AD-774 270

A DESIGN ANALYSIS OF CH-54B MAIN ROTOR HUB FABRICATED FROM COMPOSITE MATERIALS

Robert Lee Faiz

United Aircraft Corporation

Prepared for:

Army Air Mobility Research and Development Laboratory

October 1973

DISTRIBUTED BY:

NTIS

National Technical Information Service
U. S. DEPARTMENT OF COMMERCE
5285 Port Royal Road, Springfield Va. 22151

DISCLAIMERS

The findings in this report are not to be construed as an official Department of the Army position unless so designated by other authorized documents.

When Government drawings, specifications, or other data are used for any purpose other than in connection with a definitely related Government procurement operation, the United States Government thereby incurs no responsibility nor any obligation whatsoever; and the fact that the Government may have formulated, furnished, or in any way supplied the said drawings, specifications, or other data is not to be regarded by implication or otherwise as in any manner licensing the holder or any other person or corporation, or conveying any rights or permission, to manufacture, use, or sell any patented invention that may in any way be related thereto.

Trade names cited in this report do not constitute an official endorsement or approval of the use of such commercial hardware or software.

DISPOSITION INSTRUCTIONS

Destroy this report when no longer needed. Do not return it to the originator.

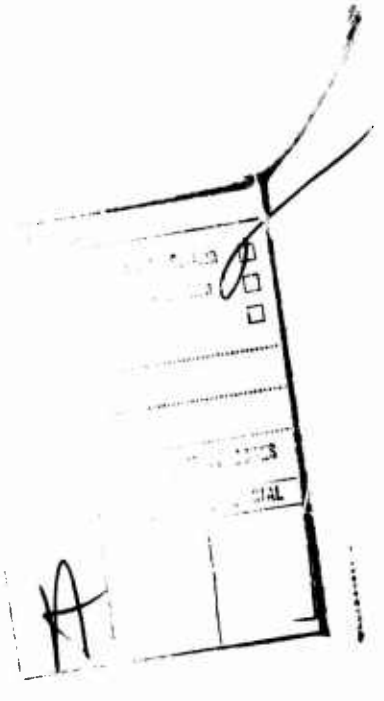

Unclassified
Security Classification

DOCUMENT CONTROL DATA - R & D

(Security classification of title, body of abstract and indexing annotation must be entered when the overall report is classified)

1. ORIGINATING ACTIVITY *(Corporate author)*

Sikorsky Aircraft Division
United Aircraft Corporation
N. Main Street, Stratford, Connecticut

2a. REPORT SECURITY CLASSIFICATION

AD774270

2b. GROUP

3. REPORT TITLE

A DESIGN ANALYSIS OF A CH-54B MAIN ROTOR HUB FABRICATED FROM COMPOSITE MATERIALS

4. DESCRIPTIVE NOTES *(Type of report and inclusive dates)*

Final Report

5. AUTHOR(S) *(First name, middle initial, last name)*

Robert L. Faiz

6. REPORT DATE	7a. TOTAL NO. OF PAGES	7b. NO. OF REFS
October 1973	224	18

8a. CONTRACT OR GRANT NO	9a. ORIGINATOR'S REPORT NUMBER(S)
DAAJ02-72-C-0104	USAAMRDL Technical Report 73-49
b. PROJECT NO. Task 1F162208A17003	
c.	9b. OTHER REPORT NO(S) *(Any other numbers that may be assigned this report)* Sikorsky Engineering Report 50827
d.	

10. DISTRIBUTION STATEMENT

Approved for public release; distribution unlimited.

11. SUPPLEMENTARY NOTES	12. SPONSORING MILITARY ACTIVITY
	Eustis Directorate, U.S. Army Air Mobility Research and Development Laboratory, Fort Eustis, Virginia

13. ABSTRACT

A design and structural analysis of a CH-54B main rotor hub fabricated from composite materials was made to assess the flightworthiness of a hub consisting basically of tension straps fabricated from graphite epoxy and fiberglass. The concept is feasible but not competitive with the production titanium hub from a weight standpoint.

238

DD FORM 1 NOV 68 1473

Unclassified
Security Classification

14. KEY WORDS	LINK A		LINK B		LINK C	
	ROLE	WT	ROLE	WT	ROLE	WT
Composite Rotor Hub Design Analysis						
CH-54B Main Rotor Head						
Composite Tension Strap Hub Concept						

DD FORM 1 NOV 68 1473

DEPARTMENT OF THE ARMY
U. S. ARMY AIR MOBILITY RESEARCH & DEVELOPMENT LABORATORY
EUSTIS DIRECTORATE
FORT EUSTIS, VIRGINIA 23604

This program was conducted under Contract DAAJ02-72-C-0104 with the Sikorsky Aircraft Division of United Aircraft Corporation.

The data contained in this report are the result of an analytical investigation of a composite-material main rotor hub designed for a CH-54B helicopter by the Whittaker Corporation, Research and Development Division. The hub is structurally and functionally equivalent to the metallic hub used on the CH-54B helicopter. The Whittaker concept was found to be basically sound, but it required some redesign to adequately resist the torsional and hub bending moments of this aircraft. Redesign consisted of structural changes in addition to increasing cross-sectional area; however, the basic filament-wound tension loop construction was maintained.

The report has been reviewed by the Eustis Directorate, U.S. Army Air Mobility Research and Development Laboratory, and is considered to be technically sound. It is published for the exchange of information and the stimulation of future composite hardware research or development.

This program was conducted under the technical management of Mr. Arthur J. Gustafson, Jr., Technology Applications Division.

Task 1F162208A17003
Contract DAAJ02-72-C-0104
USAAMRDL Technical Report 73-49
October 1973

A DESIGN ANALYSIS OF A CH-54B MAIN ROTOR HUB FABRICATED FROM COMPOSITE MATERIALS

Final Report

Sikorsky Engineering Report 50827

By

Robert Lee Faiz

Prepared by

Sikorsky Aircraft Division
United Aircraft Corporation
Stratford, Connecticut

for

Eustis Directorate
U. S. ARMY AIR MOBILITY RESEARCH AND DEVELOPMENT LABORATORY
FORT EUSTIS, VIRGINIA

Approved for public release;
distribution unlimited.

ABSTRACT

A flightworthy CH-54 main rotor hub has been designed using the composite tension strap concept developed by the Whittaker Corporation. The program was conducted in three phases. In Phase I, the structural adequacy of the tension strap hub concept was evaluated and design changes to make the hub flightworthy were defined. In Phase II, the redesign was substantiated through analysis and design drawings were prepared. In Phase III, a plan was prepared to verify, by test, the structural adequacy and flightworthiness of the design.

The study showed that the basic tension strap hub concept could not adequately react out-of-plane hub moments and rotor torque. The redesign resolved these problems by adding external vertical shear webs, tapering and deepening the hub arms, and adding clamped ring elements in the central hub regime. The weight of the redesigned hub was equal to the original concept weight, but 300 pounds heavier than the CH-54 production hub.

The rotor hub is designed to be flightworthy. Fabrication, fatigue tests, and whirl and flight tests can now proceed in discrete steps to confirm this.

FOREWORD

A CH-54 composite main rotor hub has been designed under Contract DAAJ02-72-C-0104 with the Eustis Directorate, U. S. Army Air Mobility Research and Development Laboratory, Fort Eustis, Virginia, Task 1F162208A17003. This work is part of a program to design, bench test and flight test new composite material concepts in order to evaluate benefits and limitations for helicopter applications.

The work was performed under the general direction of Mr. Arthur Gustafson of the Technology Applications Division of the Eustis Directorate. Sikorsky Aircraft's principal participants were Robert Faiz, the Project Manager, and Frank Pallone, Peter Danjoski, Hugh Taylor, and Kenneth Marshall, who performed the design material selection and analysis of the hub. The program was under the general supervision of Robert Zincone, Rotor Design Section Supervisor, and William Paul, Chief of Aircraft and Development.

TABLE OF CONTENTS

LIST OF ILLUSTRATIONS

LIST OF TABLES

LIST OF SYMBOLS

$P_{x,y,z}$; V_n; V_c; $R_{a,q}$	- force, lb
ω_p	- distributed load, lb/in.
$M_{x,y,z}$	- moment (by left-hand rule), lb-in.
ft,s,br	- applied stress, tension, shear, and bearing, $lb/in.^2$
F_{tu},F_{su}, F_{bru}	- ultimate stress, tension, shear, and bearing, $lb/in.^2$
E, F_{en}, $E_{3\sigma}$	- fatigue endurance limit, stress vs. cycles,psi
K_t	- stress concentration factor
f_{se}, $f_{3\sigma}$	- fatigue size effect and reliability factors
X,Y,Z,h	- length, in.
A	- area, $in.^2$
$I_{xx,yy,zz}$	- area moment of inertia, $in.^4$
E	- modulus of elasticity, $\frac{lb}{in.^2}$
K	- spring rate, $\frac{lb}{in.^2}$

INTRODUCTION

The high strength and stiffness-to-weight ratio of composite materials and their capability of automated molding offer potential benefits of reduced cost and increased performance and safety.[1] To explore these benefits, the Eustis Directorate has undertaken a number of programs to design and test composite blades and dynamic components. The intent of these programs is to design and ultimately flight test composite concepts on existing helicopters in order to thoroughly define structural characteristics and flightworthiness. The requirement to design with new materials for existing helicopters often results in heavy and costly structures, because the designs were made to fit on existing attachments and within existing envelopes. However, the intent of the evaluation is not necessarily to define cost and weight benefits for existing helicopters, but rather to compare directly the structural and flight characteristics of new and old structures. With these data, designers can then have more confidence in employing these concepts on new aircraft and can design a better interface that takes advantage of the weight and cost benefits of composites.

The objective of the work performed under this contract was to examine the feasibility and flightworthiness of a composite main rotor hub. The Whittaker Corporation, San Diego, developed a composite tension strap concept that could be used in a proper array to react rotor blade centrifugal forces efficiently. The concept, shown in Figure 1, has a simple, continuous, unidirectional fiber strap attached to a composite web to react in-plane shear loads. A stack of these straps could attach to a shaft to comprise a rotor hub that reacts all forces from the rotor blades and transfers them to the shaft. Ease of manufacture and potential "fail-safety" of the minimum elements were promised by this concept.

To begin the evaluation, the Eustis Directorate awarded Whittaker a contract to design and conduct preliminary fatigue tests of a rotor hub to replace the CH-54 production rotor head. The design was required to accept existing bearings to permit blade articulation. The central hub had to be designed to attach to existing shaft splines and the hub nut assembly.

The design shown in Figure 2 was derived by Whittaker to meet these requirements. The hub consists of six radially positioned cantilever beams around a central hub. These beams consist of 12 laminates of peripheral, filament-wound, glass-fiber/epoxy material to react radial centrifugal and bending stresses. Those filaments are wrapped around the steel lug, which restrains the Timken thrust bearings. Flatwise bending shear is reacted by an integral basket-shaped structure consisting of $\pm$45-degree fiberglass layers whose fibers are oriented along the principal axis. In-plane bending shear is re-

acted by similarly oriented fibers in the top and bottom plates. Torsion caused by an eccentrically applied in-plane shear load is reacted by the torque box created by the basket and top and bottom plates. The net out-of-plane thrust is transferred to the hub and shaft through 18 bolts clamping the hub laminates to the central steel hub. The net in-plane torque is reacted by six steel keys locking the hub laminates to the central hub.

Whittaker's design appeared to be inadequate in reacting out-of-plane bending and torque, and the design weight was 300 pounds heavier than the production CH-54 hub. It was considered that the next step should be to define the structural feasibility of this concept and redesign it to make it flight-worthy.

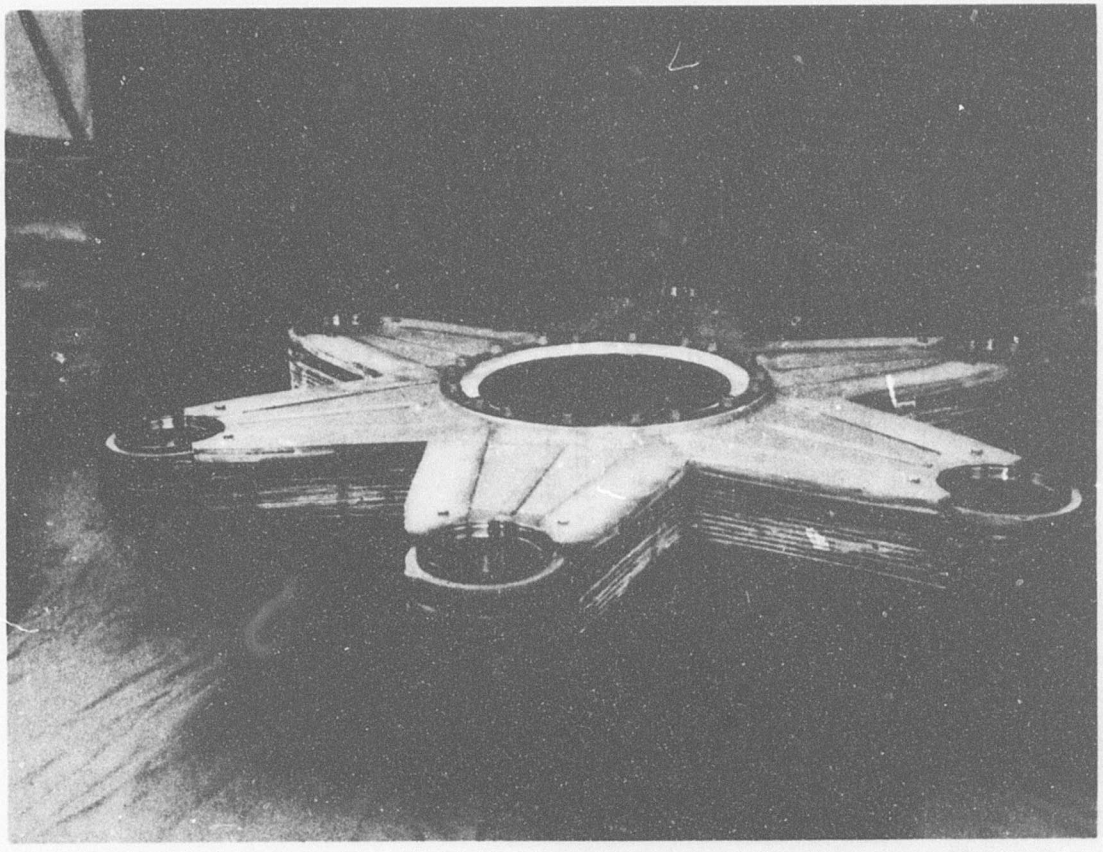

Figure 1. Whittaker Composite Hub.

PHASE I

The purpose of Phase I was to judge the structural adequacy of the proposed Whittaker hub design from the standpoint of a helicopter manufacturer and to propose design changes, if necessary, in areas of structural weakness. Incorporation of the composite hub design on an aircraft for flight evaluation must be preceded by thorough analysis of the design by the user, who has the experience to isolate key structural risk areas unfamiliar to the nonuser. Phase I made possible familiarization with the design concept, understanding of the static and fatigue properties of the composites used, and early insight into possible design flaws.

An additional purpose of Phase I was to assess the system acceptability of the composite hub design. The composite hub must integrate itself functionally into the rest of the rotor hub structure. The vibratory vertical and in-plane displacement of the composite hub arm should not degrade the pitch, flap, lag kinematic relationship of the blade.

The output of Phase I was a judgment of the ability to proceed with the basic strap concept to a flightworthy hub consistent with the design experience of a helicopter manufacturer. The significant design modifications made to the basic tension strap concept are presented in Figure 2. The incorporation of these modifications will result in increased flightworthiness of the hub.

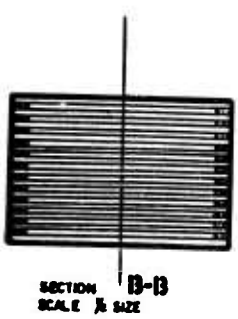

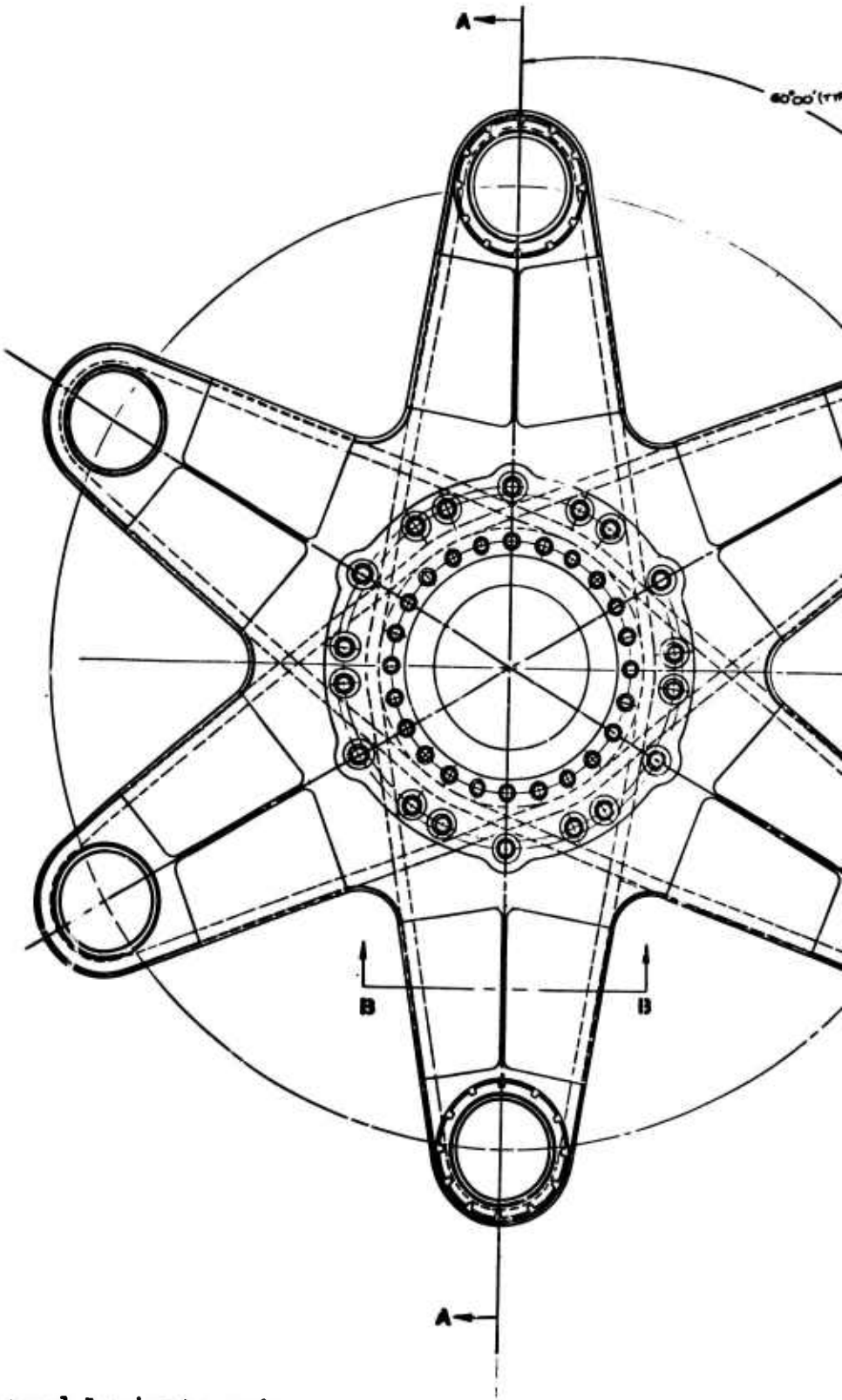

Figure 2. Splayed Laminate Hub.

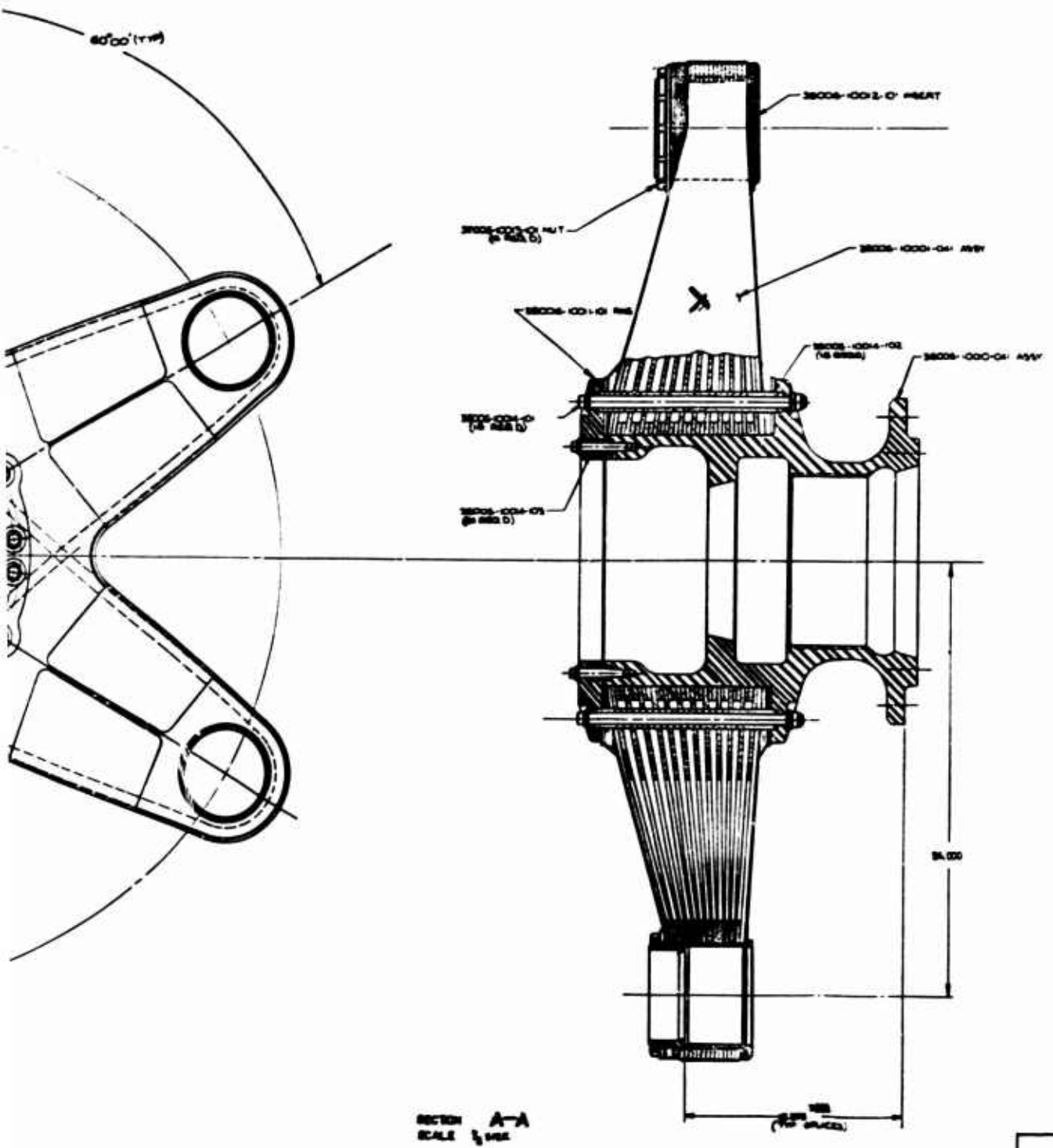

SECTION A-A
SCALE

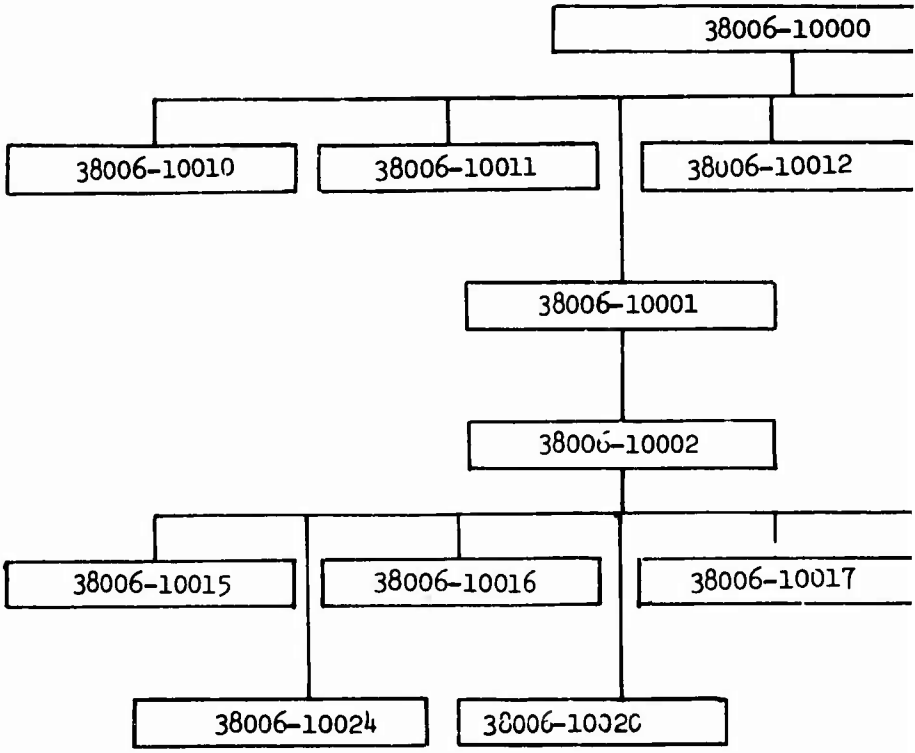

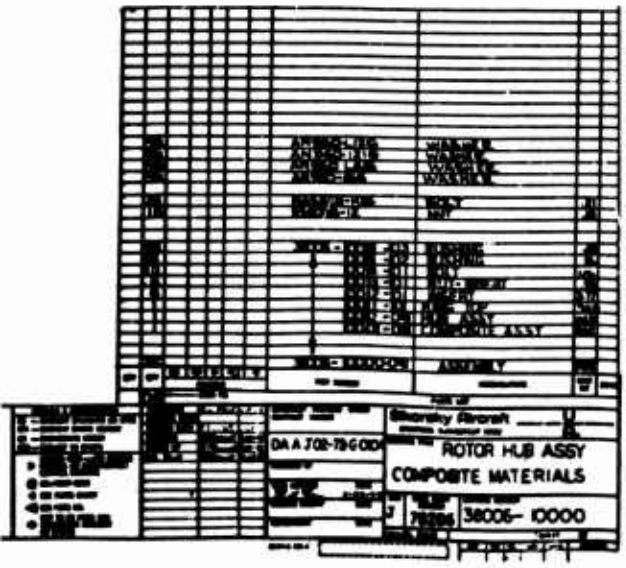

Composite Hub Draw

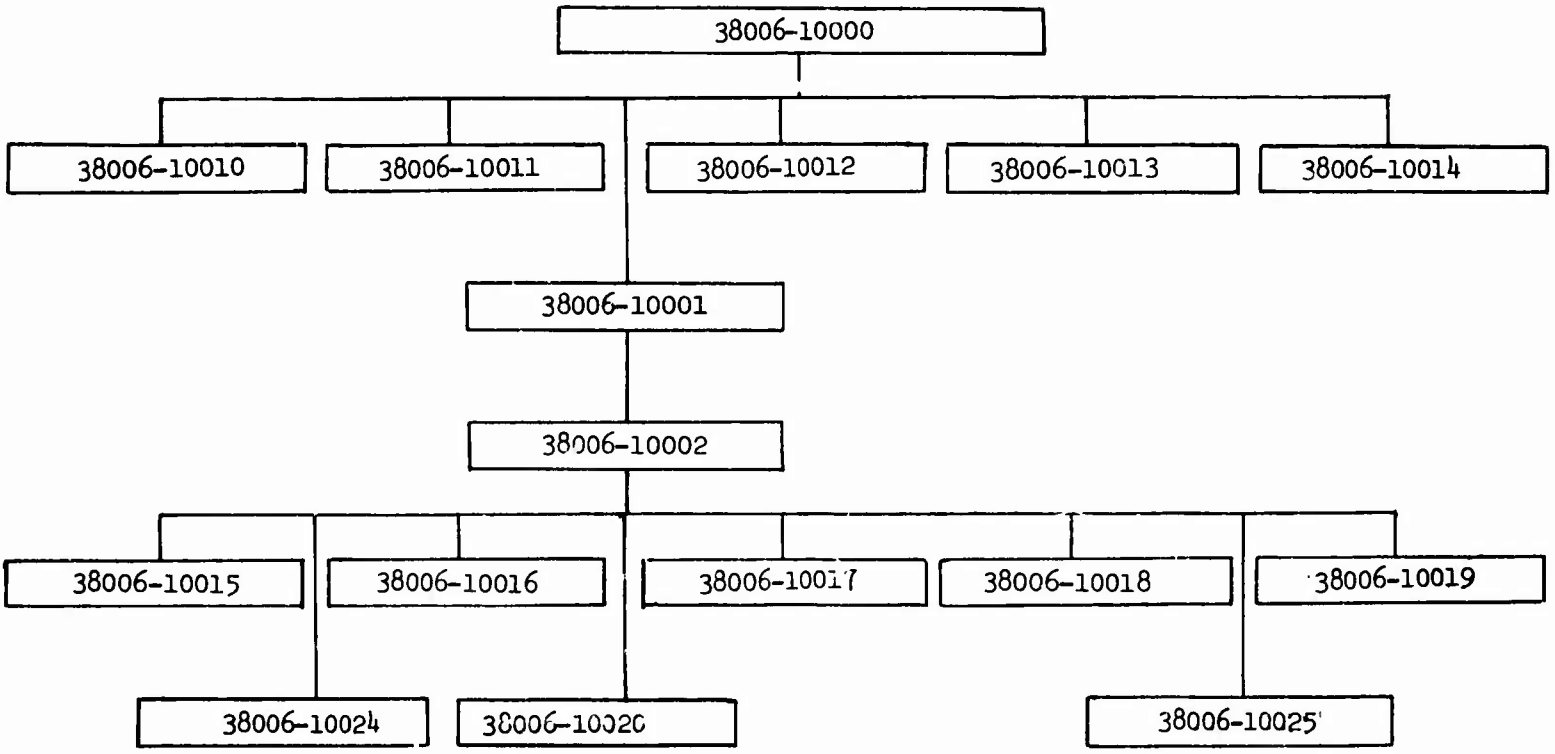

Composite Hub Drawings

DESIGN CONSIDERATIONS

The main rotor hub of a single rotor helicopter with articulated blades is subjected to steady and vibratory loads in all directions. The hub must support the weight of the vehicle, provide for the transmission of the shaft torque to the articulated hinge to drive the blades, support the large centrifugal force of each blade, and transmit the 1/rev head moments generated by blade flapping.[2] Of all these forces, the head moment derived from blade flapping and the centrifugal force are the two normally important loads. Since the head moment is the major source of vibratory stresses, it has usually controlled the basic cross-sectional sizes of the structural elements of the central hub. Centrifugal force tends to establish the basic steady stress level at which the hub operates. In critiquing the Whittaker hub design, which is built around the flat tension strap concept, the head moment and centrifugal force become most important. The strap concept naturally provides a simple reactive system to support centrifugal force: one opposing blade balances the centrifugal force of the other. However, at the flapping hinge, the head moment develops vibratory shear loads parallel to the shaft axis. These shear loads present the more difficult structural task for the Whittaker concept. Special shear-carrying provisions must be incorporated to transmit and react these shears quite apart from the loading within the tension straps (Figures 3 and 4).

ANALYTICAL EFFORT

The ever-present structural task in composite design is to transfer loads into and out of the composite usually through metal attachments and fittings. The complexity of the composite hub attachments to the main rotor shaft and blade retention components caused concern over the structural adequacy of these areas due to the transfer of loads into and out of the basic arm structure.

Preliminary investigation of the hub concept resulted in concern over the structural adequacy of the following areas:

- Load transfer into and out of the central shear basket.
- Laminate bond shear due to bending.
- Bond shear at lap joint interfaces.
- Bond shear between bearing inserts and arms.
- Bond cleavage at lower cover to arm laminate interface.
- Head moment and shaft torque transfer between central bolts, bushings, and keys.

These areas were deemed critical based on the observation that the basic weaknesses of the hub concepts were bending shear stiffness (out of plane) and head moment transfer capability. Subsequent analysis showed that these regions were structurally inadequate and that design modifications were required.[3]

Preceding page blank

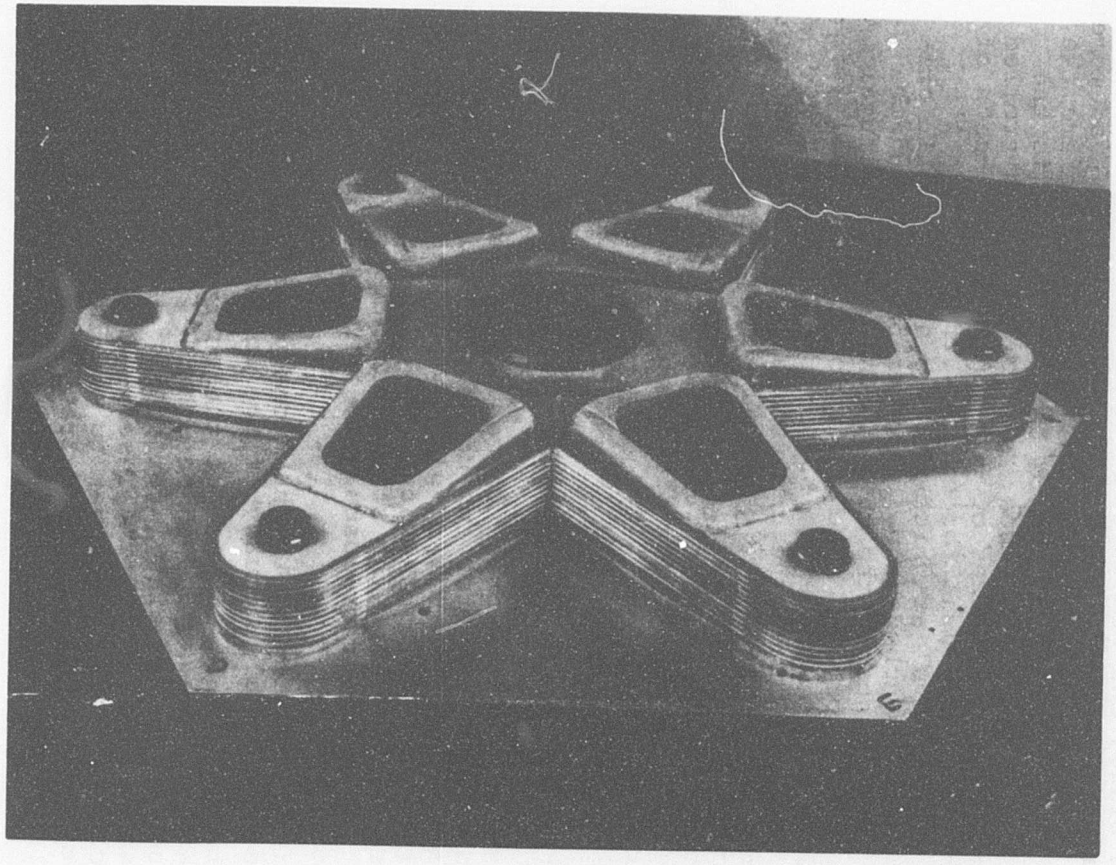

Figure 3. Composite Hub Intermediate Assembly (Shown Without Covers).

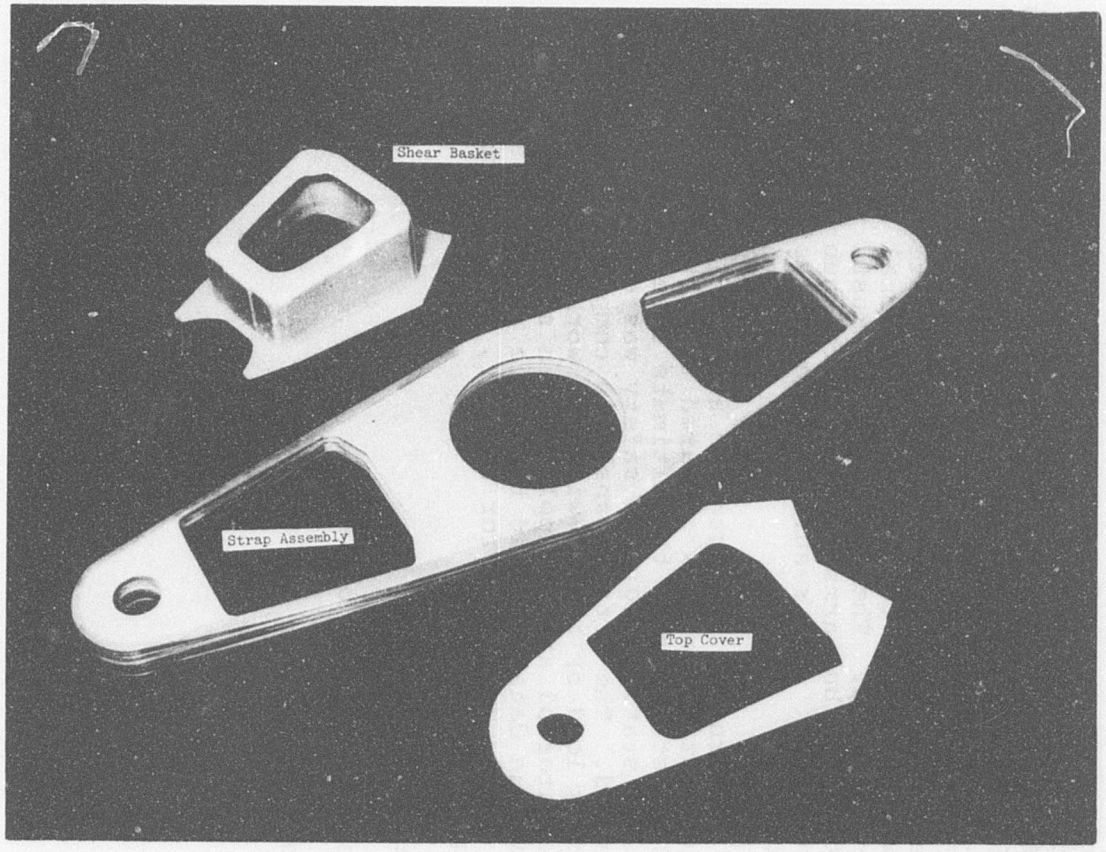

Figure 4. Primary Hub Components.

METHODS OF ANALYSIS

The initial effort involved design analysis of the initial composite hub concept prepared under Reference 1. Structural adequacy of the design was investigated. Where found inadequate, design modifications were proposed to correct the deficiency.

The methods of analysis used in the design study were similar to those used in Reference 4. The hub arm analysis is basic cantilever beam theory. The relative stiffness of the various members of the hub was taken into account when computing bending stresses.

The interface between the composite hub laminates and steel central hub was subjected to a three-dimensional finite element computer analysis. The transfer of thrust, torque, and head moment from the hub arms to the central hub was investigated with this tool. The results of the analysis are presented in Table 1.

Each area of concern was subjected to a static and fatigue analysis. The static analysis compared the ultimate load (1.5 x limit load) or stress with the ultimate stress allowable for the material. A static margin of safety was computed and a summary presented. The fatigue analysis compared the fatigue design vibratory load or stress with the working endurance limit for the material at the applied mean stress. A 50% reduction of fatigue data was used to derive a working endurance limit. This factor accounted for scatter, size effect, and surface irregularities.

The load cases were:[5]

- Autorotation, power on
- Autorotation, power off

TABLE 1. HUB REGIONS EXHIBITING STRUCTURAL INADEQUACY[3]

Failure Mode	Applied Stress/Load		Allowable		Margin Of Safety	
	Static Ult	Fatigue	Static	Fatigue	Static	Fatigue
Filament Strap Adhesive Shear Failure, Section A-A	17,645 psi	± 5550 psi	5000 psi	± 1000 psi	Neg.	Neg.
Filament Strap Overlap Adhesive Shear Failure - Hub Crotch	14,520 psi	± 2340 psi	5000 psi	± 1000 psi	Neg.	Neg.
Basket Lip to Laminate Adhesive Shear Failure - Outboard End		± 1500 psi	5000 psi	± 1000 psi		Neg.
Lower Plate to Laminate Adhesive Cleavage Failure - Outboard	314 lb/in.		10-30 lb/in.		Neg.	
Hub to Laminate Attachment Bolts - Shear Failure	160,000 psi		95,000 psi		Neg.	
Laminate Key Bearing Failure		± 29,500 psi		± 7000 psi		Neg.

HUB ARM ANALYSIS

The hub arm reacts radial, edgewise, and out-of-plane loads as a cantilever beam (Figure 5). These loads are applied at the extremities of the arm through the lag hinge bearings. Structural adequacy of the arm depends on the continuity of the shear and bending load paths. Continuity of the bending load paths is provided by the wound straps. Continuity of the shear load path is provided by the shear basket bonded to the straps. However, the shear load must be transferred into the basket at its outer end and back out at its inboard end across a bonded interface. The rate of transfer is gradual, so the basket does not react shear effectively at its extremities. The critical sections of the hub arm are at a radius of 10.9 inches and 19.5 inches from the center of rotation. These sections are close to the discontinuities created by the ends of the basket, and the basket shear capability is assumed to be zero at these points.

The original analysis of the hub arms (Reference 6) did not include the effect of chopped fiber spacers on bending stiffness. This effect cannot be neglected. These spacers are continuous from the lug bearing region to the central hub bolt region. Therefore, the arm was analyzed with the following assumptions included:

- The shear basket is not effective at Sections A-A and B-B.
- The bending shear is carried by the bond between the laminates at these sections.
- Chopped fibers are fully effective at these sections.

Analytical Results and Conclusions

Structural analysis of the hub arm revealed unacceptably high shear stresses due to bending. Sikorsky is using a similar adhesive system in a fatigue environment on main rotor blades. In this environment, the following design allowables are established:

Static Allowable Shear Stress $F_{su} = 5000$ psi

Vibratory Allowable Shear Stress $E_{3\sigma}(\text{shear}) = \pm 1000$ psi

The applied shear stresses in the bond adhesive (Figure 5) are 17,645 psi maximum ultimate and ± 5550 psi maximum vibratory. Since the applied stresses are greater than the design allowables, the static and fatigue margins of safety are negative for the adhesive.

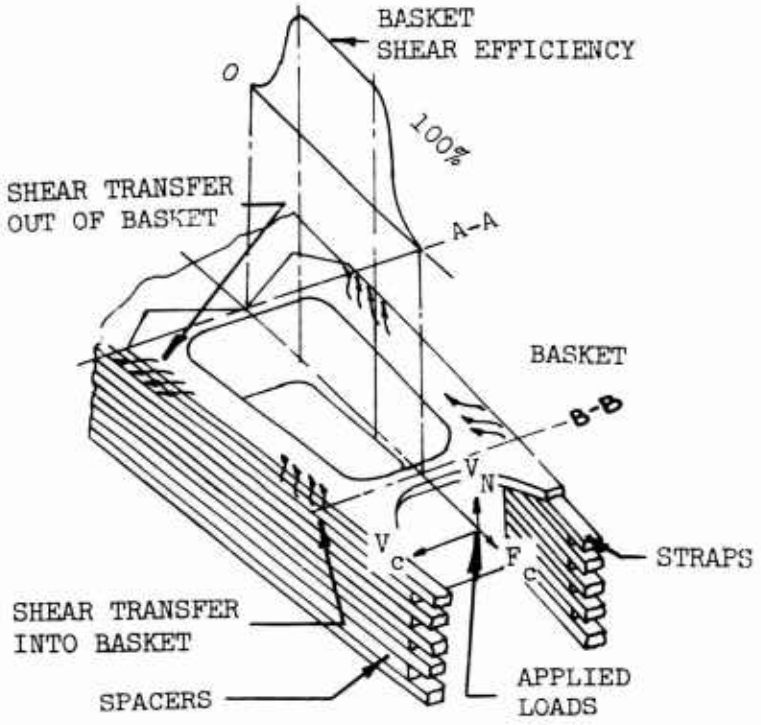

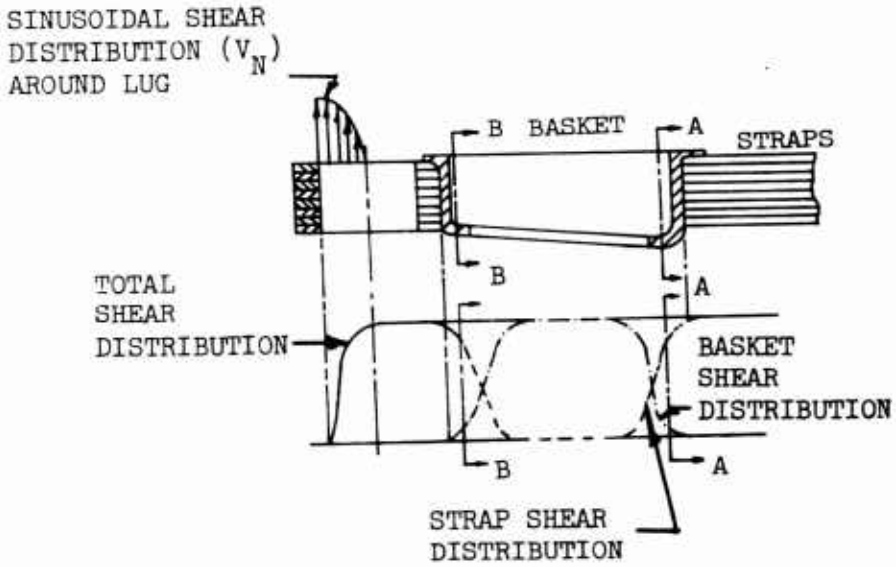

Summary of Arm Bending Shear Stresses		
SECTION	Applied Shear Stress	
	Ultimate	Fatigue
A-A	7845 psi	±2470 psi
B-B	17645 psi	±5550 psi

Figure 5. Shear Transfer Analysis in Hub Arm.

Proposed Design Modifications (Figure 6)

The primary design deficiency of the hub arm region is the bending shear discontinuity caused by the lack of a continuous shear member from the arm extremities to the central region. The design modification proposed to correct this deficiency was: placement of continuous shear strap on the outside of the hub to eliminate discontinuities and to assure that this shear web is totally effective at Sections A-A and B-B. The basket was retained to provide adequate torsional rigidity to the arms.

Preliminary Analysis Results (Table 2)

Preliminary analysis showed that the redesign was structurally feasible. The shear stresses in the vertical web were within acceptable limits. The analysis neglected the effect of the basket, but it was assumed that the continuous shear web was fully effective. It was further assumed that all of the load was carried by the shear web. The static ultimate and fatigue stresses were approximately equal to the corresponding values calculated for the shear basket in Reference 3. The shear web was sized in the detail design stage, so the stress levels and margins of safety were identical with those calculated for the shear basket.

TABLE 2. REDESIGNED ARM BENDING SHEAR STRESS

Section	Static Ultimate Shear Stress (psi)	Fatigue Shear Stress (±psi)	Static Ultimate Allowable $(Fs)_{ult}$	Fatigue Allowable (Fs)(±psi)
A-A	17215	5417	21600	±4500
B-B	22528	7089	21600	±4500

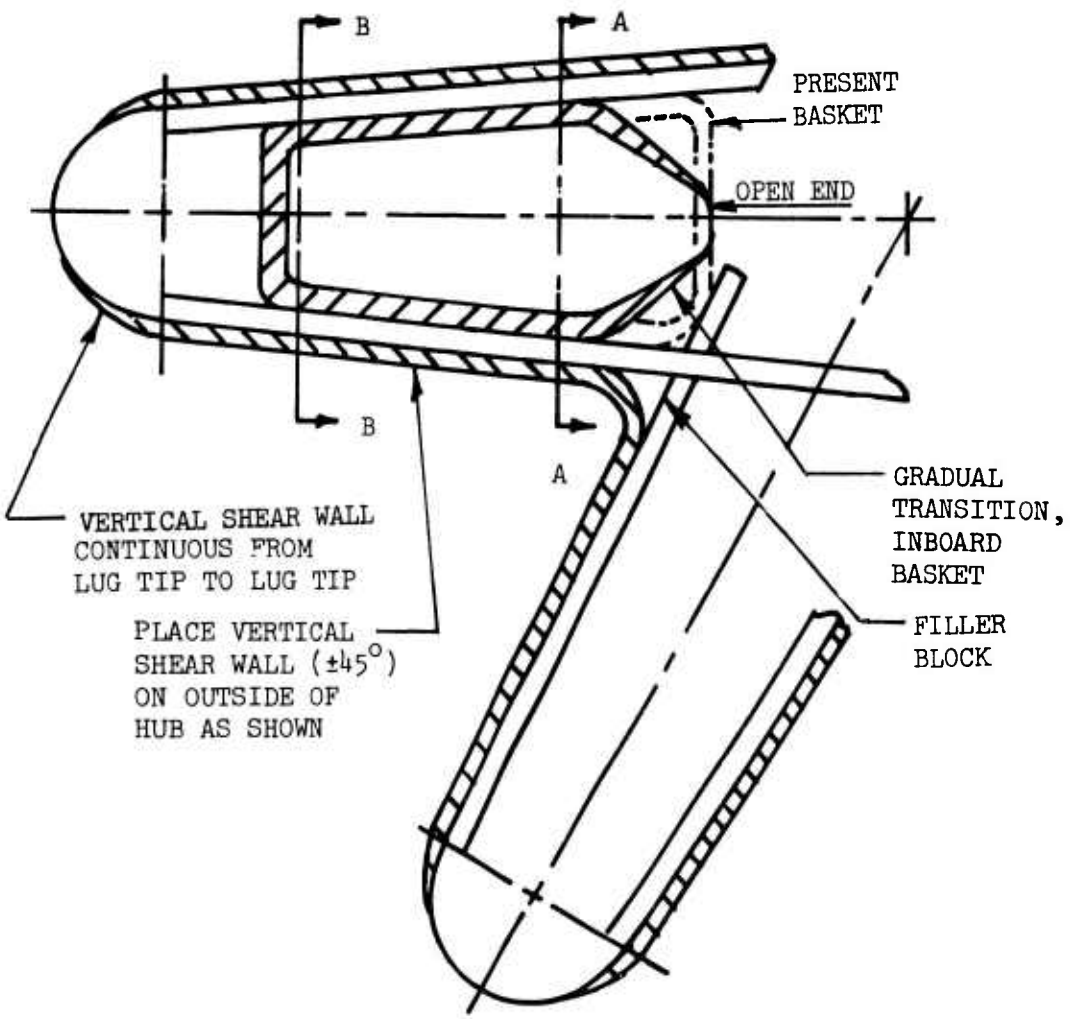

Figure 6. Design Modification for Improved Shear Transfer.

CENTRAL HUB TO LAMINATE (Figure 7)

The hub laminates are attached to the central hub with eighteen 9/16-dia steel bolts and six interlocking steel keys around the hub periphery. The shaft torque and head moment load transfer paths are redundant. The shaft torque is reacted by a combination of bearing on the keys in the tangential direction and shear in the steel attachment bolts. The head moments are reacted by a linear radial bearing distribution on the keys and by radial shear on the bolts in conjunction with a sinusoidally distributed axial bolt load. Load sharing between these redundant load paths was analyzed by use of a 3-dimensional finite-element computer analysis (Reference 3).

Analytical Results and Conclusions

Maximum bolt tension, key bearing, and bolt shear stresses for the static ultimate and fatigue cases are summarized in Table 3.

TABLE 3. LAMINATE TO HUB ATTACHMENT STRENGTH

Analysis	Loading		
	Thrust	Torque	Head Moment
Static	141,540 lb	0 * in.-lb	2.25 $(10)^6$ in.-lb
Fatigue	34,740 lb	2.5 $(10)^6$ in.-lb	0.8 $(10)^6$ in.-lb
	Reactions		
	Bolt Tension	Bolt Shear	Key Bearing
Static	19,670 lb	40,002 lb	40,000 $\frac{lb}{in.}$
Fatigue	3128 ± 3128 lb		

* Autorotation - Power-Off Condition

The loadings summarized in Table 3 resulted in the following critical hub attachment stress levels.

Aluminum spacer bearing stress due to static key bearing load of 40,000 lb/in. in 81,600 psi.

Bolt stresses due to static tension and shear loads are 80,024 psi in tension and 162,742 psi in shear.

The laminate to hub attachment was critical for static loads, because the attachment bolts would fail in shear.

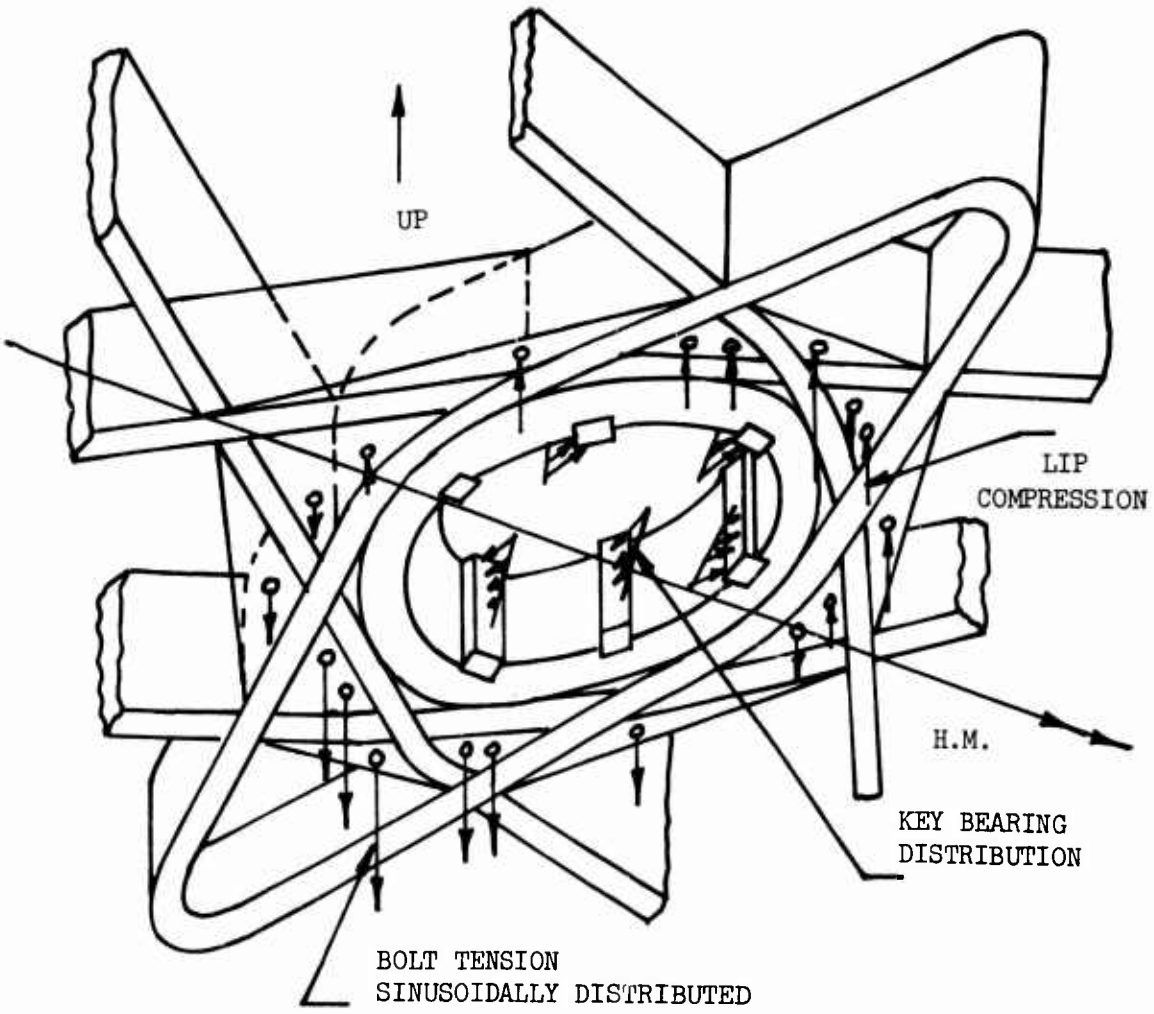

Figure 7. Laminate to Hub Load Transfer.

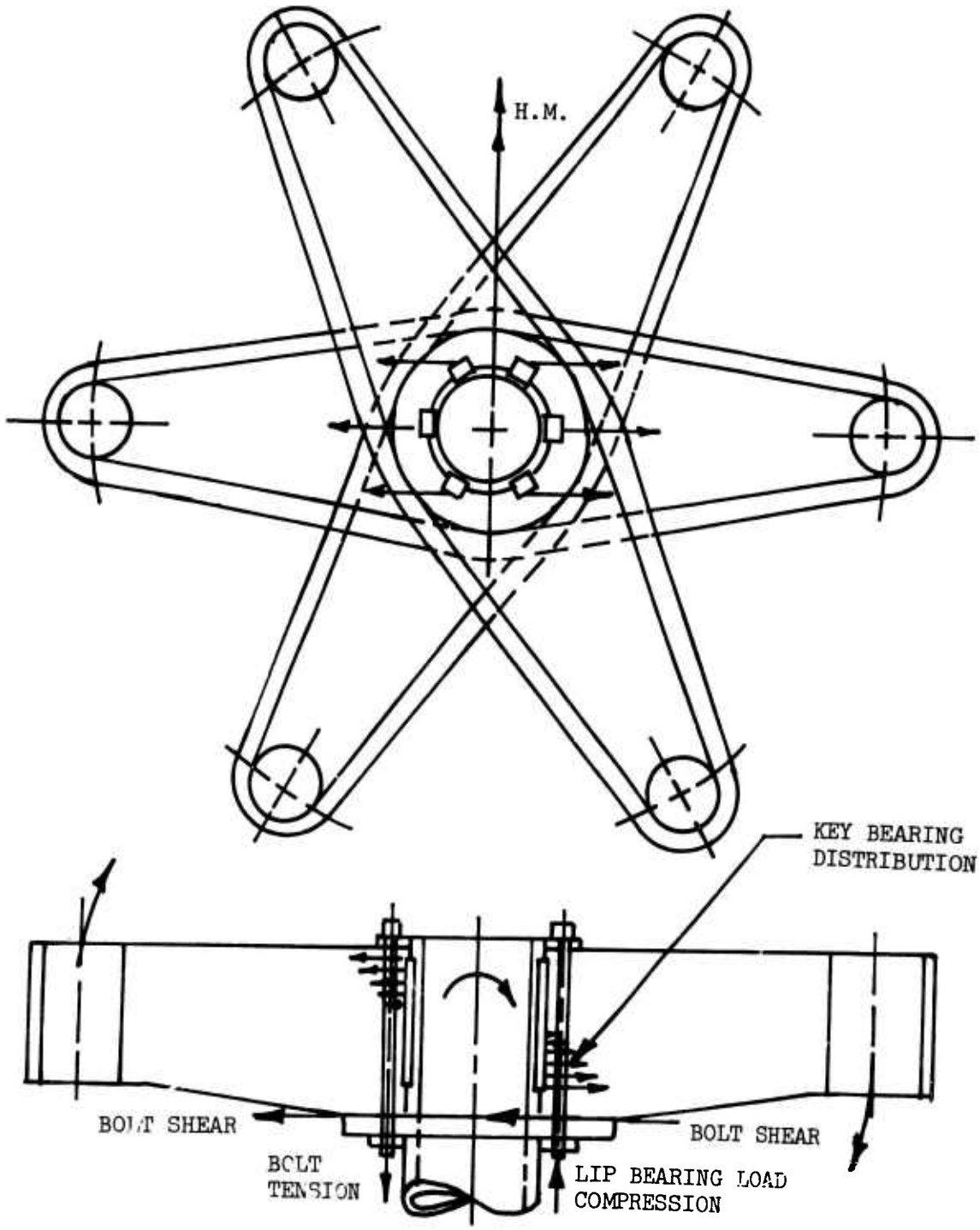

Figure 8. Hub Arm Central Bore Reactions Due to Head Moment.

Proposed Design Modifications (Figure 9)

The modified hub to laminate attachment analyzed consists of a clamp ring bolted to the top hub surface. The laminates are clamped between the clamp ring and hub lower lip by a number of through-bolts. A series of floating bushings transmits shaft torque in double shear at the clamp ring and lower lip. The head moment is reacted at the laminate through-bolt. The sinusoidally distributed out-of-plane load is reacted by a summation of bearings on the clamp ring and tension on the bolts reacted by the lower hub lip. A gap between the laminate and hub bore prevents any load transfer between the two structures in bearing.

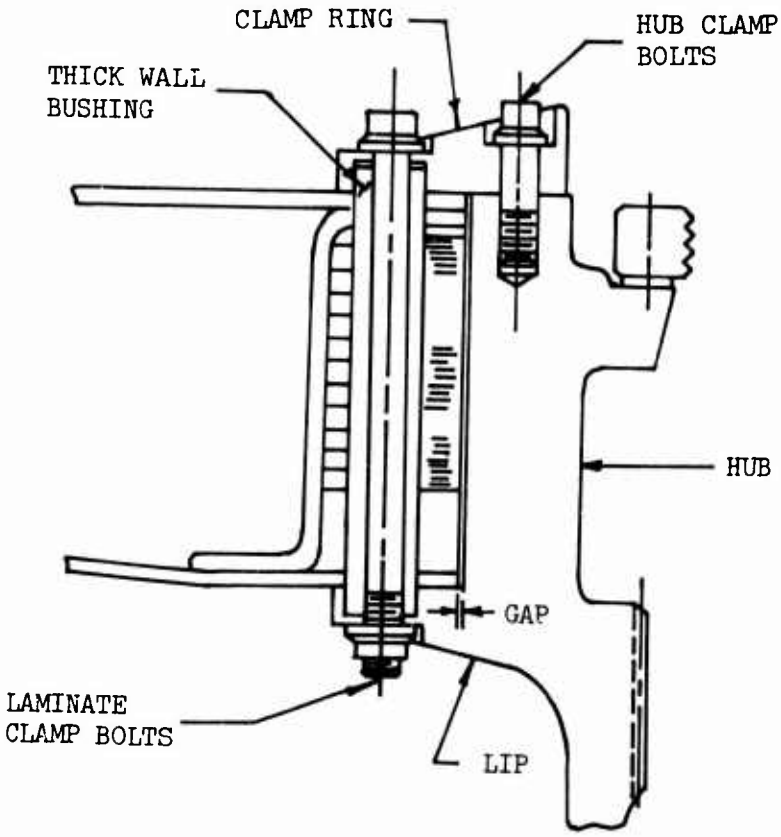

Figure 9. Improved Clamp Ring Hub Attachment.

STRAP INTERSECTION (Figure 10)

The straps form the basic structure of the individual hub arms. They are continuous from each arm to its opposite arm. To provide this continuity, the straps from adjacent arms must interlock in the crotch area of the hub. These straps carry axial bending and centrifugal loads, so they exhibit an axial strain in the intersection. Adjacent straps cross each other at an 80° angle and are bonded to each other during hub assembly. Therefore, the axial strain of one strap results in transverse strain of an adjacent strap. Unidirectional composites are structurally critical when loaded perpendicularly to the fibers, because strength is a function of the strength of the epoxy resin.

The lower adjacent straps were analyzed, because they react the highest load due to bending and centrifugal forces. The strap intersection is assumed to be a bonded reinforcement. A bonded reinforcement computer program was the analytical tool for this reinforcement.[7] This program investigates load transfer rates and magnitude as a function of adherent and adhesive material properties.

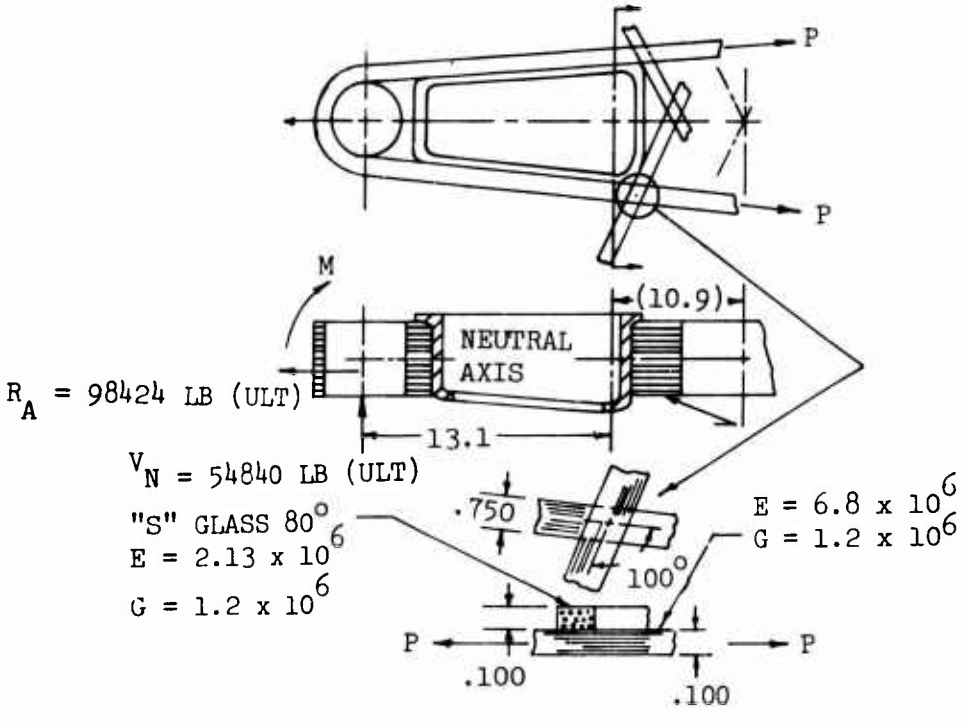

Figure 10. Strap Loading at Hub Arm Intersection.

Analytical Results and Conclusions

The static and fatigue adherent direct stresses and adhesive shear stresses resulting from the reinforcement analysis are presented in Table 4.

TABLE 4. REINFORCEMENT ANALYSIS SUMMARY

Type Load	Peak Stress (σ) (psi) Shear	Direct Lower	Direct Upper
Static (Ult)	14,520	82,590	16,940
Fatigue (Mean)	3,605	20,500	4,205
Fatigue (Vib.)	2,340	13,325	2,730

Based on Sikorsky Aircraft's experience, the ultimate shear stress for an adhesive system is 4000 psi, and the fatigue allowable is $\pm$1000 psi. Because the loads shown in Table 4 exceed these allowables, the static and fatigue margins of safety are negative.

The ultimate tensile stress for unidirectional S glass plies loaded 80° to the fibers is 11,900 psi.[8] Again, based on the data shown in Table 4, the static margin of safety is negative for the upper adherent.

Proposed Design Modifications (Figure 11)

To prevent load transfer from the lower strap adherent to the 80^{o} ply upper strap adherent, the strap interfaces should not be bonded together. Only where the aluminum shims interface with each other, should the straps be bonded together. The straps will, therefore, strain axially only.

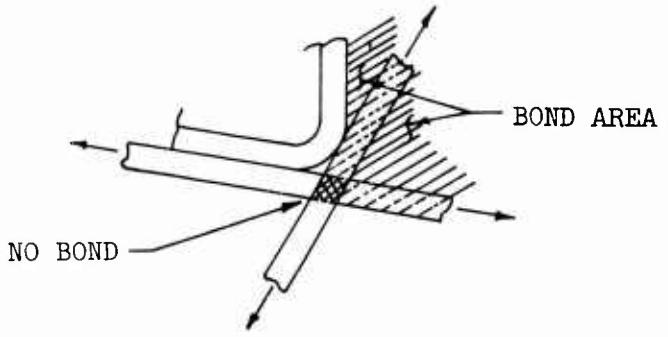

Figure 11. Strap Intersection Design Improvements To Minimize Load Transfer.

LOWER PLATE TO BASKET BOND CLEAVAGE

The lower plate is bonded to the bottom of the laminates in the lug region and to the shear basket inboard of the lug region. The bond line is parallel with the rotor plane in the lug region and angled 10° from this plane in the basket region. This change in plane creates a **"kick" load perpendicular to the bond** line. This kick load is reacted by the bond in tension or cleavage. Lower plate bending stiffness is small compared to that of the laminates. Therefore, the bending loads will be neglected, and the loads due to centrifugal force will be considered.

Only the ultimate static case is analyzed (autorotation, power off). The analysis used (Appendix II) results in an unaccepable tension load in the adhesive bonding the lower plate to the basket (Figure 12).

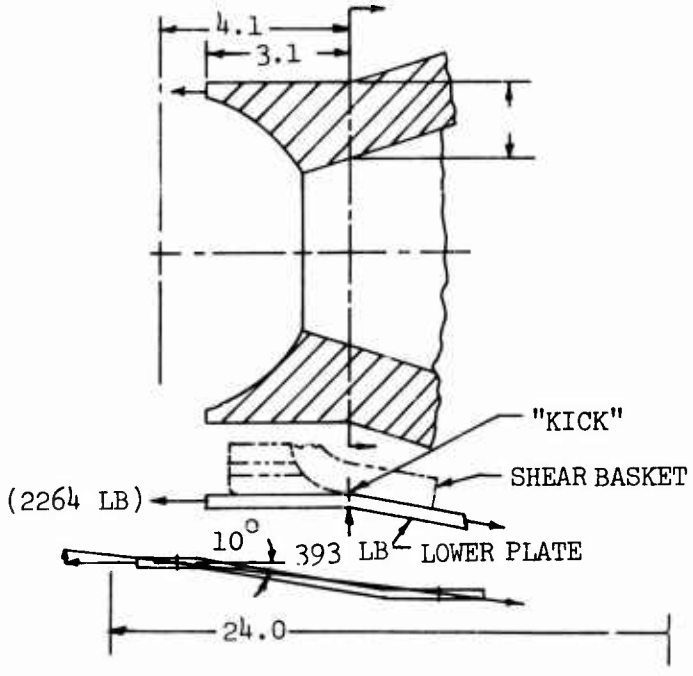

Figure 12. Critical Lower Cover Area Due to "Kick" Load.

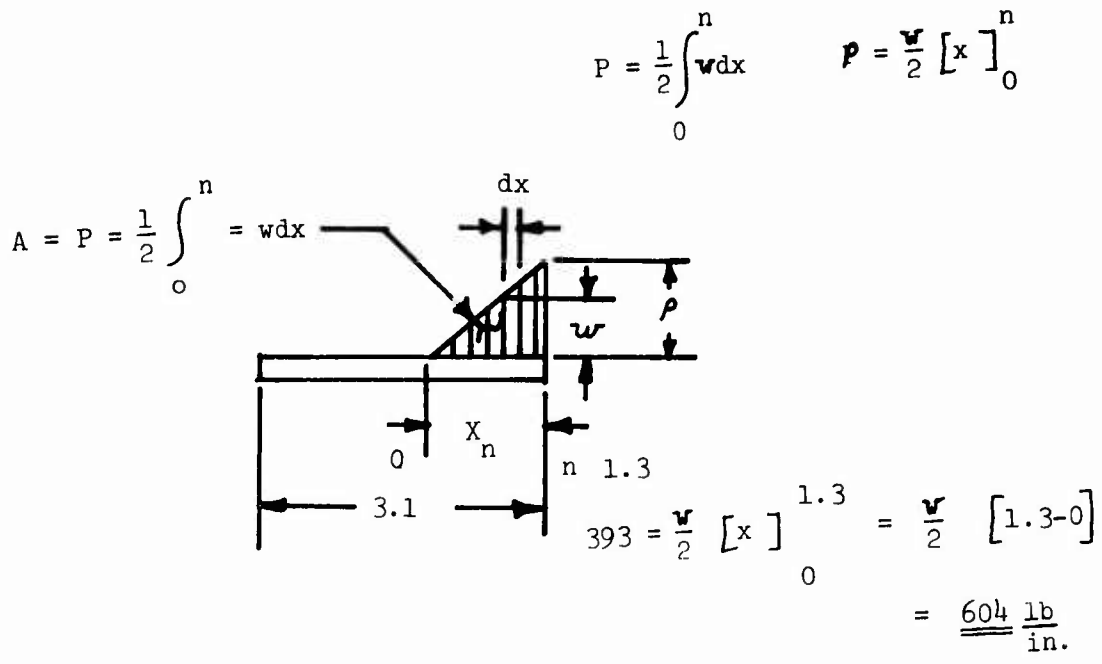

Figure 13. **Assumed "Kick" Load Distribution.**

Analytical Results and Conclusions

Adhesives are classified as class one, class two, or class three. EA 934 (Hysol) is a class-three adhesive. Such an adhesive has no peel strength, and its cleavage resistance is negligible.

However, the applied cleavage load of 393 pounds is greater than the design allowable for an adhesive, regardless of class designation. The strongest adhesives are class-one types, and have a design cleavage allowable of 30 pounds.

Proposed Design Modification

Analysis of the effect of the kick load due to the maximum total applied (98,424 lb) centrifugal load reveals that 2264 pounds are taken by one-half of the lower plate, with the reaction coming out through the lines of action of the clamping bolts. This produces a 393-pound kick load resulting from the 10° angularity.

To prevent bond cleavage, a unidirectional glass wrap is added, as defined below, to react the kick load in tension.

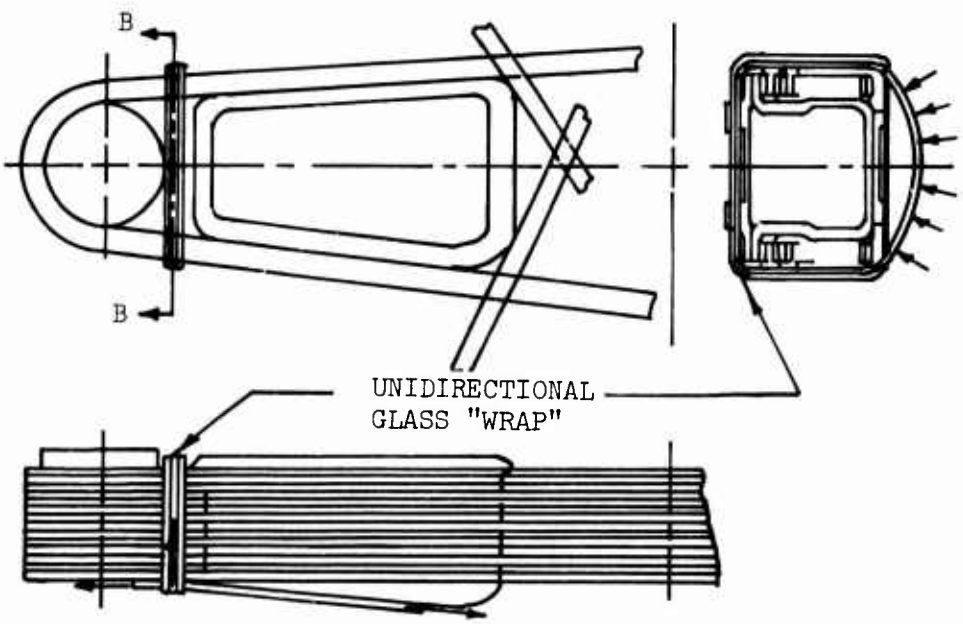

Figure 14. Tension Strap Modification To React "Kick" Load.

OUTBOARD JOINT BOND STRESS (Figure 15)

The basket lip reacts a portion of the centrifugal load. This load must be sheared into the cover adhesive bonding of the lip to the hub laminates. Due to the stiffness discontinuity at the joint end, the load transfer rate is a maximum at that point. Therefore, bond shear stress is also a maximum.

A computer program was used to analyze the load transfer rate and resultant shear stress distribution.[7] The load transfer rate and resultant shear stress distributions are analyzed as a function of adherent stiffness and geometry as well as adhesive properties.

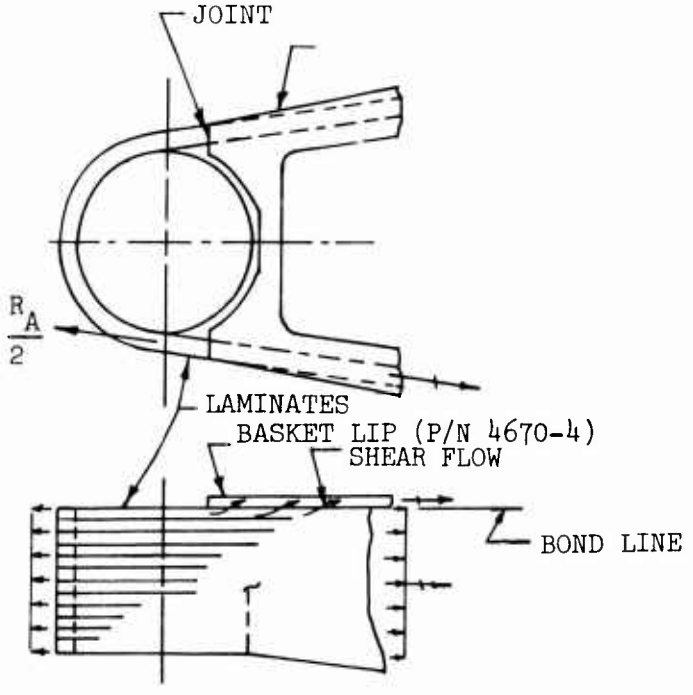

Figure 15. Assumed Load Transfer Into Basket Lip.

Analytical Results and Conclusions

The loading on the model used in the analysis consisted only of centrifugal forces (radial). Bending loads were not considered significant, as the basket is not effective in resisting in-plane and out-of-plane moments. The resultant adhesive shear stress distribution is presented below. The peak vibratory shear stress is 1.5 times the design allowable used by Sikorsky Aircraft in a fatigue environment. This allowable of ±1000 psi is based on successful use of adhesives in main rotor blades. Therefore, the basket lip to laminate bond shear stresses are unacceptable.

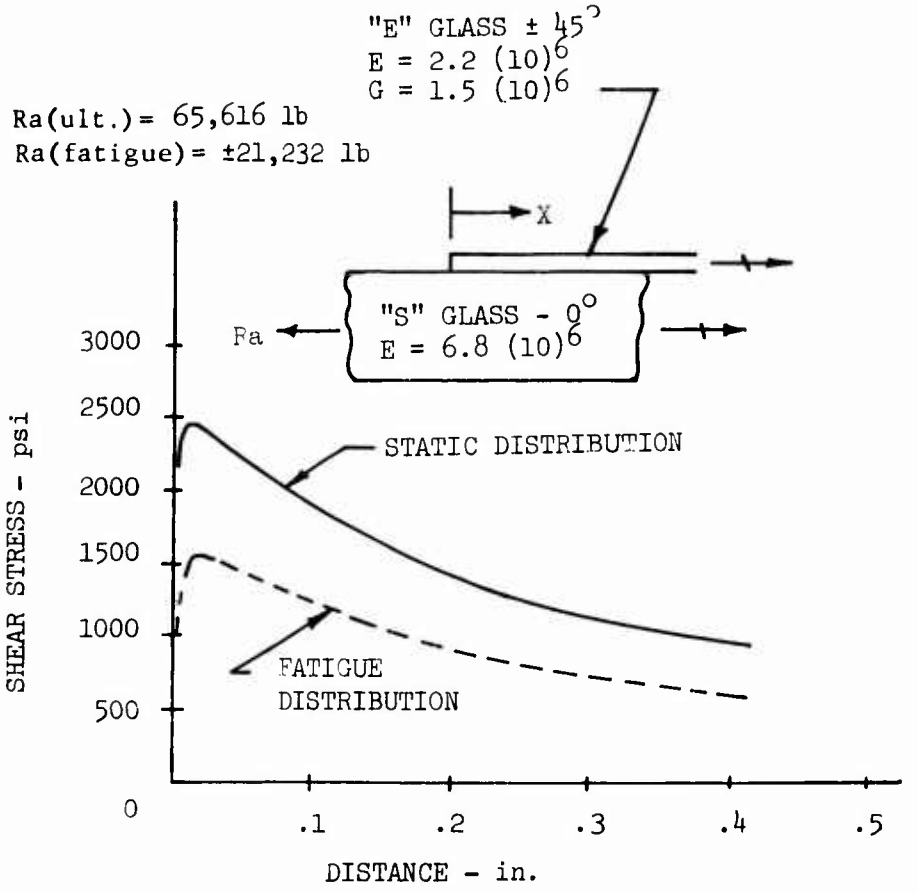

Figure 16. Resultant Shear Stress Distribution Due to Load Transfer.

Proposed Design Modification (Figure 17)

The basket lip is tapered over a length of 1 inch in order to reduce peak shear stress to an acceptable level. The optimum taper required in order to reduce the shear stress below ±1000 psi is nonlinear.

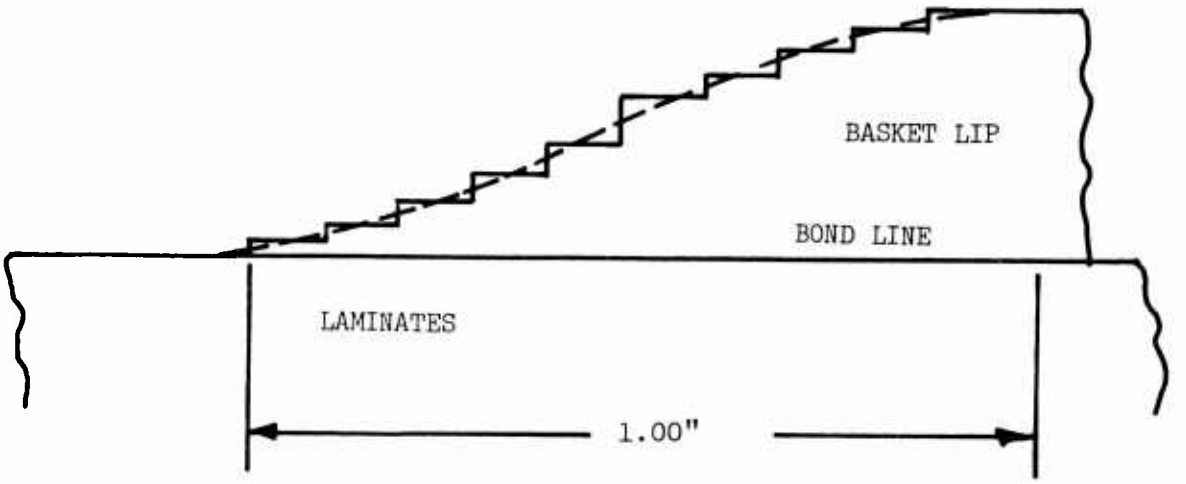

Figure 17. Improved Tapered Basket Lip.

BEARING CARTRIDGE BOND SHEAR (Figure 18)

A metal cartridge is located in the hub arm extremities to house the tapered roller lag bearings. The cartridge is held in place by bonding the outside diameter of the cartridge to the matching bore in the laminates.

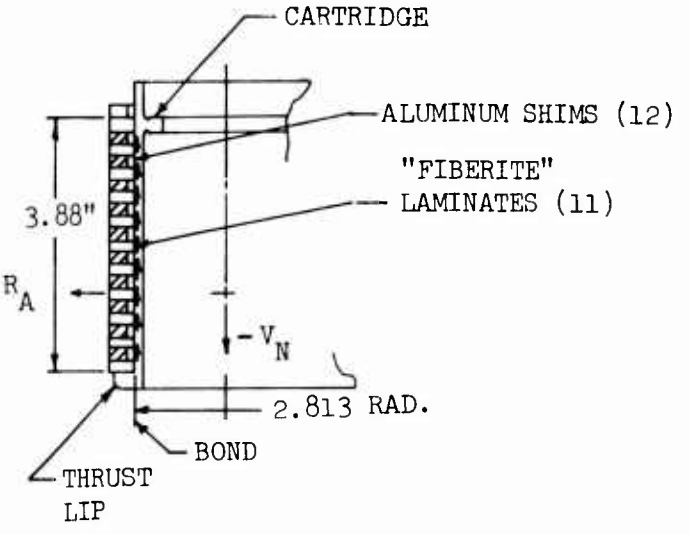

Figure 18. Downward Shear Reaction Through Bond Shear.

The positive shear (V_N), due to upward blade flapping, is reacted by the thrust lip. Negative shear ($-V_N$), due to downward blade flapping, is reacted by bond shear between the cartridge and the laminates.

Negative $V_{N_{(max)}} = -5790$ lb

due to a -4^o flapping angle

Analytical Results and Conclusions (Figure 19)

Centrifugal force will cause separation between the cartridge and laminates over the inboard periphery. Therefore, the bond will only be intact over 50% of the circumference.

$$\text{Shear Area} = 3.88\ (\pi)\ (R) = 3.88\ (\pi)\ (2.813) \quad (1)$$

$$A_s = 34.288\ \text{in}^2 \quad (2)$$

$$\text{Max. Shear Stress} = 1.5\ \frac{V_N\ (\text{MIN})}{A_s} = 1.5\ \frac{5790}{34.288} = \underline{253\ \text{PSI}} \quad (3)$$

$$\text{Allowable Shear Stress } F_{SU}\ (\text{EA 934 Adhesive}) = \underline{6500\ \text{PSI}}^{6} \quad (4)$$

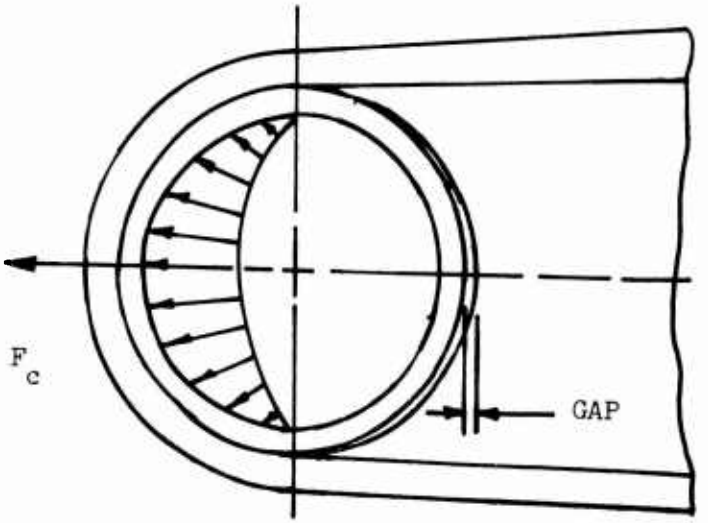

Figure 19. Resultant Back Wall Debonding Due to Hub Arm Strain.

Proposed Design Modification (Figure 20)

Although the ultimate design shear stress of 253 psi would result in a positive margin of safety, fabrication of this bonded assembly will result in a bond with a significantly lower allowable shear than that published in Reference 6.

The integrity of the bond depends on the gap between mating surfaces (proper adhesive film thickness) and slight positive pressure on the adhesive to eliminate bond voids. However, the design of the bonded assembly does not allow for control of the adhesive film thickness or allow for application of pressure on the adhesive.

The bearing cartridge is mechanically clamped to the hub and laminate extremities by the incorporation of a lock nut arrangement. The downward shear is reacted by bearing between the face of the lock nut, and the top of the arm dominates.

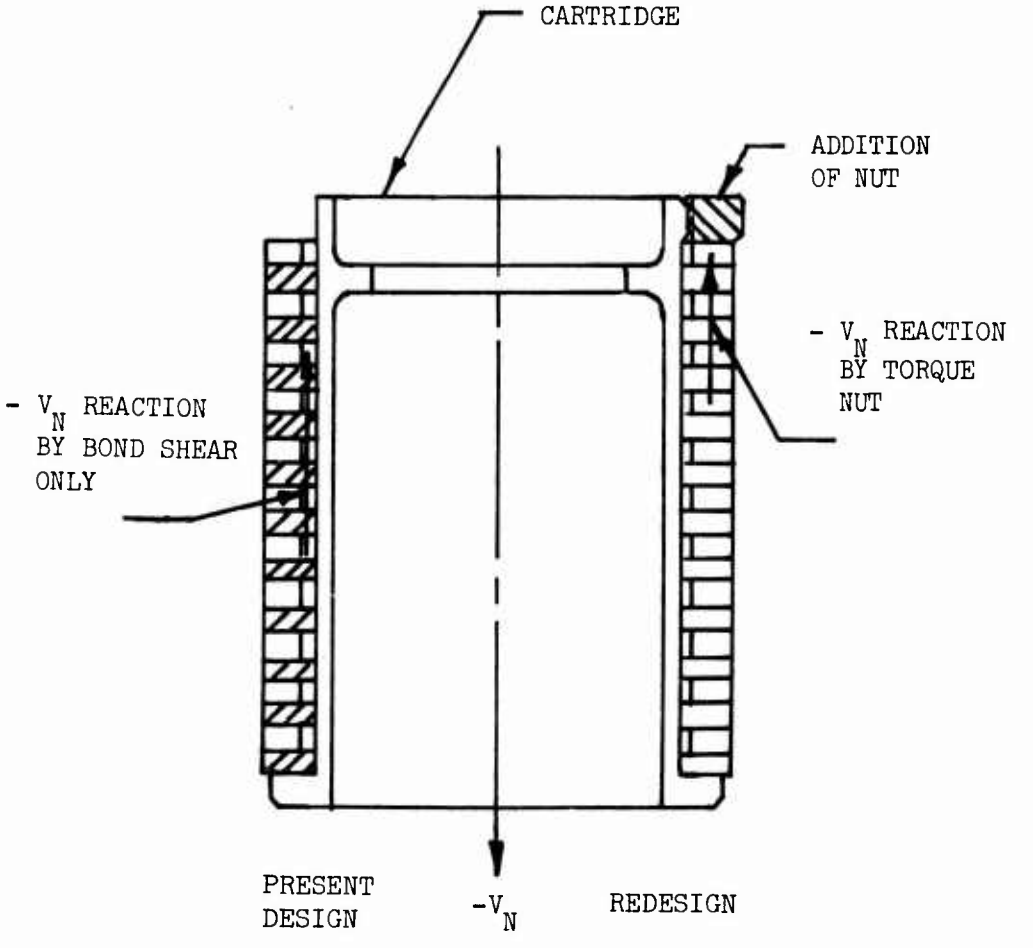

Figure 20. Mechanical Downward Shear Reaction Through Lock Nut.

PHASE II

PREPARATION OF DETAIL DRAWINGS AND SUBSTANTIATION OF THE REDESIGNED COMPOSITE HUB

The Phase II effort consisted of incorporating the tension strap concept into a redesigned, stiffer hub configuration. In addition, drawings were made of the redesigned hub, designated the splayed laminate hub.

Description of Structure (Figure 21)

The redesigned hub can be considered a series of wound straps or loops fabricated of graphite-epoxy and fiberglass-epoxy. These straps react centrifugal force and axial loads due to bending. In-plane bending shear is reacted by two shear webs laminated between the strap laminates. These shear webs are fabricated of +45° fiberglass. Out-of-plane bending shear is reacted by a vertical shear web around the periphery of the hub. This web is also fabricated of ±45° fiberglass. The vertical hinge tapered roller bearings are housed in a titanium bearing cartridge located in the six arm extremities at a radius of 24 inches. Vertical shear loads due to coning and flapping are reacted by the internal bearing cartridge lip. The laminates are attached to the titanium central hub by a series of clamp bolts and a top clamp ring. The laminates are clamped between the hub lower lip and top clamp ring by a series of 18 bolts on a 9-inch radius. Head moment is reacted by a combination of a sinusoidal bolt load distribution in tension and a sinusoidal bearing load distribution on the respective bearing lips. Rotor thrust is transferred to the central hub by a uniform bolt load and bearing load distributions. Net in-plane torque, shaft torque is transferred from the laminates to the central hub by a series of hollow bushings concentric with respect to the bolts. The central hub is splined to the main rotor shaft and located by means of split cones in a manner identical to the production CH-54B titanium rotor head assembly.

Design Improvements Summary

The basic design deficiency identified by ground testing was the inability of the Whittaker hub to react out-of-plane shear forces.[9] The reason for this was that the net flatwise stiffness of the beam was heavily influenced by the integrity of the numerous adhesive joints. The design modification added sufficient structural redundancy to minimize the effect on net strength and stiffness of the hub of local adhesive or resin system degradation.

Flatwise bending stiffness was increased by three methods. First, a more efficient continuous vertical shear web around the arm periphery replaced the original shear basket concept.

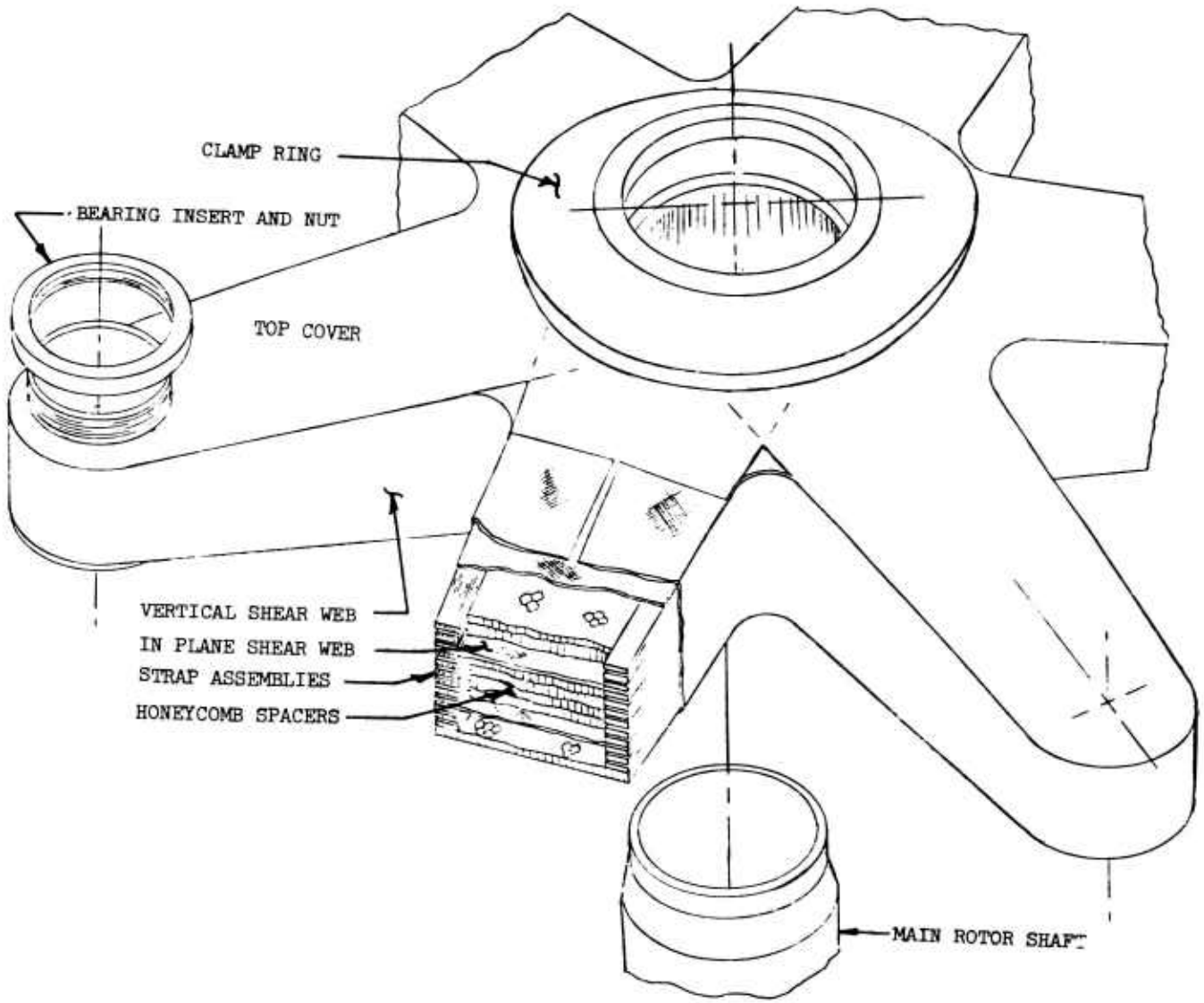

Figure 21. Splayed Laminate Composite Hub Concept.

Secondly, the loop laminates were splayed in the out-of-plane direction in order to increase the flatwise section properties of the hub arms. Finally, the extreme fiber loops were fabricated of graphite epoxy, a higher modulus material than the original fiberglass. The result was greater stiffness.

The in-plane shear load path was made redundant by incorporation of multiple shear webs. These webs are the primary shear paths and are interlaminated in the loop laminate. Also, the top and bottom covers serve as secondary in-plane shear members.

The head moment, out-of-plane load path was reacted by a sinusoidally distributed couple about the clamp ring bolt circle. The couple load was shared equally by the clamp ring and integral lip on the hub. This attachment replaced the previous attachment bolt and key attachment used on the original design. Shaft torque was reacted by a series of hollow bushings pressed into the laminates concentrically with the clamp bolts instead of the previous key arrangement.

The present CH-54B titanium hub, the Whittaker composite hub concept, and the redesigned splayed laminate hub concept were compared. This comparison is summarized in Figures 23 and 24.

The results are shown in Figure 22. The comparison was based on the relative size and weight of the three hub configurations.

Structural Analysis

The structural analysis (Appendix II) performed on the splayed laminate hub was similar to that used for the original hub concept in phase one. The hub regions analyzed were as follows:

- Hub Arm (Reference Figure 5)
    - Section A-A 10.9 in from center of rotation
    - Section B-B 19.9 in from center of rotation
    - Section through arm lug (124.0 in radius)
    - Section C-C through center of rotation
- Laminate to Hub Clamp Ring
- Central Titanium Hub Cylinder
- Lag Hinge Bearing Cartridge

Methodology (Figure 25)

The methodology used for the static and fatigue analyses was similar to that used for the production CH-54B rotor head structural analysis.[10]

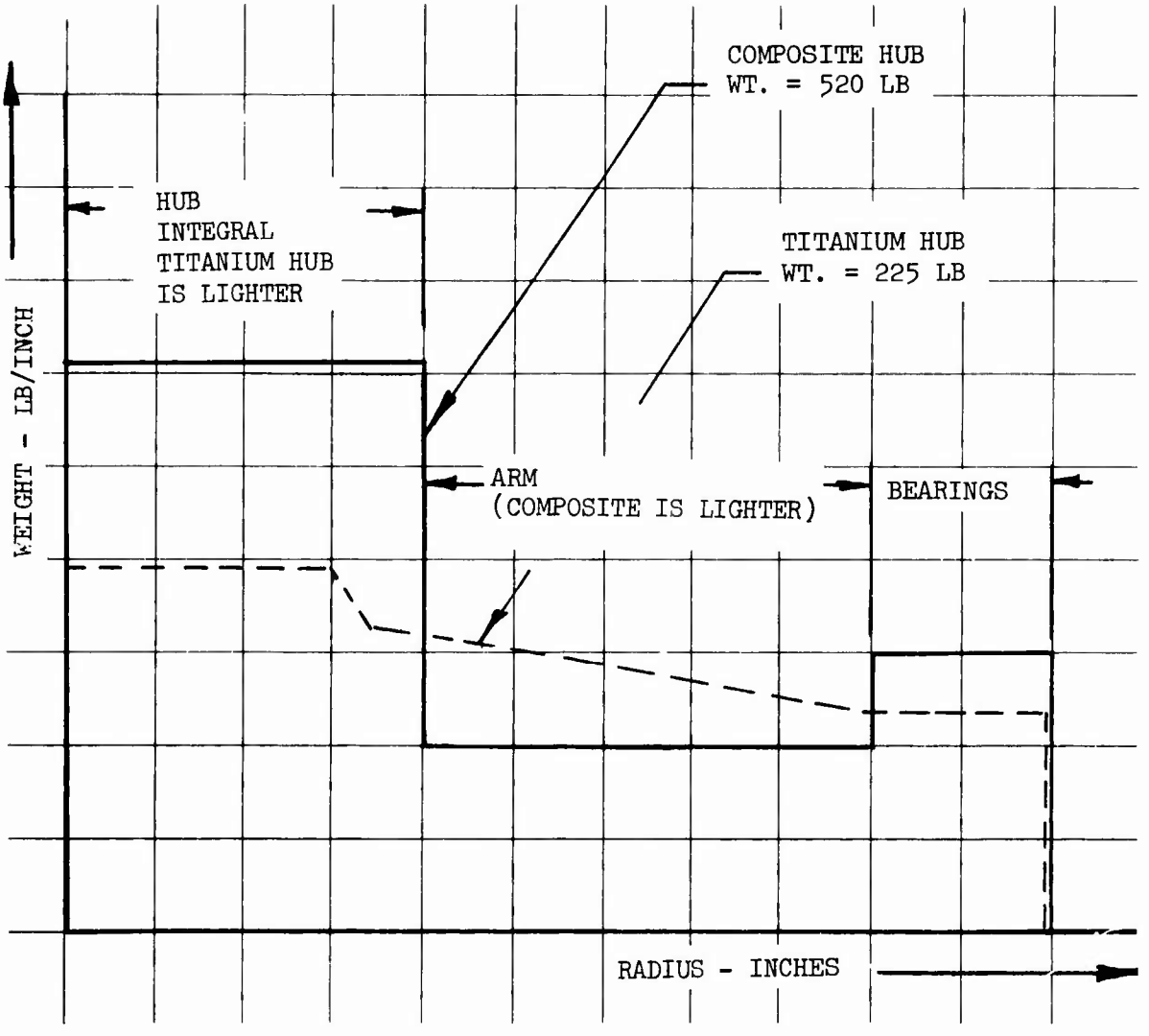

Figure 22. Hub Weight Comparison.

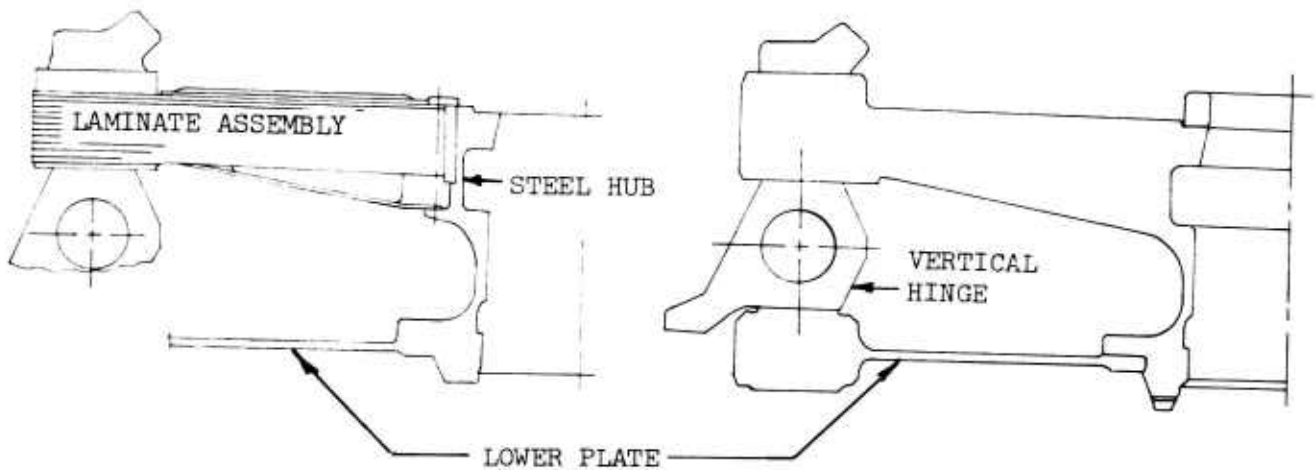

WHITTAKER CONCEPT

PRODUCTION TITANIUM

Although the Whittaker hub is approximately the same size as the present production hub, it is 300 pounds heavier and does not exhibit the strength of the titanium hub.

Figure 23. Hub Size Comparison, Whittaker and Production Hub.

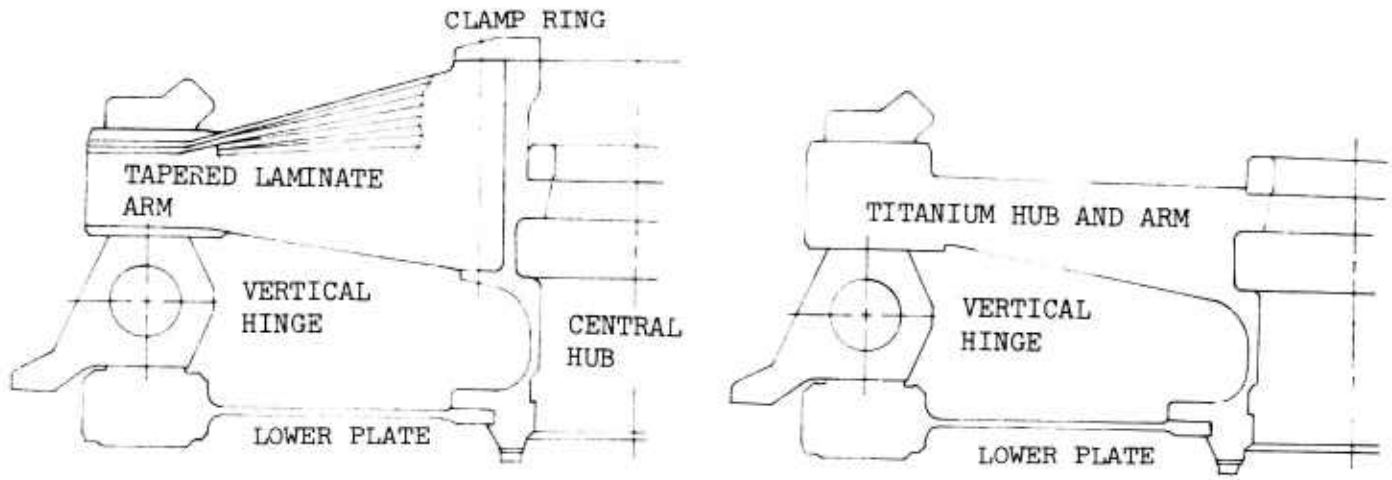

REDESIGNED SPLAYED LAMINATE HUB PRODUCTION TITANIUM HUB

The splayed laminate hub is 5 inches higher overall than the present production hub. Also, the splayed laminate hub is 300 pounds heavier, while exhibiting the same strength as the present hub.

Figure 24. Hub Size Comparison - Splayed Laminate and Production Hubs.

The static analysis used the maximum loads resulting from the most critical maneuver condition as limit. The ultimate loads and stress (1.5 times limit) were compared with the allowable ultimate stress (F_{TU}) of the material under analysis.

Fatigue analysis design vibratory loads were based on prorated mission loads spectra. These prorated loads, when applied to the component S-N data, result in a minimum of 2500 hours prior to crack initiation. Fatigue allowable stresses were based on published small-specimen endurance limits for the material under analysis. A reduction factor for size effect and reliability (test data scatter) was applied to the small specimen mean curve to obtain a working stress vs cycles to failure curve. If stress risers were in a critical region, the stress concentration factor and notch sensitivity of the material were determined. The open section working endurance limit was then reduced by the notch sensitivity factor to arrive at a component working endurance limit. The prorated fatigue (design) loads and stress levels were then compared with the working endurance limit, and the fatigue margin of safety was determined. A positive margin of safety results in a time to crack initiation in excess of 2500 hours. Also, the probability of failure at the design load level is 0.1%.

Redesigned Hub Loads (Figures 26 and 27)

The static and fatigue design loads were similar to those determined in the Phase I interim technical report.[3]

The static analysis ultimate design loads were 1.5 times the limit loads. The critical limit load condition was a symmetric pullout from a power-off autorotation (landing flare-out). The hub loadings resulting from this condition are summarized in Tables 5 and 6. In addition, the structural adequacy of components subjected to the instantaneous torque during an engine load burst restart condition was investigated.

Design loads used in the fatigue analysis were also the same as those used in Phase I. Shaft torque was equal to an in-flight steady-state value. Thrust was equivalent to that resulting at a 1g load factor at a gross weight of 42,000 pounds. The centrifugal force at each blade lug was equivalent to a main rotor speed of 185 rpm (100% NR). The head moment was equivalent to a mission prorate. This prorated head moment resulted in the same hub fatigue strength as the full mission head moment spectrum. (The production CH-54B titanium hub was substantiated using this head moment prorate.)

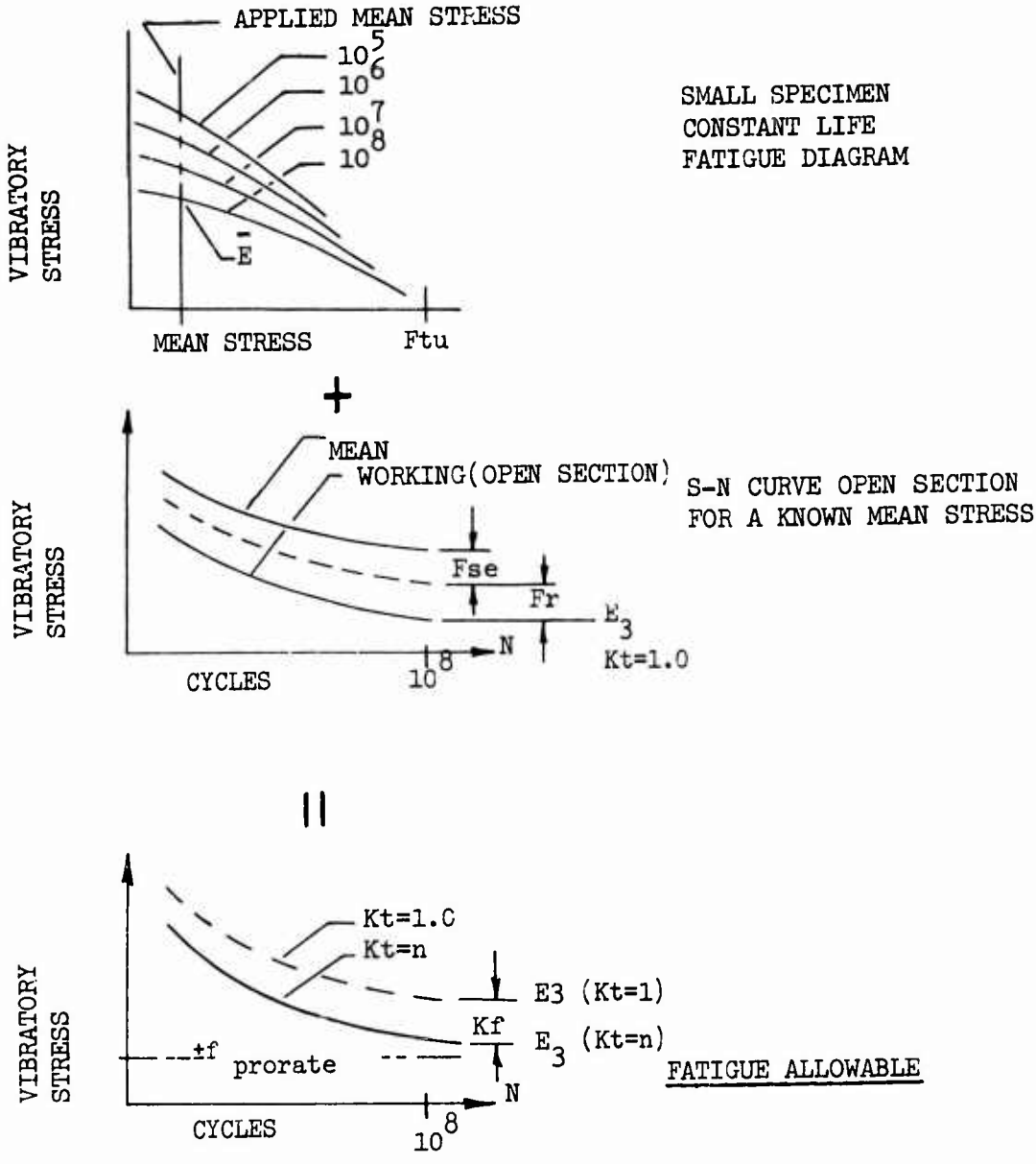

Figure 25. Fatigue Methodology Summary.

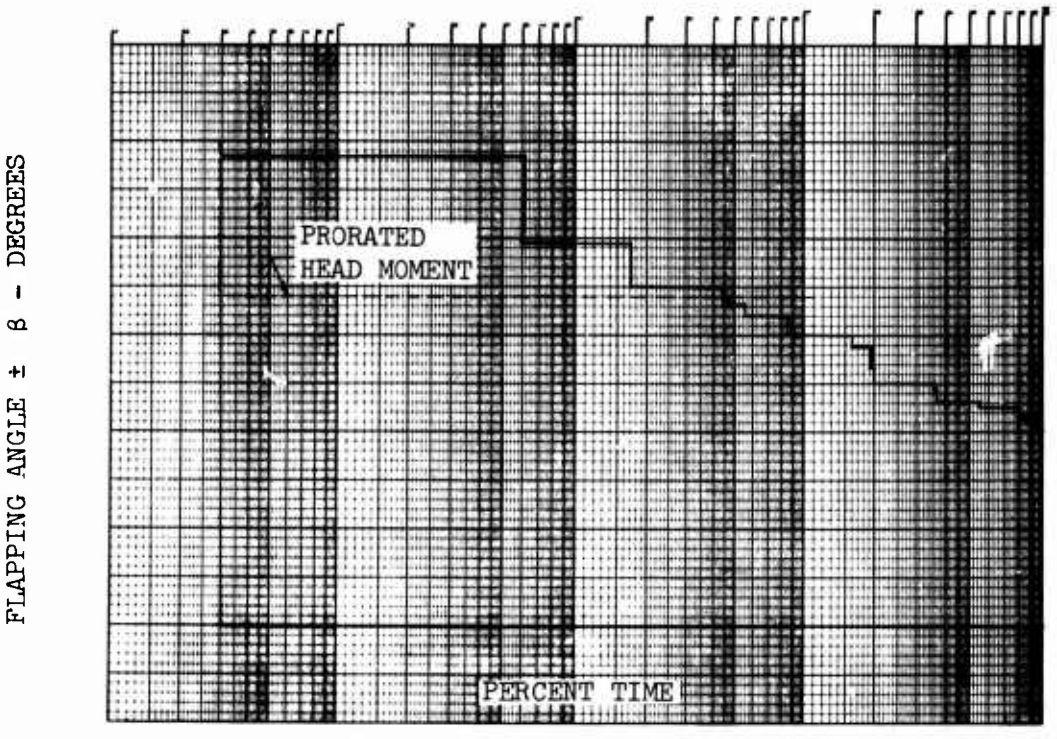

Figure 26. Mission Flapping Angle Time History.

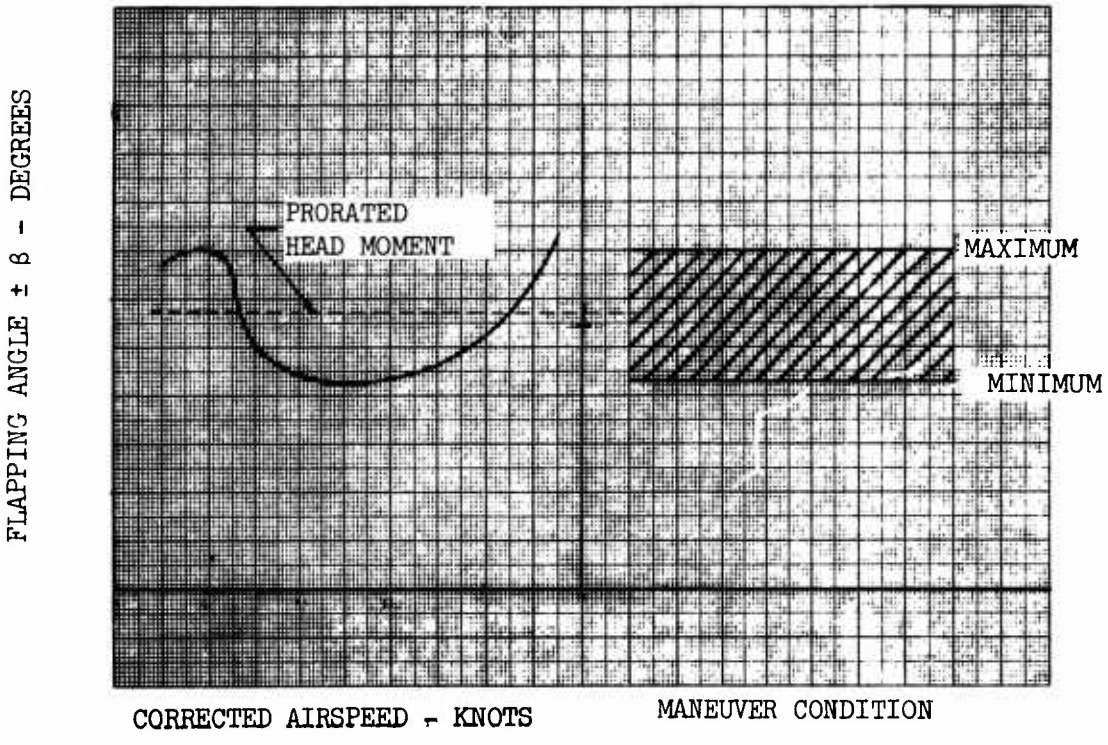

Figure 27. Flapping Angle Spectrum.

TABLE 5. STATIC LIMIT LOADS

Load	Magnitude	Flight Condition
Head Moment	$1.5\ (10)^6$ in.-lb	Symmetric Dive and Pull
Centrifugal Force	110,000 lb	Out (Autorotation)
Thrust	85,800 lb	
Shaft Torque	$2.27\ (10)^6$ in.-lb	Symmetric Dive and Pull Out (Power On)

TABLE 6. FATIGUE DESIGN LOADS

Load	Magnitude	
Head Moment	$\pm\ 0.8\ (10)^6$ in.-lb	(± 4.0 Deg. Flapping)
Centrifugal Force	83,000 lb	Prorate
Thrust		(4.0 Deg. Coning)
Damper Moment	36000 ± 36000 in.-lb	
Shaft Torque	$2.075(10)^6$ in.-lb	

The static ultimate and vibratory shears applied at the hub lugs as a result of the design conditions are shown in Tables 7 and 8.

TABLE 7. STATIC ULTIMATE LOADS

Load	Magnitude
V_N	54840 lb
V_E	13167 lb
R_A	98424 lb *

* $R_A = .595\ F_c$ (6)

TABLE 8. FATIGUE LOADS

Load	Mean	Vibratory
V_N	5734 lb	± 11523 lb
V_E	8847 lb	± 810 lb
R_A	48422 lb	± 2133 lb

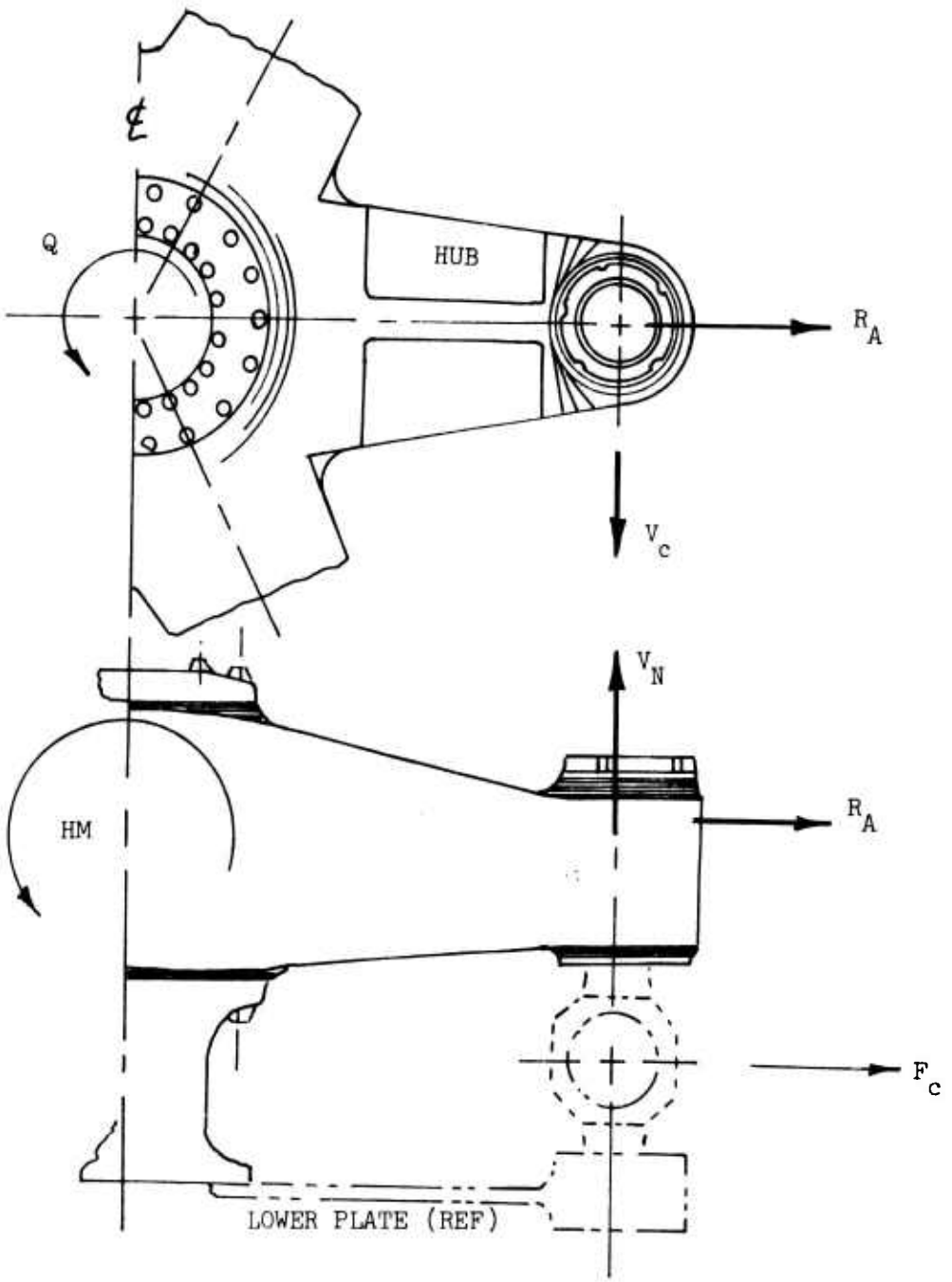

Figure 28. Summary of Hub Loadings.

The spline mode of failure shown in Figure 30 was found to be the primary structural limitation of the splayed laminate hub. The central spline region of both the composite splayed laminate hub and the present titanium hub are identical.[11] Therefore, the spline mode fatigue strength limit is valid for both.
The production titanium hub has been fatigue tested in the contractor's head and shaft test facility. The head moment vs cycles to failure for the spline mode is presented in Figure 29. The mean endurance limit for the spline mode was found to be $\pm 0.7\ (10)^6$ inch-pounds. The equivalent flapping angle is $\pm 7°$. The design head moment and flapping angle for the splayed laminate hub were $+0.8\ (10)^6$ inch-pounds and +8° respectively. As a result, all areas of the hub other than the spline have a higher fatigue strength than the primary mode.

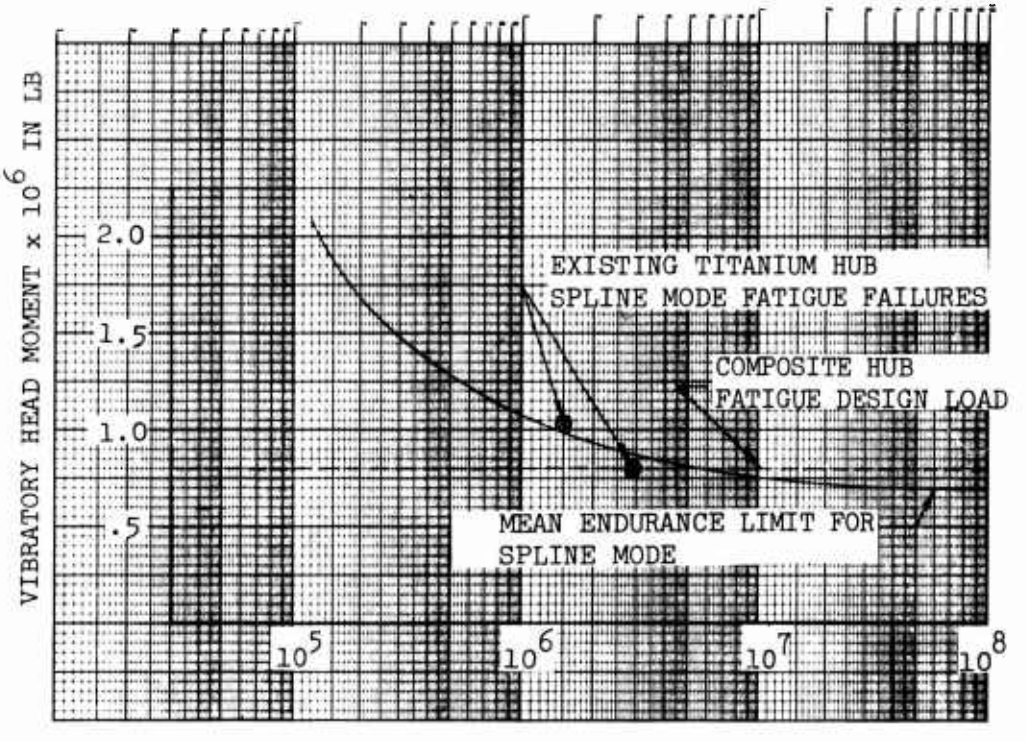

Figure 29. Test S-N Curve for Titanium Hub.

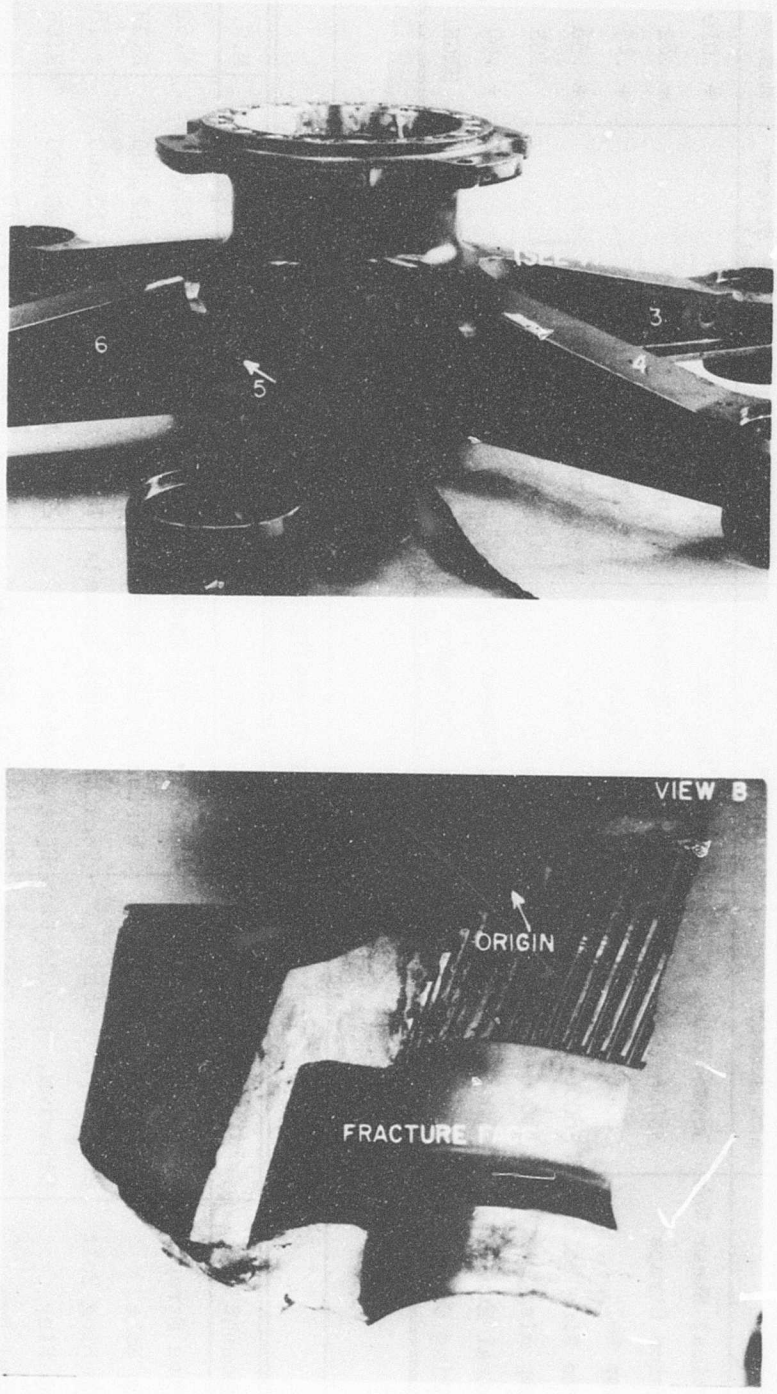

Figure 30. Titanium Hub Spline Mode Failures.

TABLE 9. STATIC STRENGTH SUMMARY

Component	Part Number	Failure Mode	Ult. Stress (psi)	Allowable Stress (psi)	M.S.
Vertical Shear Web	38006-10021	Shear in Matrix	41,640	42,000	+ .010
Tension Straps	38006-10024	Tension in G/E Straps	140,000	254,000	+ .82
Clamp Bolt	38006-10014	Tension in Bolt	125,000	180,000	+ .45
Clamp Ring Bolt	38006-10014	Tension in Bolt	132,000	180,000	+ .36
Clamp Ring	38006-10011	Ring Torsion	16,207	130,000	HIGH
Central Hub	38006-10010	Bending of Lower Lip	81,470	130,000	+ .60
Bearing Cartridge	38006-10012	Tension in Cylinder	35,610	130,000	HIGH

TABLE 10. FATIGUE STRENGTH SUMMARY

Component	Failure Mode	Failure Region	Applied Stress (psi)	Endurance (psi)	M.S.
Tension Straps	Graphite Filament	Tension in G/E Straps	32000 ± 22000	± 33,500	+.52
Clamp Bolt	Steel W/O Chafing	Tension Across Threads	80000 ± 2000	± 12,200	HIGH
Clamp Ring Bolt	Steel W/O Chafing	Tension Across Threads	78720 ± 10280	± 12,200	+.18
Clamp Ring	Titanium, Open Section	Ring Torsion	2731 ± 775	± 20,000	HIGH
Central Hub	Titanium W/O Chafing	Bending of Lower Lip	21260 ± 4060	± 10,300	±1.54
Bearing Cartridge	Titanium W/O Chafing	Tension Across Cylinder	5600 ± 5600	± 14,670	HIGH

HUB ARM (Figure 31)

The hub arm reacts the in-plane, out-of-plane, and centrifugal loads as a cantilever beam. Three sections, located at radii of 10.9 inches, 19.9 inches, and 24.0 inches, were found to be structurally critical. The sections were analyzed for in-plane and out-of-plane bending and for shear axial forces. The loading conditions used for the static and fatigue analysis were defined in Table 8. Composite material beam theory was used in the analysis. The various values of Young's modulus were taken into account when calculating bending and shear stresses.

Since the analyses of the three sections are similar, one section (A-A) is sufficient to describe the detailed development of the structural analysis (reference pages 49-51). The analytical summary is presented in graphical form. The static and fatigue cases are summarized in terms of stresses due to individual loadings as well as combined applied stresses, in order to present the degree of structural adequacy. The other critical sections analyzed that are similar to section A-A are summarized on pages 52-60.

The shear webs (in-plane and out-of-plane) were found to be structurally critical. The region involved was Section B-B. Therefore, bending shear was calculated for this section only.

The effect of the engine load burst condition (engine restart) on the in-plane shear webs was also analyzed. This instantaneous shaft torque results in a moment that is a maximum at Section A-A.

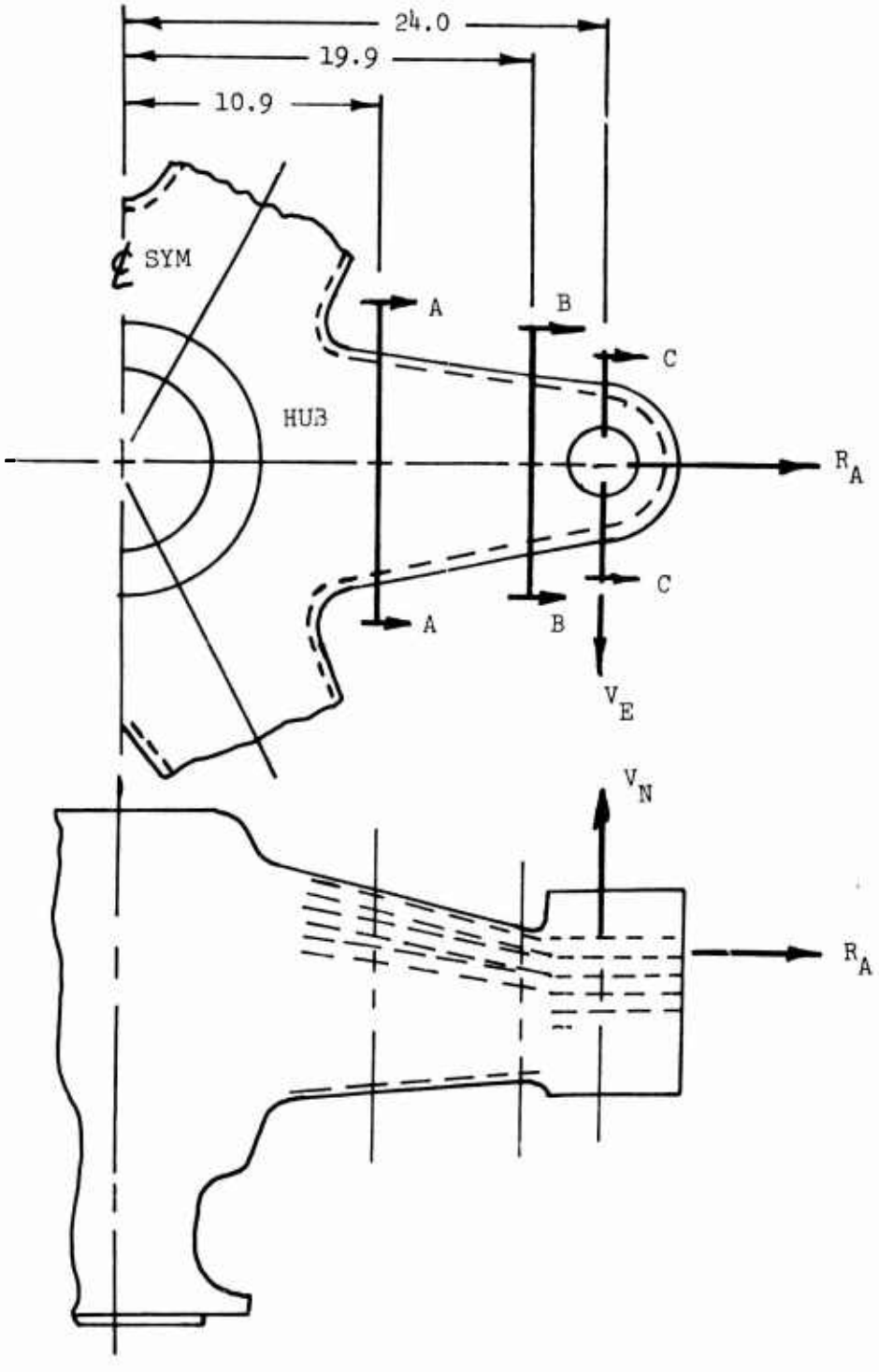

Figure 31. Structurally Critical Hub Arm Regions.

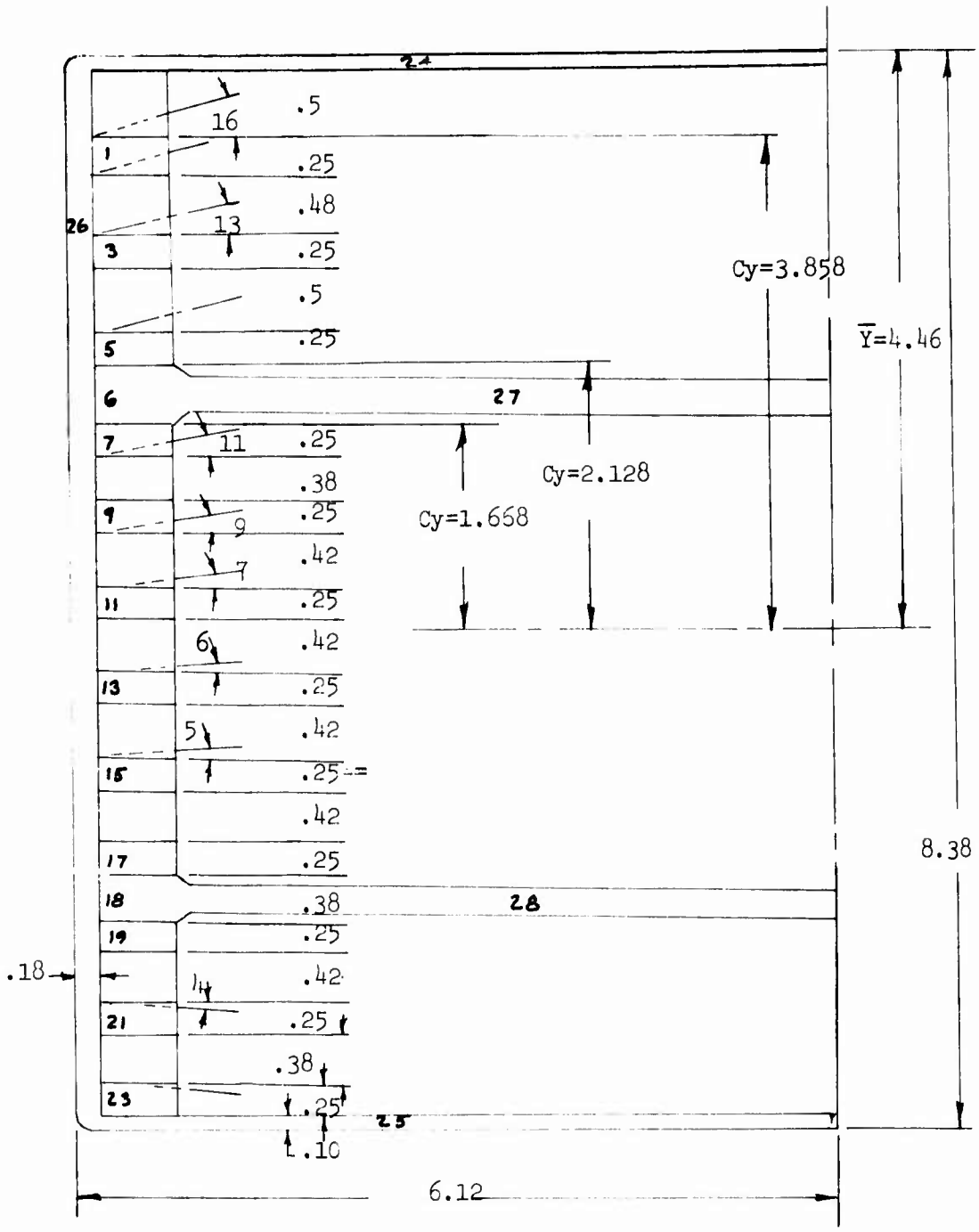

Figure 32. Section A-A of the Hub Arm.

Areas of Elements, Section A-A

A =.625 x .25 = .156 (1) (3) (5) (7) (9) (11) (13) (15) (17) (19) (21) (23) (5)

A =.625 x .46 = .297 (6) (6)

A =.625 x .38 = .237 (18) (7)

A =5.94 x .10 = .594 (24) (25) (8) (9)

A =.18 x 8.38 = 1.506 (26) (10)

A =5.315 x .25 = 1.329 (27) (28)

TABLE 11. SECTION A-A, SECTION PROPERTIES ABOUT X-X AXIS

Item	A	E $x10^6$	AE $x10^6$	Y	AEY	AEY^2	Io	EIo
1	.156	17.5	2.730	.725	1.979	1.434	.00081	.01417
3	.156	17.5	2.730	1.455	3.972	5.779	.00081	.01417
5	.156	17.5	2.730	2.205	6.019	13.271	.00081	.01417
6	.297	2.4	.071	2.560	.181	.463	.00506	.01214
7	.156	6.8	1.061	2.915	3.092	9.013	.00081	.00550
9	.156	6.8	1.061	3.545	3.761	13.332	.00081	
11	.156	6.8	1.061	4.215	4.472	18.849	.00081	
13	.156	6.8	1.061	4.885	5.182	25.314	.00081	
15	.156	6.8	1.061	5.555	5.893	32.735	.00081	
17	.156	6.8	1.061	6.225	6.604	41.109	.00081	
18	.237	2.4	.569	6.540	3.721	24.335	.00285	.00684
19	.156	17.5	2.730	6.855	18.714	128.284	.00081	.01417
21	.156	17.5	2.730	7.525	20.543	154.586	.00081	.01417
23	.156	17.5	2.730	8.155	22.263	181.554	.00081	.01417
24	.594	2.4	1.426	.050	.071	.003	.00049	.00117
25	.594	2.4	1.426	8.330	11.878	98.943	.00049	.00117
26	1.506	2.4	3.614	4.190	15.142	63.444	8.82720	21.18528
27	1.329	2.4	3.190	2.560	8.166	20.904	.00692	.01660
28	1.329	2.4	3.190	6.225	19.857	123.609	.00692	.01660
Total			36.232		161.510	956.961		21.35782

TABLE 12. SECTION A-A, SECTION PROPERTIES ABOUT Y-Y AXIS

Item	A	E $\times 10^6$	AE $\times 10^6$	X	AEX $\times 10^6$	AEX^2	Io	E Io $\times 10^6$
1	.156	17.5	2.730	5.628	15.364	86.468	.00508	.08890
3	.156	17.5	2.730					
5	.156	17.5	2.730					
6	.297	2.4	.071		.399	2.245	.00935	.02244
7	.156	6.8	1.061		5.971	33.604	.00508	.03454
9	.156	6.8	1.061					
11	.156	6.8	1.061					
13	.156	6.8	1.061					
15	.156	6.8	1.061					
17	.156	6.8	1.061					
18	.237	2.4	.569		3.202	18.020	.00773	.01855
19	.156	17.5	2.730		15.364	86.468	.00508	.08890
21	.156	17.5	2.730					
23	.156	17.5	2.730					
24	.594	2.4	1.426	2.970	4.235	12.577	1.74653	4.19167
25	.594	2.4	1.426	2.970	4.235	12.577	1.74653	4.19167
26	1.506	2.4	3.614	6.030	21.792	131.405	.00407	.00976
27	1.329	2.4	3.190	2.657	8.475	22.518	3.12801	7.50722
28	1.329	2.4	3.190	2.657	8.475	22.518	3.12801	7.50722
Total			36.232		178.823	942.292		24.18917

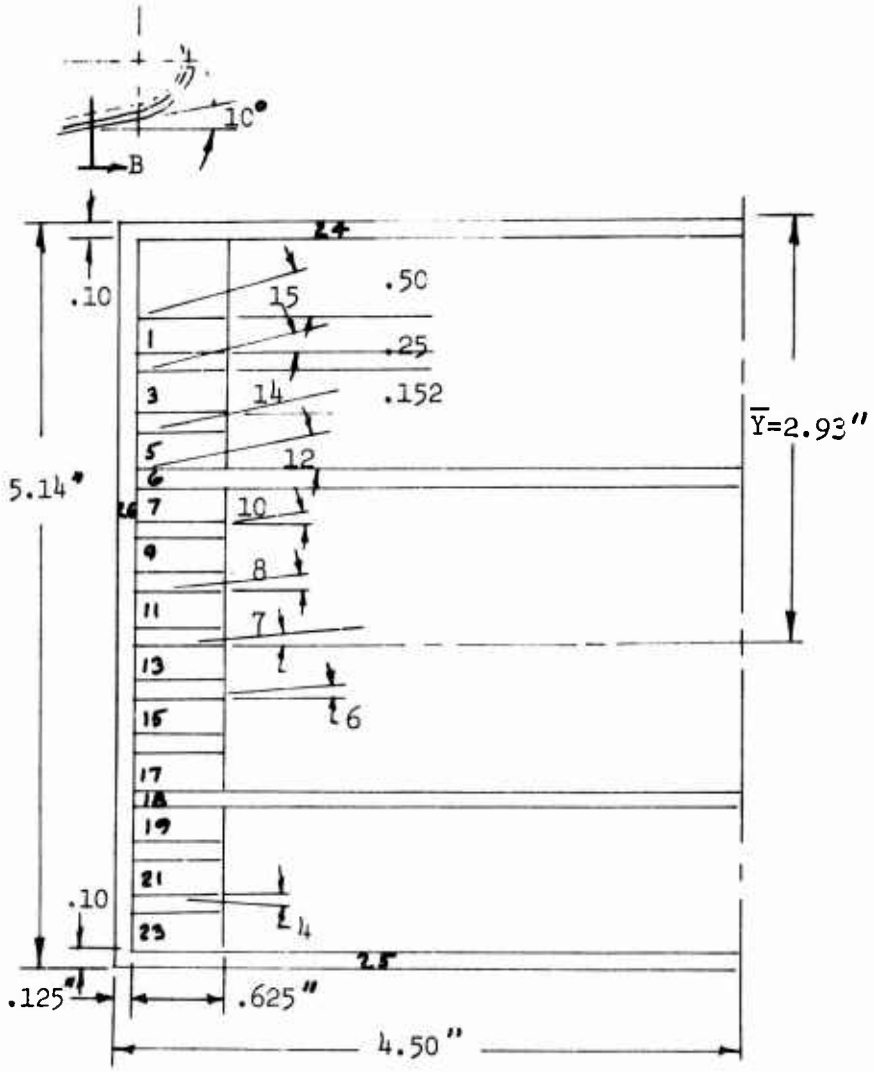

Figure 33. Section B-B of the Hub Arm.

TABLE 13. SECTION B-B, SECTION PROPERTIES ABOUT X-X AXIS

Item	A	E X 10^6	AE X 10^6	Y	AEY X 10^6	AEY^2 X 10^6	Io	EI X 10^6
1	0.156	17.5	2.73	0.725	1.97	1.43	.0008	.014
3	0.156	17.5	2.73	1.13	3.08	3.48	.0008	.014
5	0.156	17.5	2.73	1.53	4.18	6.40	.0008	.014
6	0.546	2.4	1.31	1.71	2.24	3.83	0.0007	.00171
7	0.156	6.8	1.06	1.91	2.02	3.86	.0008	.00544
9	0.156	6.8	1.06	2.31	2.45	5.66	.0008	.00544
11	0.156	6.8	1.06	2.71	2.87	7.78	.0008	.00544
13	0.156	6.8	1.06	3.110	3.3	10.26	.0008	.00544
15	0.156	6.8	1.06	3.512	3.72	13.06	.0008	.00544
17	0.156	6.8	1.06	3.914	4.14	16.19	.0008	.00544
18	0.546	2.4	1.31	4.039	5.30	21.42	.0007	.00171
19	0.156	17.5	2.73	4.289	11.71	50.24	.0008	.014
21	0.156	17.5	2.73	4.691	12.80	60.03	.0008	.014
23	0.156	17.5	2.73	4.968	13.57	67.44	.0008	.014
24	0.436	2.4	1.05	0.05	0.05	0.0025	.00036	.00086
25	0.436	2.4	1.05	5.09	5.34	27.18	.00036	.00086
26	0.643	2.4	1.54	2.57	3.96	10.18	1.4145	3.3948
	4.4790		29.00		84.94	308.44		3.51996

$$\Sigma A = (2)\ (4.4790) = 8.9580 \qquad (11)$$

TABLE 14. SECTION B-B, SECTION PROPERTIES ABOUT Y-Y AXIS

Item	A	E $(10)^6$	AE $(10)^6$	X	AEX $(10)^6$	AEX^2 $(10)^6$	Io Y	
1	.156	17.5	2.73	4.062	11.089	45.045	.0051	.0893
3	.156	17.5	2.73	4.062	11.089	45.045	.0051	.0893
5	.156	17.5	2.73	4.062	11.089	45.045	.0051	.0893
6	.563	2.4	1.35	2.25	3.038	6.834	.9492	2.278
7	.156	6.8	1.06	4.062	4.306	17.49	.0051	.0347
9	.156	6.8	1.06	4.062	4.306	17.49	.0051	.0347
11	.156	6.8	1.06	4.062	4.306	17.49	.0051	.0347
13	.156	6.8	1.06	4.062	4.306	17.49	.0051	.0347
15	.156	6.8	1.06	4.062	4.306	17.49	.0051	.0347
17	.156	6.8	1.06	4.062	4.306	17.49	.0051	.0347
18	.563	2.4	1.35	2.25	3.038	6.834	.9492	2.278
19	.156	17.5	2.73	4.062	11.089	45.045	.0051	.0893
21	.156	17.5	2.73	4.062	11.089	45.045	.0051	.0893
23	.156	17.5	2.73	4.062	11.089	45.045	.0051	.0893
24	.45	2.4	1.08	2.25	2.43	5.468	.7594	1.8226
25	.45	2.4	1.08	2.25	2.43	5.468	.7594	1.8226
26	.642	2.4	1.54	4.438	6.635	30.332	.0008	.00192
Total			29.14		118.89	430.15		8.9471

$$EI_{Y-Y} = 2\left[EA\,X^2 + EI_{OX}\right] = 2\left[430.15 + 8.9471\right](10)^6 \qquad (12)$$

$$EI_{Y-Y} = 878.2\,(10)^6 \quad PSI \qquad EA = 58.28 \times 10^6 \qquad (13)$$

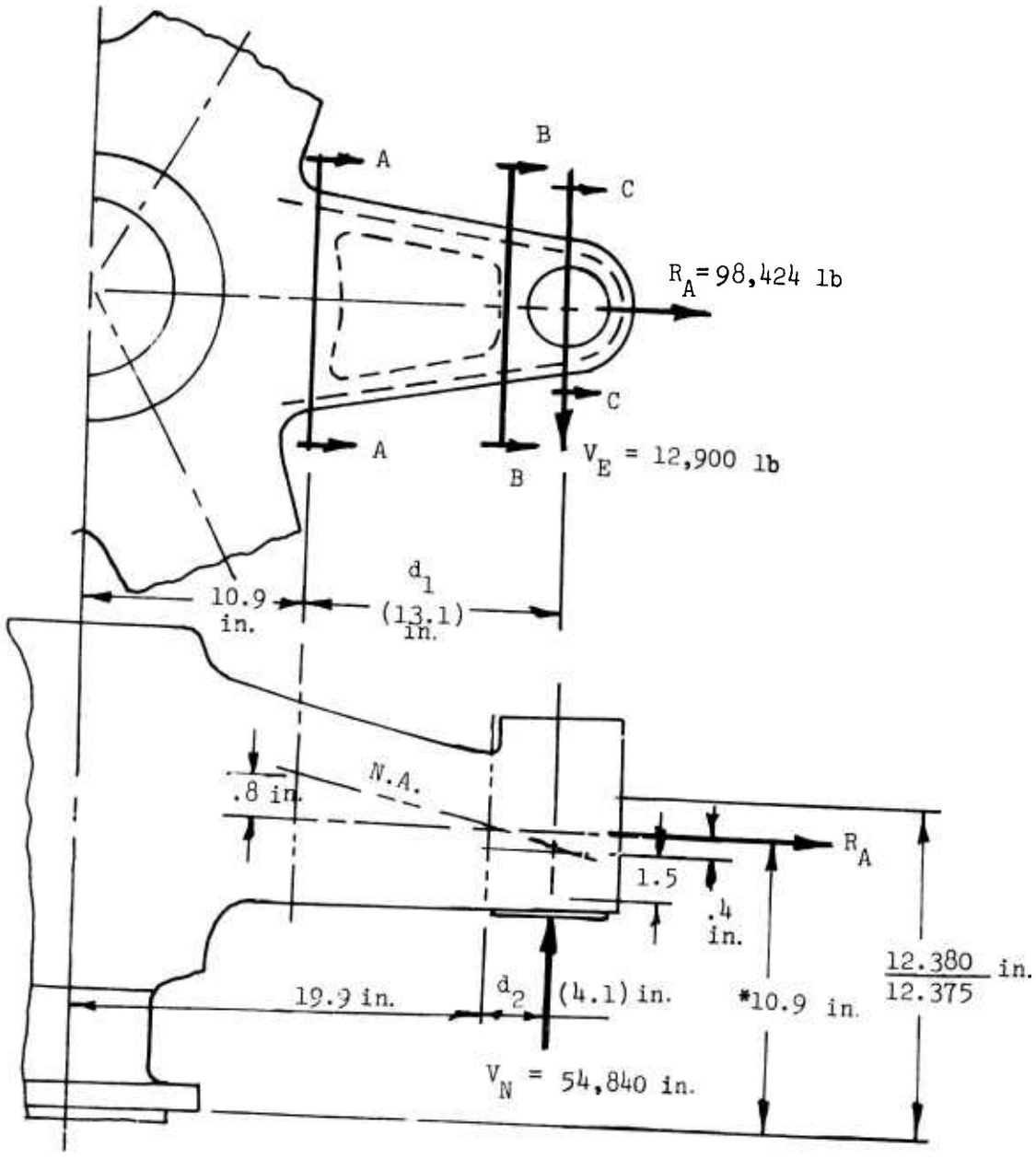

Figure 34. Ultimate Arm Loads, Autorotation, Power Off.5

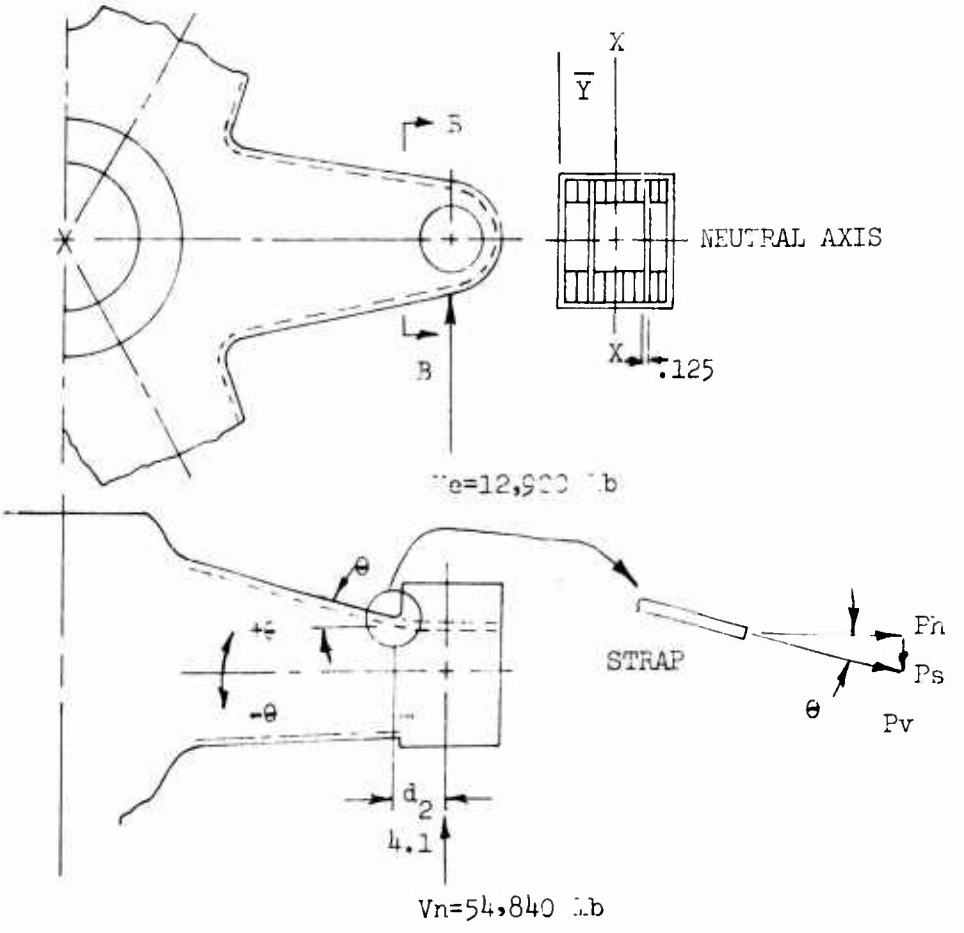

Figure 35. Ultimate Arm Loads and Critical Shear Web Regions, Autorotation, Power-On Condition.[5]

STATIC ULTIMATE TORQUE CASE -
ENGINE LOAD BURST CONDITION

$Q = 2.48 \times 10^6$ IN.-LB (Engine Torque) **(14)**

$Q_{HUBULT} = \frac{1}{2} (Q) (F.S) = (0.5) (2.48) (1.5) 10^6$ **(15)**

$V_{E/ARM} = \frac{Q_{ULT}}{(R) (N)} = \frac{1.86 \times 10^6}{(24) (6)} = \underline{12,900 \text{ LB}}$ **(16)**

N = 6 ARMS

EDGEWISE
LOAD PER
ARM

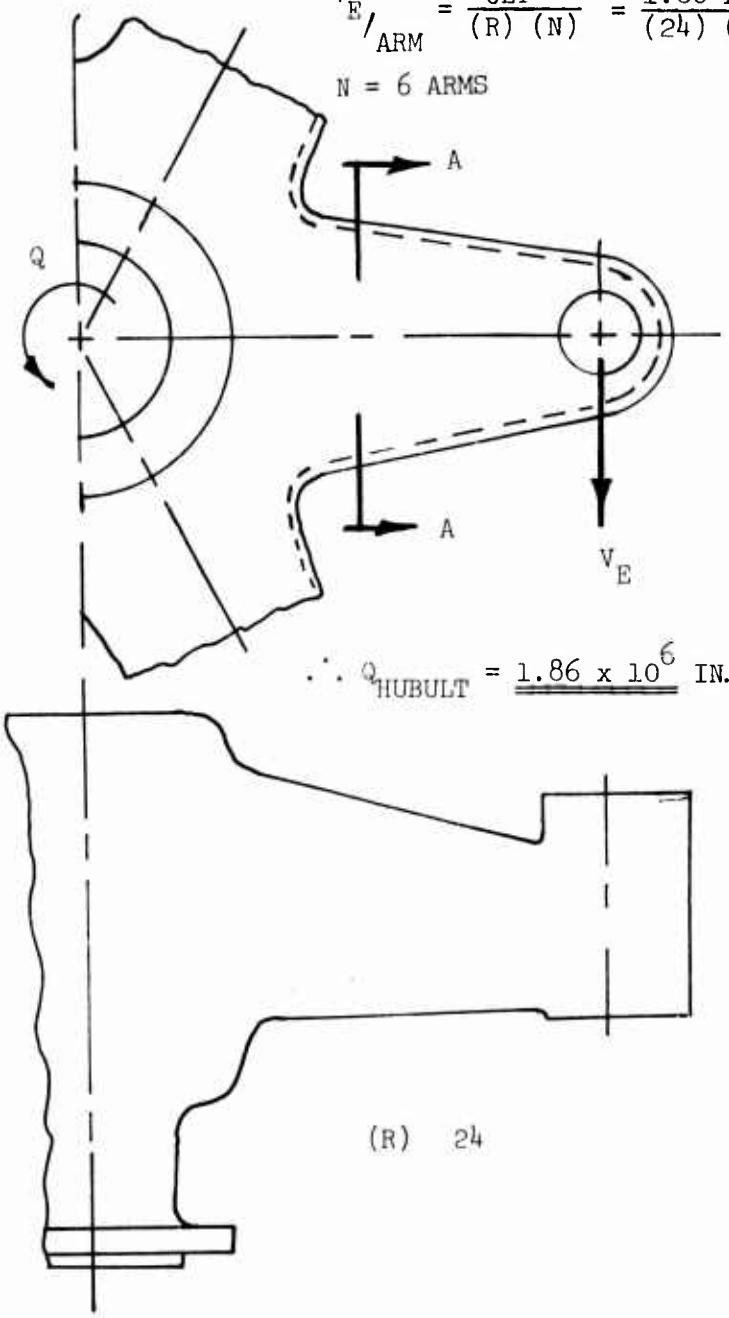

$\therefore Q_{HUBULT} = \underline{1.86 \times 10^6}$ IN.-LB

Figure 36. Ultimate Loads Due to Engine Load Burst.[12]

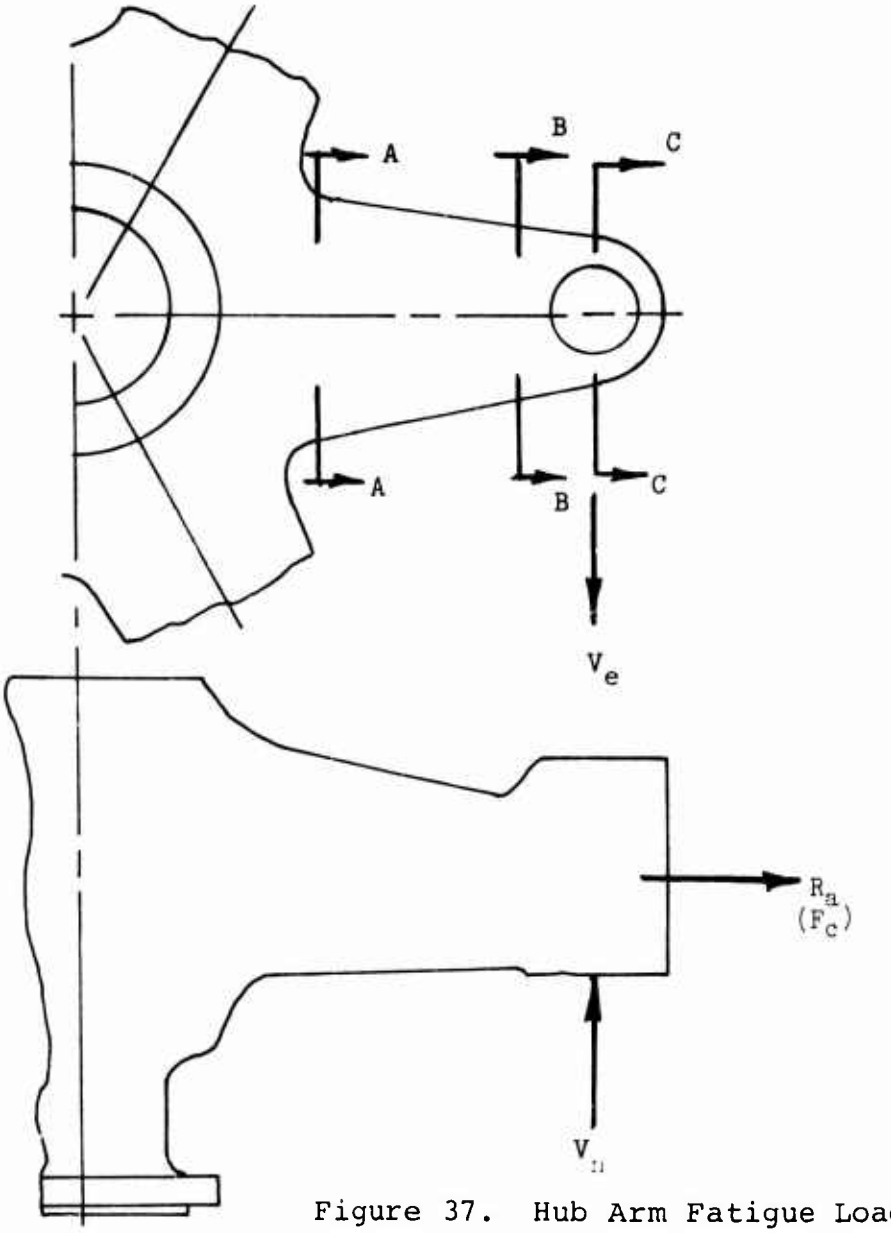

Figure 37. Hub Arm Fatigue Loading.

TABLE 15. FATIGUE LOAD SUMMARY[3]

	Fatigue Load (lb)	Mean (lb)	Vibratory (lb)
F_C	Centrifugal	48,422	± 2,133
V_E	Edgewise (In Plane, Tangential)	8,847	± 810
V_N	Flatwise (Out of Plane, Vertical)	5,734	± 11,523

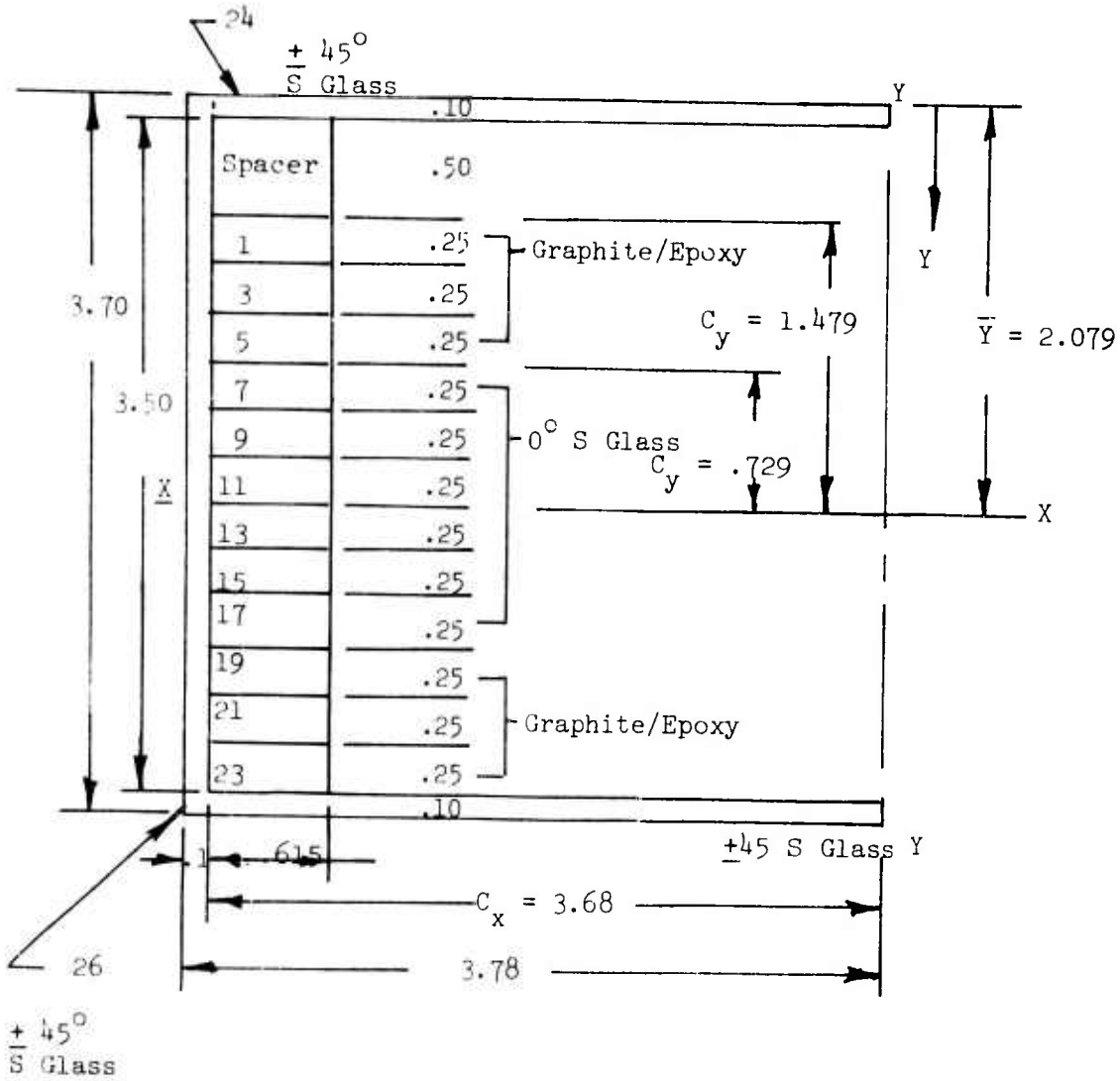

Figure 38. Section C-C of the Hub Arm.

TABLE 16. SECTION C-C, SECTION PROPERTIES ABOUT X-X AXIS

Item	A	E $\times 10^6$	AE $\times 10^6$	Y	AEY $\times 10^6$	AEY^2 $\times 10^6$	Io	EI $\times 10^6$
1	.156	17.5	2.730	.725	1.979	1.434	.00081	.01417
3				.975	2.661	2.594		
5				1.225	3.344	4.096		
7		6.8	1.060	1.475	1.563	2.305		.00550
9				1.725	1.828	3.153		
11				1.975	2.093	4.133		
13				2.225	2.358	5.246		
15				2.475	2.623	6.491		
17				2.725	2.888	7.869		
19		17.5	2.730	2.975	8.121	24.159		.01417
21				3.225	8.804	28.392		
23				3.525	9.623	33.921		
24	.368	2.4	.883	.050	.044	.002	.00030	.00072
25	.368		.883	3.650	3.222	11.760	.00030	.00072
26	.370		.888	1.850	1.642	3.037	.42210	1.01304
Total			25.394		52.793	138.582		1.13250

TABLE 17. SECTION C-C, SECTION PROPERTIES ABOUT Y-Y AXIS

Item	A	E $\times 10^6$	AE $\times 10^6$	X	AEX $\times 10^6$	AEX^2 $\times 10^6$	Io	EI $\times 10^6$
1	.156	17.5	2.730	3.305	9.022	29.817	.00508	.08890
3								
5								
7		6.8	1.060		3.503	11.577		.03454
9								
11								
13								
15								
17								
19		17.5	2.730		9.022	29.817		.08890
21								
23								
24	.368	2.4	.883	1.84	1.624	2.988	.41530	.99672
25	.368		.883	1.84	1.624	2.988	.41530	.99672
26	.370		.888	3.73	3.312	12.353	.00030	.00072
Total			25.394		81.710			2.72880

Static Ultimate and Fatigue Strength Summary - Hub Arm
(Sections A-A, B-B, and C-C) (Figures 39 - 58)

The static ultimate moments and stresses are presented graphically on the following figures and tables. The stress distributions for each applied load (M_{xx}, M_{yy}, and F_c) are plotted along with the combined stress distribution.

The mean and vibratory moments and resultant stress distributions are also presented for the individual and combined fatigue design loads. In addition, the allowable stresses for each material are superimposed on the combined stress distribution for each material. The hub arm is structurally adequate and accumulates no fatigue damage, because the allowable stress levels are greater than the applied stresses for all areas of the arm.

TABLE 18. HUB ARM SECTION PROPERTIES

Section	Distance From Hub (in.)	EIx-x $\times 10^6$	EIy-y $\times 10^6$	EA $\times 10^6$
A-A	10.9	517	1933	72
B-B	19.9	126	878	58
C-C	24.0	60	539	51

TABLE 19. HUB ARM SECTION MODULUS

	Zx-x			Zy-y	
Graphite/ Epoxy	0° S Glass	$\pm 45^\circ$ S Glass	Graphite/ Epoxy	0° S Glass	$\pm 45^\circ$ S Glass
7.6	45.6	101.1	18.6	47.8	135.6
3.1	16.4	41.7	11.5	29.4	83.5
2.3	12.0	0	8.4	21.5	0

Table 20. HUB ARM BENDING MOMENTS - STATIC ULTIMATE

Section	Mx-x (Flatwise)	My-y (Edgewise)
A-A	757,774	168,990
B-B	224,844	52,890
C-C	39,370	0

Table 21. HUB ARM MEAN AND VIBRATORY BENDING MOMENTS

Section	Mx-x (Flatwise)		My-y (Edgewise)	
	Mean (Steady)	± Vibratory	Mean (Steady)	± Vibratory
A-A	94,484	151,804	115,896	10,611
B-B	23,509	47,244	36,273	3,321
C-C	19,369	853	0	0

TABLE 22. HUB ARM STRESSES - STATIC ULTIMATE CONDITION

Section	f_b (Flatwise)			f_c (Centrifugal)			f_b (Edgewise)		
	Graphite/ Epoxy	0° S Glass	±45° S Glass	Graphite/ Epoxy	0° S Glass	±45° S Glass	Graphite/ Epoxy	0° S Glass	±45° S Glass
A-A	104,638	17,203	7,809	25,109	9,554	3,397	9,601	3,653	1,299
B-B	76,395	14,402	5,665	31,179	11,869	4,276	4,848	1,850	665
C-C	17,276	3,308	0	34,437	13,381	0	0	0	0

TABLE 23. SUMMARY OF HUB ARM MEAN STRESSES - FATIGUE DESIGN CONDITION

Section	f_b (Flatwise)			f_c (Centrifugal)			f_b (Edgewise)		
	Graphite/ Epoxy	0° S Glass	±45° S Glass	Graphite/ Epoxy	0° S Glass	±45° S Glass	Graphite/ Epoxy	0° S Glass	±45° S Glass
A-A	13,047	2,146	973	12,353	4,700	1,671	6,584	2,505	891
B-B	5,868	1,029	577	15,171	5,822	2,050	3,287	1,266	445
C-C	8,498	1,627	0	16,939	6,582	0	0	0	0

TABLE 24. SUMMARY OF HUB ARM VIBRATORY STRESSES - FATIGUE DESIGN CONDITION

Section	f_b (Flatwise)			f_c (Centrifugal)			f_b (Edgewise)		
	Graphite/ Epoxy	0° S Glass	±45° S Glass	Graphite/ Epoxy	0° S Glass	±45° S Glass	Graphite/ Epoxy	0° S Glass	±45° S Glass
A-A	20,692	3,449	1,564	544	207	74	603	230	82
B-B	11,793	2,068	1,160	668	256	90	301	116	41
C-C	374	72	0	735	286	0	0	0	0

TABLE 25. **TOTAL HUB ARM ULTIMATE STRESSES**

Type Of Stress	Graphite/Epoxy			0° S Glass			$\pm 45^{\circ}$ S Glass		
	A-A	B-B	C-C	A-A	B-B	C-C	A-A	B-B	C-C
f_b Flatwise	104,638	76,395	17,276	17,203	14,402	3,308	7,809	5,665	0
f_c Centr.	25,109	31,179	34,437	9,554	11,869	13,381	3,397	4,276	0
f_b Edgewise	9,601	4,848	0	3,653	1,850	0	1,299	665	0
Total	139,348	112,422	51,713	30,410	28,121	16,689	12,505	10,597	0

Table 26. HUB ARM MATERIAL DESIGN ALLOWABLES[8]

ULT STR	255,000 PSI Tensile	195,000 Tensile	28,900 Tensile

TABLE 27. TOTAL HUB ARM MEAN STRESSES-FATIGUE DESIGN

Type Of Stress	Graphitc/Epoxy			0° S Glass			$\pm 45^\circ$ S Glass		
	A-A	B-B	C-C	A-A	B-B	C-C	A-A	B-B	C-C
f_b Fatwise	13,047	5,868	8,498	2,146	1,029	1,627	973		0
f_c Centrif.	12,353	15,171	16,939	4,700	5,822	6,582	1,671	2,050	0
f_b Edgewise	6584	3,287	0	2,505	1,266	0	891	445	0
Total	31,984	24,326	25,437	9351	8,117	8,209	3,535	2,899	0

TABLE 28. TOTAL HUB ARM VIBRATORY STRESSES

Type Of Stress	Graphite/Epoxy			0° S Glass			$\pm 45^\circ$ S Glass		
	A-A	B-B	C-C	A-A	B-B	C-C	A-A	B-B	C-C
f_b Flatwise	20,692	11,793	374	3,449	2,068	72	1,564	1,160	0
f_c Centrif.	544	668	735	207	256	286	74	90	0
f_b Edgewise	603	301	0	230	116	0	82	41	0
Total	21,839	12,762	1,109	3,886	2,440	358	1,720	1,291	0

TABLE 29. GRAPHITE/EPOXY FATIGUE ALLOWABLES

Type of Fatigue Stress	Graphite/Epoxy		
	A-A	B-B	C-C
Mean (Steady)	31,984	24,326	25,437
Vibratory	21,839	12,762	1,109
(Vibratory Allowable)	33,750	34,500	34,500

TABLE 30. 0° S GLASS FATIGUE ALLOWABLES

Type of Fatigue Stress	0° S Glass		
	A-A	B-B	C-C
Mean (Steady)	9,351	8,117	8,209
Vibratory	3,886	2,440	358
(Vibratory Allowable)	18,500	18,750	18,750

TABLE 31. $\pm 45^{\circ}$ S GLASS FATIGUE ALLOWABLES (In Plane)

Type of Fatigue Stress	$\pm 45^{\circ}$ S Glass		
	A-A	B-B	C-C
Mean (Steady)	3,535	2,899	0
Vibratory	1,720	1,291	0
(Vibratory Allowable)	12,000	12,250	12,500

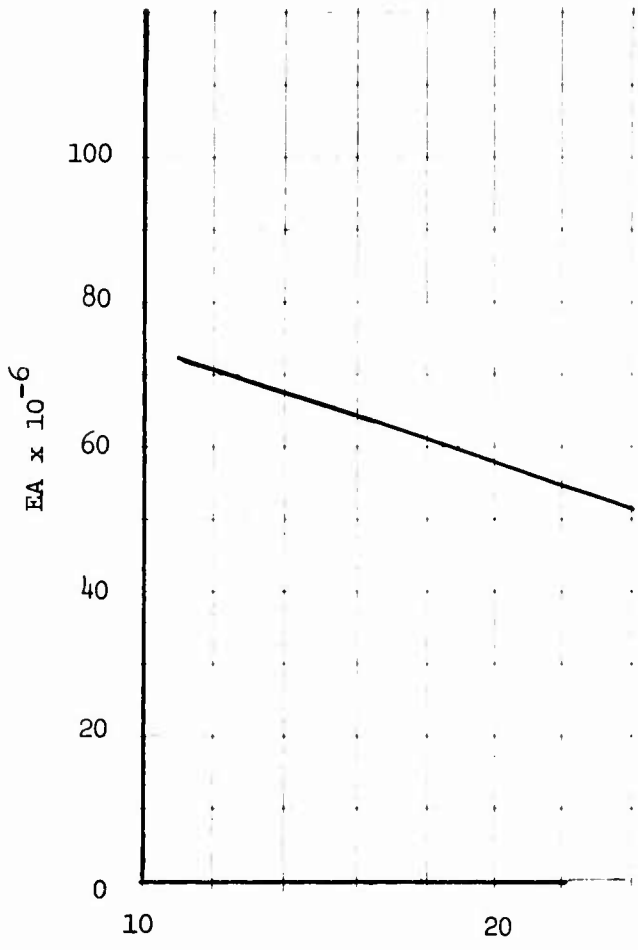

Figure 39. Hub Axial Stiffness Distribution.

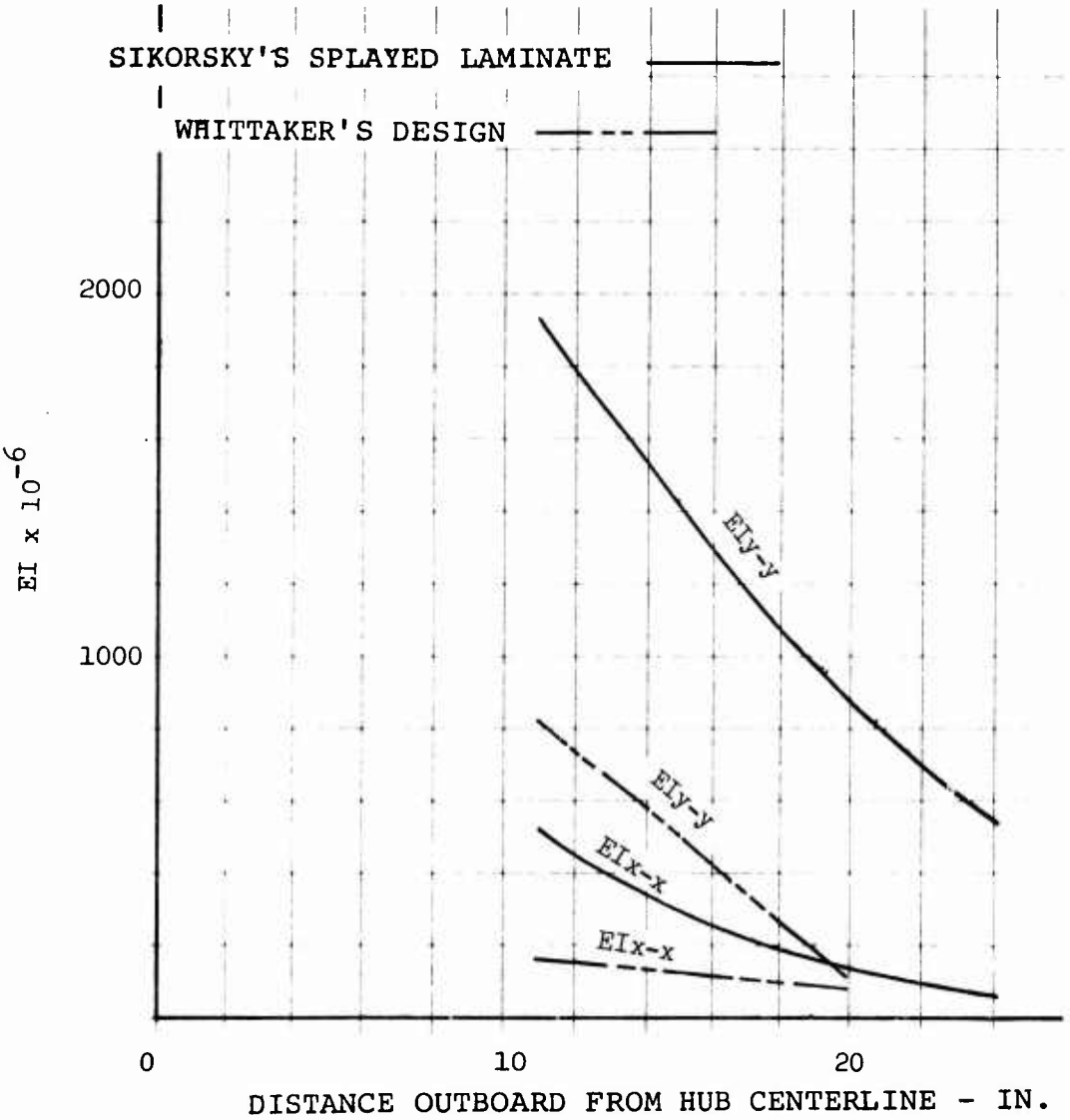

Figure 40. Hub Bending Stiffness Distribution.

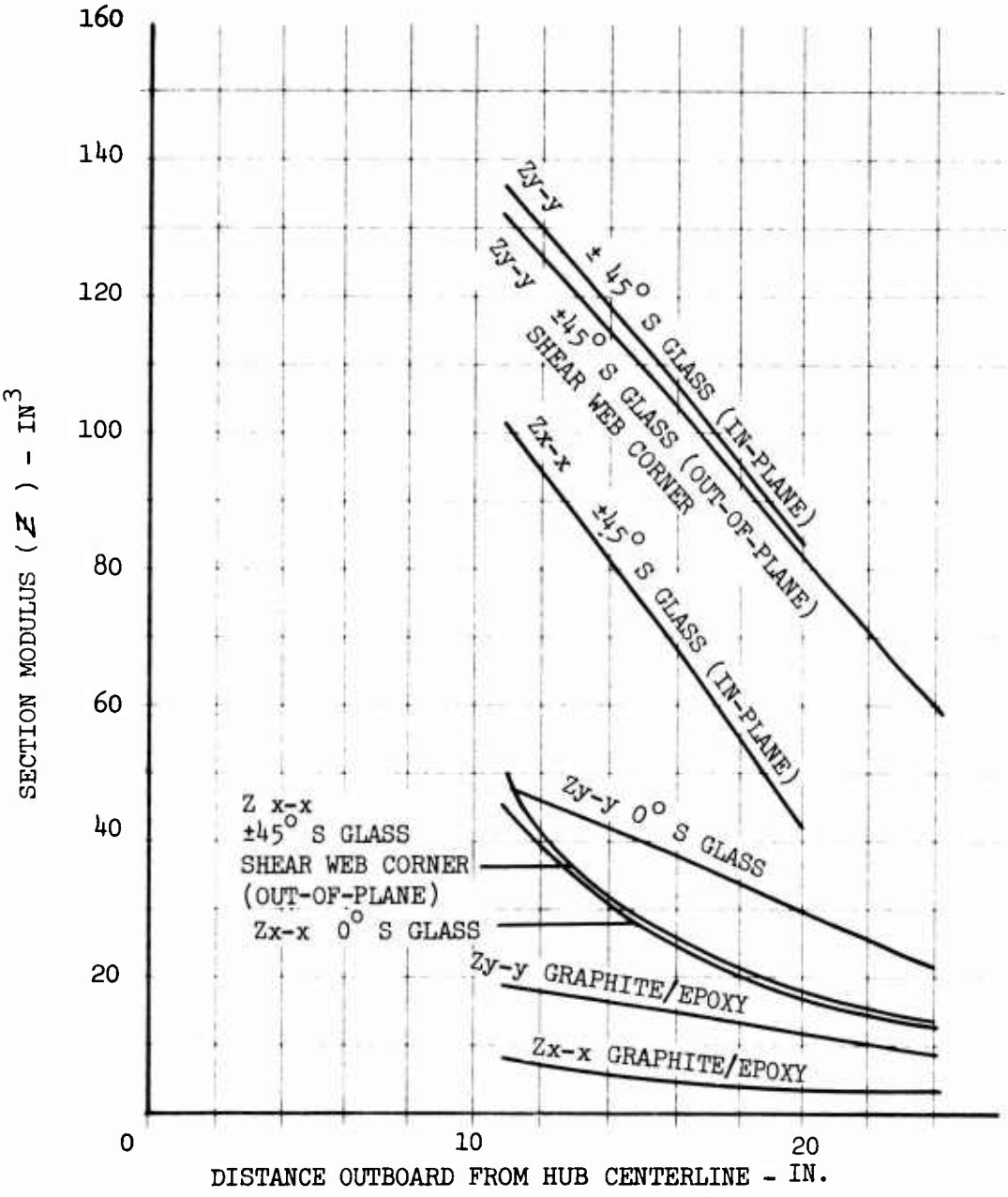

Figure 41. Hub Section Modulus Distribution.

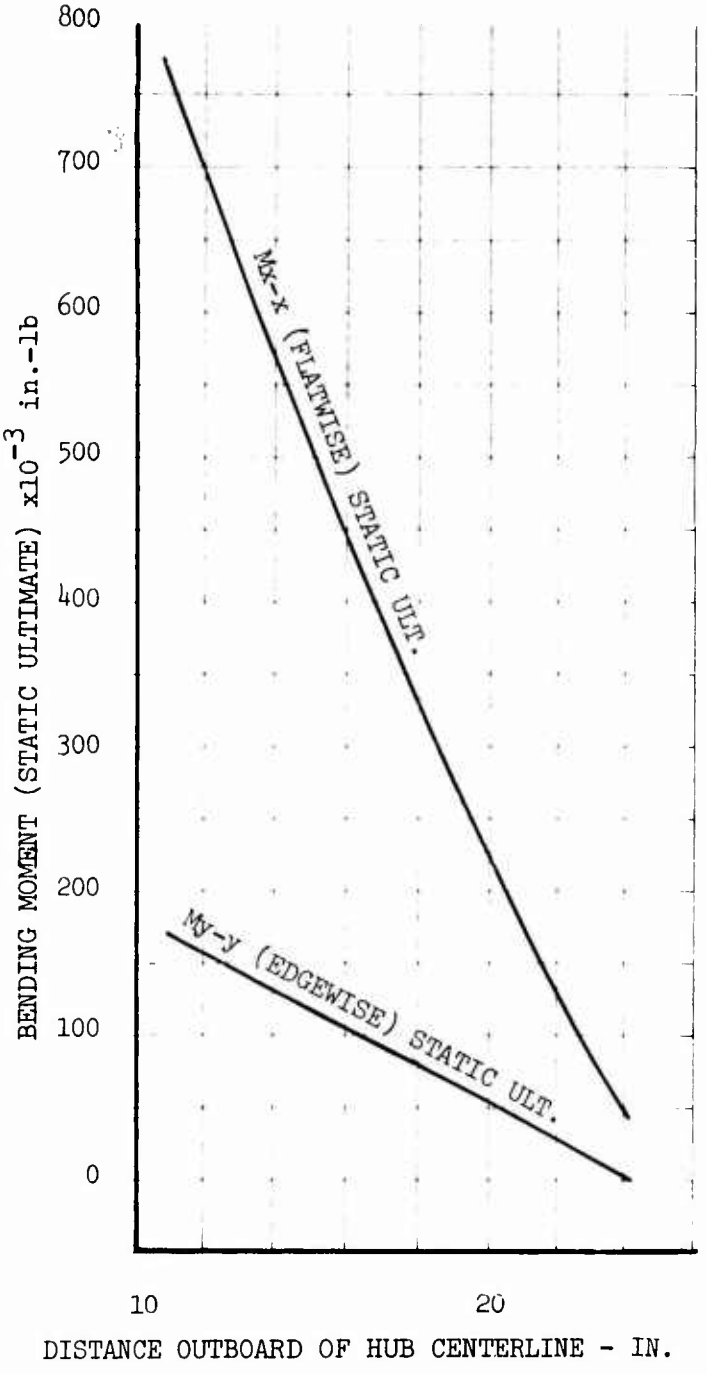

Figure 42. Static Ultimate Bending Moment Distribution.

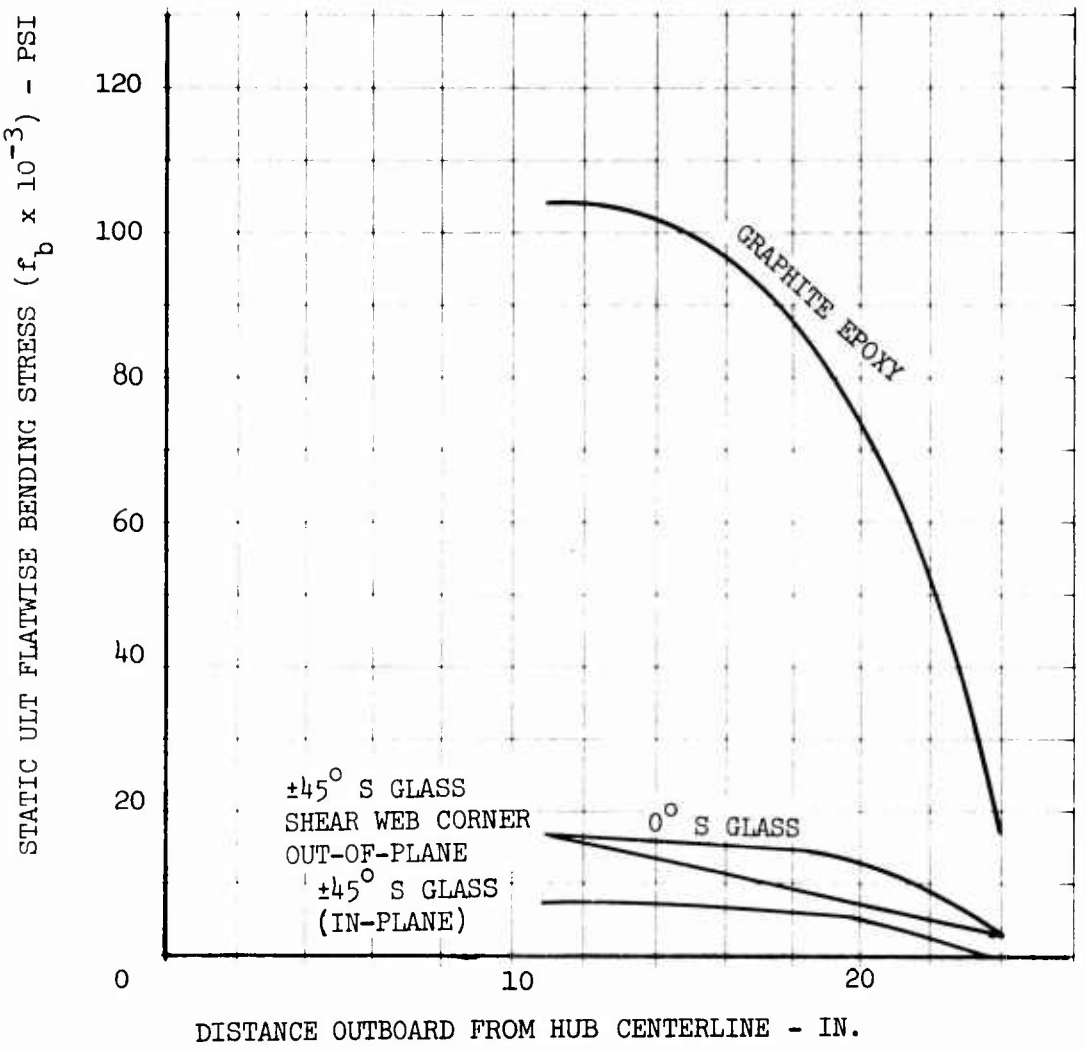

Figure 43. Static Ultimate Flatwise (About the X-X Axis) Bending Stress Distribution.

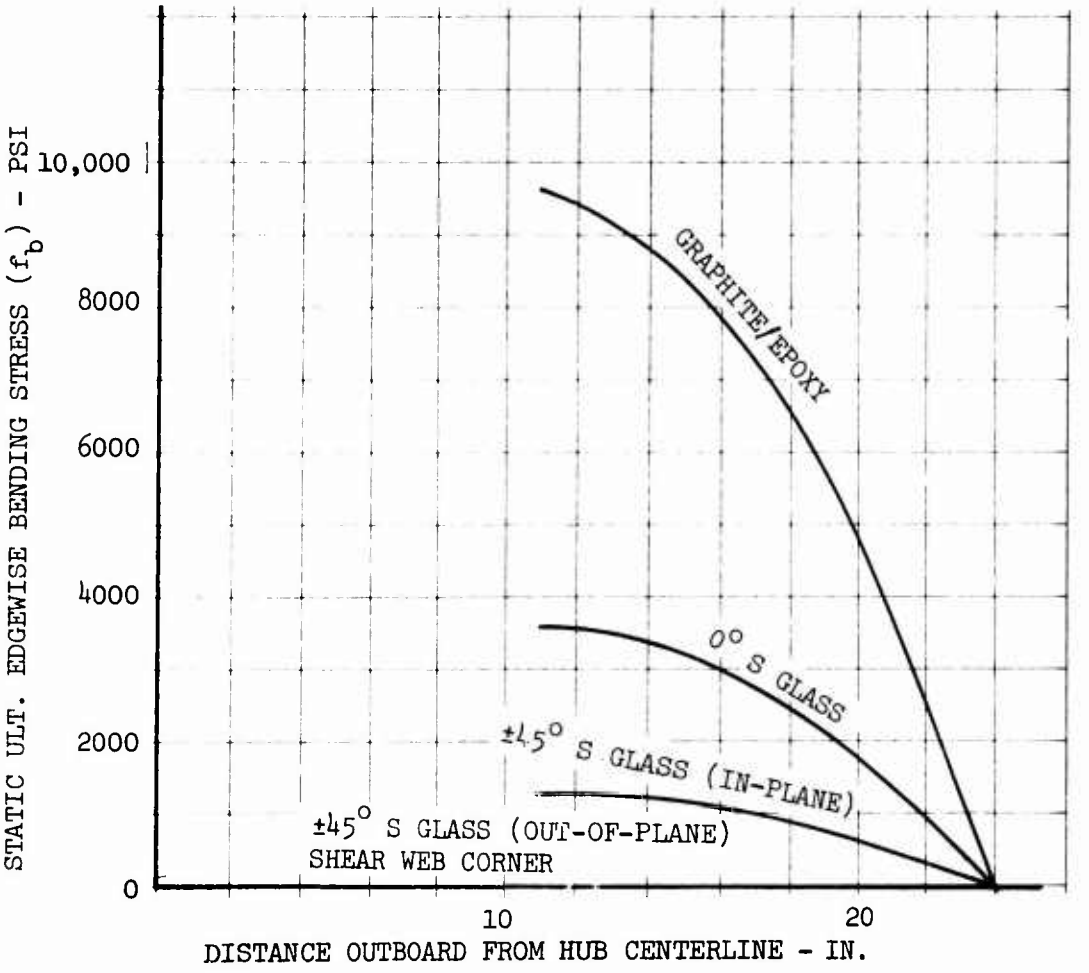

Figure 44. Static Ultimate Edgewise (About the Y-Y Axis) Bending Stress Distribution.

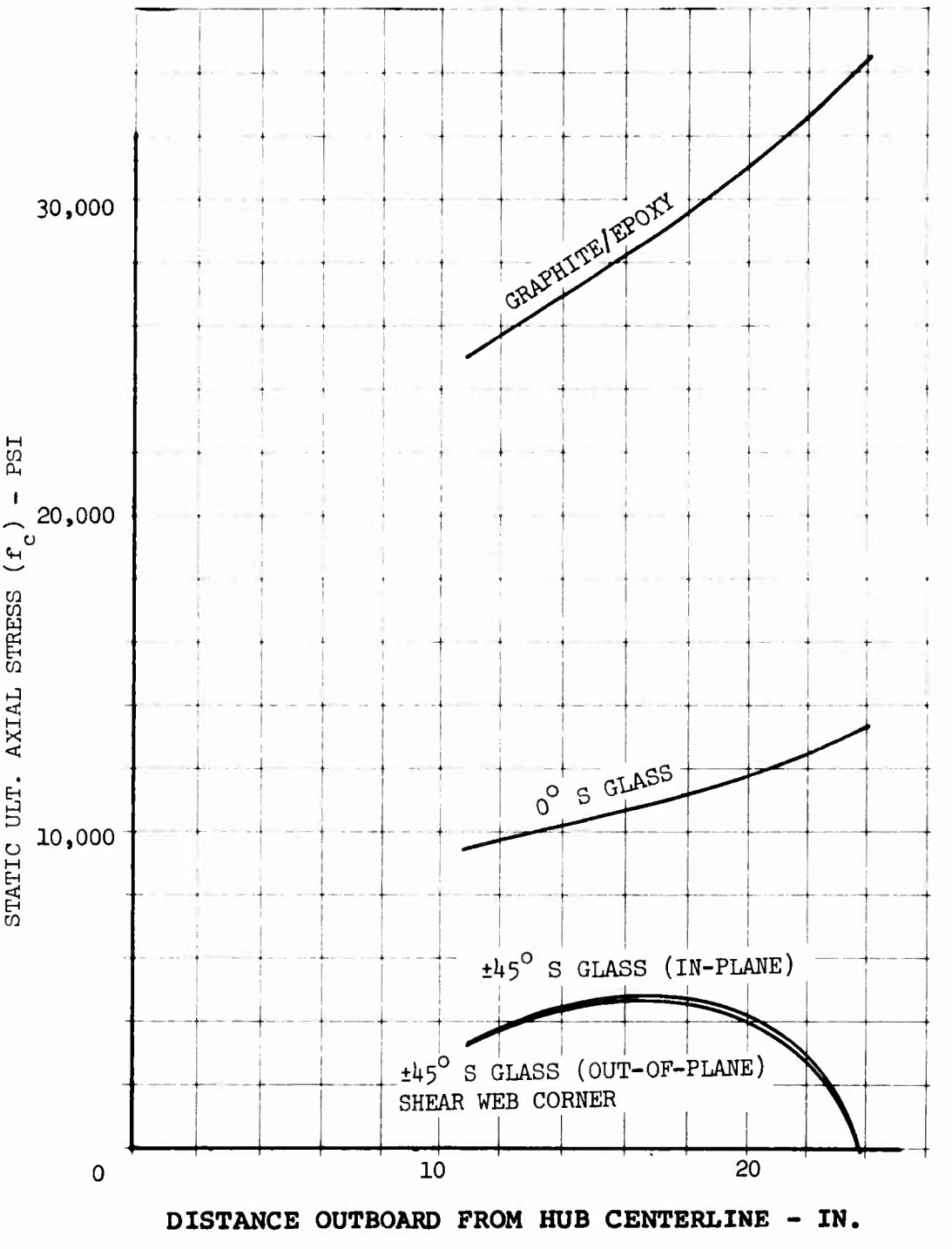

Figure 45. Static Ultimate Axial Stress Distribution.

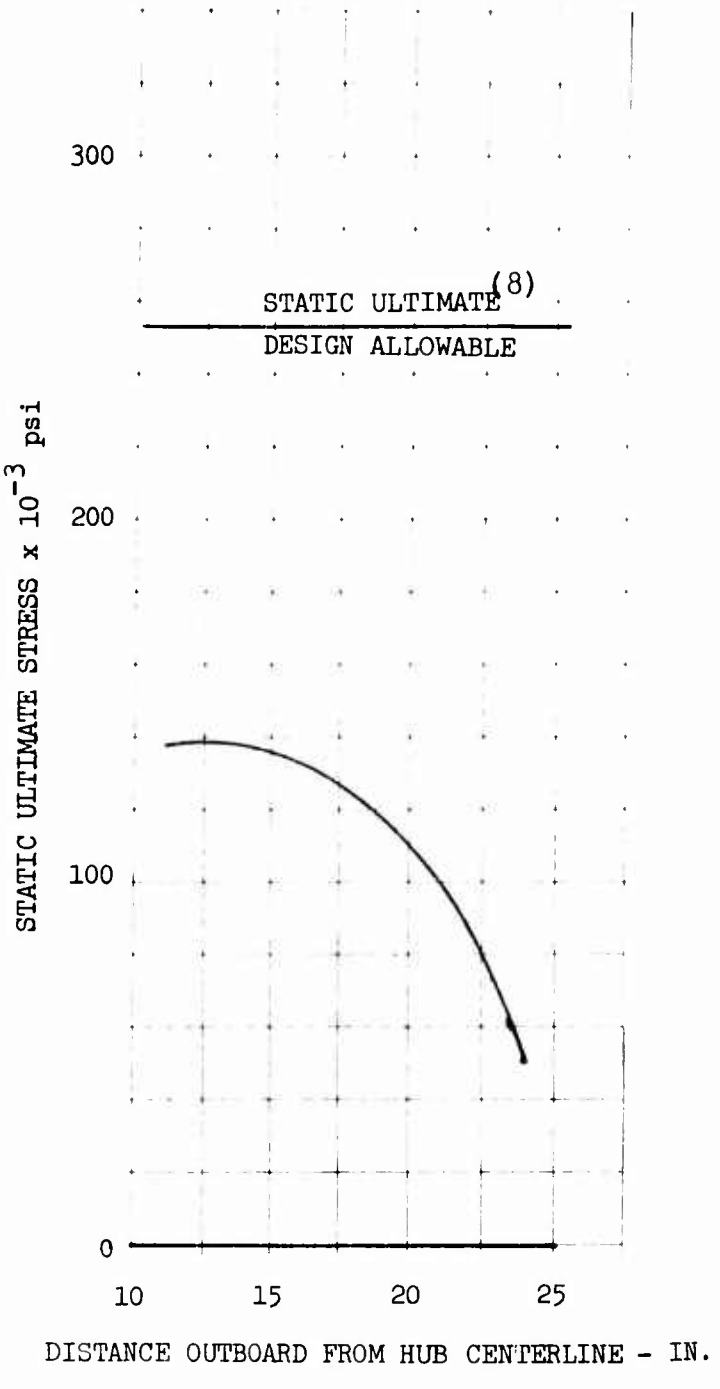

Figure 46. Total Static Ultimate and Allowable Stress Distribution - G/E Straps.

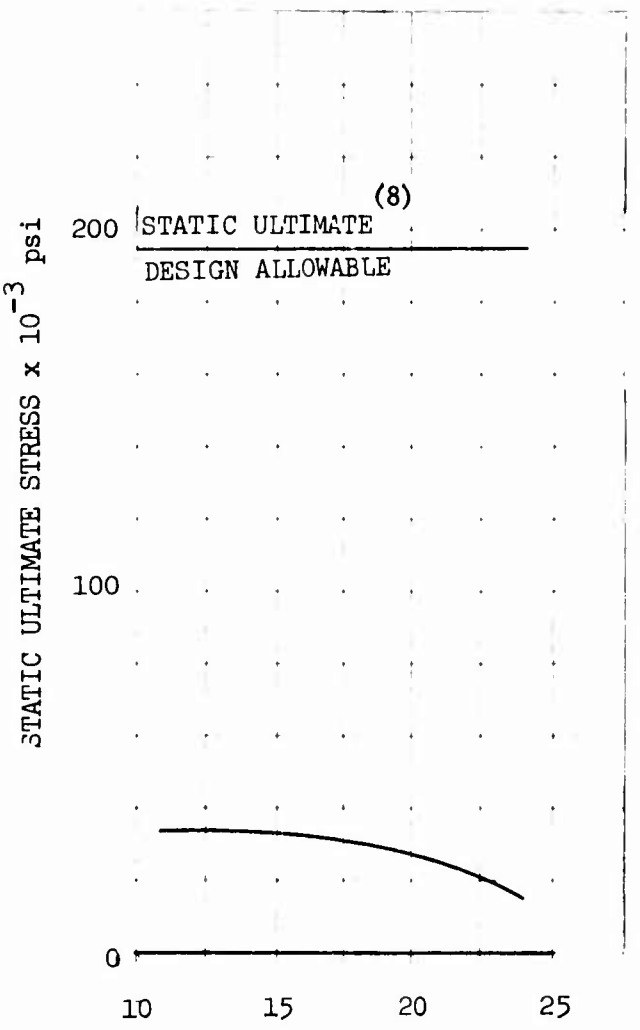

Figure 47. Total Static Ultimate and Allowable Stress Distribution - Fiberglass Straps.

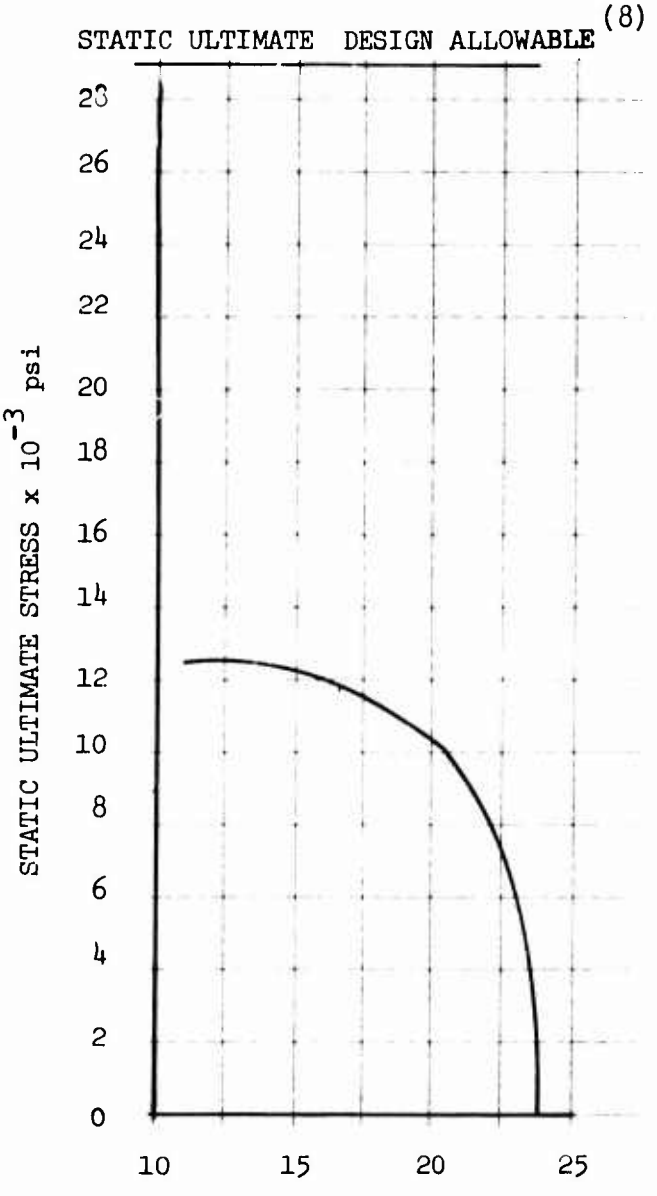

Figure 48. Total Static Ultimate and Allowable Stress Distribution-In-Plane Shear Web (±45° Glass).

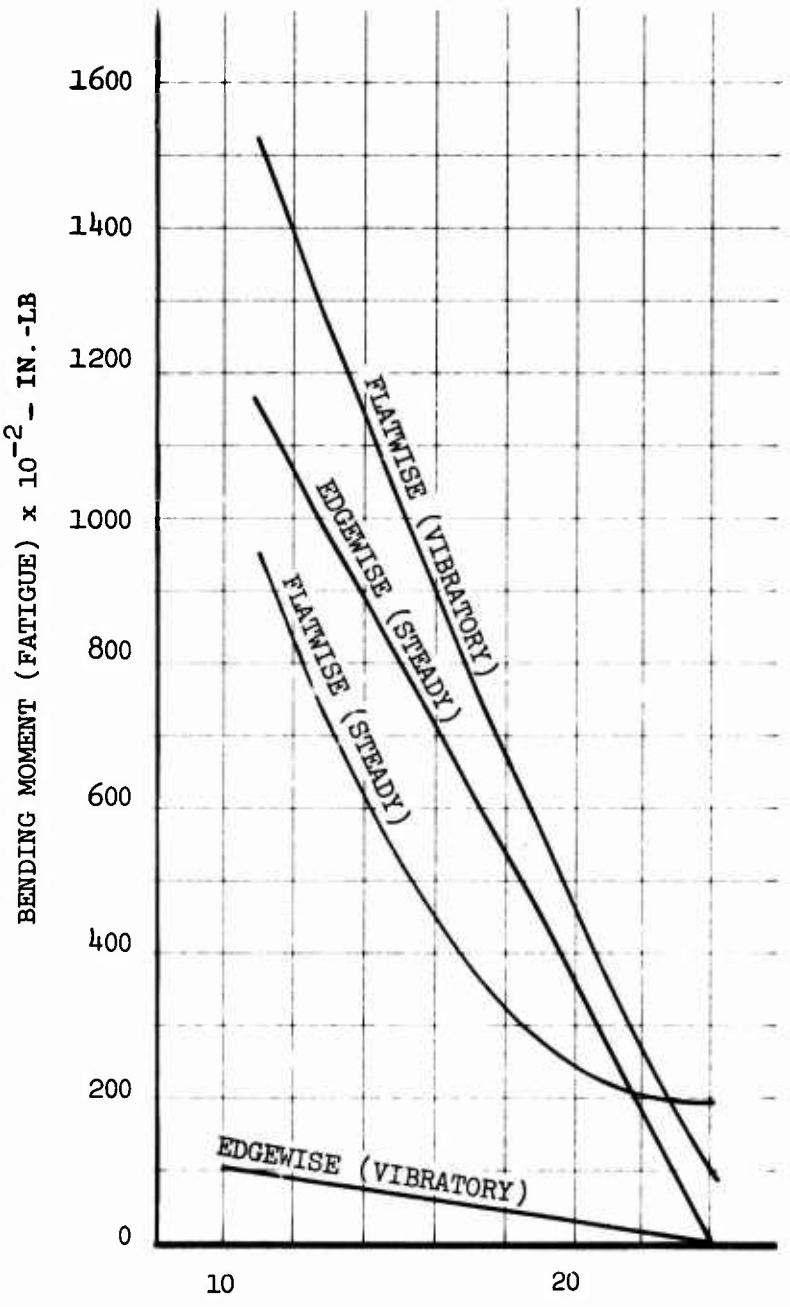

Figure 49. Design Fatigue Bending Moment Distribution.

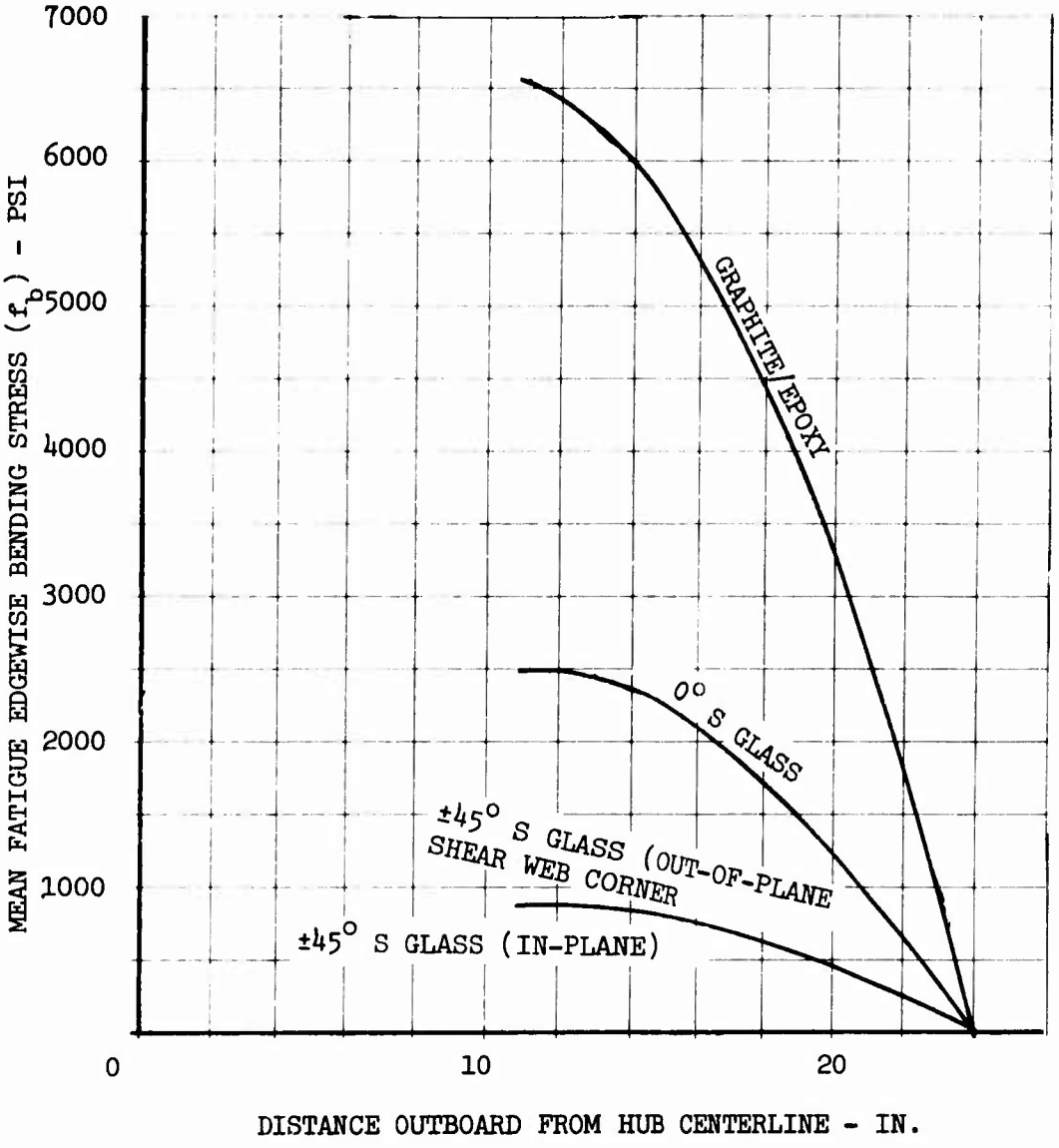

Figure 50. Mean Fatigue Edgewise (About the Y-Y Axis) Stress Distribution.

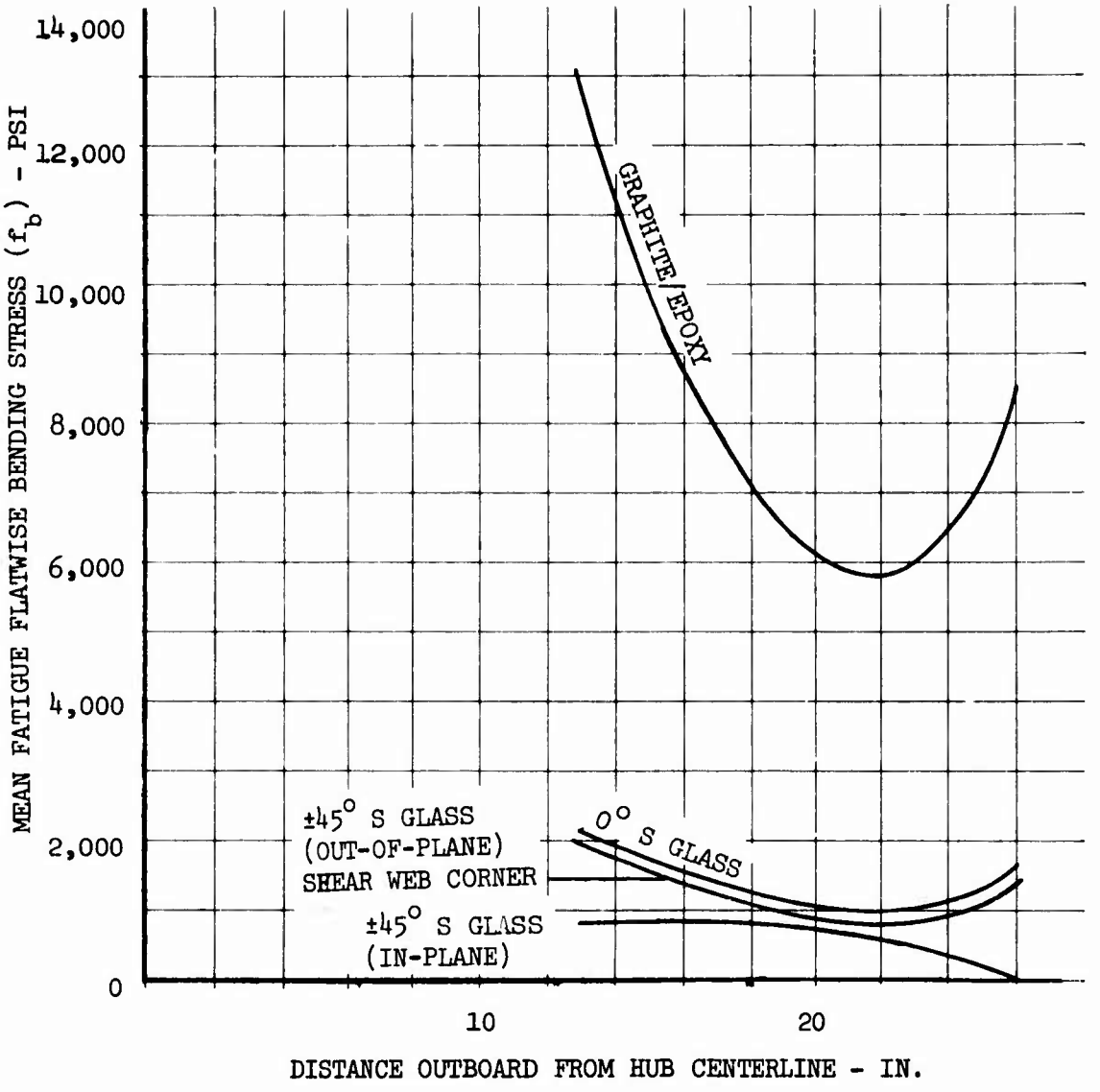

Figure 51. Mean Fatigue Flatwise (About the X-X Axis) Stress Distribution.

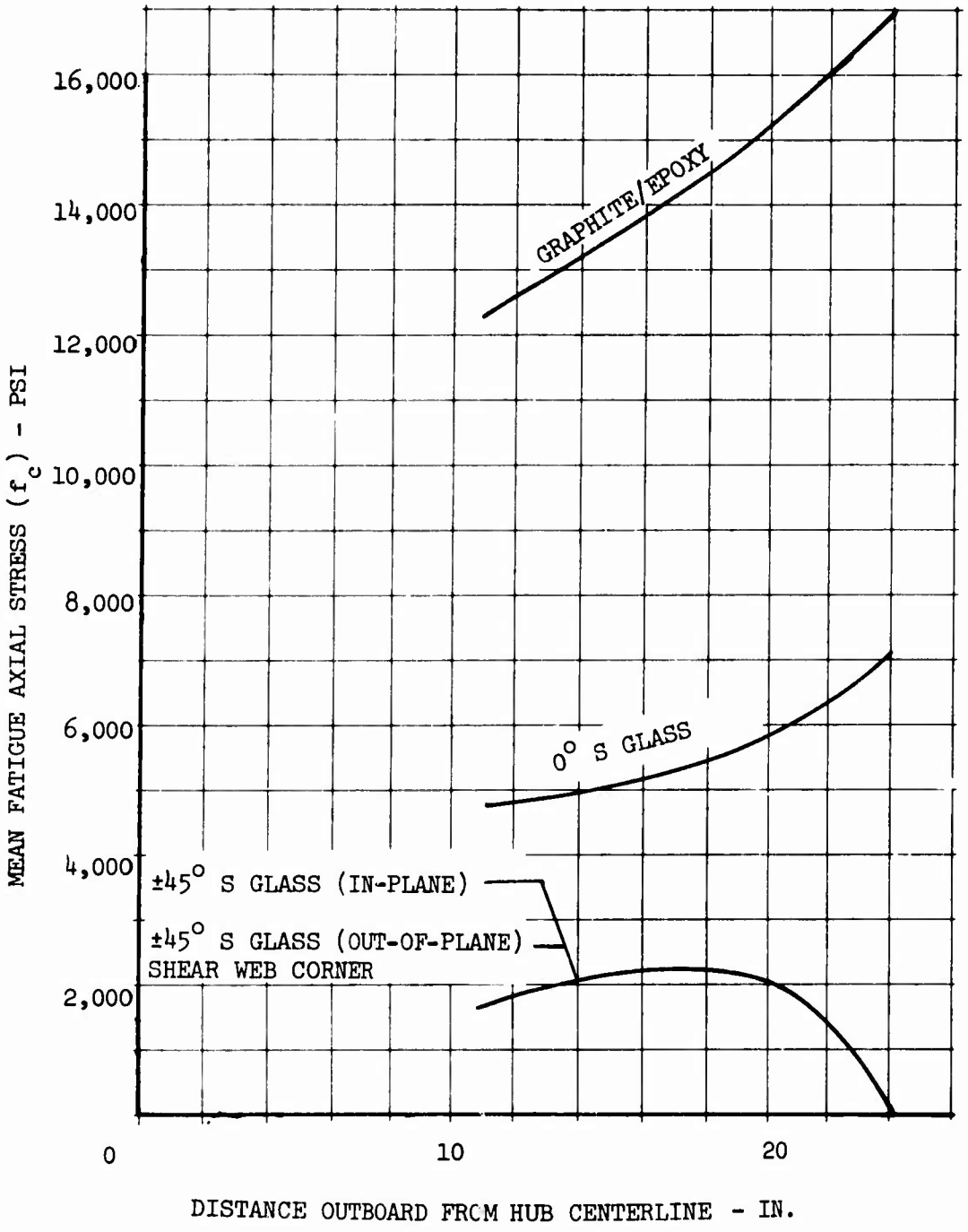

Figure 52. Mean Fatigue Axial Stress Distribution.

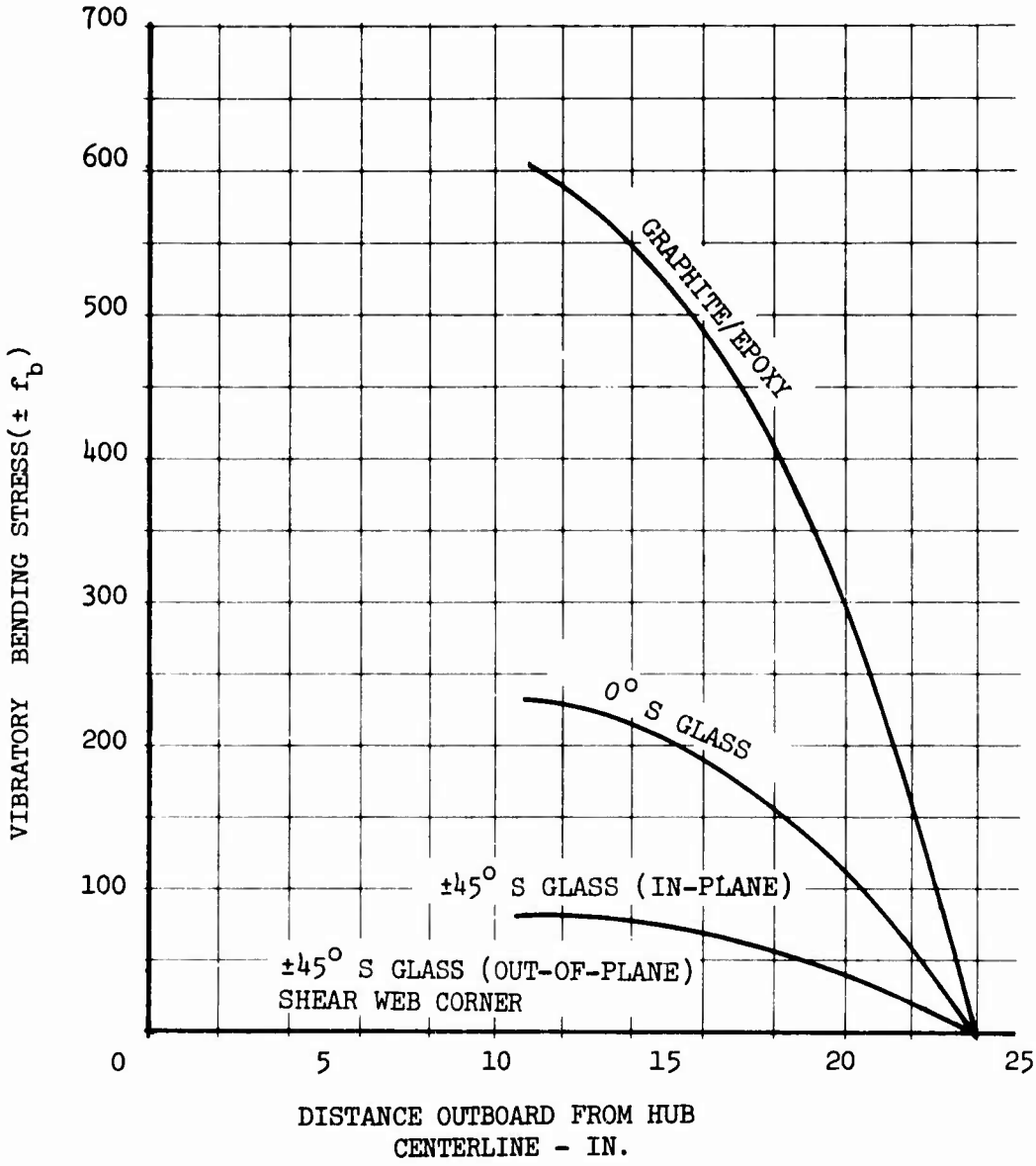

Figure 53. Vibratory Fatigue Edgewise (About the Y-Y Axis) Stress Distribution.

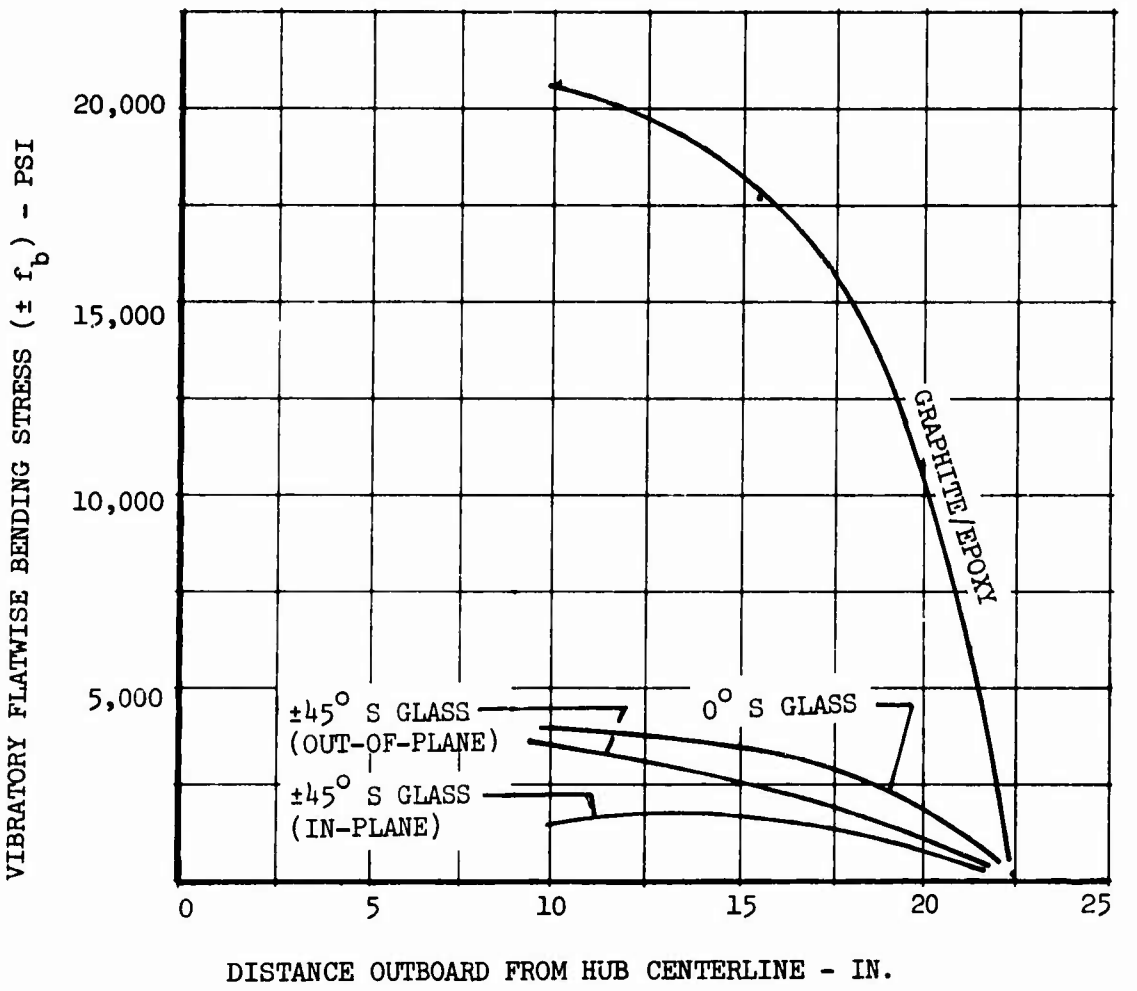

Figure 54. Vibratory Fatigue Flatwise (About the X-X Axis) Stress Distribution.

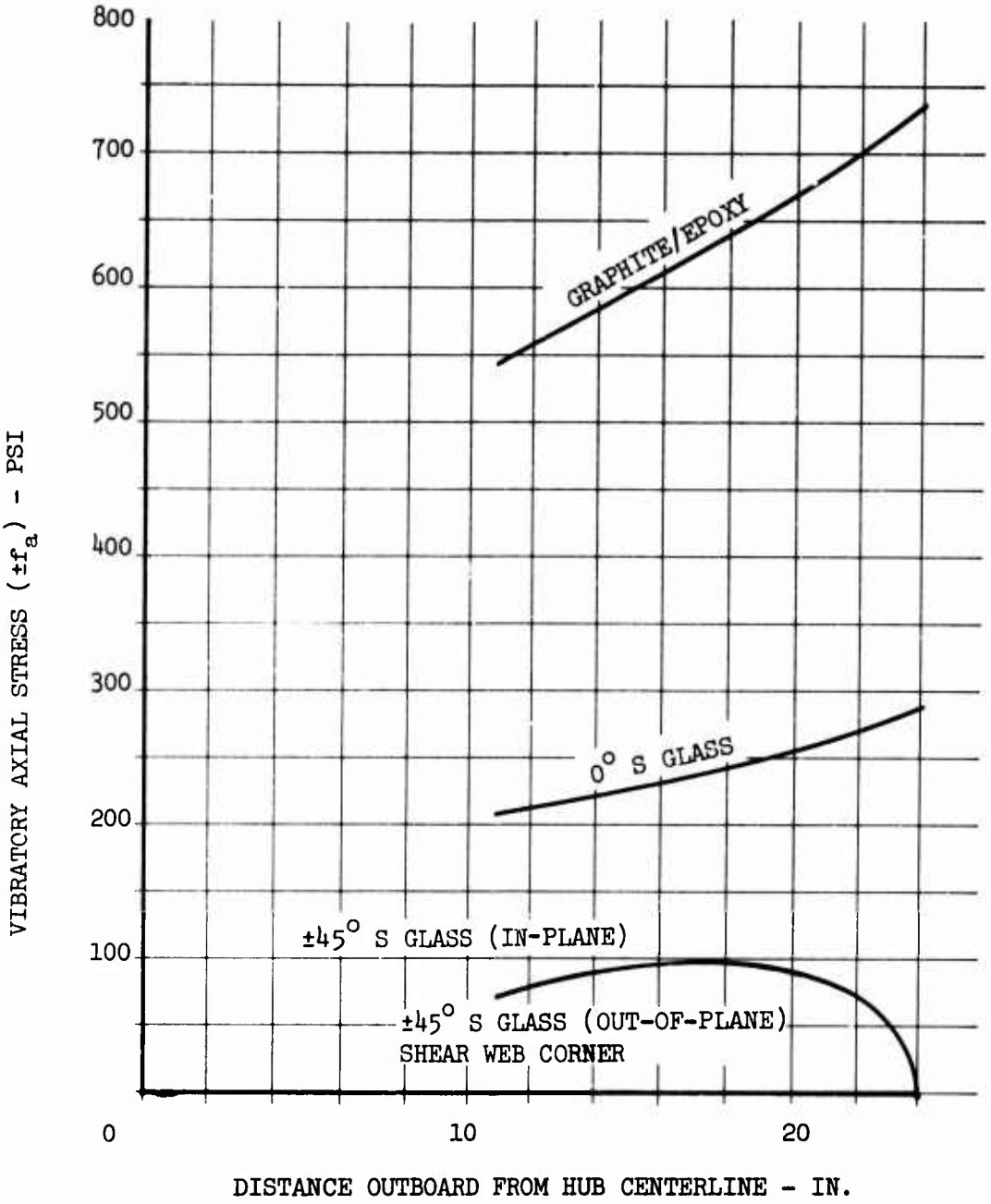

Figure 55. Vibratory Fatigue Axial Stress Distribution.

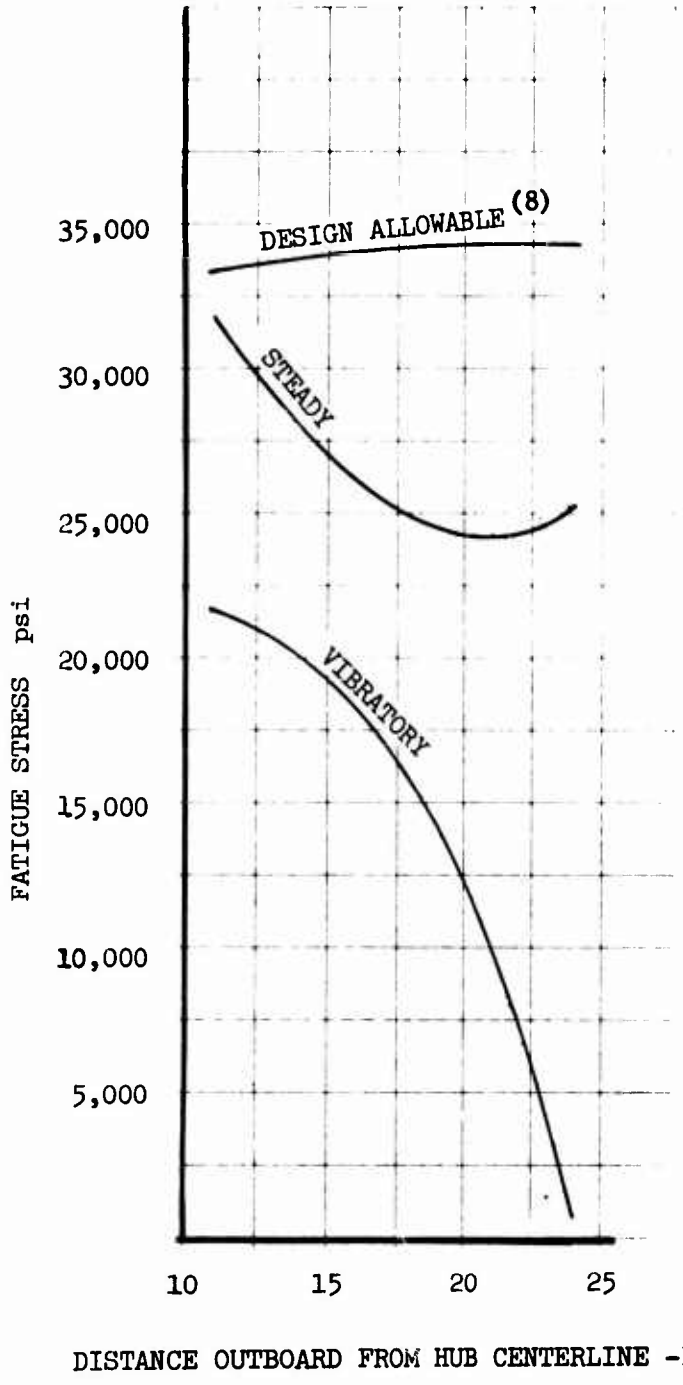

Figure 56. Design Fatigue Stress Distribution - G/E Straps.

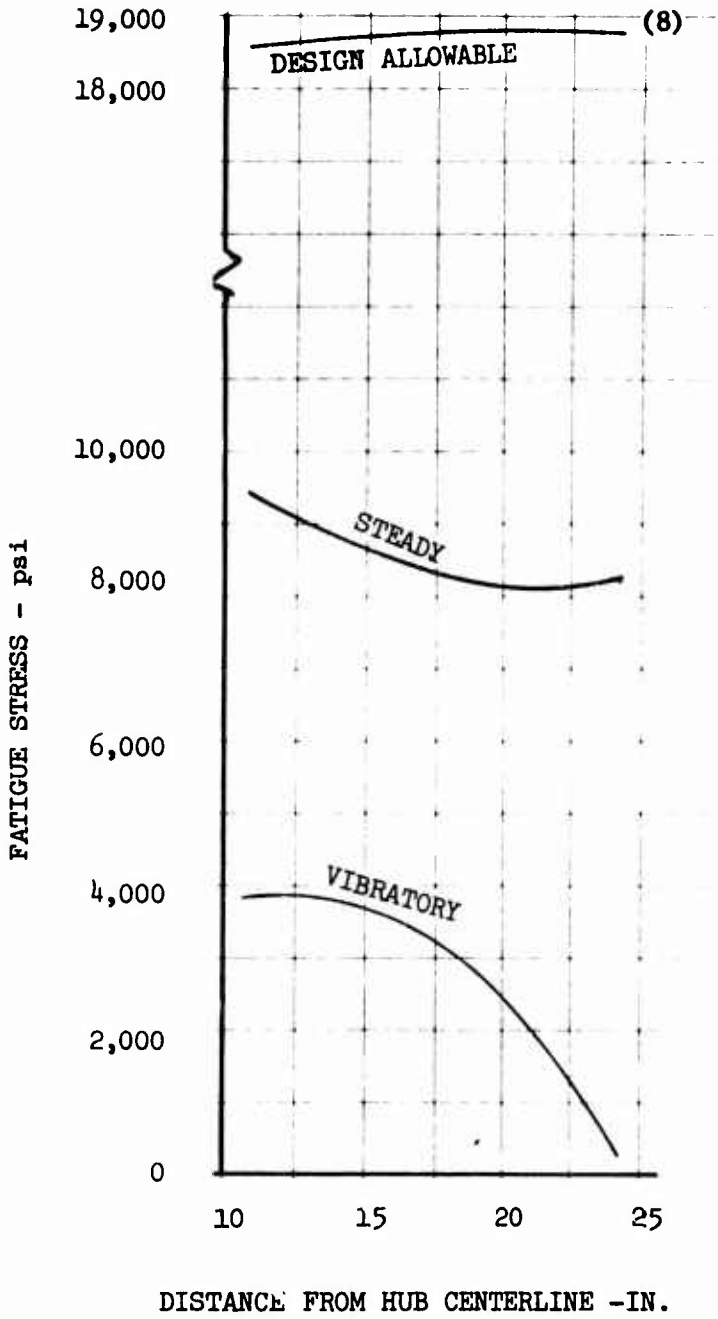

Figure 57. Design Fatigue Stress Distribution - Fiberglass Straps.

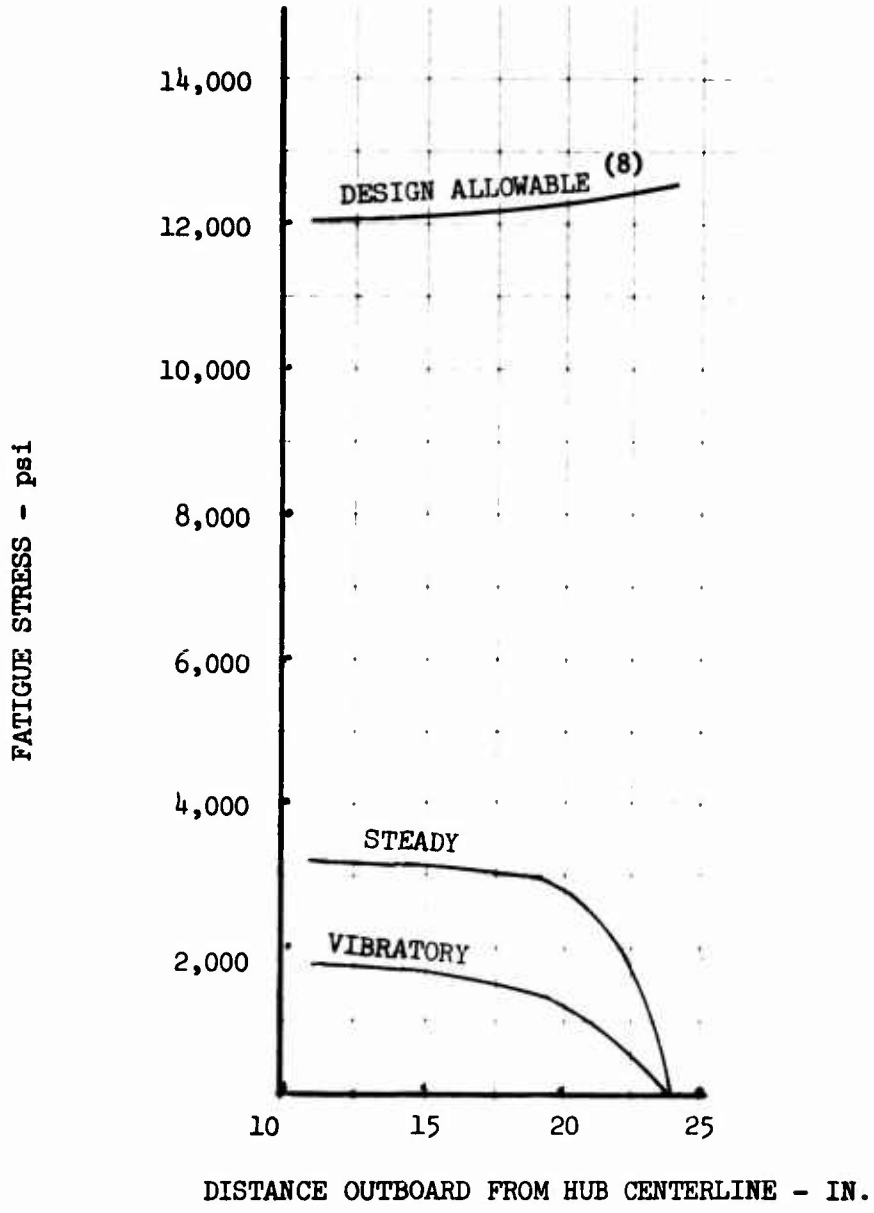

Figure 58. Design Fatigue Stress Distribution - In-Plane Shear Web (±45° Glass).

BENDING SHEAR STRESS AT CENTER OF ROTATION (Figures 59 to 61)

The six arms act as a beam with a shear load due to thrust applied at its extremities. This shear load is reacted as a constant load around the outer bolt circle. The load due to the head moment will be taken out as a sinusoidal couple around the outer bolt circle.

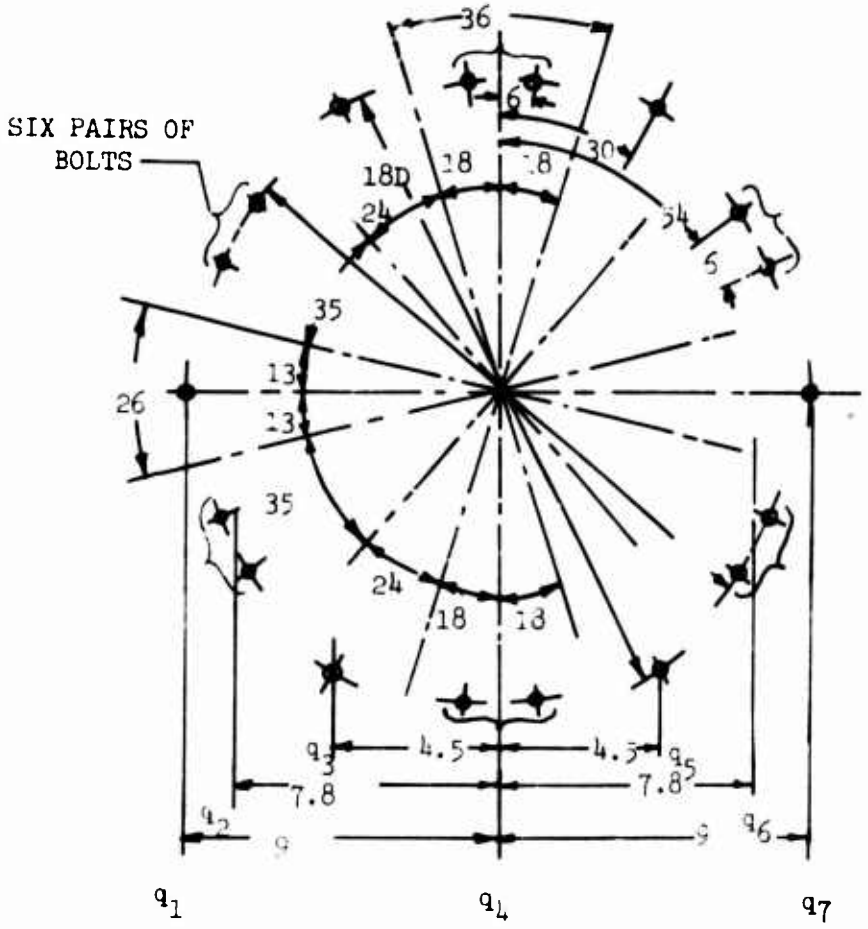

(1) ASSUMING THE SIX PAIRS OF BOLTS AT THE 17.25 BC LOCATIONS AS ONE BOLT, THERE ARE THEN TWELVE EFFECTIVE BOLTS TO REACT THE APPLIED LOADS

(2) ASSUME ALL BOLTS TO BE EFFECTIVE AT 18.0 DIA.

DEVELOPMENT OF REACTION LOADS
STATIC ULTIMATE CASE

HEAD MOMENT (HM) = 1.5×10^6 IN.-LB **(17)**

THRUST (V_N) = 31,250 LB **(18)**

Figure 59. Central Hub Clamp Bolt Geometry.

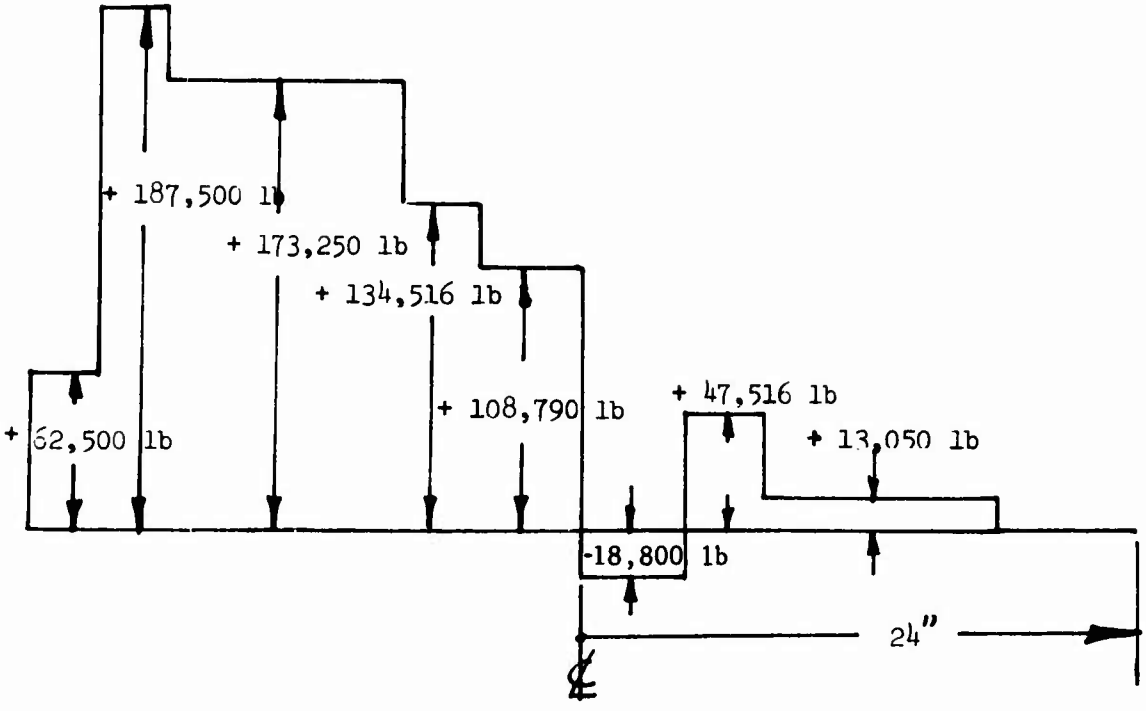

Figure 60. Resultant Static Shear Diagram.

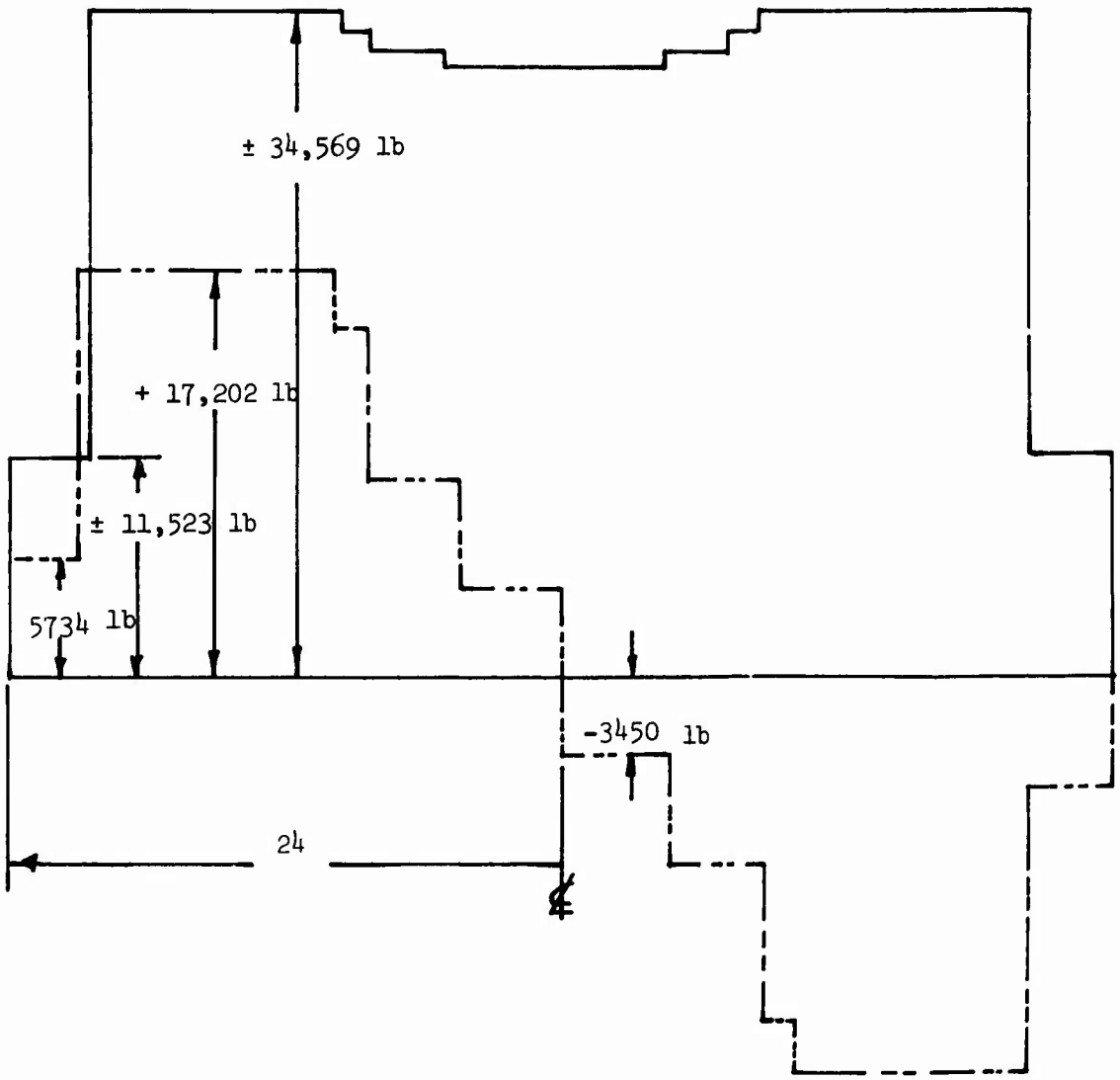

Figure 61. Resultant Fatigue Shear Diagram.

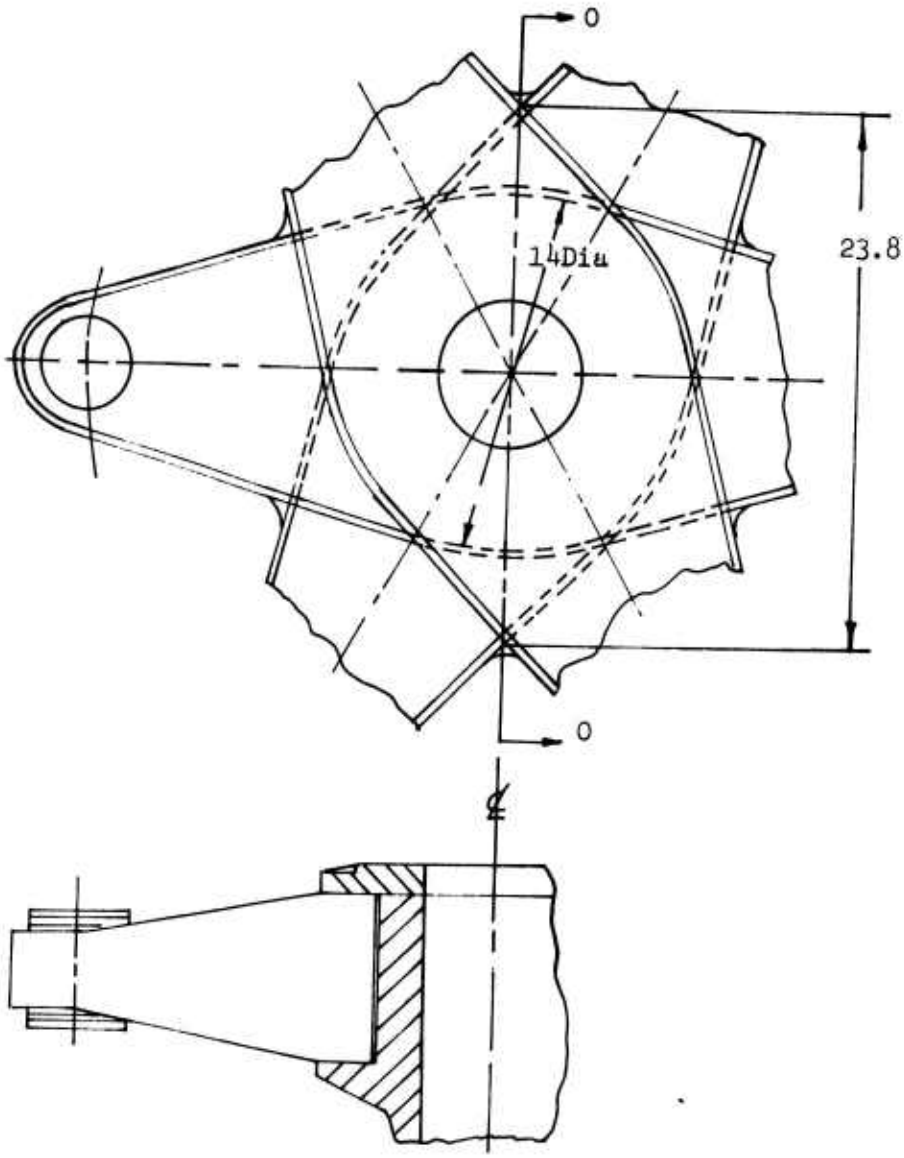

Figure 62. Critical "Beam" Section Due to Bending Shear.

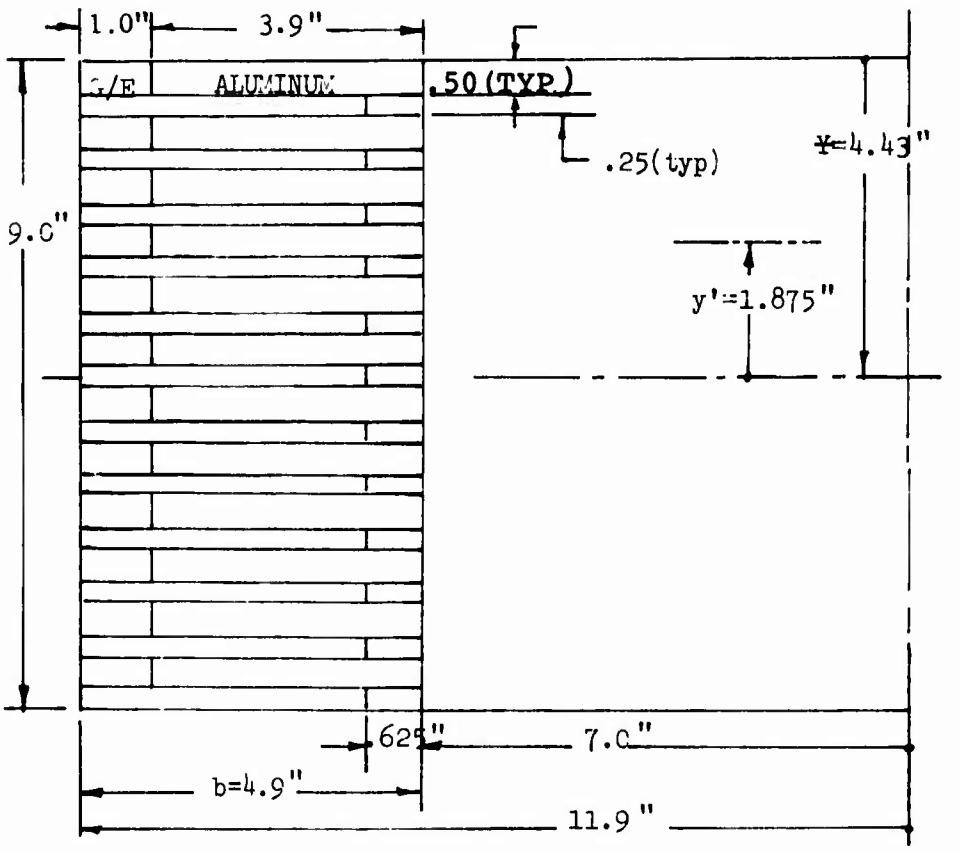

Figure 63. Section O-O Centerline of Hub.

TABLE 32.			SECTION 0-0, SECTION PROPERTIES ABOUT X-X AXIS					
Item	A	E $x10^6$	AE $x10^6$	Y	AEY	AEY^2	Io	E Io
1	.250	17.5	4.375	.250	1.093	.273	.01041	.18217
2		17.5	4.375	1.000	4.375	4.375		
3		17.5	4.375	1.750	7.656	13.398		
4		6.8	1.700	2.500	4.250	10.625		.07078
5			1.700	3.250	5.525	17.956		
6			1.700	4.000	6.800	27.200		
7			1.700	4.750	8.075	38.356		
8			1.700	5.500	9.350	51.425		
9			1.700	6.250	10.625	66.406		
10		17.5	4.375	7.000	30.625	214.375		.18217
11		17.5	4.375	7.750	33.906	262.773		
12		17.5	4.375	8.500	37.187	316.093		
13	.078	17.5	1.365	8.875	12.114	107.515	.00081	.01417
14	.250	10.0	2.500	8.500	21.250	180.625	.04062	.40620
15	.078	17.5	1.365	8.125	11.090	90.111	.00081	.01417
16	.250	10.0	2.500	7.750	19.375	150.156	.04062	.40620
17	.078	17.5	1.365	7.375	10.066	74.243	.00081	.01417
18	.250	10.0	2.500	7.000	17.500	122.500	.04062	.40620
19	.078	6.8	.530	6.625	3.511	23.262	.00081	.00550
20	.250	10.0	2.500	6.250	15.625	97.656	.04062	.40620
21	.078	6.8	.530	5.875	3.113	18.293	.00081	.00550
22	.250	10.0	2.500	5.500	13.750	75.625	.04062	.40620
23	.078	6.8	.530	5.125	2.716	13.920	.00081	.00550
24	.250	10.0	2.500	4.750	11.875	56.406	.04062	.40620
25	.078	6.8	.530	4.375	2.318	10.144	.00081	.00550
26	.250	10.0	2.500	4.000	10.000	40.000	.04062	.40620
27	.078	6.8	.530	3.625	1.921	6.964	.00081	.00550
28	.250	10.0	2.500	3.250	8.125	26.406	.04062	.40620
29	.078	6.8	.530	2.875	1.523	4.380	.00081	.00550
30	.250	10.0	2.500	2.500	6.25	15.625	.04062	.40620
31	.078	17.5	1.365	2.125	2.900	6.163	.00081	.01417
32	.250	10.0	2.500	1.750	4.375	7.656	.04062	.40620
33	.078	17.5	1.365	1.375	1.876	2.580	.00081	.01417
34	.250	10.0	2.500	1.000	2.500	2.500	.04062	.40620
35	.078	17.5	1.365	.625	.853	.533	.00081	.01417
36	.250	10.0	2.500	.250	.625	.156	.04062	.40620
Total			77.820		344.718	2156.674		6.51017

Section O-O (Figures 62 and 63)

Determination of centroid (Y') of laminates in cross-sectional area above neutral axis (assuming all of Item 25 as effective).

TABLE 33. AREA PROPERTIES

Item	$AE \times 10^6$	$AEY \times 10^6$
1	4.375	1.093
2	4.375	4.375
3	4.375	7.656
4	1.700	4.250
5	1.700	5.525
6	1.700	6.800
25	.530	2.318
26	2.500	10.000
27	.530	1.921
28	2.500	8.125
29	.530	1.523
30	2.500	6.250
31	1.365	2.900
32	2.500	4.375
33	1.365	1.876
34	2.500	2.500
35	1.365	.853
36	2.500	.625
Total	38.910	72.965

$$Y' = \frac{\Sigma AEY}{\Sigma AE} = \frac{2 \quad 72.965 \times 10^6}{2 \quad 38.910 \times 10^6} = \underline{1.875} \qquad (19)$$

Static Analysis

Shear stress in hub section laminates due to maximum static ultimate shear load

$$f_{s_{X-X}} = \frac{V_{N_{MAX}} \; EQ}{\Sigma EI_{X-X \; (2b)}} = \frac{V_{N_{MAX}} \; EAY'}{\Sigma EI_{X-X \; (2b)}} \qquad (20)$$

$$f_{s_{X-X}} = \frac{108790 \times 2 \quad 38.910 \times 10^6 \quad 1.875}{1271.948 \times 10^6 \quad (2 \times 4.9)} \tag{21}$$

$$f_{s_{X-X}} = \underline{\underline{1275}} \text{ PSI} \tag{22}$$

Margin of Safety

$$\text{M.S.}_{\text{STATIC}} = \frac{\text{Allowable Shear Stress (0°S Glass at X-X)}}{\text{Applied Shear Stress}} - 1 \tag{23}$$

$$\text{M.S.}_{\text{STATIC}} = \frac{5400}{1275} - 1 \tag{24}$$

$$\text{M.S.}_{\text{STATIC}} = 4.24 - 1 = \underline{\underline{+ 3.24}} \tag{25}$$

Fatigue Analysis

Shear stress in hub section laminates due to fatigue shear load:

The vibratory shear load/stress ratio is identical with the static ultimate load/stress ratio.

$$\text{Load/Stress}_{(\text{Ult})} = \frac{1275}{108790} \tag{26}$$

$$\text{Load/Stress}_{(\text{Ult})} = .0117 \tag{27}$$

Therefore,

$$f_{s_{(\text{Fatigue})}} = .0117 \ (V_{(\text{Fatigue})}) \tag{28}$$

$$f_{s_{(\text{Fatigue})}} = .0117 \ (3450 \pm 32559) \tag{29}$$

$$f_{s_{(\text{Fatigue})}} = 40 \text{ PSI} \pm 380 \text{ PSI} \tag{30}$$

Margin of Safety

The resin matrix of the unidirectional (0 degree) glass fiber reinforced epoxy straps is critical due to bending shear.

Based on Sikorsky Aircraft's experience with small-scale torsion test specimens fabricated of unidirectional (0 degree) fiber orientation composites, a fatigue shear allowable of ±4800 PSI at 10^7 cycles and 0 steady stress is used.

CENTRAL HUB ATTACHMENT (Figure 64)

The hub laminate assembly is clamped between the central hub lower lip and top clamp ring by 19 bolts located on a 17.25-inch bolt circle. The thrust and head moment are reacted by a constant load and two sinusoidally distributed couple loads around the bolt circle. One load path is through a bearing load distribution on the clamp ring and hub lower lip. The other is a bolt tension load distribution around the ring.

Main rotor shaft torque is transferred through the hollow bushings located concentrically with the clamp ring bolts. The geometry of the ring is identical with that of the central hub lower ring. Therefore, the similarity of the ring and lip stiffnesses results in equal load sharing between the two.

$$\text{Load} = P_{BRG}\ \text{SIN}\theta ds \quad (31)$$

$$= P_{BRG}\ \text{SIN}\theta R d\theta$$

$$= P_{BRG}\ R\int_0^{\pi} \text{SIN}\theta d\theta$$

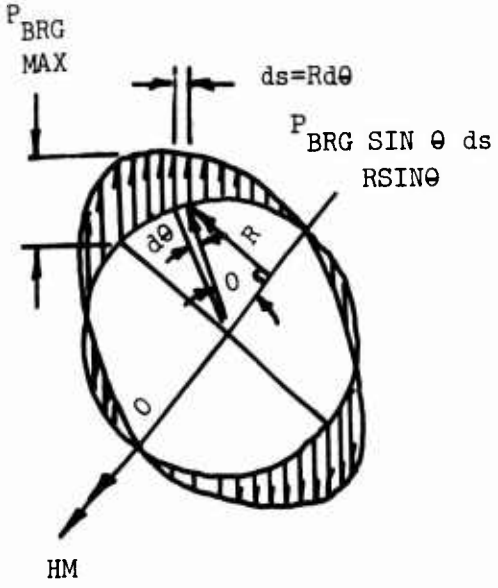

Figure 64. Sinusoidally Distributed Head Moment Reaction Around Central Hub.

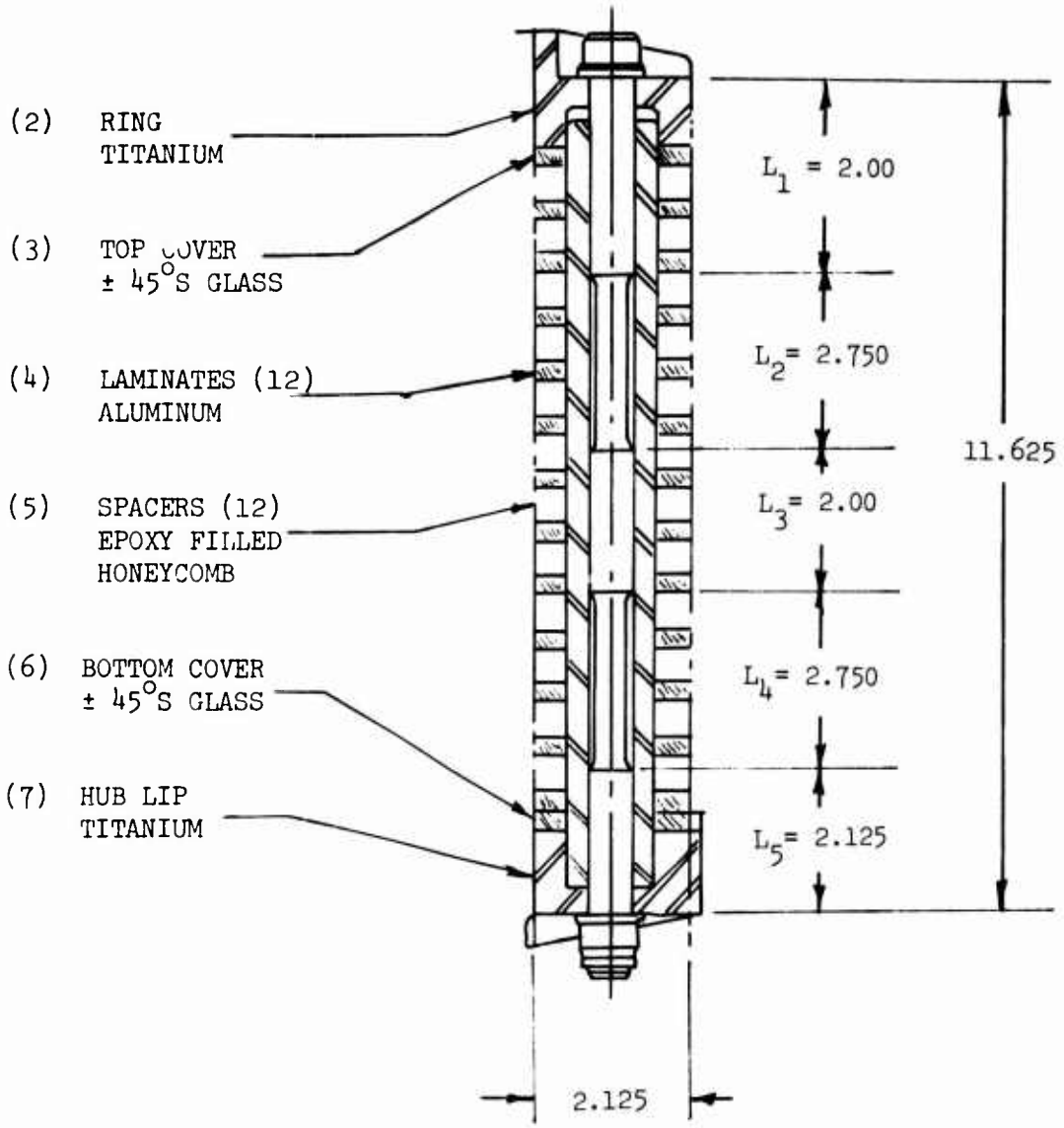

Figure 65. Clamp Bolt and Back-Up Material Geometry.

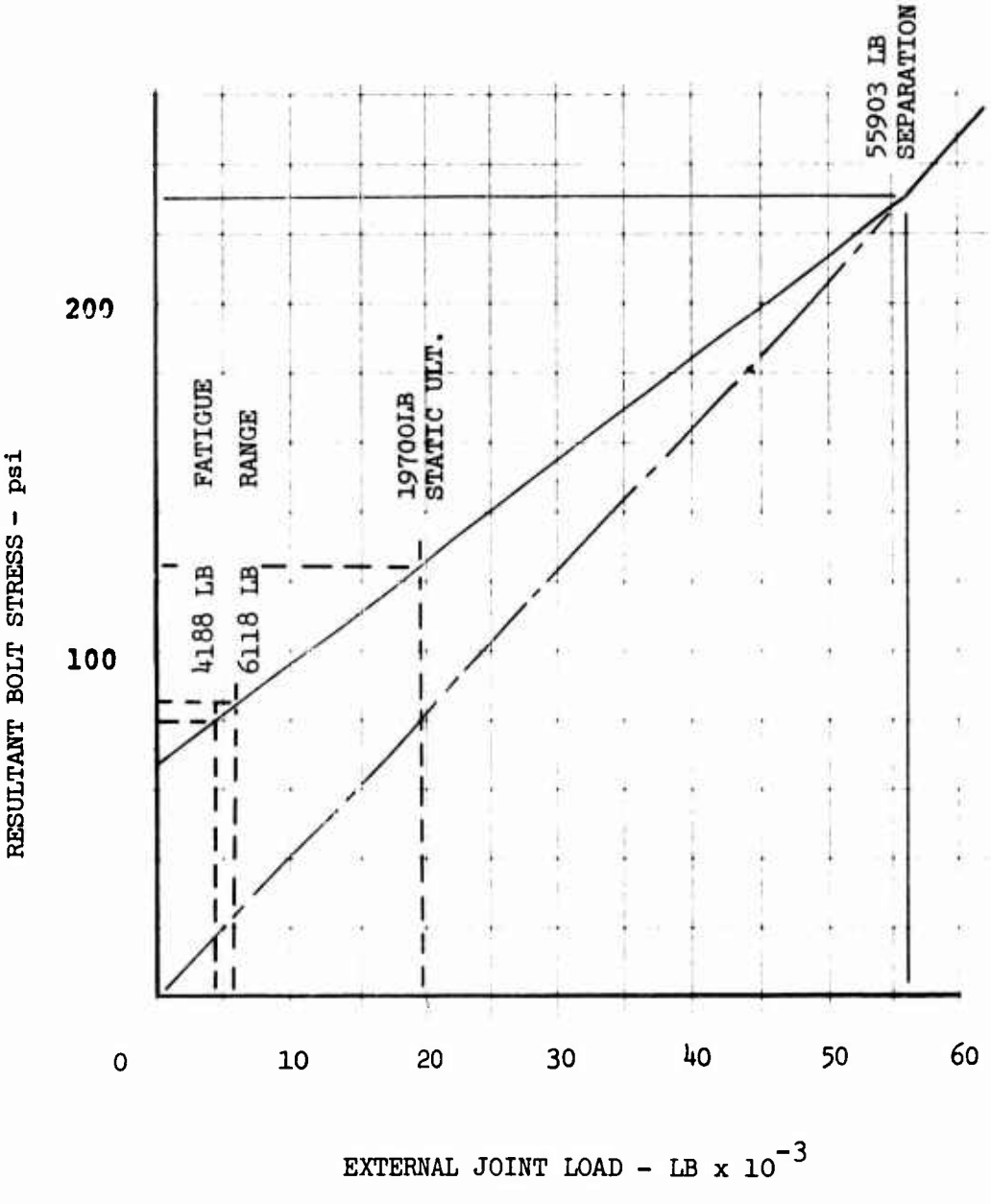

Figure 66. Clamp Bolt Load vs Joint Load.

Static Analysis (Figure 66)

For an externally applied load of 19,700 pounds ultimate, the joint does not separate, and the applied bolt stress is 125,000 psi. (Equivalent bolt load for a 5/8 bolt = 30,400 lb.)

Margin of Safety

$$F_{TU} \text{ (5/8 Bolt)} = 180{,}000 \text{ psi}^{13} \tag{32}$$

$$M.S. = \frac{F_{TU}}{f_{ULT}} = 1 \tag{33}$$

$$M.S. = \frac{180000}{125000} = 1 \tag{34}$$

$$M.S. = + .145 \tag{35}$$

Fatigue Analysis

The fatigue range of applied loads is 4118 pounds to 6118 pounds.

The resultant bolt stress range is 78000 psi to 84000 psi.

Therefore,

$$f_{bolt} = 80000 \pm 2000 \text{ psi} \tag{36}$$

Allowable Fatigue Stress

The small specimen endurance limit for 180,000-psi heat-treated steel at a steady stress of 80,000 psi is:

$$\bar{E} = \pm 50{,}000 \text{ psi}^{14} \tag{37}$$

Size Effect Factor ~ f_{SE} ~

$$f_{SE} = .7 \tag{38}$$

Reliability Factor ~ f_{3b} ~

$$f_{3\sigma} = .7 \text{ (steel)} \tag{39}$$

Stress Concentration Factor ~ K_t ~ [15]

$$K_t = 4.5 \text{ (steel threads)} \tag{40}$$

Notch Sensitivity ~ q ~

$$q = .45 \tag{41}$$

Therefore, $K_f = q\ (K_t) = 2.0$ (42)

Working Endurance Limit E_{3b}

$$E_{3_\sigma} = \bar{E} \times f_{SE} \times f_{3b} \times 1/K_f = \pm 12{,}200 \text{ psi} \quad (43)$$

Margin of Safety

$$\text{M.S. (Fatigue)} = \frac{E_{3b}}{f_{Bolt}} - 1 \quad (44)$$

$$\text{M.S. (Fatigue)} = \frac{\pm 12200}{\pm 2000} - 1 \quad (45)$$

$$\text{M.S. (Fatigue)} = + \text{ HIGH} \quad (46)$$

CLAMP TO HUB BOLT ATTACHMENT (Figure 67)

Head Moment Reaction

$$\Sigma M = M_B - M_{BRG} = 0 \tag{47}$$

Since $\frac{1}{2}$ HM = M_{BRG} (48)

$$M_B = \frac{1}{2} HM \tag{49}$$

or $\frac{1}{2}$ HM = $M_B = P_B \frac{Rx\eta}{2}$ (50)

$$P_B = \frac{HM}{R\eta} \tag{51}$$

Thrust Reaction

$$P_B = \frac{1}{2} \frac{6 V_N}{\eta} \tag{52}$$

$$P_B = \frac{3 V_N}{\eta} \tag{53}$$

Static Ultimate Case

$$HM = 225 \times 10^6 \text{ in.-lb} \tag{54}$$

$$V_N = 31{,}250 \text{ LB} \tag{55}$$

$$P_B = \frac{HM}{R} + \frac{3V_N}{\eta} \tag{56}$$

$$P_B = \frac{225 \times 10^6}{6.313 \times 24} + \frac{3 \times 31250}{24} \text{ lb} \tag{57}$$

$$P_B = 14{,}900 + 3906 \text{ lb} \tag{58}$$

$$P_B = 18{,}806 \text{ lb} \tag{59}$$

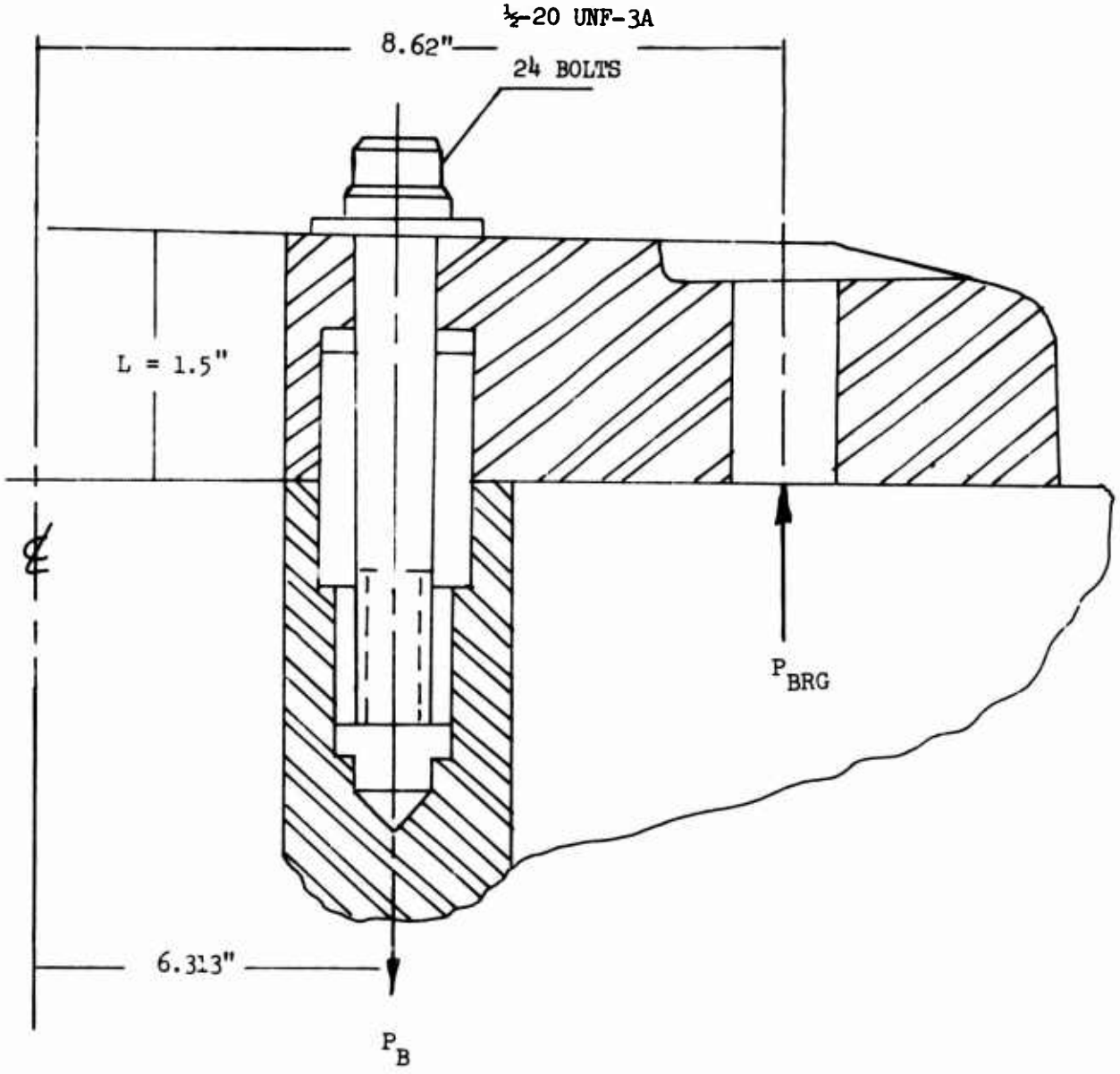

Head Moment Reaction

Pb= TENSILE BOLT LOAD
Pbrg= RING BEARING LOAD
HM= HEAD MOMENT
Vn= THRUST LOAD
n= NUMBER OF BOLTS

ASSUME THAT THE BOLT LOAD AND RING BEARING LOAD ARE SINUSOIDALLY DISTRIBUTED.

Figure 67. Clamp/Hub Bolt Geometry.

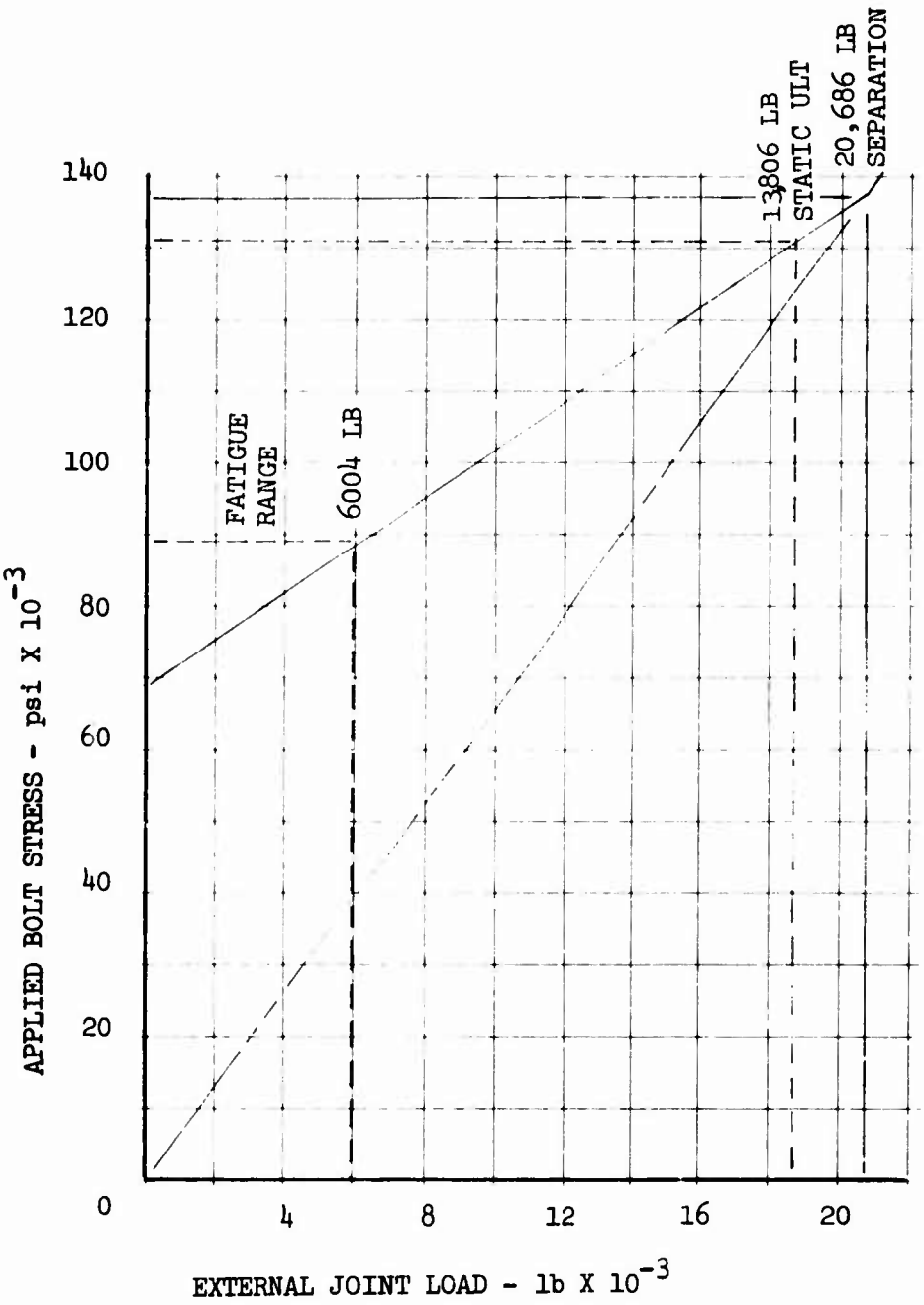

Figure 68. Clamp/Hub Bolt Load vs Joint Load.

Externally Applied Loads (Figure 68)

$$P_B = 18{,}806 \text{ pounds static ultimate} \tag{60}$$

$$\left.\begin{aligned} P_B &= 724 - 5280 = 4556 = 0 \text{ lb} \\ &= 724 + 5280 = +6004 = 6004 \text{ Max lb} \end{aligned}\right\} \text{Fatigue Range} \tag{61}$$

Static Analysis

For an externally applied load of 18,806 lb ult., the effective bolt stress is 132,000 psi ult. For a 180,000-psi heat-treat steel bolt,

$$F_{TU} = 180{,}000 \text{ psi}^{13} \tag{62}$$

Margin of Safety

$$\text{M.S. (Static)} = \frac{F_{TU}}{f_{Bolt}} - 1 \tag{63}$$

$$\text{M.S. (Static)} = \frac{180{,}000}{132{,}000} - 1 \tag{64}$$

$$\text{M.S. (Static)} = +.36 \tag{65}$$

Fatigue Analysis

The fatigue range of external bolt load is from 0 to 6004 pounds.

The corresponding bolt stress range is 68,433 to 89,000 psi.

$$\text{Therefore, } f_{Bolt} = \underline{78{,}720 \pm 10{,}280 \text{ psi}} \tag{66}$$

The ½ in. dia. bolts are made of the same material as the clamp bolts (180 KS steel). The steady stress is similar (80,000 vs 78,720 psi). Therefore, the working endurance limit is identical (E_{36}).

$$E_{36} = \pm 12{,}200 \text{ psi} \tag{67}$$

Margin of Safety

$$\text{M.S. (Fatigue)} = \frac{\pm 12{,}200}{\pm 10{,}280} - 1 = +.18 \tag{68}$$

CLAMP RING ANALYSIS (Figure 69)

Radius of Ring Centroid

$$R = \frac{\Sigma Ar}{\Sigma A} = \frac{(2.5 \times 1.0 \times 8.75) + (2.0 \times 1.5 \times 6.5)}{(2.5 \times 1.0) + (2.0 \times 1.5)}$$

$$R = \frac{21.875 + 19.5}{2.5 + 3.0} = \frac{41.375}{5.5} = \underline{\underline{7.500}} \qquad (69)$$

Moment of Inertia of Cross Section About R

$$I_R = \underline{\underline{.8588}} \qquad (70)$$

Moment of Inertia of Cross Section About Z

$$I_Z = \underline{\underline{10.7194}} \qquad (71)$$

Product of Inertia of Cross Section with Respect to R-Z

$$I_{R-Z} = \underline{\underline{.6550}} \qquad (72)$$

Effective Polar Moment of Inertia

$$J = \underline{\underline{2.4715}} \qquad (73)$$

Young's Modulus = $\underline{\underline{.16\ (10)^6}}$ Titanium 6Al-4V (74)

Torsional Modulus + $6.2\ (10)^6$

Section Modulus About R = $Z_R = \frac{IR}{C} = \frac{.85880}{.864} = \underline{\underline{.994}}\ in.^3$ (75)

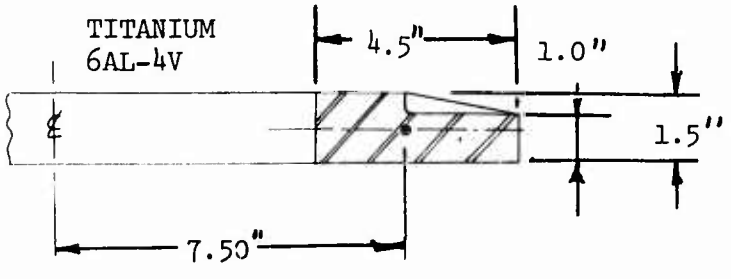

Figure 69. Clamp Ring.

STATIC ANALYSIS (FIGURES 70 to 75)

Load distribution (p_B) due to head moment

No. of Bolts, n = 24 (76)

Bolt load (P_B) = 14,900 lb static ultimate due to head moment

Bolt radius (R_b) = 6.313 (77)

$$P_{B\,(Max)} = \frac{\frac{P_B}{2\pi R_b}}{n} = \frac{14900}{\frac{2\pi \times 6.313}{24}} = \frac{14900}{1.653} = 9000 \frac{lb}{in} \quad (78)$$

THE RUNNING LOAD AND RING GEOMETRIC PROPERTIES ARE INPUTS TO A THIN CIRCULAR RING ANALYSIS COMPUTER PROGRAM. THE RESULTANT SHEARS AND MOMENTS ARE COMPUTED. 16 (Figures 71-74)

MR = MOMENT ABOUT R (RADIAL) AXIS
MT = MOMENT ABOUT T (TANGENTIAL) AXIS
MZ = MOMENT ABOUT Z (VERTICAL) AXIS

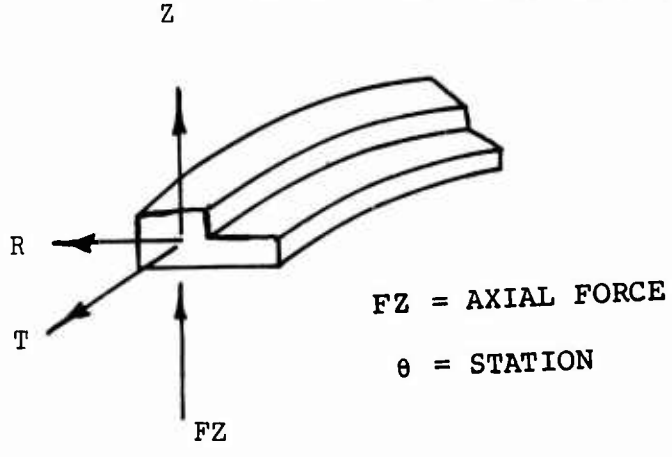

Figure 70. Clamp Ring Load Sign Convention.

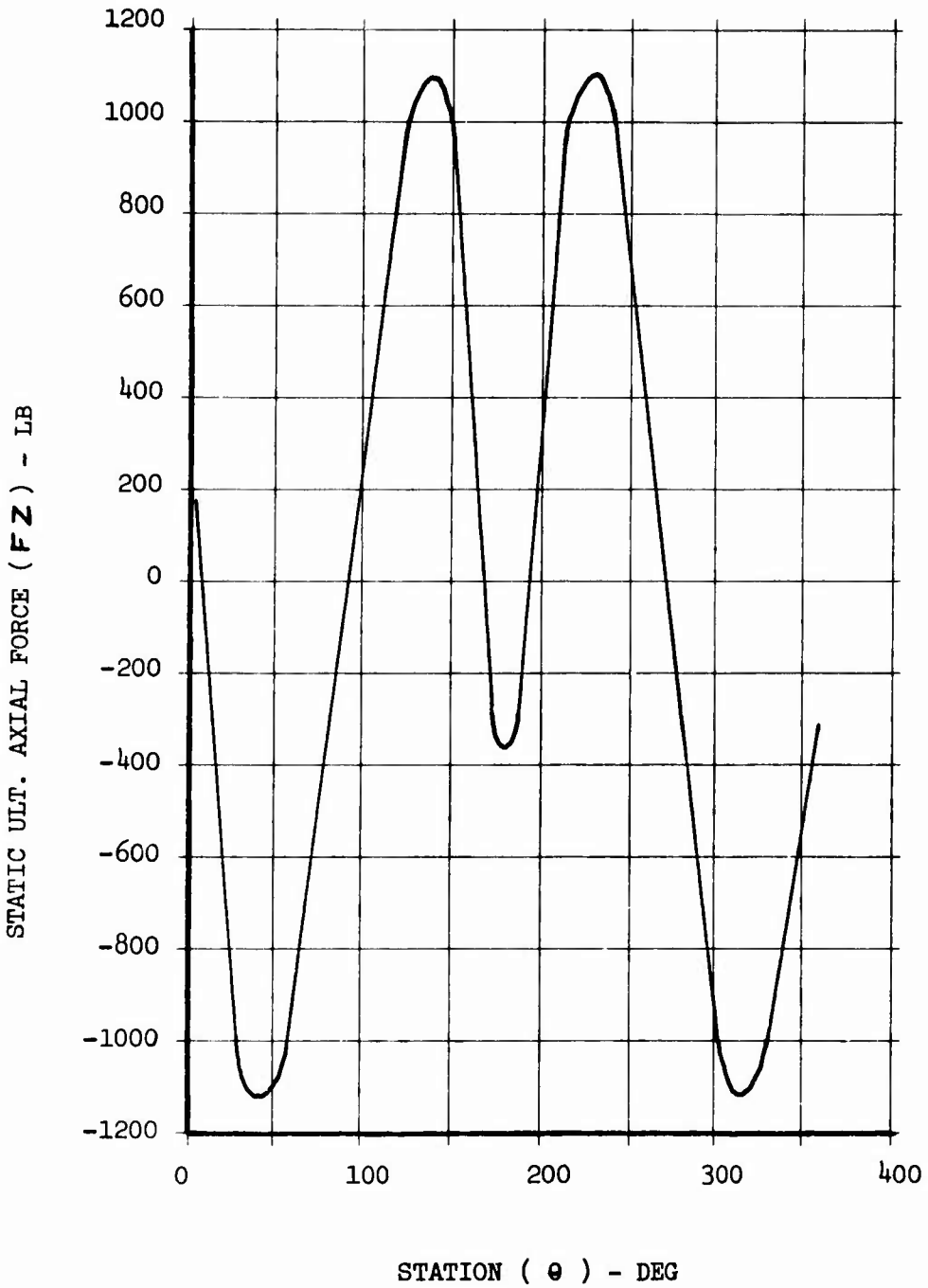

Figure 71. Clamp Ring Static Ultimate Axial Force vs Azimuth Angle.

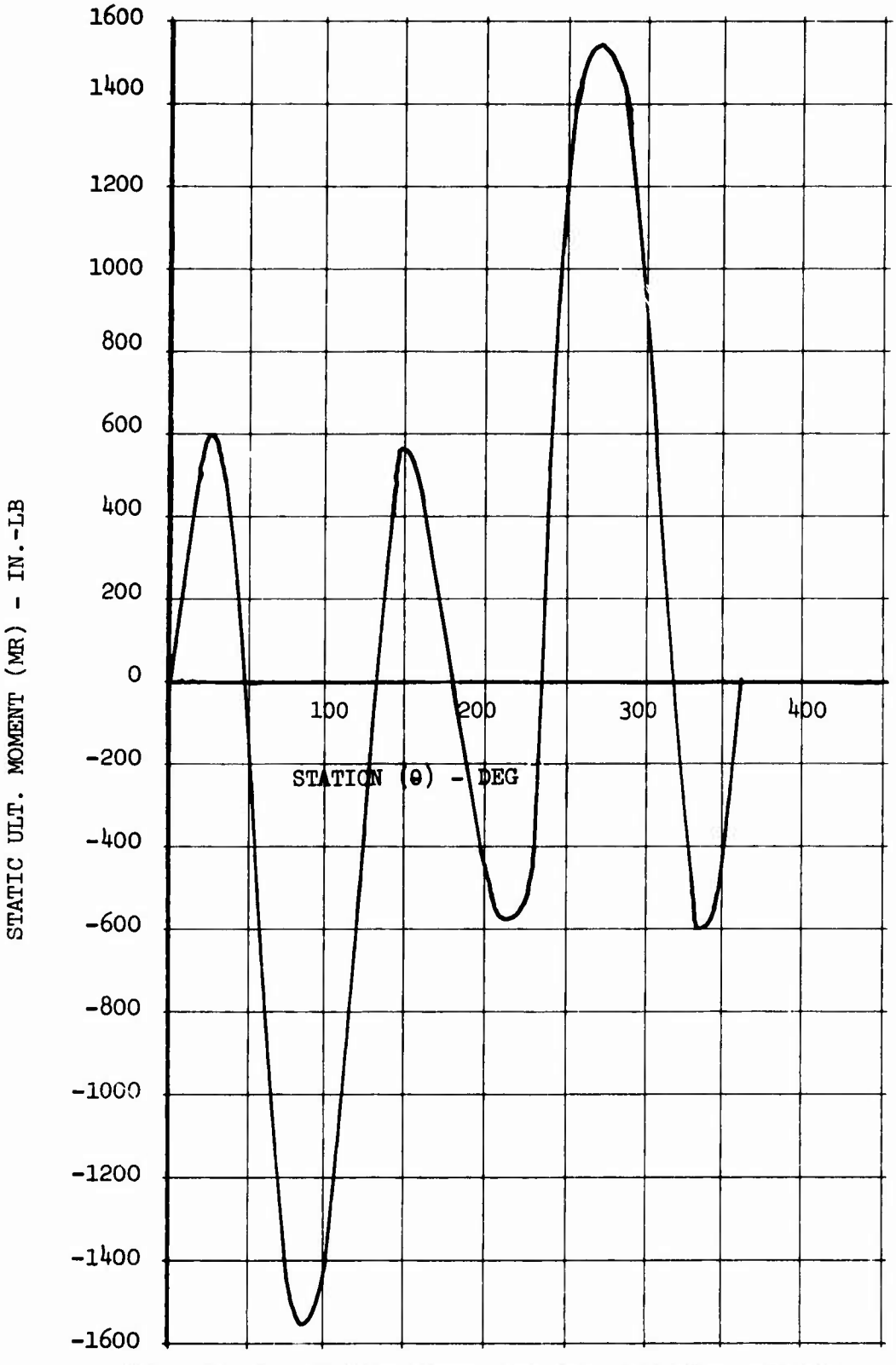

Figure 72. Clamp Ring Static Ultimate Radial Moment vs Azimuth Angle.

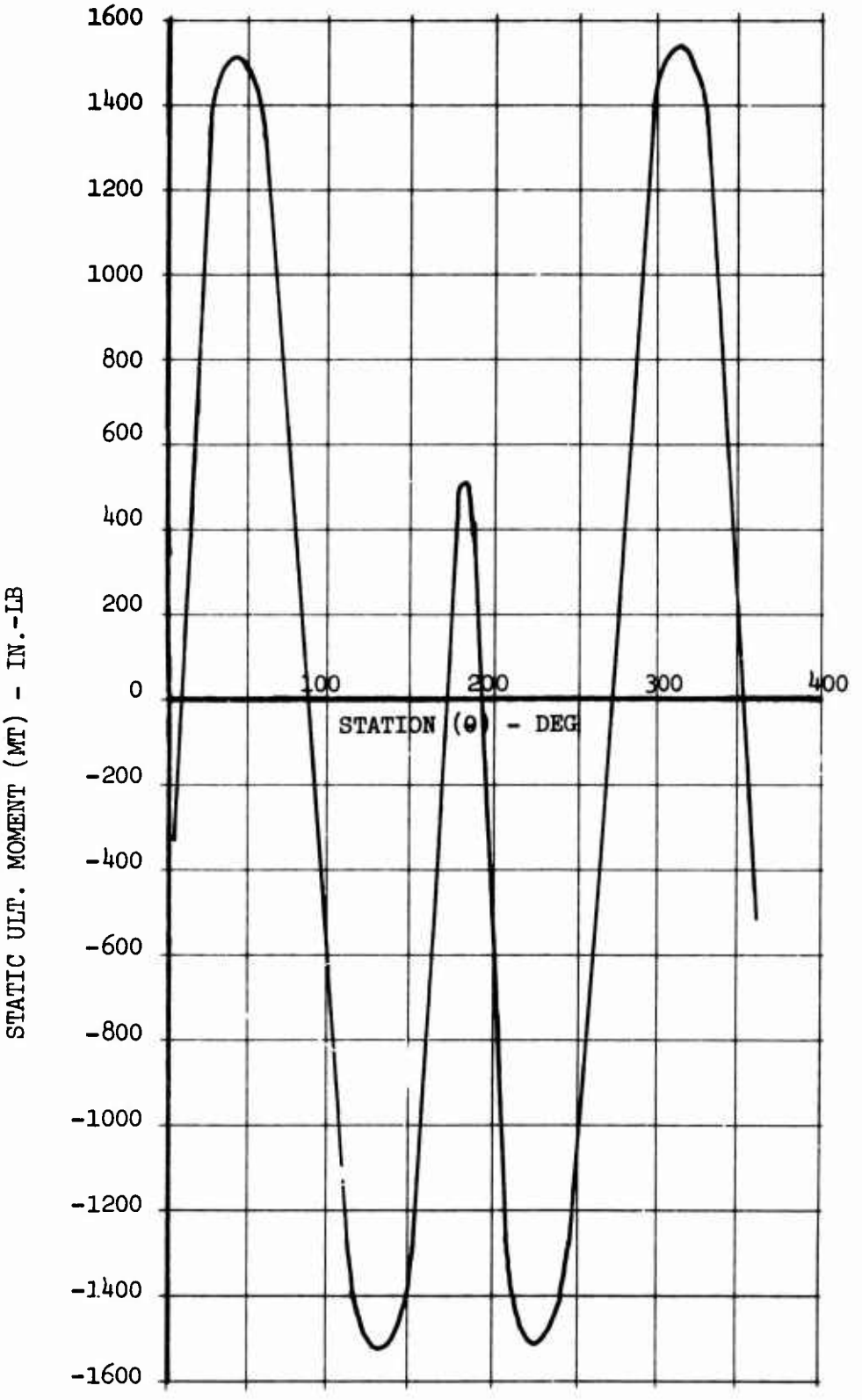

Figure 73. Clamp Ring Static Ultimate Tangential Moment vs Azimuth Angle.

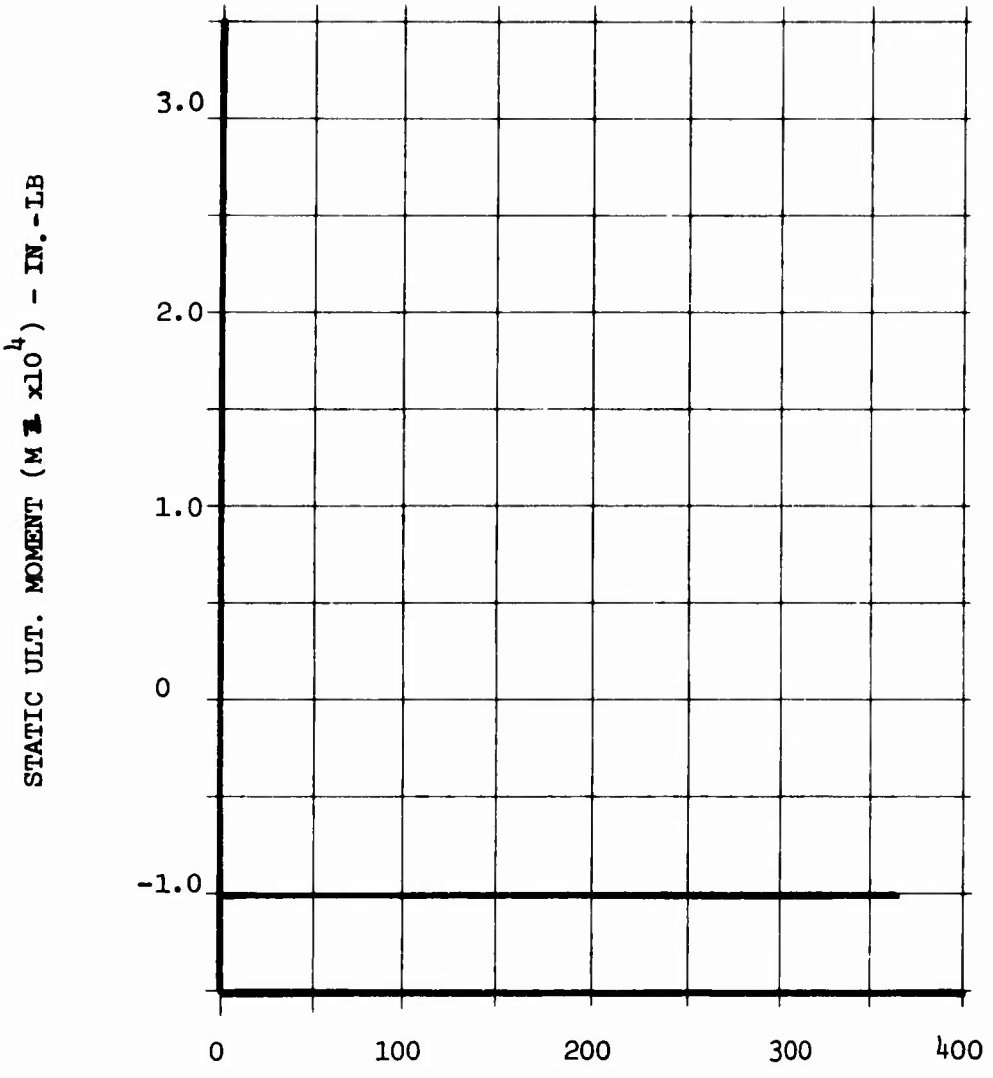

Figure 74. Clamp Ring Static Ultimate Vertical Moment vs Azimuth Angle.

Moment (M_{RC}) About Tangential Axis Due to Uniformly Distributed Load (P_{BRG}), Thrust Condition

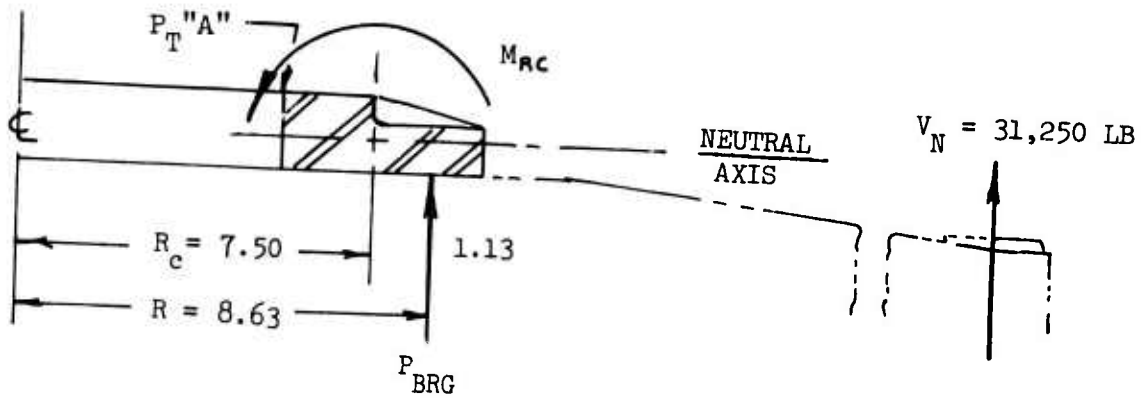

Figure 75. Clamp Ring Loading Due to Thrust.

P_{BRG} due only to thrust load in the six arms is

$$P_{BRG} = \frac{1}{2}\ \frac{6V_N}{2\pi R} = \frac{1}{2}\ \frac{6 \times 31250}{2\pi\ 8.63} = 1730\ \frac{lb}{in.} \qquad (79)$$

$$M_{RC} = P_{BRG} r = 1730\ \frac{lb}{in.} \times 1.13\ in. = 1955\ \frac{lb/in.}{in.} \qquad (80)$$

For a ring under a uniformly distributed moment acting about its axis[17]

$$f_b = \frac{M\ R}{\frac{I}{C}}\ \frac{M_{RC}\ R_C}{Z_{NA}}\ \frac{1955\ \frac{lb/in.}{in.} \times 7.50}{.994} \qquad (81)$$

$$f_b = 14{,}750\ \text{psi at Point "A"} \qquad (82)$$

Margin of Safety

Max. Static Ult Moment about Radial (R) Axis MR = 1448.4 in.-lb

At $\theta = 90°$ δ_L 270°

$$fb_r = \frac{MR}{Z_R} = \frac{14484.4}{.994} = 1457\ \text{psi} \qquad (83)$$

Max. Static Ult. Stress about Tangential (T) Axis

$$fb_t = 14{,}750 \text{ psi} \tag{84}$$

Total Applied Bending Stress (Static Ult)

$$f_{ULT} = fb_r + fb_t \tag{85}$$

$$f_{ULT} = 1457 + 14{,}750 = \underline{\underline{16207}} \text{ psi} \tag{86}$$

$$\text{M.S.} = \frac{F_{tu}}{f_{ULT}} - 1 \tag{87}$$

$$\text{M.S.} = \frac{130000}{16207} - 1 \tag{88}$$

$$\text{M.S.} = +\underline{\underline{\text{HIGH}}} \text{ (Static Ult)} \tag{89}$$

Fatigue Analysis (Figures 76 to 79)

The load distribution due to head moment is derived in the same manner as the static case:

$$\text{No. of Bolts, } h = 24 \tag{90}$$

$$\text{Bolt Load, } P_B = \pm 5280 \text{ lb} \tag{91}$$

$$\text{Bolt Radius, } R_b = 6.313 \tag{92}$$

$$P_B = \frac{\frac{P_B}{2\pi R_B}}{n} = \pm 3200 \text{ lb/in.} \tag{93}$$

Again, this load distribution and ring geometry are inputed into the ring analysis computer program, and resultant shears and moments are obtained.[16] (Figures 75-78)

Moment About Tangential Axis due to Thrust

$$V_N = 5790 \text{ lb}$$

P_{RG} due only to thrust load in the six arms is

$$P_{RG} = \frac{1}{2} \frac{6V_N}{2\pi R} = \frac{1}{2} \frac{6 \times 5790}{2\pi\ 8.63} = 321 \frac{\text{lb}}{\text{in.}}$$

$$M_{RC} = P_{BRG} r = 321 \frac{\text{lb}}{\text{in.}} \times 1.13 \text{ in.} = 362 \frac{\text{lb/in.}}{\text{in.}}$$

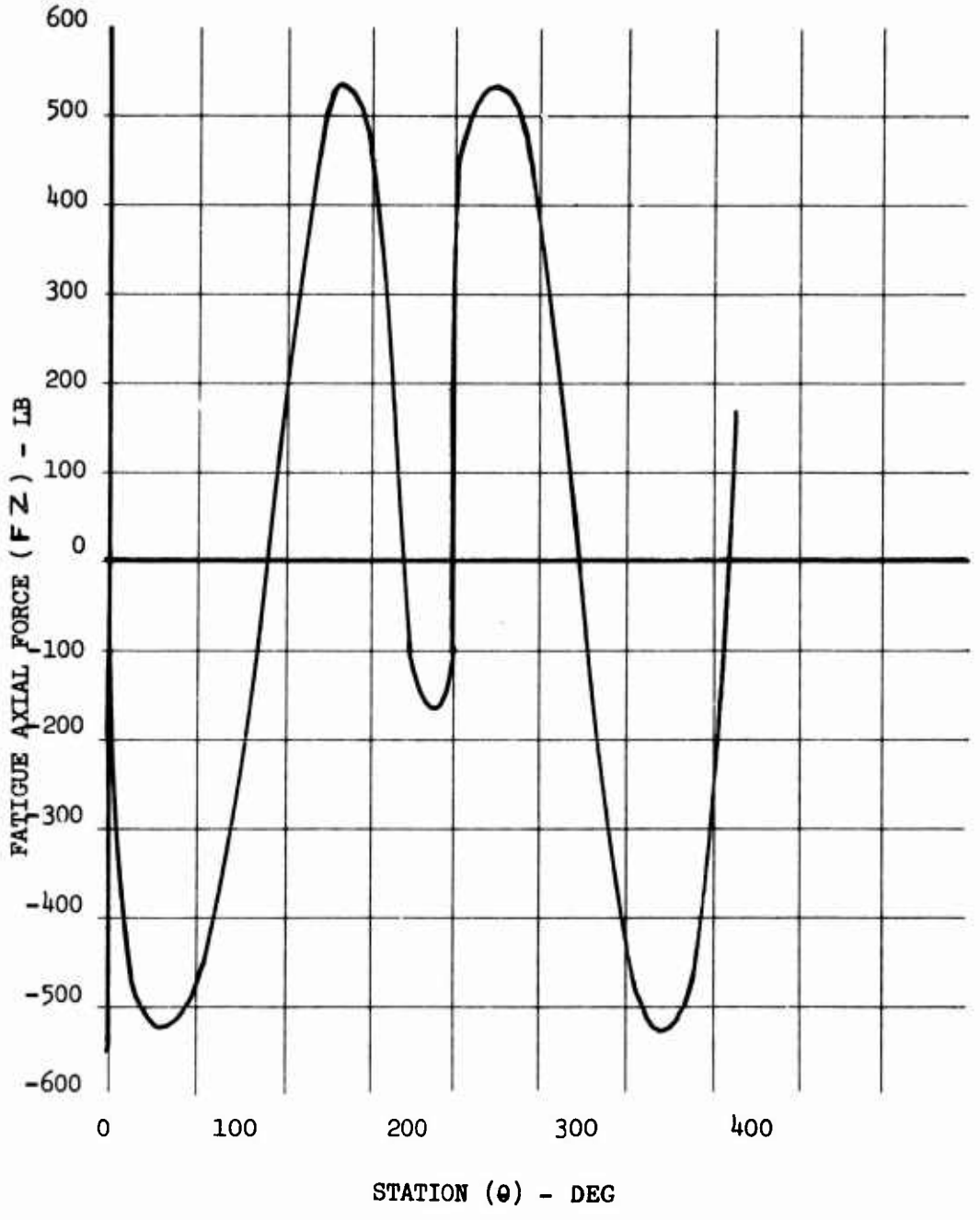

Figure 76. Clamp Ring Design Vibratory Axial Force vs Aximuth Angle.

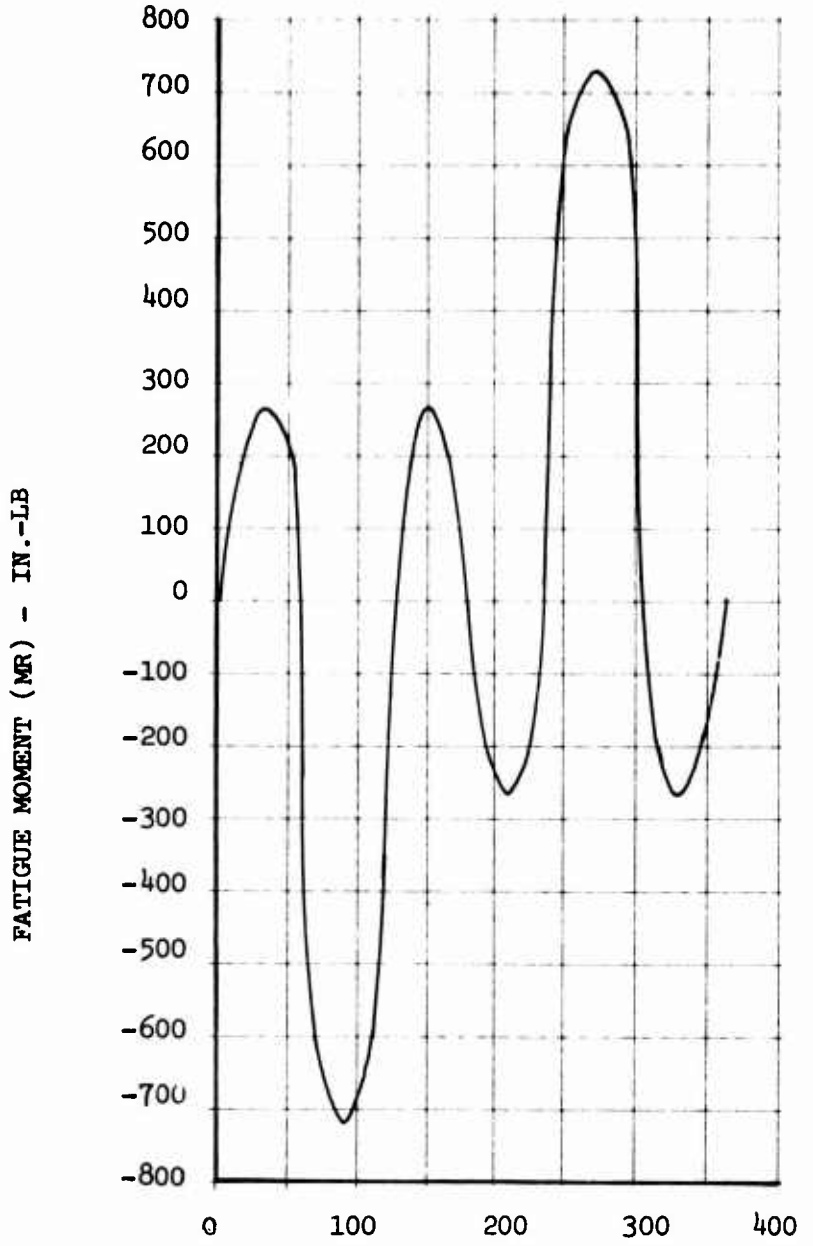

Figure 77. Clamp Ring Design Vibratory Radial Moment vs Azimuth Angle.

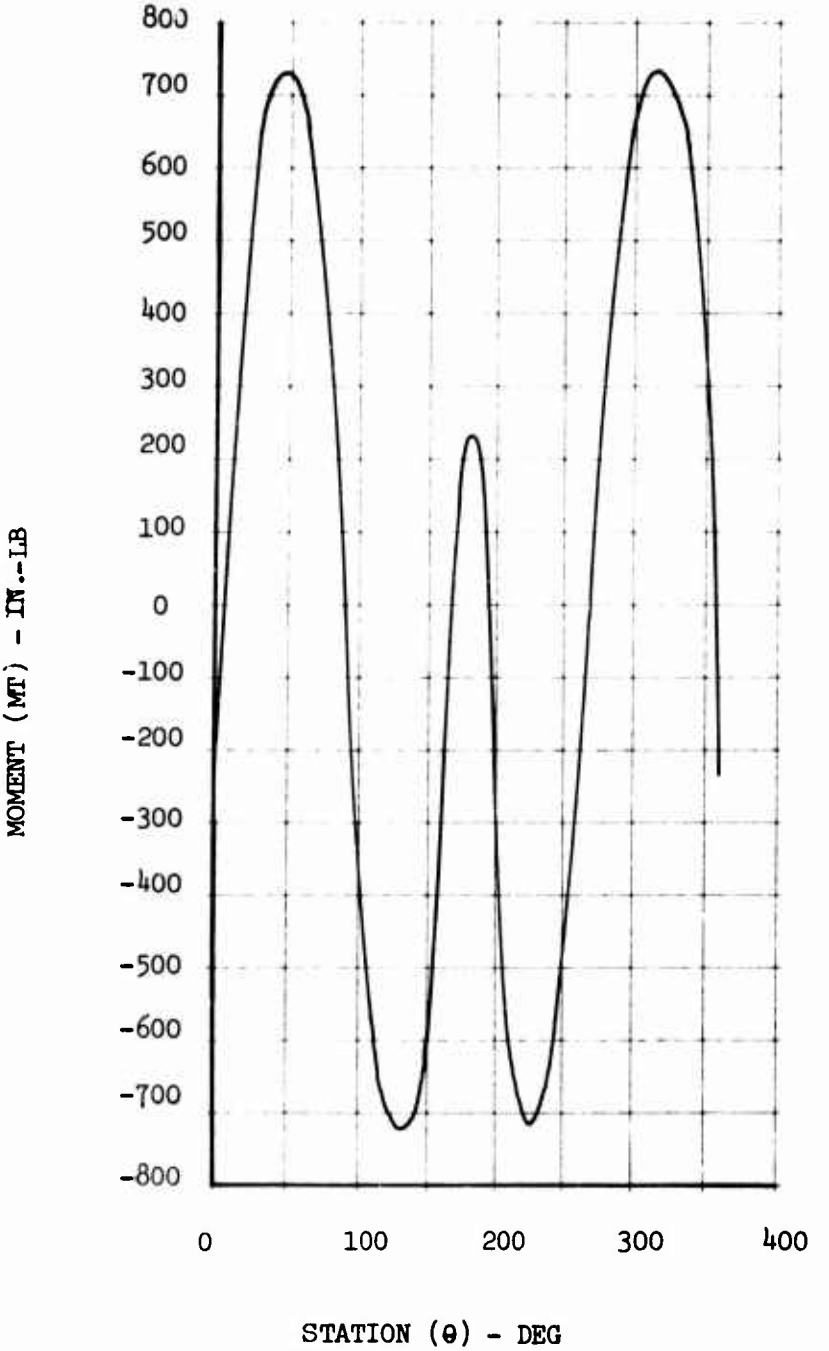

Figure 78. Clamp Ring Design Vibratory Tangential Moment vs Azimuth Angle.

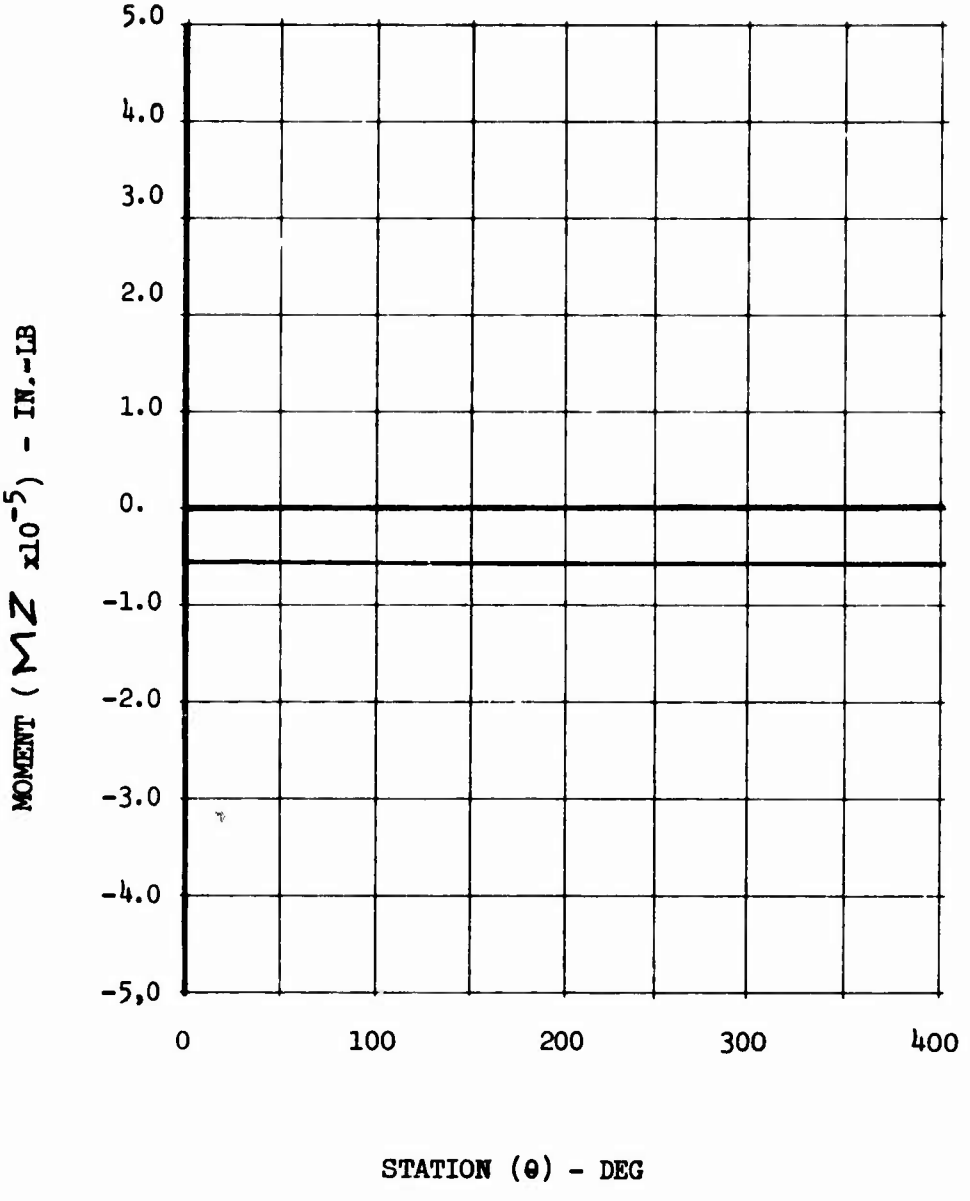

Figure 79. Clamp Ring Design Vibratory Vertical Moment vs Azimuth Angle.

For a Ring Under a Uniformly Distributed Moment Acting About Its Axis [17]

$$f_b = \frac{M\ R}{\frac{I}{C}} = \frac{M_{RC}\ R_C}{ZNA} = \frac{362\ \frac{lb/in.}{in.} \times 7.50\ in.}{.994} \quad (97)$$

$$f_b = \underline{\underline{2731}}\ psi \text{ at Point "A"} \quad (98)$$

Margin of Safety (Fatigue)

Moment About Radial Axis (M_R)

$$M_R \text{ (Peak to Peak)} = 1540\ in.\text{-}lb \quad (99)$$

$$M_R = \pm 770\ in.\text{-}lb \quad (100)$$

Moment About Z Axis (M_Z)

$$M_Z = -.5\ in.\text{-}lb \text{ (Constant)} \quad (101)$$

$$\underline{M_Z \text{ is negligible}} \quad (102)$$

Total Stress in Bending

$$f_b = 2731 + \frac{770}{Z_R} \quad (103)$$

where $Z_R = .994$ (104)

$$f_b = 2731 \pm 775\ psi \quad (105)$$

Based on the allowable fatigue stresses for 6 Al-4V titanium (Reference 14)

$$E = \pm 45{,}000\ psi \quad (106)$$

Therefore for an applied stress of ± 775 psi, the Fatigue Margin of Safety is high.

CENTRAL HUB ANALYSIS (Figure 80)

The titanium central hub forms the interface between the hub arm and the main rotor shaft. The hub can be idealized as a thick-wall cylinder with flanges located at the mid-point and base of the hub. The thrust and head moment are reacted generally by the mid-flange/arm attachment and clamp ring attachment. The thrust is assumed to be a steady running load of constant magnitude, and the head moment a vibratory sinusoidally distributed running load.

The hub region below the mid-flange is identical with the CH-53B production titanium hub. Therefore, only the upper half (above the central spline) was analyzed.

A shells-of-revolution computer program (Reference 18) was used as the analytical tool. This program defines the peak stress level as well as the stress range around the periphery of the hub. The allowable stress levels used were based on titanium (6AL-4V) forging data.[14]

Static Analysis (Figure 81)

The outside surface of Element No. 30 was found to be critical in compression.

$$f_c = 81{,}470 \text{ PSI Ultimate} \tag{107}$$

$$F_{cu} = F_{TU} \text{ for 6AL-4V Titanium} \tag{108}$$

$$F_{TU} = 130{,}000 \text{ PSI}^{13} \tag{109}$$

Margin of Safety

$$\text{M.S. (Static)} = \frac{F_{TU}}{f_{e\,(ULT)}} - 1 \tag{110}$$

$$\text{M.S. (Static)} = \frac{130{,}000}{81{,}470} = 1 \tag{111}$$

$$\text{M.S. (Static)} = +.60 \tag{112}$$

Fatigue Analysis (Figures 82 to 84)

The outside surface of Element No. 30 is critical in fatigue.

Stress range is from +17,200 to -25,320 psi

$$\text{Mean} = \frac{\text{MAX} + \text{MIN}}{2} = \frac{25{,}320 + 17{,}200}{2} = 21{,}260 \text{ lb}$$

$$\text{Vibratory} = \frac{\text{MAX} - \text{MIN}}{2} = \frac{25{,}320 - 17{,}200}{2} = \pm 4060 \text{ lb}$$

Fatigue Allowable

The small specimen endurance limit for a slightly worked 6AL-4V titanium forging with a thick cross section $\bar{E}$ at a mean stress of 21,260 psi[14]:

$$\bar{E} = \pm 21{,}000 \text{ psi (Open Section, Shot Peened)} \tag{116}$$

Size Effect Factor f_{SE}

$$f_{SE} = .7 \tag{117}$$

Reliability Factor $f_{3\sigma}$

$$f_{3\sigma} = .7 \tag{118}$$

Since the element size in the critical region inputed into the computer analysis is fine enough to take into account stress gradients, the stress concentration is neglected. Therefore, the K_T was assumed to be unity.

The working endurance limit $E_{3\sigma}$ is

$$E_{3\sigma} = \bar{E} \times f_{SE} \times f_{3\sigma} \tag{119}$$

$$E_{3\sigma} = \pm 21{,}000 \ (.7) \ (.7) \tag{120}$$

$$E_{3\sigma} = \pm 10{,}300 \text{ psi} \tag{121}$$

Margin of Safety

$$\text{M.S. (Fatigue)} = \frac{E_{3\sigma}}{\sigma_s} = -1 \tag{122}$$

$$\text{M.S. (Fatigue)} = \frac{\pm 10{,}300}{\pm 4060} = -1 \tag{123}$$

$$\text{M.S. (Fatigue)} = +1.54 \tag{124}$$

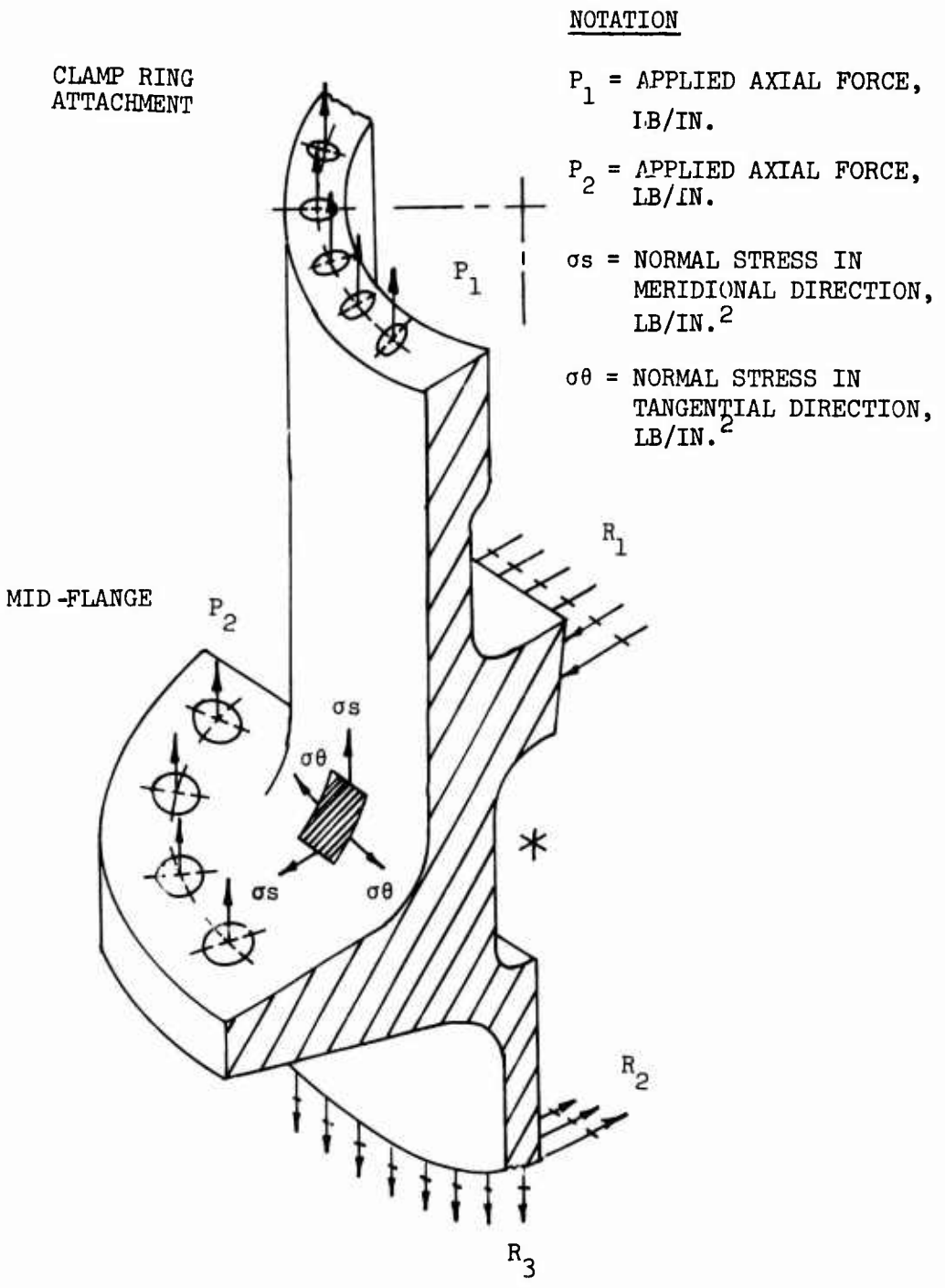

Figure 80. Central Titanium Hub Applied Loads and Reactions.

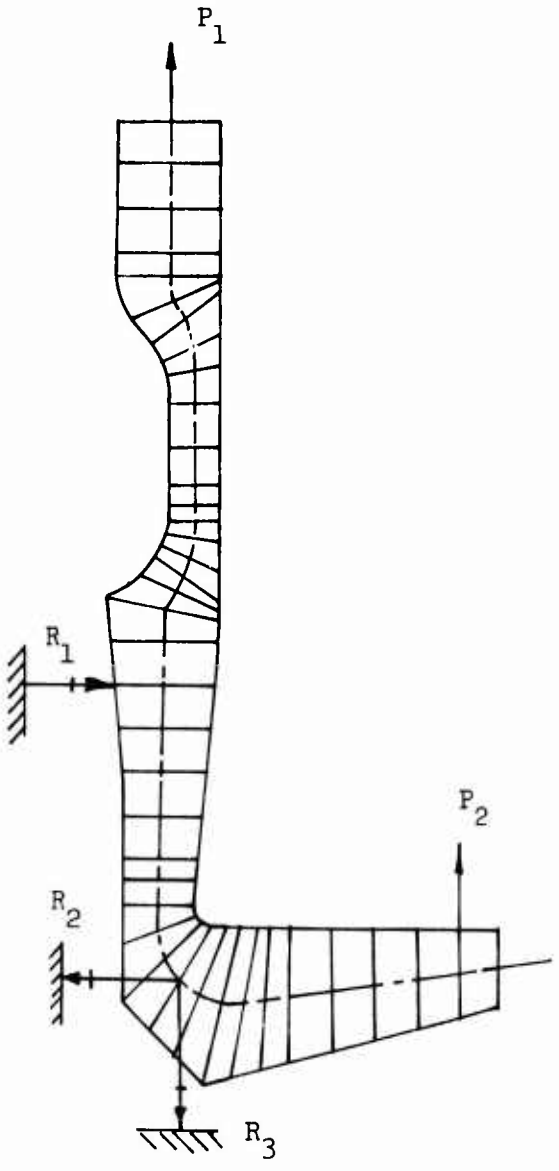

CASE	UNIFORM DISTRIBUTION DUE TO THRUST		SINUSOIDAL DISTRIBUTION DUE TO HEAD MOMENT	
	P_1 lb/in.	P_2 lb/in.	P_1 lb/in.	P_2 lb/in.
STATIC ULT.	-1730	-1730	-4800	-4800
FATIGUE	-321	-321	-1712	-1712

Figure 81. Central Hub Finite Element Computer Model.

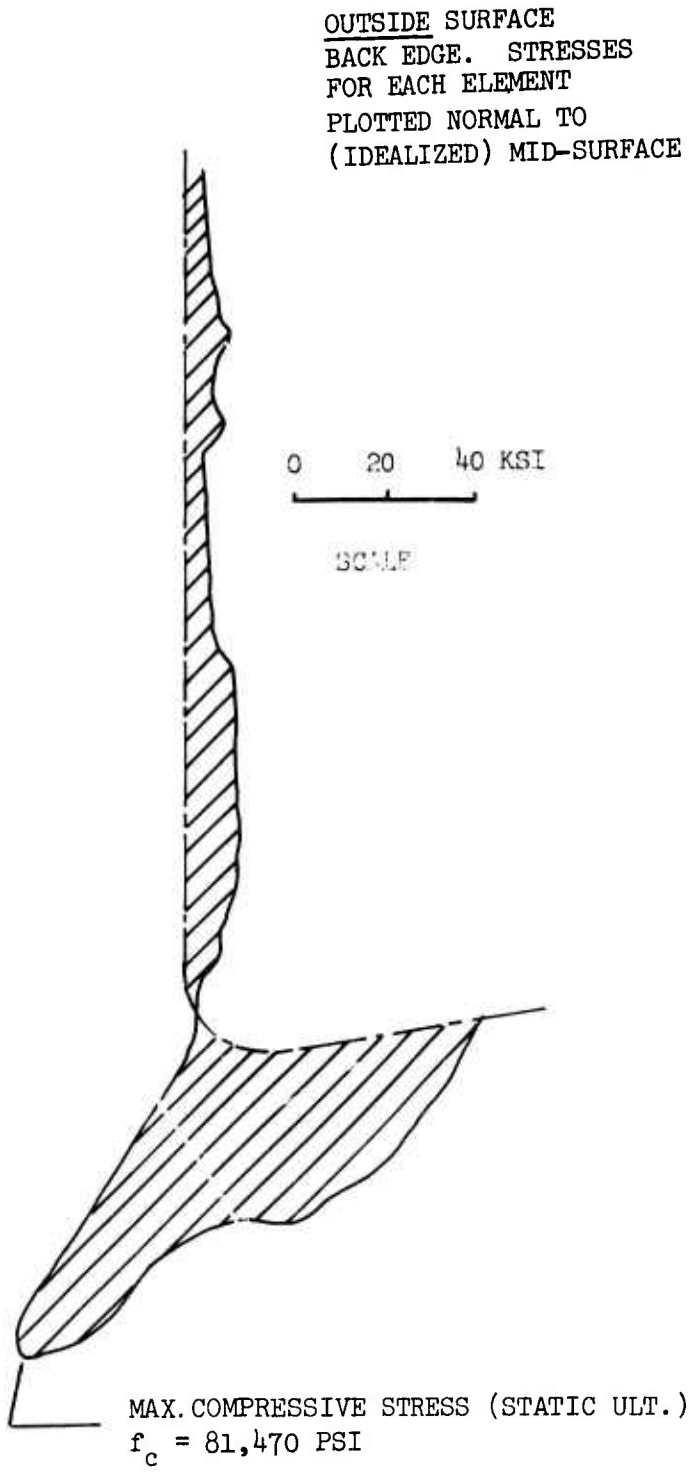

Figure 82. Central Hub Stress Distribution (O.D.) Ultimate Load Case.

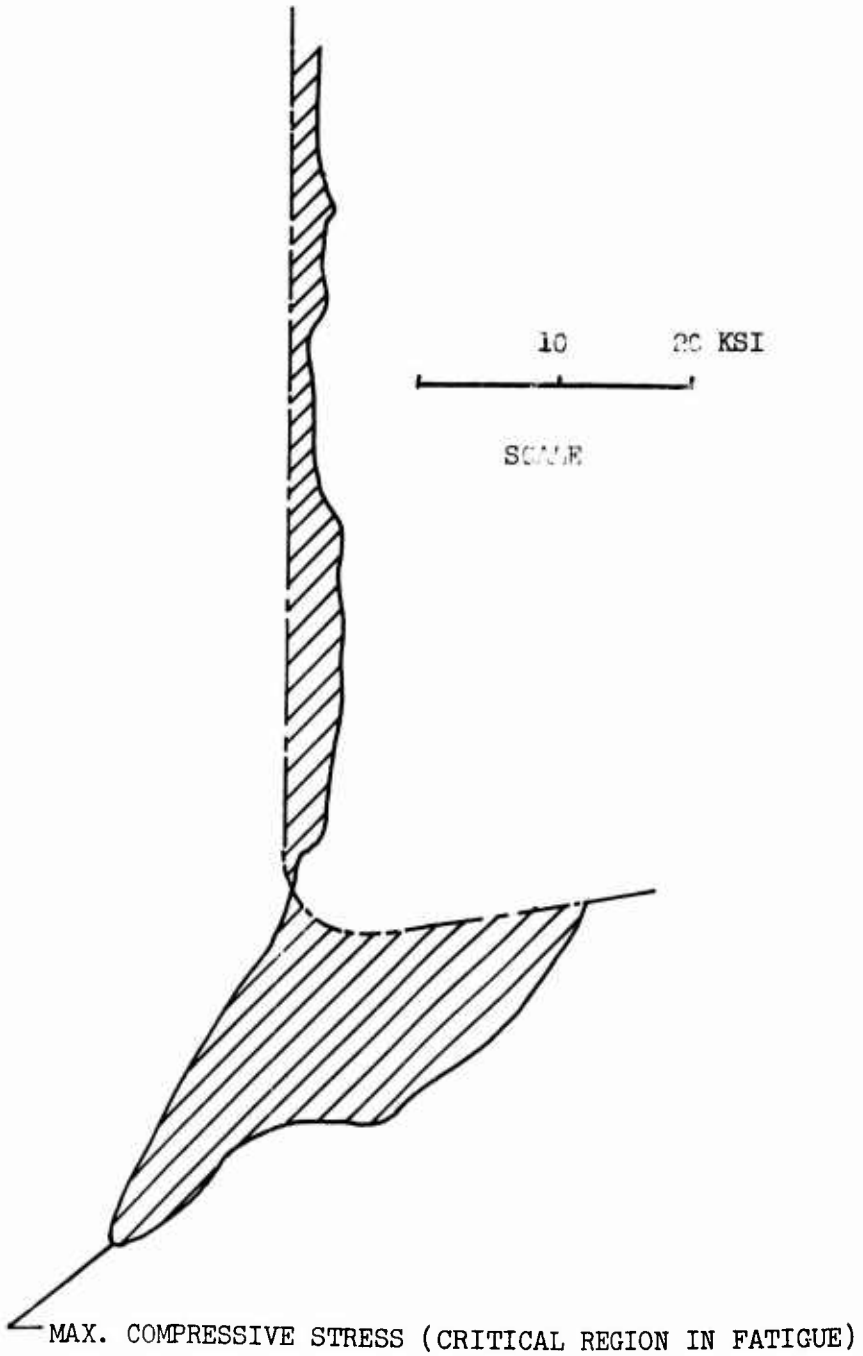

Figure 83. Central Hub Stress Distribution (O.D.) Fatigue Load Case.

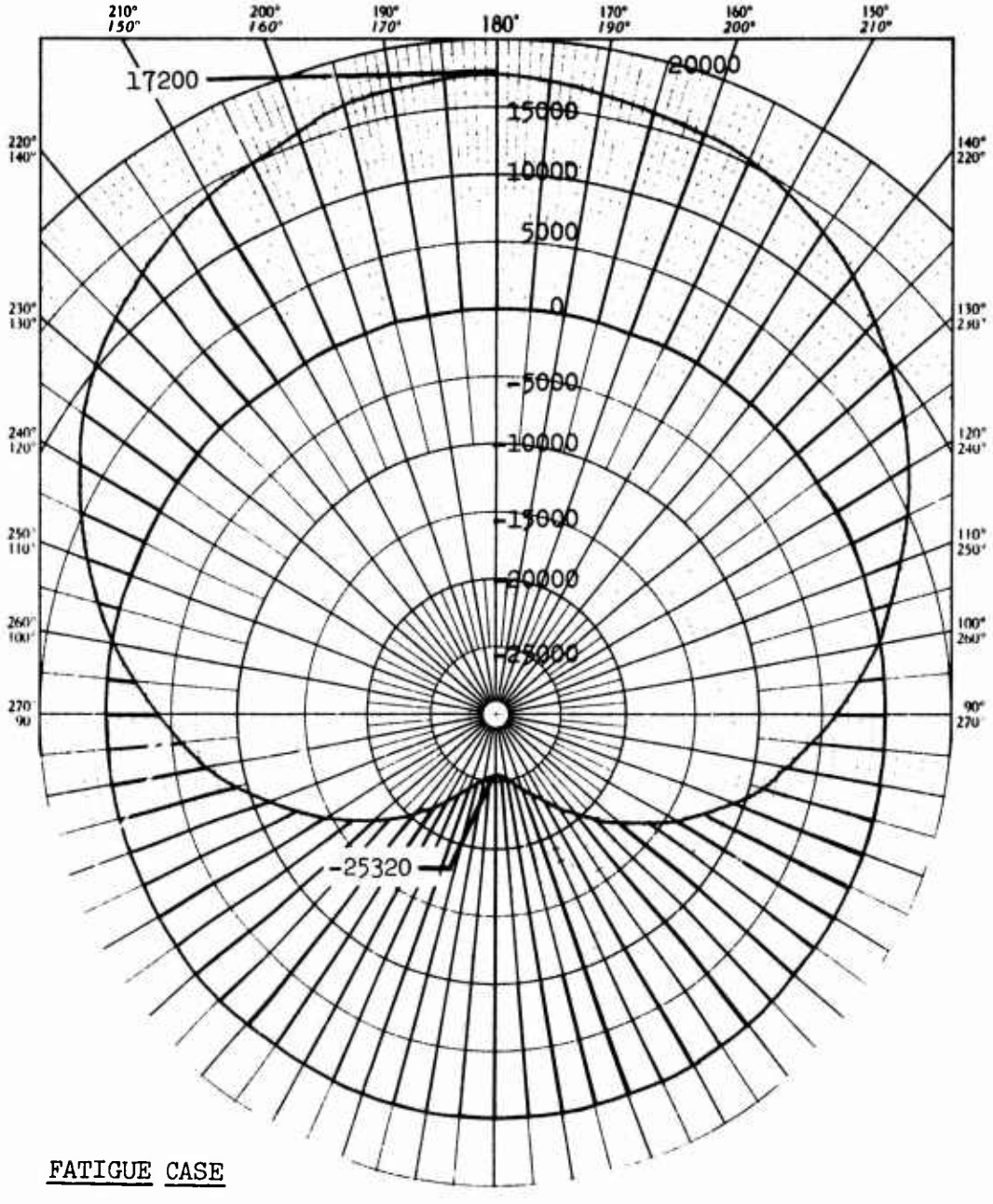

FATIGUE CASE

ELEMENT NO. 30

σs (NORMAL STRESS) VS
θ (AZIMUTH POSITION)

Figure 84. Central Hub Stress Distribution Around Periphery at Critical Element.

BEARING CARTRIDGE (Figure 85)

The main rotor blade lag hinge is incorporated in the hub 24 inches from the center of rotation. The lag motion is provided by a set of preloaded tapered roller bearings. These bearings are housed in a titanium cartridge inserted into the bore in the arm extremities. The cartridge is clamped to the laminate assembly with a ring nut.

The blade coning and flapping motion results in an out-of-plane (vertical) shear force being applied to the bearings. This shear force (V_N) is reacted by the lower cartridge lip (when upward) or the cartridge nut (when downward). Preliminary analysis indicates that Section A-A is critical for both the upward and downward shear load conditions.

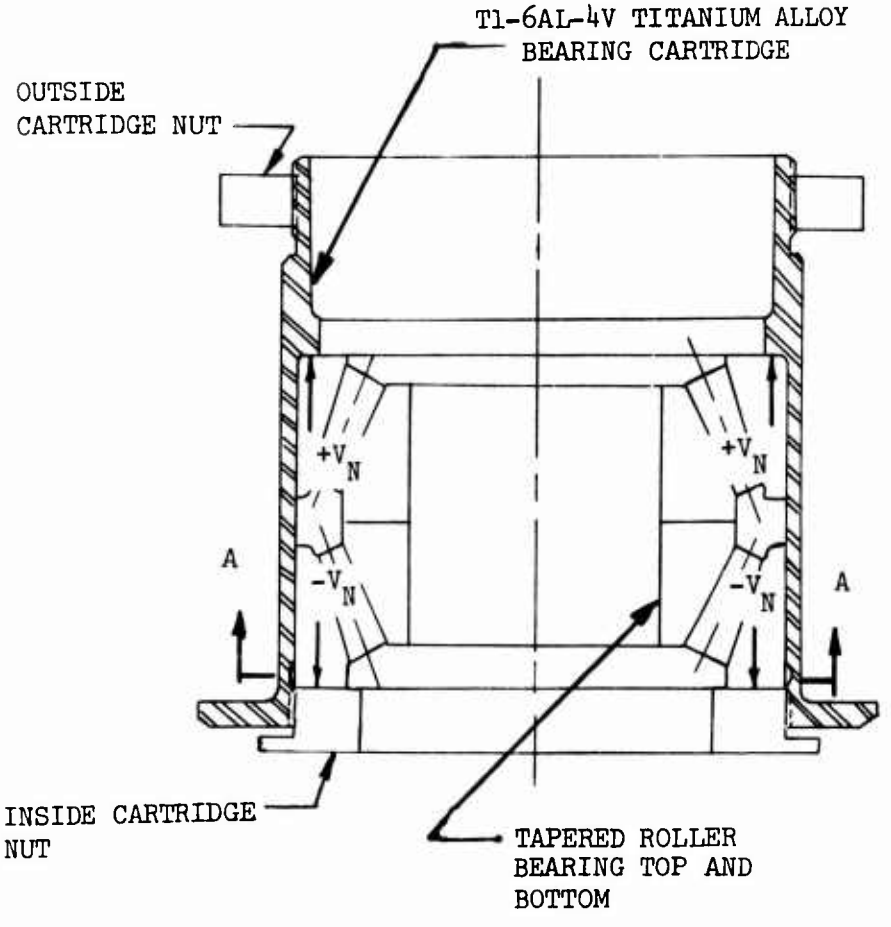

Figure 85. Hub Arm Bearing Cartridge Loading.

Bearing Cartridge Analysis

Section A-A is critical for both positive and negative vertical shear (V_N) loading.

A - Area
ID - Inside Diameter
OD - Outside Diameter

$$A = \frac{\pi}{4} (OD)^2 - (ID)^2 \qquad A = \frac{\pi}{4} (5.7)^2 - (5.525)^2 = 1.54 \text{ sq in.} \tag{125}$$

Static Analysis

$V_{N\ ULT} = 54840$ lb $\quad F_{tu} = 130{,}000$ psi[13] ULT Tensile Stress (Allowable Stress)

$$\frac{V_{N\ ULT}}{A} = \frac{54840}{1.54} \tag{126}$$

$$= 35{,}610 \text{ PSI (Applied Stress)} \tag{127}$$

Margin of Safety (Static Ultimate

$$M.S. = \frac{\text{Allowable Stress}}{\text{Applied Stress}} - 1 \tag{128}$$

$$M.S. = \frac{130{,}000}{35610} = -1 + \text{HIGH} \tag{129}$$

Preliminary analysis indicates that Section A-A is critical. Section A-A is subjected to a tension load whether the out-of-plane shear (V_N) is acting upward or downward. The relationship between the tensile load at A-A and the out-of-plane shear is determined. Also, the assumed variation of tensile load at Section A-A is determined.

Fatigue Analysis (Figure 85)

Equivalent fatigue stress at bearing cartridge Section A-A = f_{tAA} = $\frac{V_{N\ A\text{-}A\ (Assumed)}}{A_{A\text{-}A}}$

$$V_{N_{A\text{-}A}} = 8630 \pm 8630,\ V_{N_{A\text{-}A}}\ (Max) = 17260 \tag{130}$$

$$f_{t_{A\text{-}A}} = \frac{8630 \pm 8630}{1.54} \tag{131}$$

$$f_{t_{A\text{-}A}} = \underline{\underline{5600 \pm 5600 \text{ psi}}} \tag{132}$$

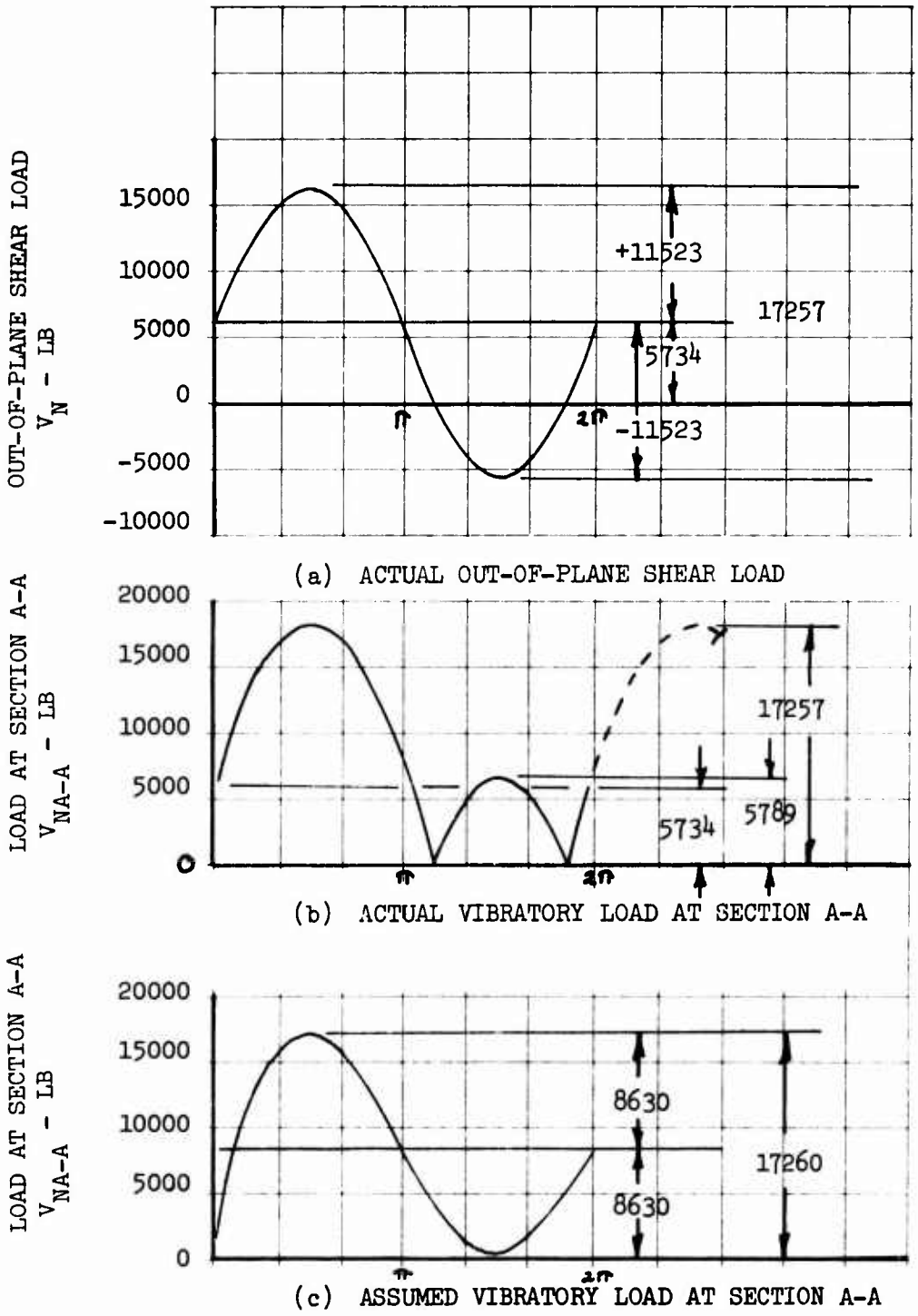

Figure 86. Out-of-Plane Shear Loading and Resultant Stress at Section A-A.

Allowable Stress

6 AL-4V Titanium Alloy
(Moderately thick section, moderately worked, shot peened)

The mean small specimen endurance ~ $\bar{E}$ ~ limit at a mean stress of 5600 psi

$$\bar{E} = 45{,}000 \text{ psi}^{14} \tag{133}$$

The working endurance limit for an open smooth section E 3σ ($K_t = 1$)

$$E\,3_\sigma = \bar{E}\,(f_s)\,(f_R) \tag{134}$$

where f_s = Size Effect Factor = .7 (135)

f_R = Reliability Factor = .7 (136)

Therefore,

$$E\,3_{\sigma(K_t=1)} = \pm 22{,}000 \text{ psi} \tag{137}$$

Stress Concentration Factor K_t For Section A-A Assumed as a Flat Bar with a Shoulder Fillet (in Tension)[15]

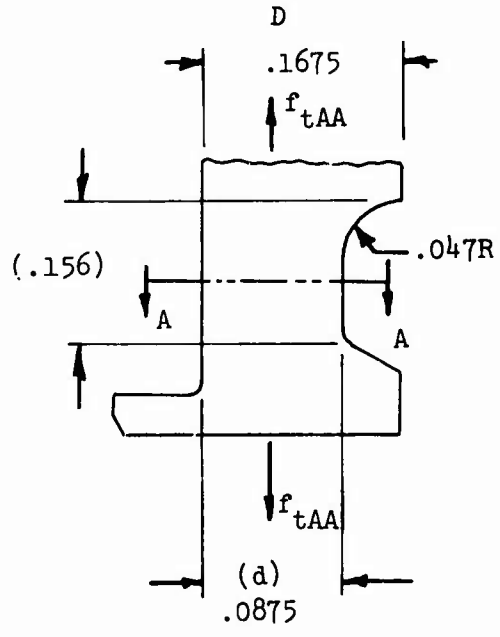

Figure 87. Section A-A Geometry.

$$\frac{D}{d} = \frac{.1675}{.0875} = 1.91 \tag{138}$$

$$K_t = 1.5$$

$$\frac{r}{d} = \frac{.047}{.0875} = .54 \tag{139}$$

Working endurance limit for a K_t of 1.5 $E_{3b\ (K_t = 1.5)}$

$$E_{3\sigma\ (K_t = 1.5)} = \frac{E_{3\sigma\ (K = 1)}}{1.5} = \frac{\pm 22{,}000}{1.5} = \pm 14{,}670 \text{ psi Allowable} \tag{140}$$

Margin of Safety (Fatigue)

$$M.S. = \frac{\pm 14{,}670}{\pm 5600} - 1 = + \text{HIGH} \tag{141}$$

Static Analysis

Ultimate Tensile Load at Section A-A = V_N (ULT) = 54,840 lb (142)

$$f_{tAA} = \frac{V_{N(ULT)}}{A} \tag{143}$$

$$f_{tAA} = \frac{54840}{1.54} \tag{144}$$

$$f_{tAA} = 35{,}050 \text{ psi ult} \tag{145}$$

FTU (6AL-4V Titanium) = 130,000 psi

Margin of Safety M.S. ULT

$$M.S.\ ULT = \frac{F_{tu}}{f_{tAA}} - 1 \tag{146}$$

$$M.S.\ ULT = \frac{130{,}000}{35{,}050}^{13} - 1 \tag{147}$$

$$M.S.\ ULT = + \text{HIGH} \tag{148}$$

ANALYTICAL SUMMARY

The incorporation of the proposed design modifications into the basic tension strap hub concept results in a rotor head that is structurally flightworthy. The modified composite hub, called the splayed laminate hub, has approximately twice the bending strength of the original configuration at the same weight. The two basic flaws of the original design have been eliminated: lack of vertical shear resistance, and head moment transfer to the central hub.

Tapering the hub arm by incorporating tapered spacers has improved the strength of the hub in reacting out-of-plane shears. The flatwise bending stiffness is increased, due to the increased depth of the arm at the inboard end. Also, the graphite straps located at the extremities of the arm cross section react part of the out-of-plane shear load. These straps are inclined so that the axial reactive force due to bending results in a component out-of-plane that is equal to 25% of applied shear load. This additional shear load path is redundant with respect to the primary vertical shear load path of the web located around the hub periphery.

The head moment transfer in the central hub is now structurally adequate for all static and fatigue load conditions. The reaction to the head moment is across a large-diameter bolt circle instead of an inefficient bearing couple around the hub diameter. The clamp ring permits sufficient clamping of the laminated assembly to eliminate rocking between the laminates and central hub. This clamp ring arrangement was chosen from a number of concepts by virtue of its low risk, but this low risk results in a weight penalty. A more efficient attachment would involve an extensive development program.

With the incorporation of the design modifications into the basic tension strap concept, the main rotor hub becomes structurally more efficient from a weight standpoint. The redesigned hub has twice the bending strength of the original hub when reacting out-of-plane load paths are provided. Also, the load transfer across bonded joints is minimized. Adhesives are loaded in shear only in areas where there is adequate bond to provide adequate load transfer rates.

CONCLUSIONS

1. A flightworthy hub can be designed employing the strap concept provided provisions are made to transfer the shear loads perpendicular to the straps. The off-axis strap concept selected is one way of overcoming the shear deficiency of the flat strap concept.

2. When mechanical interface constraints are imposed on the application of composites, a less than optimum solution results. The redesigned hub is 270 lb heavier than its titanium counterpart. This overweight would not be present if greater design freedom was allowed.

3. The higher hub weight will not present an effective evaluation of the strap concept during a fabrication and test follow-on program.

4. The three-dimensional complexity of the central hub strap junction area can only be structurally substantiated by full-scale testing. The large stiffness changes occurring across strap layers can induce a three-dimensional stress stage very difficult to qualify.

5. No alteration of the existing bearing lives in the vertical hinge area is expected. The redesigned hub has a stiffness that is equivalent to the titanium hub. Therefore, bearing axis rotations due to hub deflections will be unchanged.

6. The redesigned hub has static and fatigue strength margins equal to or greater than the existing titanium hub.

PHASE III

The objective of Phase III was to define a plan for developing the splayed laminate concept into a flightworthy structure. The plan includes manufacturing development, ground fatigue and whirl test, and limited flight test.

The manufacturing plan will develop tooling capable of fabricating the individual components and assemblies within the dimensional tolerance and with the appropriate properties specified by the design organization. This plan will also involve a design trade-off study, which will identify and incorporate design changes to facilitate fabrication.

Ground testing will consist of static and fatigue testing of a complete hub assembly under combined thrust, torque, centrifugal force, and head moment. The strength of the composite hub will be compared with the strength of the existing titanium hub. If the resulting static and fatigue strength is found to be adequate, a stress and motion survey and a limited endurance test will be performed on a whirl test facility. On completion of ground testing, a decision will be made as to the flight adequacy of the rotor head used in the whirl test program. If found satisfactory, a flight test of not longer than ten hours will be performed. The composite rotor head will be instrumented and installed on a CH-54B aircraft, and a structural shakedown flight test will be performed.

This section of the report contains a summary of the effort required during the hardware development phase, as well as a proposed schedule for the development, fabrication, and testing of a composite hub.

Appendix I contains the detail fabrication, static and fatigue testing, and flight test plans. The manufacturing development plan was formulated by Whittaker Corporation, under contract to Sikorsky Aircraft.

HUB CONFIGURATION FINALIZATION, DESIGN, AND FABRICATION

Review configuration by USAAMRDL, Sikorsky, and Whittaker. If additional hub design trade-offs are required, conduct design concept refinement studies. Conduct weight reduction program.

Fabricate and test structural models of high-risk areas to reveal high-stress areas and failure modes that can be corrected prior to full-scale fabrication. Test to failure up to two specimens of at least three high-risk areas.

Fabricate wooden mock-up of full-scale hub to confirm structural load path interactions in the central hub zone. Modify detail geometry of laminates on the mock-up if necessary.

Prepare detail design drawing and conduct detail structural analysis of splayed laminate composite hub.

Conduct manufacturing risk reduction effort. Fabricate tooling and laminate subassemblies in order to define tooling and fabrication problems. Whittaker Corporation will participate in development of tooling and cure cycles.

Procure material for three hubs and one spare. Fabricate and test sample coupons to verify material properties.

Fabricate tooling required to manufacture details, subassemblies, and assemblies for three complete hubs.

Identify strain gage locations to be applied to subassemblies.

Fabricate and instrument three hubs.

The contracting agency shall supply details and assemblies required to assemble one rotor head.

Assemble one rotor head.

Statically test one hub to limit head moment, thrust, and shaft torque. Measure hub arm bending and radial spring rates and deflections.

GROUND TEST

Fatigue test the static test hub plus one additional hub under normal flight loads, with accelerations on head moment only, in accordance with the structural substantiation process used for the CH-53A main rotor head (Reference 11). Apply overspeed RPM cycles at specified intervals during fatigue testing. Test rotor heads to failure or 4 $(10)^6$ cycles, whichever occurs first. Compare hub strength with the existing endurance limit of the CH-53A titanium hub (Reference SER-65068).

After laboratory testing, check two fatigue test heads for bending and radial stiffness. Tear down these hubs for engineering evaluation of failure modes, stiffness degradation, etc. Evaluate overall design. Document design improvements for increased strength, lower weight, and lower cost, if necessary. Submit final report containing structural substantiation, test results, and final evaluation. Establish adequacy of the hub for flight testing.

A report will be submitted documenting the results of the small

specimen tests risk reduction and static test results.

The ground test results and subsequent engineering analysis and structural evaluating will be documented and a report submitted.

WHIRL AND FLIGHT TEST

Conduct whirl test of the third hub if the fatigue and static strength, based on tests, proves to be structurally adequate for flight testing.

Whirl test, if conducted, will include functional check (interference, etc.), stress and motion survey, and 20-hour unaccelerated flight loads endurance test, including start-stop and ground-air-ground. (The primary objective of the whirl test is to assess the operational compatibility of the composite hub with the remaining metallic elements of the rotor head. An inspection procedure will be established based upon the ground test data to detect hub premature failures.)

Conduct safety-of-flight review between AAMRDL and Sikorsky to verify flightworthiness of the whirl test hub. Determine bending and axial stiffness. Compare with values prior to ground testing.

Assuming safety-of-flight review board approval, request bailment of a CH-54B aircraft from the Army for flight test purposes. Instrument the splayed laminate hub rotor head to measure blade motions, control loads, and stress levels at critical regions of the hub as determined by ground testing. Conduct flight test within a limited CG and payload envelope. Flight test envelope and duration will be determined based on 10-hour structural shakedown flight test program.

Upon completion of flight testing, check hub stiffness against previous values.

Submit flight test report to AAMRDL.

APPENDIX I
HARDWARE DEVELOPMENT PLAN

STATIC AND FATIGUE TEST PLAN TECHNICAL APPROACH

Two composite rotor hubs will be subjected to static and dynamic test loads simulating flight conditions to expose fracture modes and provide strength data for comparison with existing CH-54B titanium rotor hub data and to substantiate structural adequacy for the proposed flight test program.

The first hub will be subjected to the following static test loads:

(a) Centrifugal load (equiv to 117% N/r) of 1,140,000 lb/arm

(b) Thrust load of 50,000 lb

(c) Torque load 160,000 ft/lb

During these tests, deflections and stresses will be measured at critical locations to provide data for correlation with design calculations.

The first hub will then be subjected to fatigue loading simulating steady and vibratory flight conditions except that, in order to provide strength data within a reasonable time period, applied head moment will be accelerated well above levels observed in flight.

The purpose of the test is to demonstrate a strength at least equivalent to that of a titanium hub. Differences in S/N curve shapes for hub materials make selection of load level extremely important.

Figure 87 shows the selected test level for the first splayed laminate composite hub and curve shapes for titanium, S-glass, and graphite materials. At a test level of ± 1.06 in./lb x 10^6 head moment, the titanium core of the hub is expected to fracture at about 10^6 cycles. If a fracture occurs, unknown (but potential) fracture modes in the composite materials must be treated as fractures and will result in calculated crack initiation times approximately the same as the titanium spline.

If a lower test level were selected and a graphite fracture occurred at a corresponding higher number of cycles, similar calculations would certainly indicate a lower crack initiation time for the composites.

In the event of an early fracture of the spline, this part of

the hub will be replaced and testing continued (Figure 90).

A hub fracture other than in the spline will be treated conservatively as a fracture mode for all materials, and crack initiation times (based on a 70% working curve) will be calculated for each curve shape. Recommended replacement time will be based on the lowest of these.

During the fatigue tests, the condition of the rotor will be checked by repeating static deflection measurements every 250,000 cycles. On completion of 10^6 cycles, the hub will be subjected to a residual static strength test under combined centrifugal load and head moment.

If the first test reaches 10^6 cycles with no composite failure, the second hub will be tested at the same load level to provide a second data point. Should the spline fail, the titanium core will be replaced as necessary and testing continued until a composite fracture is achieved or 5×10^6 cycles are reached.

If the first hub fractures early in the composite material, a lower load level will be selected to determine if the hub is structurally adequate to support the proposed flight test program.

Statement of Work - (Test Section)

Static Tests

Perform static strain and deflection tests of first hub under

(a) Centrifugal load

(b) Thrust load

(c) Torque

Determine spring rates of hub under each type of loading.

Test of First Hub

Fatigue test composite hub in head and shaft test facility at a load level designed to fracture spline at 10^6 cycles.

Repeat static tests as per above every 250,000 cycles.

Determine changes in spring rates.

If spline fracture occurs significantly prior to 10^6 cycles, replace titanium bore and continue testing to 10^6 cycles.

On completion of 10^6 cycles, perform residual strength test to

fracture or 2 x normal flight load under combined centrifugal and head moment loading.

Test of Second Hub

If test of the first hub reaches 10^6 cycles, test second hub at same load level to 5 x 10^6 cycles or fracture, whichever occurs first, replacing the titanium spline as required up to a maximum of four times.

If an early fracture of the first hub occurred in the composite material, test of the second hub will be at a load level selected to demonstrate structural adequacy for the proposed flight test program.

Test Facility (Figures 89 and 91)

The head and shaft test facility at Sikorsky Aircraft has the unique capability of safely testing a helicopter main rotor hub to complete fracture. Instead of rotating the shaft and rotor head to generate the required loading, the shaft is held stationary. Cyclic loads are applied to the rotor head in such a way that it experiences the steady and vibratory loads developed in flight. Instrumentation and visual observations of the hub are simple. Even in the event of unexpected fracture, there is little kinetic energy to dissipate.

The test machine uses hydraulic rams to simulate blade centrifugal loads at each of the arms of the rotor head. The outboard ends of these cylinders are attached to the inner ring of a gimballed ring assembly. The ring assembly is so driven that the lines of action of the simulated centrifugal loads nutate, imparting 1-per-rev vibratory loads and motions to the rotor head similar to those experienced in flight. Thrust loads are induced by coning the centrifugal loading cyclinders. This is accomplished by lowering the main rotor shaft with respect to the gimbal rings so that the vertical component of the applied ram loads provides the required thrust. Similarly, torque is induced by rotating the shaft with respect to the gimbal rings. The tangential component of the applied ram loads provides the required torque.

The facility has been used successfully to develop and substantiate the H-53 and H-54 rotor head and shaft.

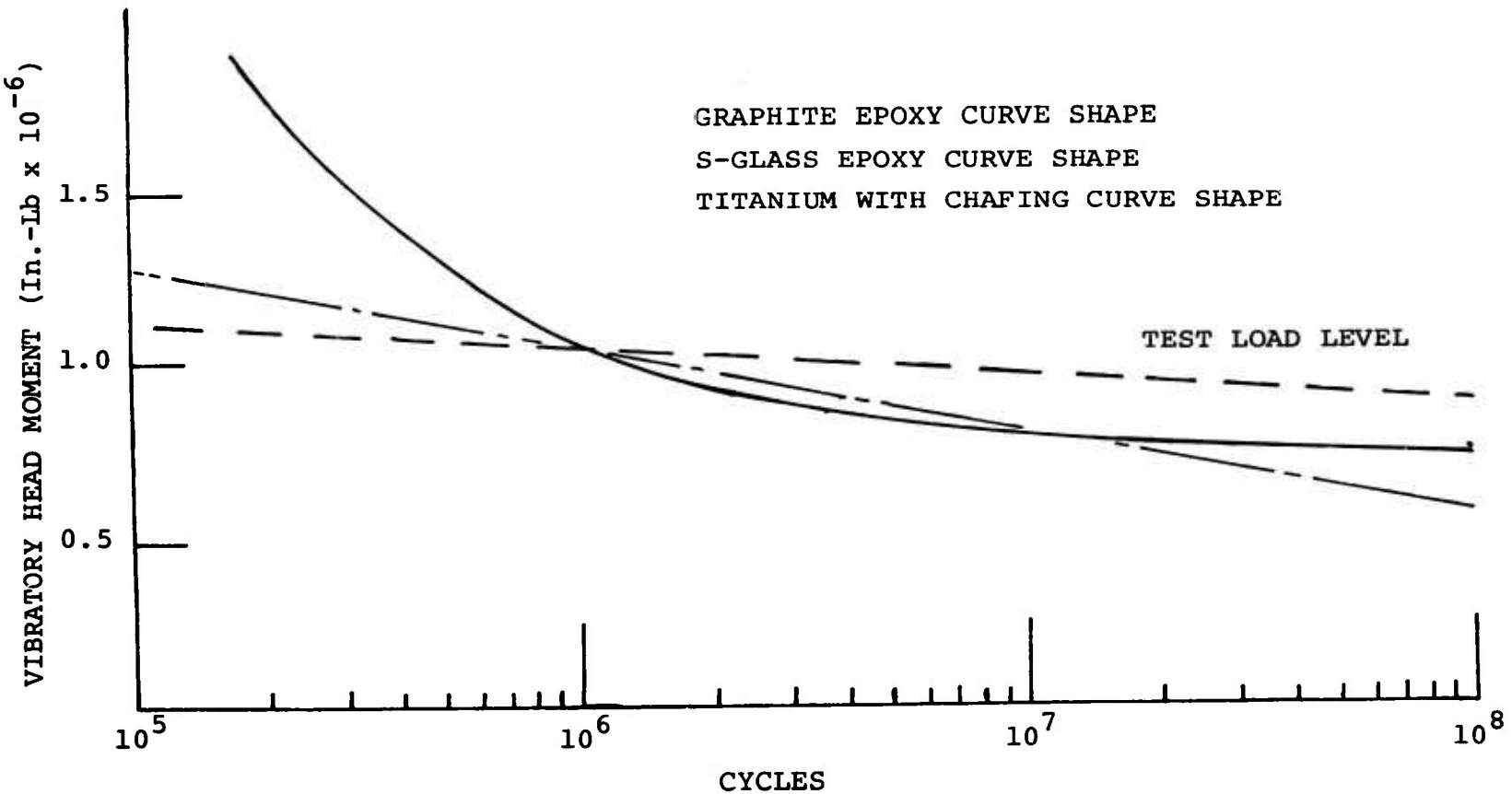

Figure 88. Selection of Test Load Level.

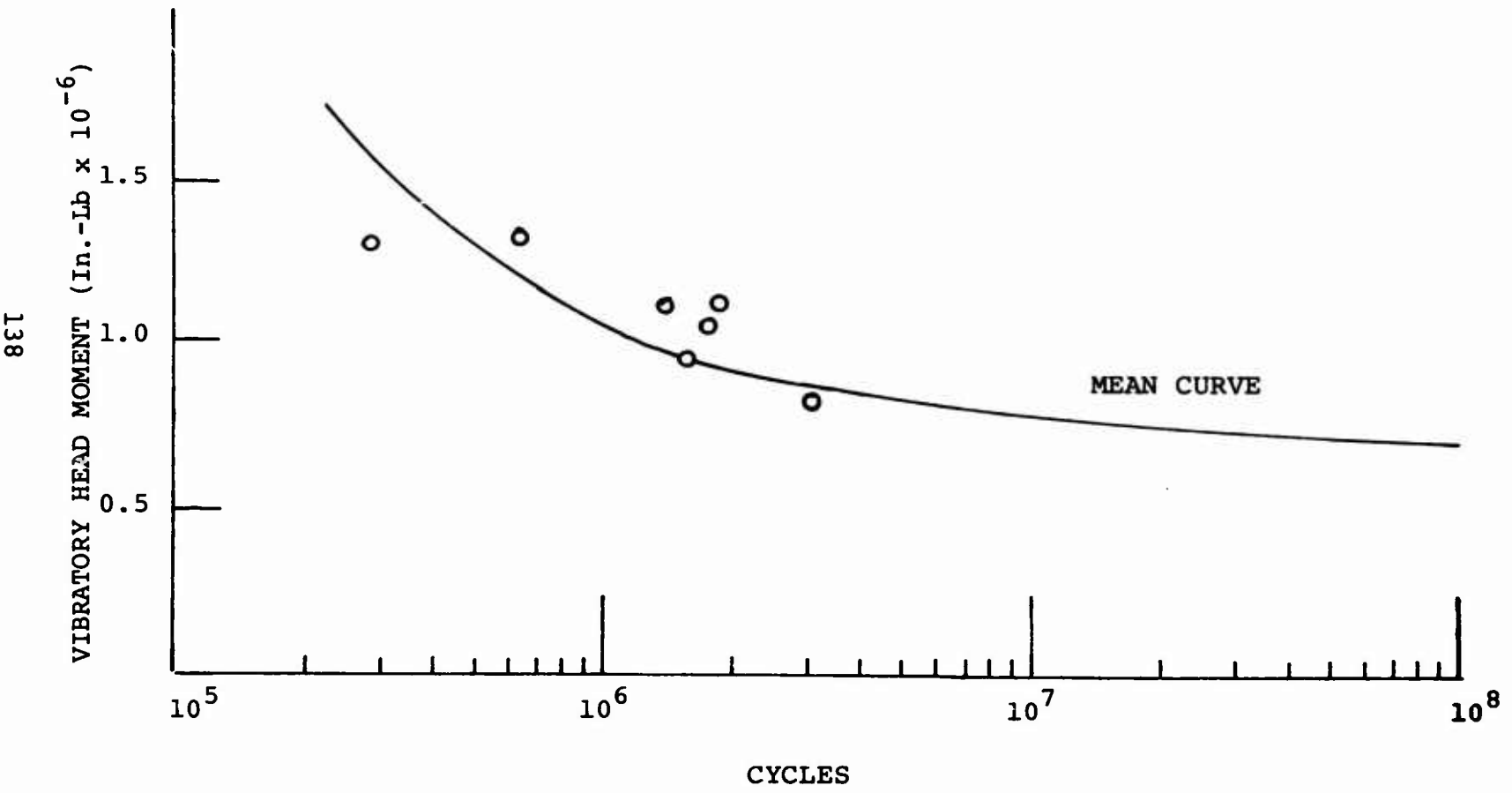

Figure 89. CH-53A/54B Main Rotor Hub Fatigue Test Data.

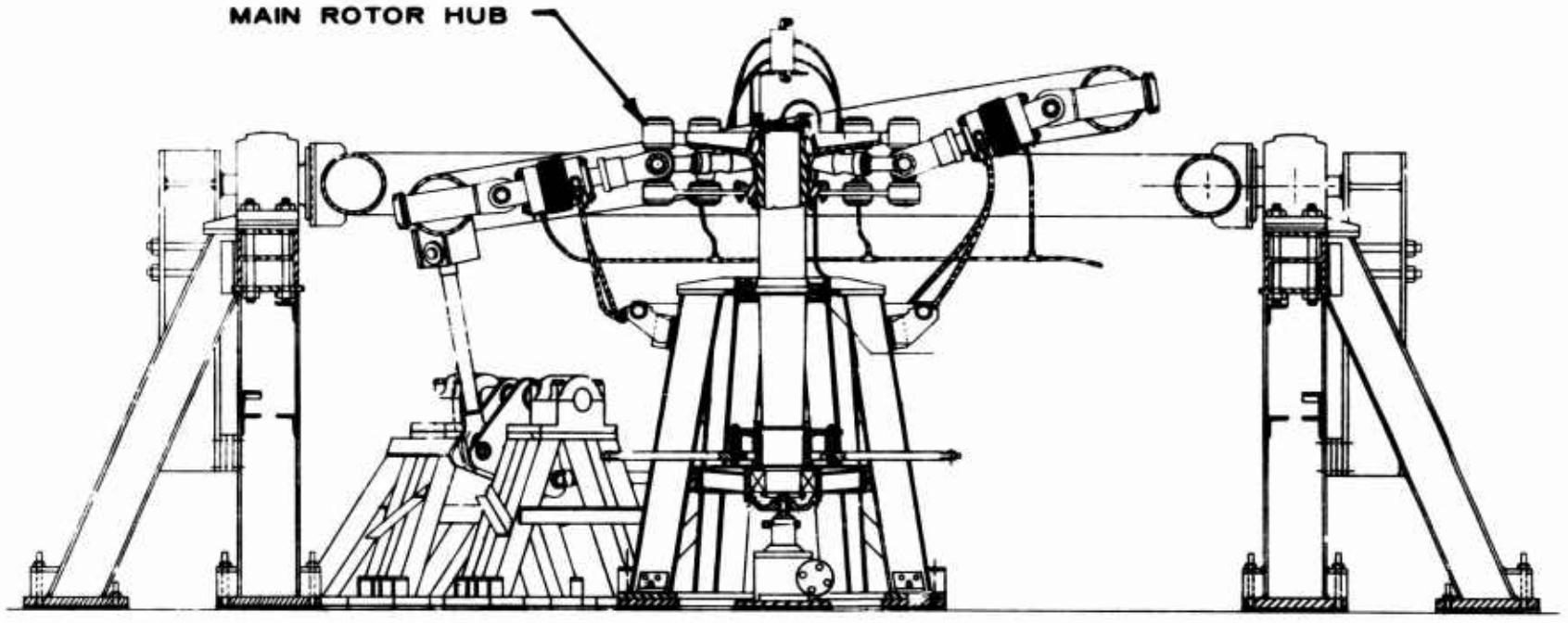

Figure 90. Main Rotor Head and Shaft Test Facility.

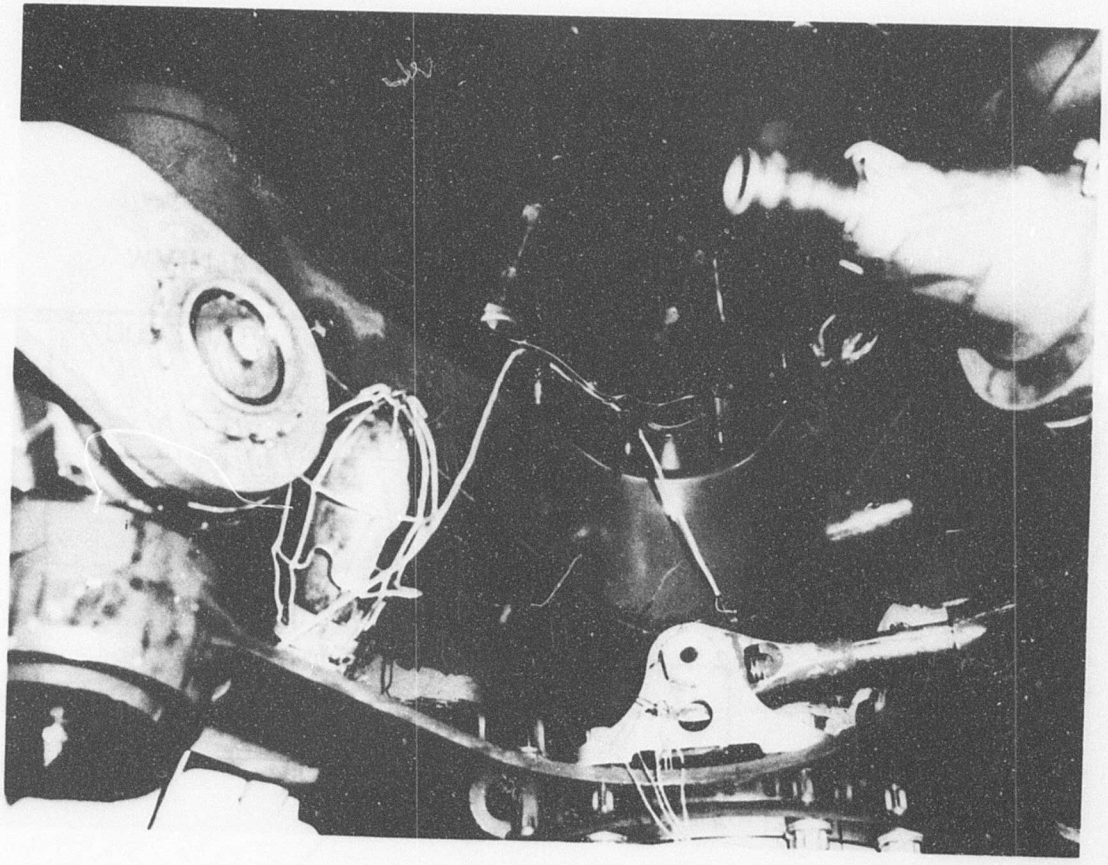

Figure 91. Main Rotor Hub Installed in Test Facility. Spline Mode Crack Propagation to Outside of Hub Shown.

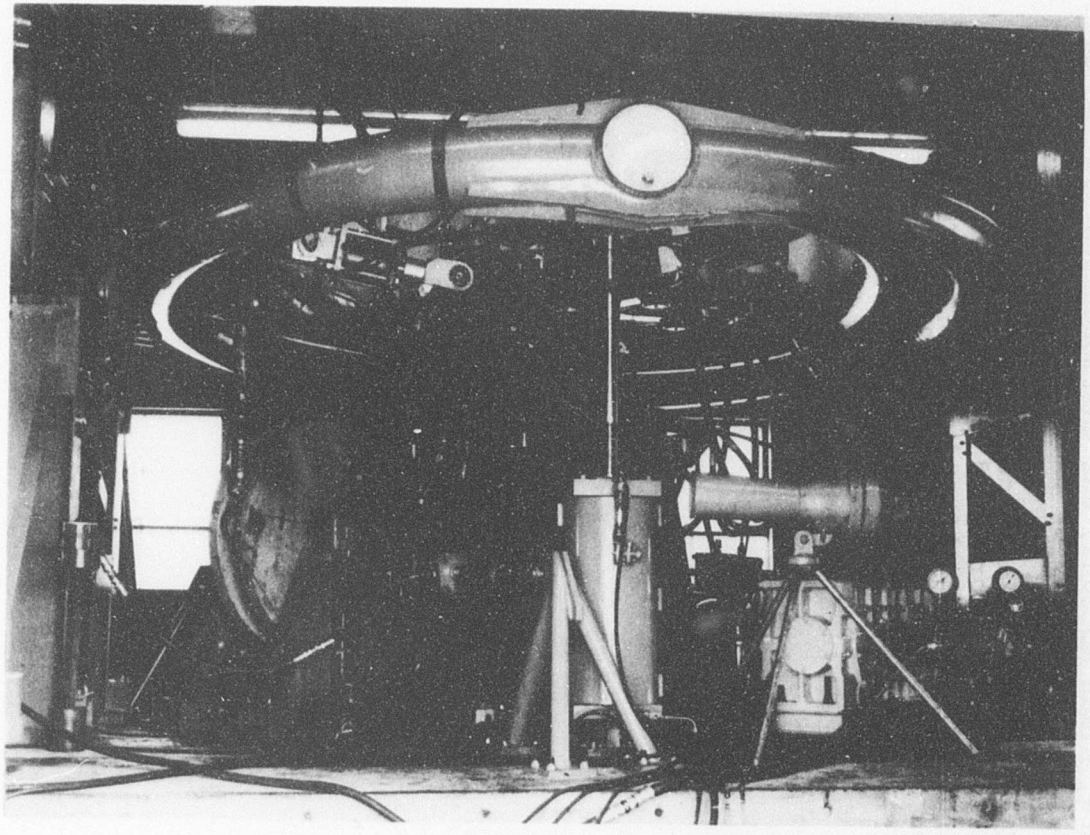

Figure 92. Test Facility With Hub Installed.

STRUCTURAL SHAKEDOWN FLIGHT TEST PLAN - TECHNICAL APPROACH

A structural shakedown flight test program will be conducted at the Sikorsky Aircraft facility. Sufficient strain gages, vibration transducers, blade motions, and thermocouples will be used to demonstrate the feasibility of the composite rotor hub.

Instrumented flight tests will be conducted throughout the normal test airspeed and rotor speed envelope of the aircraft. Flights will include level flight and normal neutral center of gravity, and an intermediate gross weight (38,000 lb) at the forward, neutral, and aft center-of-gravity limits.

FLIGHT TEST PLAN

Model: CH-54B

G.W.: Minimum and 38,000 lb.
C.G.: 326, 336, 349 inches

Conditions	Measure
All	Main Rotor pushrod load, MRβ, MRθ, main rotor shaft bending, main rotor rotating scissors load, vertical accel. main rotor centerline, in-plane accel. main rotor centerline, vert. accel. CRH #1 arm, vert. accel. CRH #2 arm, in-plane accel. CRH #2 arm, in-plane accel. CRH #2 arm, vert. accel. at C.G., strain gages on the composite rotor hub to be placed in the laminations (15), thermocouples on the composite rotor hub to be replaced in the laminations (3).
	NOTE: Pushrod load, hub stresses, MRβ, and MR shaft bending will be monitored by telemetry for safety of flight.
1.	Minimum G.W. @ 336 in. C.G.
2.	38,000 lb. G.W. @ 336 in. C.G.
3.	38,000 lb. G.W. @ 326 in. C.G.
4.	38,000 lb. G.W. @ 349 in. C.G.

Plan A (Cond. 1 & 2) Yardwork

Item	Units	
1.	1	Rotor engagement, slow.
2.	3	Flat pitch @ 90, 100, and max. % Nr.
3.	1	Qualitatively assess mechanical ability at 100% Nr.
4.	1	Start forward taxi.
5.	1	Taxi @ 100% Nr.
6.	1	Lift off to hover @ 100% Nr.
7.	4	Hover @ 96, 100, 104, and max. % Nr.
8.	2	Longitudianl and lateral reversals, mild; @ hover @ 100% Nr.
10.	3	Paces rearward flight 10 kt @ 100% Nr and recovery.

Item	Units	
11.	1	Aborted takeoff and approach at 100% Nr.
12.	1	Landing @ 100% Nr.
	19 Units	total units 50

NOTE: Photo coverage will be provided for 1st flight.

Plan B (Cond. 1 & 2) 2000 ft. Hd

Item	Units	
1.	1	Hover @ 100% Nr.
2.	1	Take off and fly once around pattern @ 100% Nr.
3.	1	Approach normal.
4.	1	Take off and climb out 70 kts @ 100% Nr. normal power.
5.	4	Level flight 60 kt @ 96, 100, 104, and max. % Nr.
6.	6	Level flight 20, 40, 60, 80, and 100 kt @ 100% Nr.
7.	4	Level flight 90 kt @ 96, 100, 104, and max. % Nr.
8.	1	Rough Approach.
9.	1	Transition to hover.
10.	1	Hover IGE @ 100% Nr.
	21 Units	total units 40

Plan C (Cond. 3 & 4) Yardwork

Item	Units	
1.	1	Rotor engagement (normal).
2.	1	Hover OGE @ 100% Nr.
3.	4	Left side flight @ 100% Nr; 10, 20, and 30 kt and recovery.
4.	4	Right side flight @ 100% Nr; 10, 20, and 30 kt and recovery.
5.	3	Rearward flight @ 100% Nr; 10 and 20 kt and recovery.
6.	1	Left hover turn @ 100% Nr (15 sec)
7.	1	Right hover turn @ 100% Nr (15 sec)
8.	2	Hover @ 100% Nr longitudinal and lateral reversal.
9.	1	Hover IGE @ 100% Nr.
10.	1	Hover IGE @ 100% Nr.
	19 Units	total units 38

Plan D (Cond. 3 & 4) 2000 ft. Hd

Item	Units	
1.	4	Hover @ 96, 100, 104, and max. % Nr.
2.	1	Normal power takeoff and climbout, 70 kt @ 100% Nr.
3.	4	Level flight 60 kt @ 96, 100, 104, and max. % Nr.
4.	8	Level flight 20, 40, 60, 80, 100, 110, 115 kt @ 100% Nr.
5.	4	Level flight 105 kt @ 96, 100, 104, and max. % Nr.
6.	6	70 kt @ 100% Nr, left and right turns @ 15°, 30° AOB and recovery.
7.	2	70 kt @ 100% Nr, longitudinal and lateral reversal.
8.	1	70 kt @ 100% Nr, symmetrical pullout.
9.	4	Autorotation @ 70 kt max., 100% and min. % Nr and recovery.
10.	1	Normal approach.
11.	1	Hover @ 100% Nr.
	36 Units	total units 72

Plan E (Cond. 3 & 4) 2000 ft. Hd

Item	Units	
1.	4	Hover @ 96, 100, 104, and max. % Nr.
2.	1	Max. power takeoff and climb, 70 kt @ 100% Nr
3.	3	Climb 40 kt and 90 kt @ 100% Nr max. power
4.	6	105 kt @ 100% Nr, left and right turns @ 15° and 30° AOB and recovery.
5.	2	105 kt @ 100% Nr, longitudinal and lateral reversals.
6.	1	105 kt @ 100% Nr, symmetrical pullout.
7.	5	Autorotation @ 105 kt, max. 100 and min. % Nr and recovery.
8.	3	Partial power descent 70 kt @ 100% Nr, 500, 1000 and 1500 fpm ROD.
9.	3	Partial power descent 105 kt @ 100% Nr, 500, 1000, and 1500 fpm ROD.
10.	1	Rough approach.
11.	1	Hover @ 100% Nr.
12.	1	Rotor engage, rapid.

31 Units total units 62

NOTE: Composite rotor hub will be inspected after each flight.

Test Sequence

Flight	Plan	Cond.	Flt. Time	Comments
1	A	1	.7	Yardwork.
2	B	1	.7	Level flight.
3	A	2	.7	Yardwork.
4	B	2	.7	Level flight.
5	C	3	.7	Yardwork.
6	D	3	1.2	Level flight.
7	E	3	1.0	Level flight & maneuvers.
8	C	4	.7	Yardwork.
9	D	4	1.2	Level flight.
10	E	4	1.0	Level flight & maneuvers.

Total Flight Hours = 8.6

MANUFACTURING DEVELOPMENT PLAN

Introduction

Fabrication of the rotor hub includes development tasks that range from straightforward material evaluation, e.g., foam selection, to more complex areas such as loop manufacture and adhesive formulation. The latter two conditions require rigorous investigation and consideration of the design, stress analysis, and processing factors. The following discussion outlines a development plan that proceeds from relatively simple tasks to tasks of increasing risk and complexity.

Foam Selection

A foam filler is used in two areas of hub fabrication: (1) as a filler encapsulated by aluminum or laminated boundaries and (2) as a fillet section covered by an external, glass shear-web sheath. In these functions, it must be compatible with the assembly adhesive and capable of withstanding the environment imposed by the adhesive and by laminated shear-web curing.

Although foam-adhesive compatiblity can be evaluated readily, temperature and pressure parameters impose more serious restrictions. Curing of a glass/epoxy laminate usually requires a pressure ranging from 50 to 90 psi and a time-temperature schedule of 4 hours at 350°F or an equivalent of 16 hours at 250°F. This schedule would also accommodate any standard adhesive cure. These conditions imply the use of a foam having a density of approximately 2 to 10 lb/ft^3.

Since each hub assembly incorporates approximately 2 ft^3 of foam, the lowest density material capable of withstanding the imposed lamination pressure and temperature profile should be selected. Inherent in this selection is the evaluation of shrinkage and outgassing properties under the required cure schedule in order to provide retention of hub dimensions without introducing surface anomalies during cover installations and external shear web bonding.

The actual density of the cured form not only is determined by the formulation, but is strongly influenced by temperature and geometry of the cavity in which it flows and cures. Therefore, as part of the density-compression evaluation task, test specimens should be obtained from castings foamed in a representative cavity. This procedure will also establish the foam charge weight most applicable to the specified cavities.

Cover Fabrication

The construction of laminated covers entails use of +45° S-glass epoxy prepreg in multiple plies to produce a cover thickness of

0.10 inch. An evaluation profile of the cover shows a contour consisting essentially of three surfaces. This contour, or more specifically the inner cover surface, must conform closely to the geometry of the laminated loop buildup in order to achieve a uniformly thin continuous bond line of satisfactory shear behavior.

Depending on the adhesive, a satisfactory bond line is usually within the range of .002 to .010 inch thickness. Tolerance on this thickness is determined by the stress analysis based on adhesive properties. Physically, it is limited by the precision with which the internal cover surface can be produced. Correct cover conformation can be achieved only by establishing the final composite hub surfaces based on the resultant cumulative manufacturing component tolerances for the loops and spacers, and the control of the distortion of the laminated cover that may be experienced during cure.

The former condition can be determined from previous experience and initial fabrication of each of the components. The latter condition can be confirmed only by investigation of layup patterns and curing conditions. Previous laminated covers have displayed up to 1/2 inch displacement in end loop evaluation and serious mismatching with composite hub contours, resulting in low interlaminar shear strengths and highly irregular bond lines. Minor variations in cured laminate thickness can occur, but should introduce no contoured molding surface.

Spacer Fabrication

The proposed design includes molded composite spacers between each of the laminated loop assemblies. A taper from approximately 1/2 inch to essentially zero is indicated. Some finite minimum thickness is obtainable with sheet molding compounds, but the absolute practical minimum thickness remains to be determined. Assuming that this dimension lies between .002 to .010 inch, the usual range of acceptable bond line thickness, the inherent characteristics of precision molding must be determined. These parameters include charge weight, preform shape, and preform location within the die cavity. Sequential evaluation of these variables, together with a regulated schedule of curing conditions, will produce a precision-molded component. Molding temperature, dwell time, pressure application, and cure duration must be determined for a representative spacer geometry.

Web (In-Plane) Fabrication

The fabrication of in-plane glass shear webs, interspersed in the composite hub assembly in place of every fourth molded spacer, required precision molding of approximately 50 plies of glass epoxy prepreg. Normally, materials of this type are

fabricated as oversize laminates in thicknesses up to 1/4 inch and machined to final size. The proposed geometry in the spacer configuration precludes this possibility. The proposed design, tapering from 0.5 inch to zero, must again accommodate a finite minimum molding thickness. For a glass/epoxy prepreg, this dimension approaches .0075 inch. The maximum thickness, however, indicates that at least 50 plies are required. To achieve the outline dimensions without excessive machining costs, the indicated technique is matched mold forming. In order to accomplish this configuration as a lamination from a prepreg containing approximately 40% resin content, the prepreg must be mixed with dry glass fibers to produce a reasonable laminate approaching 30% resin content with the proper dimensions. The proportion of dry glass to prepreg and the appropriate pressure, time, and temperature schedule must be established.

Boss Fabrication

Several alternatives are available for fabrication of the aluminum-glass bosses on the covers. The bosses could be laid up and co-cured with the covers. The bosses could be fabricated independently and adhesively bonded to the covers. They could be assembled, cured, and later bonded to the covers using several plies of fresh prepreg material to achieve the bond.

The first alternative is not desirable, because control of the aluminum-glass boss material on the glass/epoxy cover is not readily possible during the cure of the covers. Prefabrication of the bossing rings is possible, but subsequent bonding of these cured rings may not provide the substantially uniform bond line necessary for structural integrity.

The third alternative, prefabrication of the boss ring laminates and subsequent attachment of these rings to the cured covers using fresh prepreg, should provide firm bonding and also accommodate the geometries associated with the bonding areas. Structural integrity of the joint produced with this technique can be verified with relatively small specimens. Simultaneous examination of the lay-up procedure can also be conducted. The bearing boss, in particular, represents a thick wall section of approximately 50 plies that should be evaluated for representative ply thickness and, if possible, manufactured using a lamination procedure developed specifically for the composite bosses.

Shear Web (External) Fabrication

The entire hub surface, extending from the mounting ring diameters to the end of each arm, is essentially encapsulated by an epoxy/glass fiber shear web. This sheath is composed of six relatively independent sections. Each section provides increased wall thickness and $\pm 45°$ glass fiber orientation at

the vertical sides of the arm. A wall thickness of 0.1 inch requires approximately 13 plies of laid-up prepreg. The contour of the web, the continuous fiber orientation, and the high structural requirements dictate the use of narrow tapes for these webs. Every section could consume as many as 1000 pieces. If each section were divided into two parts, the volume and the time for lay-up directly on the composite hub still precludes in situ fabrication. Therefore, the shear web sections should be fabricated as preformed elements consisting of six mating pairs laid up on contoured male molds dimensioned to the outline surfaces of the hub arms.

The large number of individual prepreg pieces associated with the shear web sections justifies the effort to optimize the manufacturing procedure. An attempt to minimize the prepreg lay-up patterns and reduce the volume of pieces handled is essential in establishing a practical manufacturing method. Once lay-up patterns have been optimized, steel rule dies can be used to expedite the cutting of the repetitive prepreg shapes.

Experience with smaller but similar multi-ply preformed shear web sections has shown that deep freezing in sealed packages after lay-up is a workable timesaving technique that can be applied to glass/epoxy preforms. This method is best used when the mold design is a true representation of the composite hub surface. Consequently, the final fitting and bonding of the shear web sections can proceed rapidly through the cure cycles, one each for the upper and then the lower overlapping sections.

Since the bonding adhesive and the S-glass epoxy prepreg are cured simultaneously, a hybrid curing schedule must be developed that will accommodate both materials. Satisfactory co-curing studies can be conducted using small specimens of the representative materials, autoclave curing conditions, and physical evaluation of the fabricated specimens.

Laminated Loop Fabrication

The filament-wound laminated loop assemblies are vital components in the composite hub assembly. They provide primary structural integrity, form the basis for hub fabrication, and directly influence most of the other components and fabrications. Manufacture of the loops is also a substantial portion of the hub fabrication costs.

One design premise must be assured for this type of filament-wound component: the cross-sectional area of the continuous unidirectional S-glass laminate windings must be constant.

If a final design analysis permits a lower lamination volume, simplification of loop contours, or reduction of individual

laminated loop designs, both tooling and manufacturing costs could be reduced. Certain areas of processing may require improvements.

The winding mold design should provide for three or more loop configurations within a single winding fixture. This would markedly reduce the processing time per loop by permitting single preheat, winding, and curing times for multiple units. As many filament rovings of high volume, perhaps three or more 60-end glass prepreg rovings, could be wound simultaneously in each loop gap.

A winding fixture must be developed to feed the selected multiple roving combination to a representative laminated loop assembly. Once this apparatus demonstrates the fiber feed system mechanically, the prime winding variables are superimposed to provide prepreg roving conditions suitable for curing. Temperature of mold, roving temperature, winding speed, and filament tension all contibute to a well-compacted laminated loop assembly and dimensional control. Mechanical compaction, using pressure application during the winding, may also be beneficial. It may also be necessary to apply additional compacting pressure continuously during the cure cycle to provide structural integrity of the cured part.

As mentioned earlier, projected tooling costs are relatively high for this single component. Associated with this direct expense are the indirect disadvantages that can be incurred if mold material and mold design are not carefully selected. The mold material must be considered in terms of service conditions, cost (both initial and rework), and weight. Steel molds are serviceable, but pose logistic problems in terms of mass and machining costs. A high-temperature glass/epoxy mold material is feasible and should be evaluated.

Composite Hub Assembly

Adhesive bonding can be accomplished using adhesive film of various types or viscous liquids, which may include particulate filling agents. Films, supported or free standing, are used frequently for bonding smooth, matched surfaces with heat and pressure. The assembly of the composite hub would rarely present a bonding surface of this nature. An additional disadvantage of adhesive films is the mode of application, which includes cutting, fitting, and lay-up.

A viscous liquid bonding agent offers a wide choice of curing schedules, ranging from ambient conditions through various combinations of heat and pressure. Final selection of adhesive formulation is directed by design stress analysis requirements. Candidate materials qualifying in terms of adequate stress performance can be further screened on the basis of adequate pot life and viscosity.

Actually, two adhesives could be used. An ambient curing system for bearing cartridge and foam filler installation would be suitable, since pot life is not critical for these operations. The composite hub assembly does demand a substantial pot life of 4 to 8 hours and, consequently, elevated temperature curing. Modifications of the adhesive cure schedule must be made to achieve conditions compatible with the co-curing of external shear web. Manual application of the adhesive by brush or spatula to all laying surfaces as they occur during assembly buildup would provide the best assurance of filling all interfacial surfaces and joints. Subsequent pressure application during cure produces adhesive extrusion as a visual indication of complete bond line filling when a small excess of adhesive is applied during assembly. The possiblility of adding inert fillers to the adhesive formulation should be examined as a method of enhancing viscosity, provided that the inherent bonding strength of the adhesive is not degraded.

Shear strength verification is accomplished with an established cure schedule and each material combination included in the composite hub assembly. Surface preparations for specimens tested to establish the ultimate shear strength values must incorporate the manufacturing procedure applicable to the particular components under evaluation.

Work Statement

The engineering development plan leading to successful manufacture of the proposed main rotor hub encompasses several areas of investigation:

Examine each of the composite components (including laminated covers, molded spacers, in-plane webs, aluminum/glass bosses, external shear webs and laminated loops) for the specific processing parameters pertinent to design and fabrication.

Confirm at least two material selections, foam and adhesive, through initial screening studies and ultimate mechanical property testing. (Additional attention is directed to the co-curing of the bonding adhesive and the external shear web. A similar task may be devoted to the exploration of alternative methods for fabricating the aluminum/glass composite mounting bosses.)

Task	Engineering Development Objective
Foam Selection	- Adhesive compatibility - Low density with 100-psi compressive strength - Thermal stability-shrinkage and outgassing - Charge weight
Cover Fabrication	- Contour definition - Lamination tool design - Prepreg lay-up pattern - Laminate contour control
Spacer Fabrication	- Minimum molding thickness - Charge weight - Preform shape and location - Cure schedule
Web (In-Plane) Fabrication	- Minimum molding thickness - Prepreg lay-up pattern - Dry glass/prepreg ratio - Cure schedule
Boss Fabrication	- Single-step lamination procedure - Bond joint strength - Cure schedule
Shear Web (External) Fabrication	- Prepreg lay-up patterns - Lay-up procedure - Co-curing schedule
Laminated Loop Fabrication	- Mold design and material selection - Filament volume and quantity - Multiple roving winding fixture design and demonstration - Winding parameters - Compaction factors - Cure schedule
Composite Hub Assembly	- Shear stress requirements - Adhesive shear stress vs bond line thickness - Adhesive post life - Adhesive viscosity control - Cure schedule - Shear stress verification with all material combinations

When each task is completed to the satisfaction of the design, stress, and fabrication requirements, preliminary process specifications should be formalized for individual manufacturing

operations. Similar specifications should also be prepared for the quality control of raw materials used in the manufacturing processes. These procedures will reflect the tolerances associated with each processing condition.

APPENDIX II

SPLAYED HUB ANALYTICAL CALCULATIONS

The following contains the detail analysis of the redesigned, splayed-laminate hub as defined in Phase II. The calculations were used to derive the loads, section properties, and stresses for the following areas:

- Hub Arm
    - . Section A-A
    - . Section B-B
    - . Section C-C
- Hub Center of Rotation (Section O-O)
- Central Hub Attachment
    - . Clamp Ring Bolts
    - . Clamp to Hub Bolts

The results of the analysis and the static and fatigue strengths determined are summarized in the main body of this report.

Calculations for Section A-A Section Properties (Reference Table 11)

$$Io = \frac{bh^3}{12}$$

$$Io = \frac{.625 \times 25^3}{12} = .00081 \quad (1)(3)(5)(7)(9)(11)(13)(15)(17)(19)(21)(23)$$

$$Io = \frac{.625 \times .46^3}{12} = .00506 \quad (6)$$

$$Io = \frac{.625 \times .38^3}{12} = .00285 \quad (18)$$

$$Io = \frac{5.94 \times .10^3}{12} = .00049 \quad (24)(25)$$

$$Io = \frac{.18 \times 8.38^3}{12} = 8.82720 \quad (26)$$

$$Io = \frac{5.315 \times 25^3}{12} = .00692 \quad (27)(28)$$

$$\bar{Y} = \frac{AEY}{AE} = \frac{161.510 \times 10^6}{36.232 \times 10^6} = \underline{\underline{4.458}}$$

$$\Sigma EI_{X-X} = 2 \ \Sigma AEY^2 + \Sigma EIo - AE\bar{Y}^2$$

$$\Sigma EI_{X-X} = 2 \quad 956.961 \times 10^6 + 21.358 \times 10^6 - (36.232 \times 10^6)\ 4.458^2$$

$$\Sigma EI_{X-X} = 2 \quad 978.319 \times 10^6 - 720.066 \times 10^6 = 2 \quad 258.853 \times 10^6$$

$$\Sigma EI_{X-X} = \underline{\underline{516.506 \times 10^6}}$$

$$\Sigma EA = 2 \quad 36.232 \times 10^6 = \underline{\underline{72.464 \times 10^6}}$$

$$Io = \frac{.25 \times .625^3}{12} = .00508 \quad (1)(3)(5)(7)(9)(11)(13)(15)(17)(19)(21)(23)$$

$$Io = \frac{.46 \times .625^3}{12} = .00935 \quad (6)$$

$$Io = \frac{.38 \times .625^3}{12} = .00773 \quad (18)$$

$$Io = \frac{.10 \times 5.94^3}{12} = 1.74653 \quad (24) \quad (25)$$

$$Io = \frac{8.38 \times .18^3}{12} = .00407 \quad (26)$$

$$Io = \frac{.25 \times 5.315^3}{12} = 3.12801 \quad (27) \quad (28)$$

$$\Sigma EI_{Y-Y} = 2 \quad AEX^2 + \quad EIo \quad = 2 \quad 942.292 \times 10^6 + 24.18917 \times 10^6$$

$$\Sigma EI_{Y-Y} = 2 \quad 966.481 \times 10^6 \quad = \underline{1932.962 \times 10^6}$$

Section Modulus Calculations

Graphite/Epoxy

$$Z_{X-X} = \frac{EI_{X-X}}{ECy} = \frac{516.506 \times 10^6}{(17.5 \times 10^6)\ 3.858} = \underline{7.650}$$

$$Z_{Y-Y} = \frac{EI_{Y-Y}}{ECx} = \frac{1932.962 \times 10^6}{(17.5 \times 10^6)\ 5.94} = \underline{18.594}$$

0° S Glass

$$Z_{X-X} = \frac{516.506 \times 10^6}{(6.8 \times 10^6)\ 1.668} = \underline{45.537}$$

$$Z_{Y-Y} = \frac{1932.962 \times 10^6}{(6.8 \times 10^6)\ 5.94} = \underline{47.855}$$

$\pm 45^\circ$ S Glass

$$Z_{X-X} = \frac{516.506 \times 10^6}{(2.4 \times 10^6)\ 2.128} = \underline{101.132}$$

$$Z_{Y-Y} = \frac{1932.962 \times 10^6}{(2.4 \times 10^6)\ 5.94} = \underline{135.589}$$

Calculations for Section B-B Section Properties (Reference Table 13)

$$Io = \frac{bh^3}{12} = (0.625)\ (0.25)^3 = .0008 \text{ in.}^4$$

(1)(2)(3)(5)(7)(9)(11)(13)(15)(17)(19)(21)(23)

$$I_o = \frac{(4.375)\ (0.1)^3}{12} = 00036 \text{ in.}^4$$

25 24

$$I_o = \frac{(4.375)\ (0.1^{\text{illegible}})^3}{12} \cdots 0.0007 \qquad I_o = \frac{(0.125)\ (5.14)^3}{12} = 1.4145 \text{ in.}^4$$

26

$$EI_{X-X} = 2 \quad AEY^2 - A\bar{Y}^2 + Io\ E$$

$$125.98 \times 10^6 = 2 \quad 308.44 - 29.00\ (2.93)^2 + 3.51 \quad (10^6)$$

Section Modulus Calculations

Graphite Epoxy

$$Z_{XX} = \frac{EI_{XX}}{EC_Y} = \frac{126 \times 10^6}{(17.5)\ (2.33)\ 10^6} = 3.09 \text{ in.}^3$$

$$Z_{YY} = \frac{878.2 \times 10^6}{(17.5)\ (4.38)\ 10^6} = 11.46 \text{ in.}^3$$

0° S Glass

$$Z_{XX} = \frac{126 \times 10^6}{(6.8)\ (1.13)\ 10^6} = 16.39$$

$$Z_{YY} = \frac{878.2 \times 10^6}{(6.8)\ (4.375)\ 10^6} = 29.39$$

$\pm 45^\circ$ S Glass

$$Z_{XX} = \frac{126 \times 10^6}{(2.4)\ (1.26)\ 10^6} = 41.67 \text{ in.}^3$$

$$Z_{YY} = \frac{878.2 \times 10^6}{(24)\ (4.38)\ 10^6} = 83.5 \text{ in.}^3$$

Static Analysis, Section A-A (Reference Table 22)

Bending Moment (Flatwise)

$$M_{X-X} = V_N d_1 + .4\ R_A$$

$$M_{X-X} = 54840 \times 13.1 + .4 \times 98424$$

$$M_{X-X} = 718404 + 39370 = \underline{\underline{75774}} \text{ in.-lb}$$

Bending Moment (Edgewise)

$$M_{Y-Y} = V_E d_1$$

$$M_{Y-Y} = 12{,}900 \times 13.1 = \underline{\underline{168990}} \text{ in.-lb}$$

Bending Stresses (Flatwise)

Graphite/Epoxy

$$f_{b_{xx}} = \frac{M_{X-X}}{Z_{X-X}} = \frac{757774}{7.650} = 99055$$

0° Glass

$$f_{b_{x-x}} = \frac{757774}{45.537} = 16630$$

$\pm 45^\circ$ S Glass

$$f_{b_{x-x}} = \frac{757774}{101.132} = 7493$$

Resultant Flatwise Bending Stresses (In Fiber Plane)

Graphite/Epoxy

$$f_b = \frac{f_{b_{x-x}}}{\cos 10^\circ \cos 16^\circ} = \frac{99055}{.94665} = \underline{\underline{104638}} \text{ psi}$$

0° S Glass

$$f_b = \frac{f_{b_{x-x}}}{\cos 10^\circ \cos 11^\circ} = \frac{16630}{.96671} = \underline{\underline{17203}} \text{ psi}$$

$\pm 45^\circ$ S Glass

$$f_b = \frac{f_{b_{xx}}}{\cos 10^\circ \cos 13^\circ} = \frac{7493}{.95956} = \underline{\underline{7809}} \text{ psi}$$

Centrifugal Stresses

Graphite/Epoxy

$$f_c' = \frac{R_A E}{AE} = \frac{98424\ (17.5 \times 10^6)}{72.464 \times 10^6} = 23{,}769 \quad \text{psi}$$

0° S Glass

$$f_c' = \frac{98424\ (6.8 \times 10^6)}{72.464 \times 10^6} = 9236 \quad \text{psi}$$

$\pm 45^\circ$ S Glass

$$f_c' = \frac{98424\ (2.4 \times 10^6)}{72.464 \times 10^6} = 3260 \quad \text{psi}$$

Resultant Centrifugal Stress (In Fiber Plane)

Graphite/Epoxy

$$f_c = \frac{f_c'}{\cos 10^\circ \cos 16^\circ} = \frac{23769}{.94665} = \underline{\underline{25{,}109}} \quad \text{psi}$$

0° S Glass

$$f_c = \frac{f_c'}{\cos 10^\circ \cos 11^\circ} = \frac{9236}{.96671} = \underline{\underline{9554}} \quad \text{psi}$$

$\pm 45^\circ$ S Glass

$$f_c = \frac{f_c'}{\cos 10^\circ \cos 13^\circ} = \frac{3260}{.95956} = \underline{\underline{3397}} \quad \text{psi}$$

Bending Stresses (Edgewise)

Graphite/Epoxy

$$f_{b_{Y-Y}} = \frac{M_{Y-Y}}{Z_{Y-Y}} = \frac{168990}{18.594} = 9088 \quad \text{psi}$$

0° S Glass

$$f_{b_{Y-Y}} = \frac{168990}{47.855} = 3531 \quad \text{psi}$$

$\pm 45^\circ$ S Glass

$$f_{b_{Y-Y}} = \frac{168990}{135.589} = 1246 \quad \text{psi}$$

Resultant Edgewise Bending Stress (In Fiber Plane)

Graphite/Epoxy

$$f_b = \frac{f_{b_{Y-Y}}}{\cos 10^\circ \cos 16^\circ} = \frac{9088}{.94665} = \underline{9601} \text{ psi}$$

0° S Glass

$$f_b = \frac{f_{b_{Y-Y}}}{\cos 10^\circ \cos 11^\circ} = \frac{3531}{.96671} = \underline{3653} \text{ psi}$$

$\pm 45^\circ$ S Glass

$$f_b = \frac{f_{b_{Y-Y}}}{\cos 10^\circ \cos 13^\circ} = \frac{1246}{.95956} = \underline{1299} \text{ psi}$$

Section A-A is critical for the load burst condition

$$M_{Y-Y} = V_E (R-10.9) = (12900)(24-10.9)$$

$$= (12,900)(13.1) = 168,990 \text{ in.-lb}$$

Section Modulus (Graphite Epoxy)

$$Z_{Y-Y} = 18.6 \text{ in.}^3$$

$$f_{b_{Y-Y}} = \frac{M_{Y-Y}}{Z_{Y-Y}} = \frac{168,990}{18.6} = 9085 \text{ psi}$$

$$\therefore f_b = \frac{9085}{\cos 10^\circ \cos 16^\circ} = \frac{9085}{(0.985)(0.961)} = 9,597 \text{ psi}$$

Edgewise bending stress due to engine burst condition.

Edgewise bending stress resulting from the static ultimate condition at Section A-A in the critical graphite epoxy strap is 9601 psi. (Symmetric dive and pullout, autorotation power on.)

Therefore, the engine load burst condition is not critical.

Fatigue Analysis, Section A-A (Reference Tables 23 and 24)

Bending Moment, Flatwise Mean (Steady)	Vibratory
$M_{X-X} = V_N d_1 + .4 F_c$	
$M_{X-X} = 5734 \times 13.1 + 4 \times 48422$	$M_{X-X} = \pm 11{,}523 \times 13.1 + .4 (\pm 2133)$
$M_{X-X} = 75{,}115 + 19{,}369$	$M_{X-X} = \pm 150{,}951 + \pm 853$
$M_{X-X} = \underline{94484}$ in.-lb	$M_{X-X} = \pm \underline{151{,}804}$ in.-lb
Bending Moment, Edgewise	
$M_{Y-Y} = V_E d_1$	
$M_{Y-Y} = 8847 \times 13.1$	$M_{Y-Y} = \pm 810 \times 13.1$
$M_{Y-Y} = \underline{115{,}896}$ in.-lb	$M_{Y-Y} = \pm \underline{10{,}611}$ in.-lb
Bending Stresses, Flatwise	
Graphite/Epoxy	
$f_{b_{X-X}} = \frac{M_{X-X}}{Z_{X-X}} = \frac{94{,}484}{7.650}$	$f_{b_{X-X}} = \frac{M_{X-X}}{Z_{X-X}} = \frac{\pm 151{,}804}{7.650}$
$f_{b_{X-X}} = 12{,}351$ psi	$f_{b_{X-X}} = \pm 19{,}844$ psi
0° S Glass	
$f_{b_{X-X}} = \frac{94{,}484}{45.537} = 2075$ psi	$f_{b_{X-X}} = \frac{\pm 151{,}804}{45.537} = \pm 3334$ psi
$\pm 45^\circ$ S Glass	
$f_{b_{X-X}} = \frac{94{,}484}{101.132} = 934$ psi	$f_{b_{X-X}} = \frac{\pm 151{,}804}{101.132} = \pm 1501$ psi

Resultant Flatwise Bending Stress (In Fiber Plane)

Graphite/Epoxy

$$f_b = \frac{f_{b_{X-X}}}{\cos 10^\circ \cos 16^\circ} = \frac{12,351}{.94665}$$

$$f_b = 13047 \text{ psi}$$

$$f_b = \frac{f_{b_{X-X}}}{\cos 10^\circ \cos 16^\circ} = \frac{\pm 19844}{.94665}$$

$$f_b = \pm 20692 \text{ psi}$$

0° S Glass

$$f_b = \frac{2075}{\cos 10^\circ \cos 11^\circ} = 2146 \text{ psi}$$

$$f_b = \frac{\pm 3334}{.96671} = \pm 3449 \text{ psi}$$

$\pm 45^\circ$ S Glass

$$f_b = \frac{934}{\cos 10^\circ \cos 13^\circ} = 973 \text{ psi}$$

$$f_b = \frac{\pm 1501}{.95956} = \pm 1564 \text{ psi}$$

Centrifugal Stresses

Graphite/Epoxy

Mean

$$f'_c = \frac{F_c E}{AE}$$

$$f'_c = \frac{48422 \ (17.5 \times 10^6)}{72.464 \times 10^6}$$

$$f'_c = 11694 \text{ psi}$$

Vibratory

$$f'_c = \frac{\pm 2133 \ (17.5 \times 10^6)}{72.464 \times 10^6}$$

$$f'_c = \pm 515 \text{ psi}$$

0° S Glass

$$f'_c = \frac{48422 \ (6.8 \times 10^6)}{72.464 \times 10^6}$$

$$f'_c = 4544 \text{ psi}$$

$$f'_c = \frac{\pm 2133 \ (6.8 \ 10^6)}{72.464 \times 10^6}$$

$$f'_c = \pm 200 \text{ psi}$$

$\pm 45^\circ$ S Glass

$$f'_c = \frac{48422 \ (2.4 \times 10^6)}{72.464 \times 10^6}$$

$$f'_c = 1604 \text{ psi}$$

$$f'_c = \frac{\pm 2133 \ (2.4 \times 10^6)}{72.464 \times 10^6}$$

$$f'_c = \pm 71 \text{ psi}$$

Resultant Centrifugal Stress (In Fiber Plane)

Graphite/Epoxy

$$f_c = \frac{f_c'}{\cos 10^\circ \cos 16^\circ}$$

$$f_c = \frac{11694}{.94665} = \underline{\underline{12,353}} \text{ psi}$$

$$f_c = \frac{\pm 515}{.94665} = \underline{\underline{\pm 544}} \text{ psi}$$

0° S Glass

$$f_c = \frac{f_c'}{\cos 10^\circ \cos 11^\circ}$$

$$f_c = \frac{4544}{.96671} = \underline{\underline{4700}} \text{ psi}$$

$$f_c = \frac{\pm 200}{.96677} = \underline{\underline{\pm 207}} \text{ psi}$$

$\pm 45^\circ$ S Glass

$$f_c = \frac{f_c'}{\cos 10^\circ \cos 13^\circ}$$

$$f_c = \frac{1604}{.95956} = \underline{\underline{1671}} \text{ psi}$$

$$f_c = \frac{\pm 71}{.95956} = \underline{\underline{\pm 74}} \text{ psi}$$

Bending Stresses, Edgewise

Graphite/Epoxy

$$f_{b_{Y-Y}} = \frac{M_{Y-Y}}{Z_{Y-Y}} = \frac{115,896}{18.594}$$

$$f_{b_{Y-Y}} = 6233 \text{ psi}$$

$$f_{b_{Y-Y}} = \frac{\pm 10611}{18.594}$$

$$f_{b_{Y-Y}} = \pm 571 \text{ psi}$$

0° S Glass

$$f_{b_{Y-Y}} = \frac{115896}{47.855}$$

$$f_{b_{Y-Y}} = 2422 \text{ psi}$$

$$f_{b_{Y-Y}} = \frac{\pm 10611}{47.855}$$

$$f_{b_{Y-Y}} = \pm 222 \text{ psi}$$

$\pm 45^{\circ}$ S Glass

$$f_{b_{Y-Y}} = \frac{115896}{135.589} \qquad f_{b_{Y-Y}} = \frac{\pm 10611}{135.589}$$

$$f_{b_{Y-Y}} = 855 \text{ psi} \qquad f_{b_{Y-Y}} = \pm 78 \text{ psi}$$

Resultant Edgewise Bending Stresses (In Fiber Plane)

Graphite/Epoxy

$$f_b = \frac{f_{b_{Y-Y}}}{\cos 10^{\circ} \cos 16^{\circ}}$$

$$f_b = \frac{6233}{.94665} \qquad f_b = \frac{\pm 571}{.94665}$$

$$f_b = \underline{\underline{6584}} \text{ psi} \qquad f_b = \underline{\underline{\pm 603}} \text{ psi}$$

0° S Glass

$$f_b = \frac{f_{b_{Y-Y}}}{\cos 10^{\circ} \cos 11^{\circ}}$$

$$f_b = \frac{2422}{.96671} \qquad f_b = \frac{\pm 222}{.96671}$$

$$f_b = \underline{\underline{2505}} \text{ psi} \qquad f_b = \underline{\underline{\pm 230}} \text{ psi}$$

$\pm 45^{\circ}$ S Glass

$$f_b = \frac{f_{b_{Y-Y}}}{\cos 10^{\circ} \cos 13^{\circ}}$$

$$f_b = \frac{855}{.95956} \qquad f_b = \frac{\pm 78}{.95956}$$

$$f_b = \underline{\underline{891}} \text{ psi} \qquad f_b = \underline{\underline{\pm 82}} \text{ psi}$$

Static Analysis - Section B-B (Reference Table 22)

Bending Moment

$$M_{XX} = V_N d = (54840.0)\ (4.1) = 224{,}844 \text{ in.-lb}$$

$$M_{YY} = (12900)\ (4.1) = 52890 \text{ in.-lb}$$

Bending Stresses (Flatwise)

Graphite Epoxy

$$f_{bXX} = \frac{M_{XX}}{Z_{XX}} = \frac{224{,}844}{3.09} = 72765 \text{ psi}$$

0° S Glass

$$f_{bXX} = \frac{224{,}844}{16.39} = 13718.34 \text{ psi}$$

$\pm 45^\circ$ S Glass

$$f_{bXX} = \frac{224{,}844}{41.67} = 5395.8 \text{ psi}$$

Bending Stresses In Fiber of Strap (Flatwise)

Graphite Epoxy

$$f_b = \frac{f_{bXX}}{(\cos 10^\circ)\ (\cos\ )} = \frac{72765}{(\cos 10^\circ)\ (\cos 15^\circ)} = \frac{72765}{(0.966)\ (0.986)} = 76395.63 \text{ psi}$$

0° S Glass

$$f_b = \frac{13718.3}{(0.986)\ (0.986)} = 14402.5 \text{ psi}$$

$\pm 45^\circ$ S Glass

$$f_b = \frac{5395.8}{(0.986)\ (0.966)} = 5665.05 \text{ psi}$$

Centrifugal Stresses (Direct)

Graphite Epoxy

$$f'_c = \frac{R_A E}{AE} = \frac{(98424)\ (17.5)\ (10^6)}{2\ (29.00)\ (10^6)} = 29696.88$$

$\pm 45^\circ$ S Glass

$$f'_c = \frac{(98424)\ (2.4)\ (10^6)}{2\ (29.00)\ (10^6)} = 4072.71 \text{ psi}$$

0° S Glass

$$\frac{(9842)\ (6.8)\ 10^6}{(58)\ 10^6} = 11539.36 \text{ psi}$$

Centrifugal Stresses (In Fiber of Strap)

Graphite Epoxy

$$f_c = \frac{f'_c}{\cos 10^\circ \cos\theta} = \frac{29696.88}{\cos 10^\circ \cos 15^\circ} = 31178.81$$

0° S Glass

$$\frac{11539.36}{(0.986)\ (.986)} = 11869.5 \text{ psi}$$

$\pm 45^\circ$ S Glass

$$\frac{4072.71}{(0.986)\ (0.966)} = 4275.9 \text{ psi}$$

Bending Stress (Edgewise)

Graphite Epoxy

$$f_{b_{YY}} = \frac{M_{YY}}{Z_{YY}} = \frac{52890}{11.46} = 4615.18 \text{ psi}$$

0° S Glass

$$\frac{52890}{29.39} = 1799.59 \text{ psi}$$

$\pm 45^\circ$ S Glass

$$\frac{52890}{83.5} = 633.413 \text{ psi}$$

Bending Stresses in Fiber of Strap (Edgewise)

Graphite Epoxy

$$f_b = \frac{f_{b_{YY}}}{\cos 10^\circ \cos\theta} = \frac{4615.18}{(0.986)\ (0.966)} = 4847.88 \text{ psi}$$

0° S Glass

$\frac{1799.59}{(0.986)\ (0.986)} = 1851.43$ psi

$\pm 45^\circ$ S Glass

$\frac{633.413}{(0.986)\ (0.966)} = 665.350$ psi

Fatigue Analysis, Section B-B (Reference Tables 23 and 24)

Bending Moment

Mean Steady

$M_{XX} = V_N d_Z = (5734)\ (4.1)$

$= 23509$ in.-lb

$M_{YY} = V_E d_Z$

$M_{YY} = (8847)\ (4.1) = 36273$ in.-lb

Vibratory

$M_{XX} = \pm (11523)\ (4.1)$

$= \pm 47244$ in.-lb

$M_{YY} = \pm (810)\ (4.1) = \pm 3321$ in.-lb

Bending Stresses (Flatwise)

Graphite Epoxy

$f_{b_{XX}} = \frac{M_{XX}}{Z_{XX}} = \frac{23509}{3.09} = 7608.09$ psi

$\frac{\pm 47244}{3.09} = \pm 15289.3$ psi

$\pm 45^\circ$ S Glass

$f_{b_{XX}} = \frac{23509}{41.67} = 564.17$ psi

$\frac{\pm 47244}{41.67} = 1133.77$ psi

0° S Glass

$f_{b_{XX}} = \frac{23509}{23.43} = 1003.37$ psi

$\frac{\pm 47244}{23.43} = \pm 2016.39$ psi

Resultant Flatwise Bending Stresses (In Fiber Plane)

Graphite Epoxy

$f_b = \frac{5651.20}{\cos 10^\circ \cos 16^\circ} = 5900$ psi

$f_b = \frac{\pm 11356.73}{.94665} = \pm 12050$ psi

0° S Glass

Mean (Steady

$\frac{1003.37}{\cos 10^\circ \cos 13^\circ} = 1035$ psi

Vibratory

$\frac{\pm 2016.39}{0.96671} = \pm 2060$ psi

$\pm 45^{\circ}$ S Glass

$$\frac{564.7}{\cos 10^{\circ} \cos 11^{\circ}} = 580 \text{ psi}$$

$$\frac{\pm 1133.77}{0.9596} \pm 1180 \text{ psi}$$

Centrifugal Stresses

Mean (Steady)

Vibratory

Graphite Epoxy

$$f_{c_d} = \frac{F_c E}{\Sigma AE} = \frac{(48422)\ (17.5)\ 10^6}{(58)\ 10^6}$$

$$= 14610 \text{ psi}$$

$$\pm \frac{(2133)\ (17.5)\ (10^6)}{(58)\ 10^6} = 644$$

0° S Glass

$$f_{c_d} \frac{48422\ (6.8)\ (10)^6}{(58)\ (10)^6} = 5677 \text{ psi}$$

$$f_{c_d} = \pm \frac{2133\ (6.8)}{58\ (10)^6}\ (10)^6 = \pm 250 \text{ psi}$$

$\pm 45^{\circ}$ S Glass

$$f_{c_d} = \frac{48422\ (2.4)\ (10)^6}{58\ (10)^6} = 2000 \text{ psi}$$

$$f_{c_d} = \frac{\pm (2133)\ (2.4)\ 10^6}{(58)\ 10^6} = 88 \text{ psi}$$

Resultant Centrifugal Stresses (In Fiber Plane)

Graphite Epoxy

$$f_c = \frac{14610}{\cos 10^{\circ} \cos 16^{\circ}} = 15171 \text{ psi}$$

$$f_c = \frac{\pm 644}{0.94665} = 668$$

0° S Glass

$$f_c = \frac{567.7}{\cos 10^{\circ} \cos 11^{\circ}} = 5822 \text{ psi}$$

$$\frac{\pm 250.0}{0.96691} = \pm 256.4 \text{ psi}$$

$\pm 45^{\circ}$ S Glass

$$f_c = \frac{2000}{\cos 10^{\circ} \cos 13^{\circ}} = 2050 \text{ psi}$$

$$\frac{88}{0.9596} = \pm 90 \text{ psi}$$

Bending Stresses (Edgewise)

Graphite Epoxy

$$f_{b_{YY}} = \frac{M_{YY}}{Z_{YY}} = \frac{36273}{11.46} = 3165 \text{ psi} \qquad f_{b_{YY}} = \frac{\pm 3321}{11.46} = \pm 289.79 \text{ psi}$$

0° S Glass

$$f_{b_{YY}} = \frac{36273}{29.39} = 1234.20 \text{ psi} \qquad f_{b_{YY}} = \frac{\pm 3321}{29.39} = 113 \text{ psi}$$

$\pm 45^{\circ}$ S Glass

$$f_{b_{YY}} = \frac{36273}{83.5} = 434.40 \text{ psi} \qquad f_{b_{YY}} = \frac{\pm 3321}{83.5} = \pm 39.77 \text{ psi}$$

Resultant Edgewise Bending Stresses (In Fiber Plane)

Mean (Steady	Vibratory

Graphite Epoxy

$$f_b = \frac{3165.18}{\cos 10^{\circ} \cos 16^{\circ}} = 3286 \text{ psi} \qquad f_b = \frac{\pm 289.79}{0.94665} = \pm 300 \text{ psi}$$

0° S Glass

$$f_b = \frac{1234.20}{\cos 10^{\circ} \cos 11^{\circ}} = 1270 \text{ psi} \qquad f_b = \frac{\pm 113}{.96671} = \pm 115 \text{ psi}$$

$\pm 45^{\circ}$ S Glass

$$f_b = \frac{434.40}{\cos 10^{\circ} \cos 13^{\circ}} = 445 \text{ psi} \qquad f_b = \frac{\pm 39.77}{.9596} = \pm 40 \text{ psi}$$

The portion of out-of-plane shear reacted by the splayed laminates is a function of the strap stiffness and inclination. The in-plane shear webs are assumed to carry no out-of-plane shear.

Table 34. SECTION B-B, GEOMETRIC PROPERTIES AND SHEAR RESISTANCE

Item	A	E x 10^6	AEx 10^6	Y	AEY	θ	TAN θ	P_H	P_V
* 1	0.156	17.5	2.73	2.205	6.02	15	.2679	11000	3000
* 3		17.5	2.73	1.803	5.00	14	.2493	9000	2300
*5 5		17.5	2.73	1.401	4.15	12	.2125	7407	1600
* 7		6.8	1.06	1.026	1.10	10	.1763	1970	350
* 9		6.8		.624	.66	8	.1405	1200	170
* 11		6.8		.222	.24	7	.1227	430	55
13		6.8		.012	.013	6	.1051	-23	-2
15		6.8		.414	.44	4	.0699	-780	-50
17		6.8		.816	.87	0	0	-1550	0
19		17.5	2.73	1.181	3.22	0	0	-5750	0
21		17.5	2.73	1.583	4.32	-4	-.0699	-7720	550
23		17.5	2.73	1.985	5.50	-7	-.1227	-9820	1210
* 24	0.436	2.4	1.05	2.88	3.03	15	.2679	5408	1500
25	0.436	2.4	1.05	2.16	2.30	-7	-.1227	-4110	505
Total									11188

where

$$P_H = \frac{V_N \times d_2 \, AEY}{EI_{XX}}$$

$$P_H = \frac{54840 \times 4.1 \times AEY}{125.98}$$

$$P_H = 1785 \times AEY$$

$$P_V = P_H \, TAN \, \theta$$

$$\therefore \Sigma P_V = 2 \, P_V = 2 \times 11188 = \underline{\underline{22376}} \text{ lb}$$

* Loads in fibers above neutral axis are considered positive.

P_H = In-Plane Shear Load

P_V = Out-of-Plane Shear Load

V_N = Applied Load (Out-of-Plane)

d_2 = Distance to Section B-B from point of load application

EI_{XX} = Total Section Property for Section B-B

Resultant Applied Shear Load (V_{N_R}) Carried by Vertical Shear Web

$$V_{N_R} = V_N - \Sigma P_V$$

$$V_{N_R} = 54840 - 22358 = 32,464 \text{ lb}$$

TABLE 35. SECTION B-B, Σ AEY	
Item	AEY X 10^6
1	6.02
3	5.00
5	4.15
7	1.10
9	.66
11	.24
24	3.03
Total	20.20

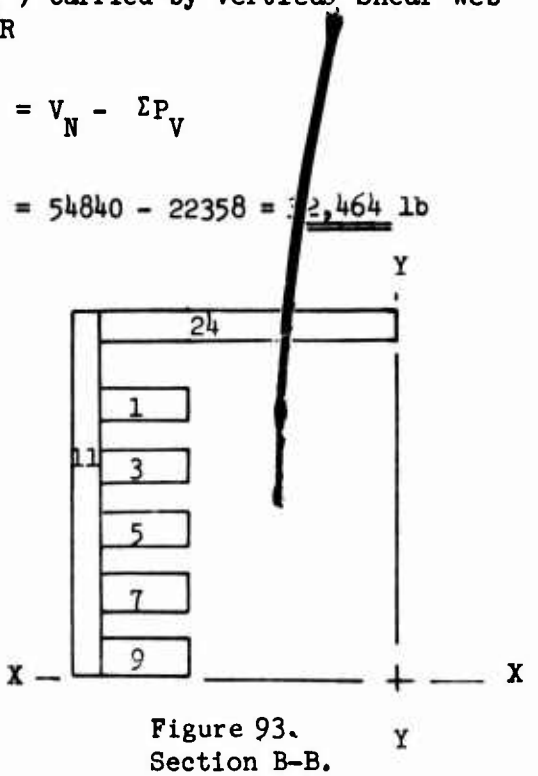

Figure 93. Section B-B.

$$\Sigma AEY = (20.20 \times 10^6) = 40.40 \times 10^6$$

Shear Stress in Out-of-Plane Webs

$$f_{s_{X-X}} = \frac{(V_{NR})_{\Sigma EQ}}{(I_{X-X})(2b)} = \frac{(V_N)_{\Sigma AEY}}{(EI_{X-X})(2b)}$$

$$f_{s_{X-X}} = \frac{32464\ (40.40 \times 10^6)}{(125.98 \times 10^6)\ (2 \times .125)} = 41640$$

MARGIN OF SAFETY

$$M.S = \frac{\text{Allowable Shear Stress}}{\text{Applied Shear Stress}} - 1$$

$$M.S = \frac{42000}{41640} - 1 = 1.010 - 1 = +.010$$

In-Plane Shear Web Analysis (About Y-Y Axis)

Sum of Products of AEX (10^6) Between Y-Y (Neutral) Axis and Most Extreme Fiber.

$$\Sigma AEX\ (10^6) = 2\ (118.89 \times 10^6) = 237.78 \times 10^6$$

TABLE 36. SECTION B-B, Σ AEX

Item	AEX (10^6)
1	2.73
3	2.73
5	2.73
7	1.06
9	1.06
11	1.06
13	1.06
15	1.06
17	1.06
19	2.73
21	2.73
23	2.73
24	1.05
25	1.05
Total	24.84

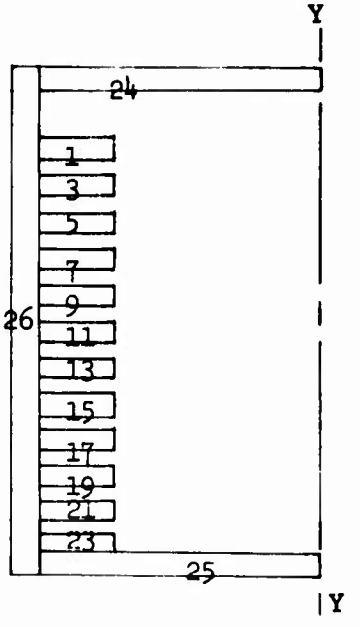

Figure 94. Section B-B.

Shear Stress in (In-Plane) Shear Webs

$$f_{s_{Y-Y}} = \frac{V_E\ \Sigma EQ}{\Sigma I_{Y-Y}\ (2d)} = \frac{V_E\ \Sigma AEX}{\Sigma I_{Y-Y}\ (2d)}$$

$$f_{s_{Y-Y}} = \frac{12900\ (237.78 \times 10^6)}{878.2 \times 10^6\ (2 \times .125)} = 13{,}970$$

MARGIN OF SAFETY

$$M.S. = \frac{\text{Allowable Shear Stress}}{\text{Applied Shear Stress}} = -1$$

$$M.S. = \qquad M.S. = \frac{42000}{13970} = -1$$

$$M.S. = 3.006 - 1 = +\underline{2.0}$$

Calculations for Section C-C Section Properties (Reference Table 16)

$$Io = \frac{.10 \times 3.70^3}{12} = .42210$$

$$\bar{Y} = \frac{\Sigma AEY}{\Sigma AE} = \frac{52.793 \times 10^6}{25.394 \times 10^6} = \underline{2.079}$$

$$\Sigma EI_{X-X} = 2 \left[\Sigma AEY^2 + \Sigma EIo - \Sigma AE\bar{Y}^2\right]$$

$$\Sigma EI_{X-X} = 2 \left[138.582 \times 10^6 + 1.13250 \times 10^6 - (25.394 \times 10^6)(2.079)^2\right]$$

$$\Sigma EI_{X-X} = 2 \left[138.582 \times 10^6 + 1.13250 \times 10^6 - 109.759 \times 10^6\right]$$

$$\Sigma EI_{X-X} = 2 \left[29.955 \times 10^6\right] = \underline{59.911 \times 10^6}$$

$$\Sigma EA = 2 \left[25.394 \times 10^6\right] = \underline{50.788 \times 10^6}$$

$$Io = \frac{3.70 \times .10^3}{12} = .00030$$

$$\Sigma EI_{Y-Y} = 2 \quad \Sigma AEX^2 + \Sigma EIo$$

$$\Sigma EI_{Y-Y} = 2 \left[266.693 \times 10^6 + 2.72880 \times 10^6\right]$$

$$\Sigma EI_{Y-Y} = 2 \left[269.4218 \times 10^6\right]$$

$$\Sigma EI_{Y-Y} = 538.844 \times 10^6$$

Section Modulus Calculations

Graphite/Epoxy

$$Z_{X-X} = \frac{EI_{X-X}}{E\, C_Y} = \frac{59.911 \times 10^6}{(17.5 \times 10^6)\ 1.479} = \underline{2.314}$$

$$Z_{Y-Y} = \frac{EI_{Y-Y}}{E\, C_X} = \frac{538.844 \times 10^6}{(17.5 \times 10^6)\ 3.68} = \underline{8.367}$$

0° S Glass

$$Z_{X-X} = \frac{59.911 \times 10^6}{(6.8 \times 10^6)\ .729} = \underline{12.085}$$

$$Z_{Y-Y} = \frac{538.844 \times 10^6}{(6.8 \times 10^6)\ 3.68} = \underline{21.532}$$

Static Analysis - Section C-C (Reference Table 22)

Bending Moment (Flatwise)

$$M_{X-X} = .4\ R_A$$

$$M_{X-X} = .4 \times 98424 = \underline{39370}\ \text{in.-lb}$$

Bending Moment (Edgewise)

$$M_{Y-Y} = 0$$

Bending Stress (Flatwise)

Graphite/Epoxy

$$f_{b_{X-X}} = \frac{M_{X-X}}{Z_{X-X}} = \frac{39370}{2.314} = 17014\ \text{psi}$$

0° S Glass

$$f_{b_{X-X}} = \frac{39370}{12.085} = 3258\ \text{psi}$$

Resultant Flatwise Bending Stresses (In.Fiber Plane)

Graphite Epoxy

$$f_b = \frac{f_{b_{X-X}}}{\cos 10^{\circ} \cos 0^{0}} = \frac{17014}{.98481} = \underline{17276}\ \text{psi}$$

0° S Glass

$$f_b = \frac{3258}{.98481} = \underline{3308}\ \text{psi}$$

Centrifugal Stresses

Graphite/Epoxy

$$f_c = \frac{R_A E}{\Sigma AE} = \frac{98424\ (17.5 \times 10^6)}{50.788 \times 10^6} = 33914 \text{ psi}$$

0° S Glass

$$f_c = \frac{98424\ (6.8 \times 10^6)}{50.788 \times 10^6} = 13178 \text{ psi}$$

Resultant Centrifugal Stresses (In Fiber Plane)

Graphite/Epoxy

$$f_c = \frac{f_c}{\cos 10^\circ \cos 0^\circ} = \frac{33914}{.98481} = \underline{34437} \text{ psi}$$

0° S Glass

$$f_c = \frac{13178}{.98481} = \underline{13381} \text{ psi}$$

Development of a Static Ultimate Margin of Safety for the 0° Glass Lug Straps

The analytical method used to calculate the ultitmate margin of safety was developed and reported in Reference 6.

Ultimate Bending Stress Summary

- Static ult. flatwise bending stress (f_b) due to out-of-plane shear = 3308 psi
- Static ult. axial stress (f_a) due to centrifugal load = 13,381 psi

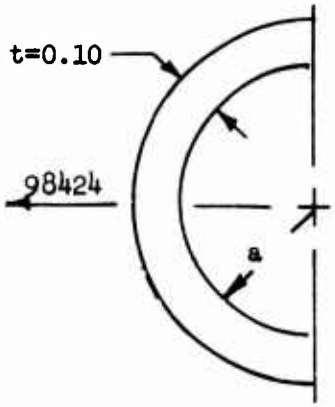

$\therefore$ AV = $f_b + f_c$ = 3308 + 13,381 psi

= 16,689 psi

$$a = 3.68; \frac{t}{a} = \frac{.10}{3.68} = .02717$$

Notation:

σr = Applied Radial Compression Stress

$\sigma\theta$ = Applied Tangential Tensile Stress

$\sigma r^* = F_{c_{90^\circ}}$ = Allowable Radial Compression Stress

= 25,000 psi @ 160° F

$\sigma\theta^* = F_{tu_{0^\circ}}$ = Allowable Tangential Tensile Stress

= 180,000 psi @ 160° F

$$\sigma r_{MAX} = 1.13\ \sigma \frac{t}{a}$$

$$\sigma r_{MAX} = 1.13 \times 16689 \times .02717$$

$$\sigma r_{MAX} = 512 \text{ psi Ult.}$$

$$\sigma\theta = 1 + .079 \left(\frac{t}{d}\right)^2 \sigma AV$$

$$\sigma\theta = 1 + .079\ (.02717)^2\ 16689 = 1 + .079\ (.00073)\ 16689$$

$$\sigma\theta = 1 + .00005\ \ 16689 = 16689 \text{ psi Ult.}$$

$$M.S. = \frac{1}{\left\{\left[\frac{\sigma r_{MAX}}{\sigma r^*}\right]^2 - \left[\frac{\sigma r_{MAX}}{\sigma r^* \sigma\theta^*} + \frac{\sigma\theta}{\sigma\theta^*}\right]^2\right\}^{\frac{1}{2}}} - 1$$

$$M.S. = \frac{1}{\left\{\left[\frac{(-512)}{25000}\right]^2 - \left[\frac{(-512)\ (16689)}{(25000)\ (180000)} + \frac{16689}{180000}\right]^2\right\}^{\frac{1}{2}}} - 1$$

$$M.S. = \frac{1}{\left\{(-.02048)^2 - \left[\frac{(-1)\ (\ 1\ )}{(48.83)\ (10.785)} + (.09271)\right]^2\right\}^{\frac{1}{2}}} - 1$$

$$M.S. = \frac{1}{\left\{(.00041) - \frac{(-1)}{526.63} + .00859\right\}^{\frac{1}{2}}} - 1$$

$$M.S. = \frac{1}{\left[.00041 + .00189 + .00859\right]^{\frac{1}{2}}} - 1$$

$$M.S. = \frac{1}{\left[.01089\right]^{\frac{1}{2}}} - 1 = \frac{1}{.10435} - 1$$

$$M.S. = 9.58 - 1$$

$$M.S. = + \underline{\underline{HIGH}}$$

Fatigue Analysis - Section C-C Reference Tables 23 and 24)

Bending Moment, Flatwise

Mean (Steady)	Vibratory
$M_{X-X} = .4\ F_c = .4 \times 48422$	$M_{X-X} = .4\ (\pm 2133)$
$M_{X-X} = \underline{\underline{19369}}$ in.-lb	$M_{X-X} = \pm \underline{\underline{853}}$ in.-lb

Bending Stresses (Flatwise)

Graphite/Epoxy

$f_{b_{X-X}} = \frac{M_{X-X}}{Z_{X-X}} = \frac{19369}{2.314}$	$f_{b_{X-X}} = \frac{\pm 853}{2.314}$
$f_{b_{X-X}} = 8370$ psi	$f_{b_{X-X}} = \pm 369$ psi

0° S Glass

$f_{b_{X-X}} = \frac{19369}{12.085}$	$f_{b_{X-X}} = \frac{853}{12.085}$
$f_{b_{X-X}} = 1603$ psi	$f_{b_{X-X}} = \pm 71$ psi

Resultant Flatwise Bending Stresses (In Fiber Plane)

Graphite/Epoxy

$$f_b = \frac{f_{b_{X-X}}}{\cos 10^\circ \cos 0^\circ}$$

$$f_b = \frac{8370}{.985}$$

$$f_b = \underline{\underline{8498}} \text{ psi}$$

$$f_b = \frac{\pm 369}{.985}$$

$$f_b = \pm \underline{\underline{374}} \text{ psi}$$

0° S Glass

$$f_b = \frac{1603}{.985}$$

$$f_b = \underline{\underline{1627}} \text{ psi}$$

$$f_b = \frac{\pm 71}{.985}$$

$$f_b = \pm \underline{\underline{72}} \text{ psi}$$

Centrifugal Stresses,

Graphite/Epoxy

$$f_c' = \frac{F_c E}{AE}$$

$$f_c' = \frac{48422\ (17.5 \times 10^6)}{50.788 \times 10^6}$$

$$f_c' = 16685 \text{ psi}$$

$$f_c' = \frac{\pm 2133\ (17.5 \times 10^6)}{50.788 \times 10^6}$$

$$f_c' = \pm 735 \text{ psi}$$

0° S Glass

$$f_c' = \frac{48422\ (6.8 \times 10^6)}{50.788 \times 10^6}$$

$$f_c' = 6483 \text{ psi}$$

$$f_c' = \frac{\pm 2133\ (6.8 \times 10^6)}{50.788 \times 10^6}$$

$$f_c' = \pm 286 \text{ psi}$$

Resultant Centrigugal Stresses (In Fiber Plane)

Graphite/Epoxy

$$f_c = \frac{f'_c}{\cos 10^\circ \cos 0^\circ}$$

$$f_c = \frac{16685}{.985} \qquad f_c = \frac{\pm 735}{.985}$$

$$f_c = \underline{16939} \text{ psi} \qquad f_c = \pm \underline{746} \text{ psi}$$

0° S Glass

$$f_c = \frac{6483}{.985} \qquad f_c = \frac{286}{.985}$$

$$f_c = \underline{6582} \text{ psi} \qquad f_c = \pm \underline{290} \text{ psi}$$

Calculations For Section 0-0 Loads (Reference page 87)

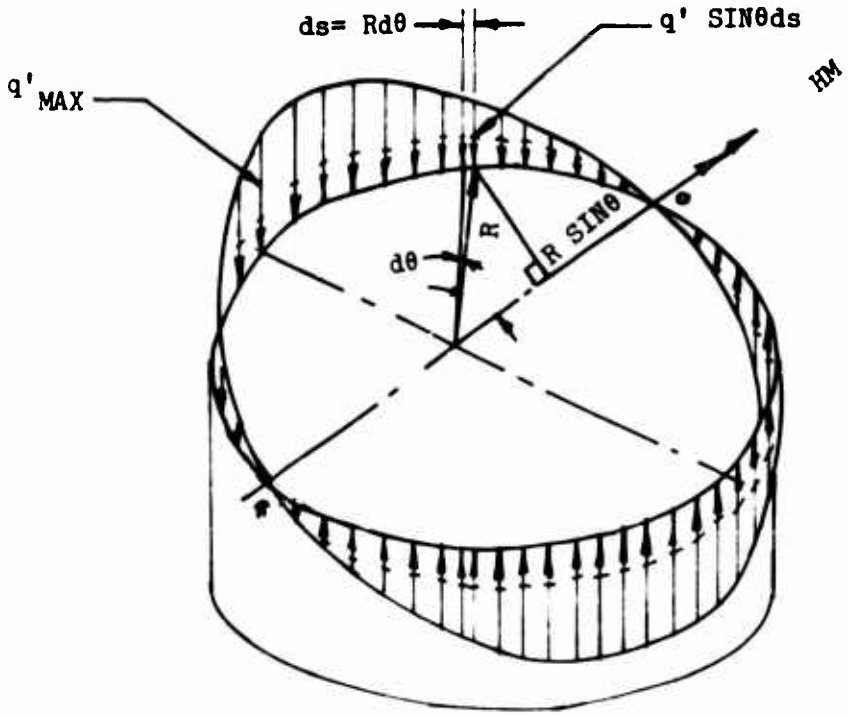

Figure 95. Hub Sinusoidal Head Moment Reaction at Clamp Bolts.

Head Moment Reactive Loads - Static Ultimate

q' = Force distribution on outer bolt circle, lb maximum at load, zero at ends in.

q = Load per bolt, lb

$$\text{LOAD} = q' \text{SIN}\theta ds = q'\text{SIN}\theta R d\theta = q'R\int_0^{2\pi} \text{SIN}\theta d\theta$$

$$\text{HM} = \left\{ q'R\int_0^{2\pi} \text{SIN}\theta d\theta \right\} R \text{SIN}\theta = q'R^2\int_0^{2\pi} \text{SIN}^2\theta d\theta$$

$$\text{HM} = q'R^2 \left[\frac{\theta}{2} - \frac{\text{SIN}2\theta}{4} \right]_0^{2\pi} = q'R^2 \left[\frac{2\pi}{2} - \frac{\text{SIN}2\pi}{4} \right] =$$

$$\pi q' R^2$$

$$\therefore q' = \frac{HM}{\pi R^2} \left[\text{MAX } \frac{\text{lb}}{\text{in.}} \right]$$

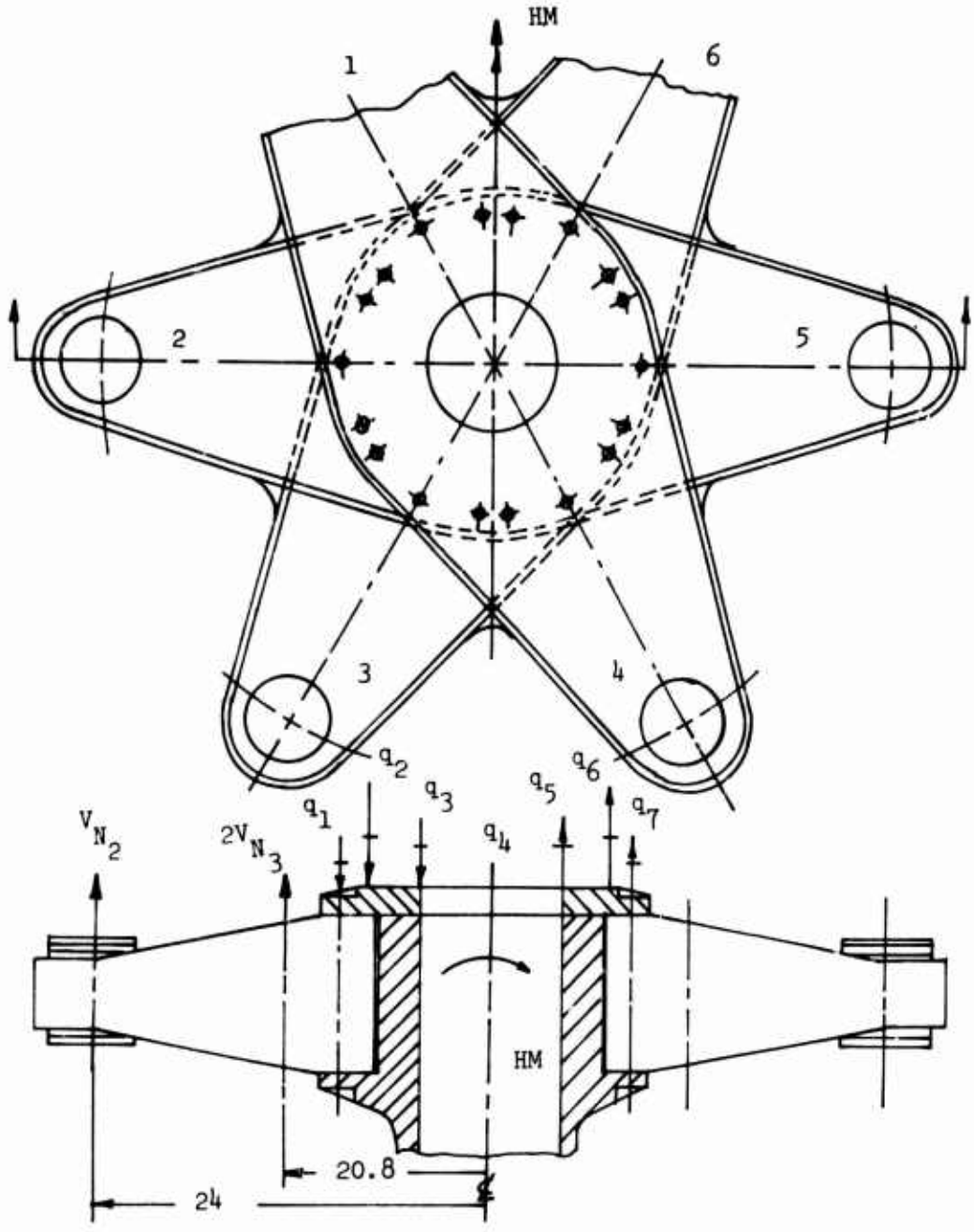

Figure 96. Head Moment Loading and Reactions - Ultimate Case.

$$q = \int_{\theta_1}^{\theta_2} \frac{HM}{\pi R^2} \text{ SIN}\theta \; d\theta = \frac{HM}{\pi R^2} \int_{\theta_1}^{\theta_2} \text{SIN}\theta d\theta$$

$$\therefore q = -\frac{HM}{\pi R^2} \left[\text{COS}\theta\right]_{\theta_1}^{\theta_2} \text{ lb}$$

TABLE 37. SINUSOIDALLY DISTRIBUTED BOLT LOAD

BOLT NO.	ANGLE DEG	ANGLE COS	BOLT LOAD q	EQUIVALENT BOLT LOAD PER STATION q_3	q_2	q_1	q_5	q_6	q_7
1	26	.898	- 600			-600			
2	35	.819	-1067		-1067				
3	24	.913	- 513	-513					
4	0	0	0						
5	24	.913	513				513		
6	35	.819	1067					1067	
7	26	.898	600						600
8	35	.819	1067					1067	
9	24	.913	513				513		
10	0	0	0						
11	24	.913	- 513	-513					
12	35	.819	-1067		-1067				
Total				-1026	-2134	-600	1026	2134	600

$$q = -\frac{HM}{\pi R^2} \left[\text{COS}\theta\right]_{\theta_1}^{\theta_2} = -\frac{HM}{\pi R^2} \left[\text{COS}\theta_2 - \text{COS}\theta_1\right]$$

$$q = -\frac{(1.5 \times 10^6)}{\pi 9^2} \left[\text{COS } 26^\circ - \text{COS } 0^\circ\right]$$

$$q = -\frac{(1.5 \times 10^6)}{x81} \left[.898 - 1.00\right]$$

$$q = -5895 (-.102)$$

$$q = 600 \text{ lb} \quad \text{BOLT } (1), (7)$$

$$q = 5895 \quad \text{COS } 35^\circ - \text{COS}0^\circ = 1067 \text{ lb} \quad \text{BOLT } (2) \; (12) \; (8) \; (6)$$

$$q = -5895 \left[\cos 24^\circ - \cos 0^\circ\right] = 513 \text{ lb}$$ BOLT (3) (11) (5) (9)

$$q = -5895 \left[\cos 0^\circ - \cos 0^\circ\right] = 0 \text{ lb}$$ BOLT (4) (10)

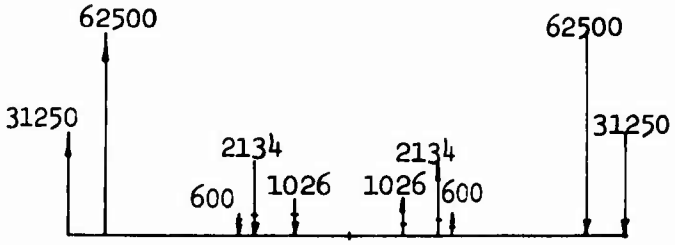

Figure 97. Hub Beam Loading - Ultimate Head Moment.

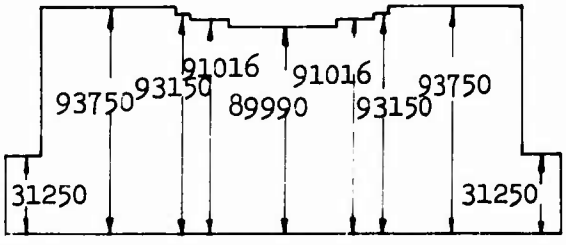

Figure 98. Resultant Shear Diagram.

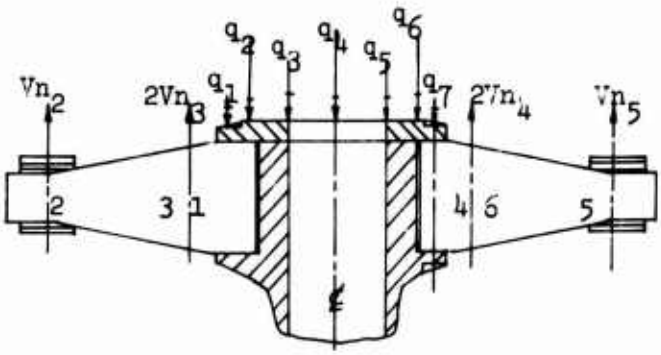

Figure 99. Thrust Loads and Reactions Ultimate Case.

Thrust Reaction Loads - Static Ultimate Case

$$q' = \frac{6V_N}{\pi D}, \quad \frac{lb}{in.}$$

$$q = \frac{6V_N}{\pi D} \times C, \text{ lb}$$

where D = Bolt circle, in.
(Assume all loads acting at 18.00 in.)

C = Arc Length between bolts, in.

C = 1/2 Dθ

θ = Central angle, radians

$57.296 \frac{\text{Deg}}{\text{Rad}} \times 6.284 \text{ Rad} = 360^{\circ}$ $C = \pi \times 18 = 56.548$ In.,

$6 \times V_N = 6 \times 31250$

$6 V_N = 187500$

$C = \frac{1}{2} \times 18 \times 454 = 4.086$ (1), (7)

$C = \frac{1}{2} \times 18 \times .611 = 5.499$ (2), (8), (6), (12)

$C = \frac{1}{2} \times 18 \times .419 = 3.711$ (3), (5), (9), (11)

$C = \frac{1}{2} \times 18 \times .628 = 5.625$ (4), (10)

$$q = \frac{6V_N}{\pi D} C$$

$q = \frac{6 \times 31250}{\pi \times 18} \times 4.086 = 13,650$ (1) (7)

$q = 3315.73 \times 5.499 = 18,300$ (2) (8) (6) (12)

$q = 3315.73 \times 3.711 = 12,350$ (3) (5) (9) (11)

$q = 3315.73 \times 5.625 = 18,800$ (4) (10)

TABLE 38. UNIFORMLY DISTRIBUTED BOLT LOAD

BOLT NO.	ANGLE DEG θ	ANGLE RAD θ	ARC LGTH. C in.	BOLT LOAD q-lb	EQUIVALENT BOLT LOAD PER STATION q_4-lb	q_3-lb	q_2-lb	q_1-lb	q_5-lb	q_6-lb	q_7-lb
1	26	.454	4.086	-13650				-13650			
2	35	.611	5.499	-18300			-18300				
3	24	.419	3.711	-12350		-12350					
4	36	.628	5.625	-18800	-18800						
5	24	.419	3.711	-12350					-12350		
6	35	.611	5.499	-18300						-18300	
7	26	.454	4.086	-13650							-13650
8	35	.611	5.499	-18300						-18300	
9	24	.419	3.711	-12350					-12350		
10	36	.628	5.625	-18800	-18800						
11	24	.419	3.711	-12350		-12350					
12	35	.611	5.499	-18300			-18300				
TOTAL	360	6.284	56.262	-187500	-37600	-24700	-36600	-13650	-24700	-36600	-13650

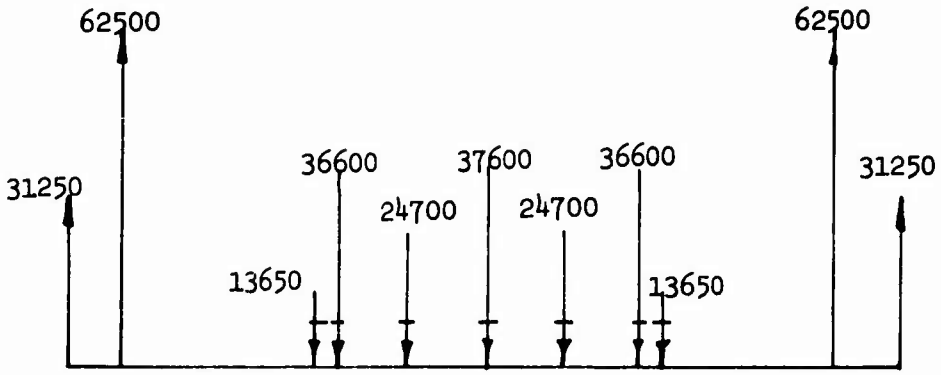

Figure 100. Hub Beam Loading - Ultimate Thrust Case.

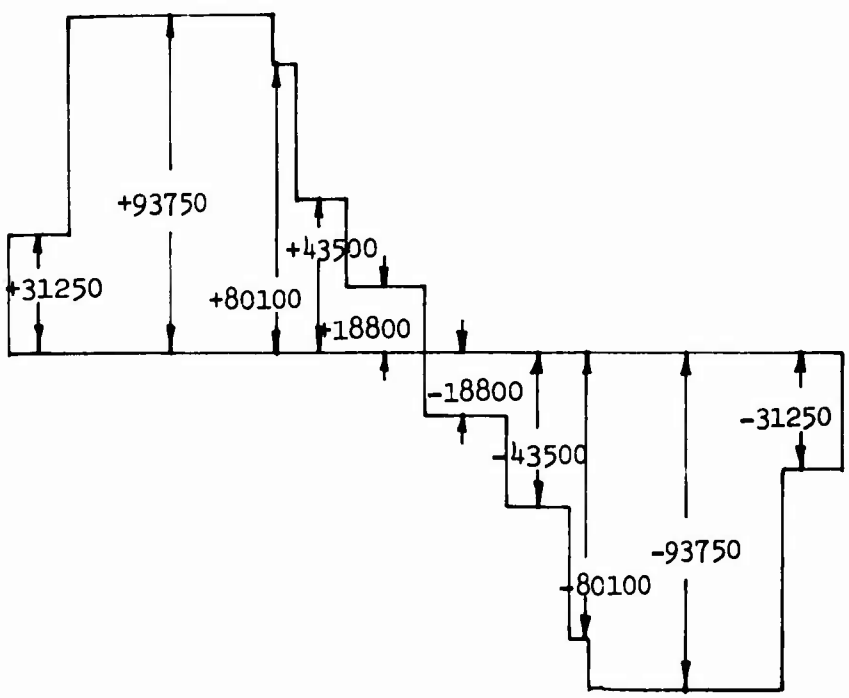

Figure 101. Resultant Shear Diagram.

TABLE 39. RESULTANT STATIC BOLT LOAD DISTRIBUTION

LOAD	V_{N_2} -lb	$2V_{N_3}$-lb	q_1-lb	q_2-lb	q_3-lb	q_4-lb	q_5-lb	q_6-lb	q_7-lb	$2V_{N_4}$-lb	V_{N_5}-lb
HEAD											
MOMENT	+31250	+93750	+93150	+91016	+89990	0	+91016	+93150	+93750	+31250	0
THRUST	+31250	+93750	+80100	+43500	+18800	+18800	-43500	-80100	-93750	-31250	-31250
TOTAL	+62500	+187500	+173250	+134516	+108790	-18800	+47516	+13050	0	0	0

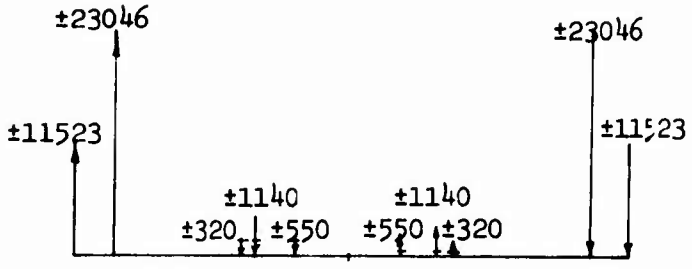

Figure 102. Hub Beam Loading - Fatigue Head Moment Case.

Head Moment Reative Loads - Fatigue Case

$$H\,M = \pm .8 \times 10^6 \text{ in.-lb}$$

$$V_N = 5734 \pm 11523 \text{ lb}$$

$$q = \frac{HM\ (\text{Fatigue Vibratory})}{HM\ (\text{Static Ult})} \times q\ (\text{Static Ult})$$

$$q = \frac{.8 \times 10^6}{1.5 \times 10^6} \times 600 = .533 \times 600 = 320 \text{ lb} \quad \text{BOLT } ①, ⑦$$

$$q = .533 \times 1067 = 570 \text{ lb} \quad \text{BOLT } ②, ⑫, ⑧, ⑥$$

$$q = .533 \times 513 = 275 \text{ lb} \quad \text{BOLT } ③, ⑪, ⑤, ⑨$$

$$q = .533 \times 0 = 0 \text{ lb} \quad \text{BOLT } ④, ⑩$$

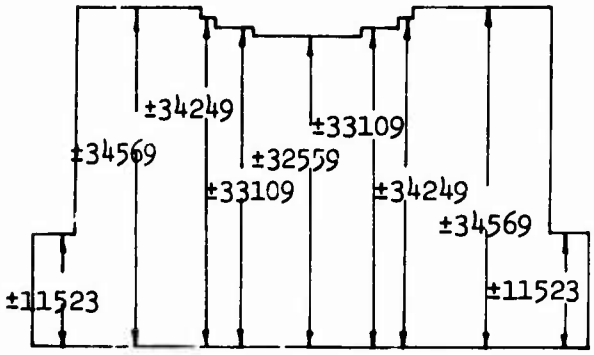

Figure 103. Resultant Shear Diagram.

TABLE 40. SINUSOIDALLY DISTRIBUTED BOLT LOADS

BOLT NO.	BOLT LOAD q-lb	q_3-lb	q_2-lb	q_1-lb	q_5-lb	q_6-lb	q_7-lb
1	-(±320)			-(±320)			
2	-(±570)		-(±570)				
3	-(±275)	-(±275)					
4	0						
5	±275				±275		
6	±570					±570	
7	±320						±320
8	±570					±570	
9	±275				±275		
10	0						
11	-(±275)	-(±275)					
12	-(±570)		-(±570)				
TOTAL		-(±550)	-(±1140)	-(±320)	±550	±1140	±320

Thrust Reaction Loads Fatigue Case

$$q = \frac{V_N \text{ (Fatigue Mean)}}{V_N \text{ (Static Ult)}} \times q \text{ (Static Ult)}$$

$$q = \frac{5734}{31250} \times 13{,}650 = 2504 \quad (1)\ (7)$$

$$q = .18348 \times 18300 = 3358 \quad (2)\ (8)\ (6)\ (12)$$

$$q = .18348 \times 12.350 = 2266 \quad (3)\ (5)\ (9)\ (11)$$

$$q = .18348 \times 18.800 = 3450 \quad (4)\ (10)$$

TABLE 41. UNIFORMLY DISTRIBUTED BOLT LOADS

Bolt No.	Bolt Load q	q_4-lb	q_3-lb	q_2-lb	q_1-lb	q_5-lb	q_6-lb	q_7-lb
1	-2504				-2504			
2	-3358			-3358				
3	-2266		-2266					
4	-3450	-3450						
5	-2266					-2266		
6	-3358						-3358	
7	-2504							-2504
8	-3358						-3358	
9	-2266					-2266		
10	-3450	-3450						
11	-2266		-2266					
12	-3358			-3358				
Total	-34404 ($6V_N$)	-6900	-4532	-6716	-2504	-4532	-6716	-2504

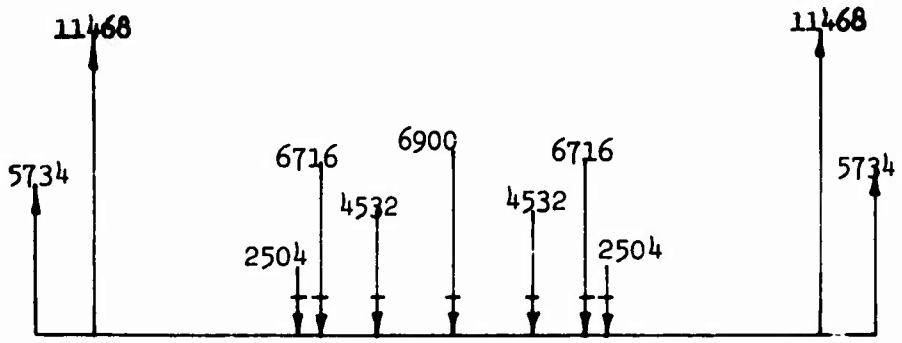

Figure 104. Hub Beam Loading - Fatigue Thrust Case.

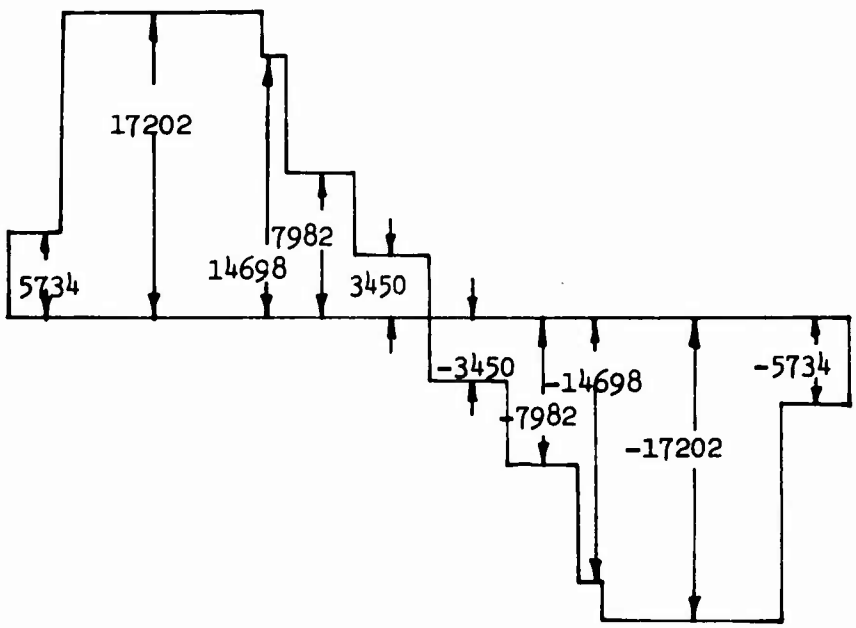

Figure 105. Resultant Shear Diagram.

Calculations for Section 0-0 Properties (Reference Table 32)

$$Io = \frac{bh^3}{12}$$

$$Io = \frac{1.0 \times .50^3}{12} = .01041 \text{ (1) through (12)}$$

$$Io = \frac{3.9 \times .50^3}{12} = .04062 \text{ (14), (16) (36)}$$

$$Io = \frac{.625 \times .250^3}{12} = .00081 \text{ (13), (15) (35)}$$

$$\bar{Y} = \frac{\Sigma AEY}{\Sigma AE} = \frac{2\ (344.718 \times 10^6)}{2\ (77.820 \times 10^6)} = \underline{4.430}$$

$$\Sigma EI_{X-X} = 2 \quad \Sigma AEY^2 + \Sigma EIo - \Sigma AE\bar{Y}^2$$

$$\Sigma EI_{X-X} = 2 \quad 2156.674 \times 10^6 + 6.510 \times 10^6 - (77.820 \times 10^6)\ 4.430^2$$

$$\Sigma EI_{X-X} = 2 \quad 2163.184 \times 10^6 - 1527.209 \times 10^6 = 635.974 \times 10^6$$

$$\Sigma EI_{X-X} = \underline{1271.948 \times 10^6}$$

$$\Sigma EA = 2 \quad 77.820 \times 10^6$$

$$\Sigma EA = 155.640 \times 10^6$$

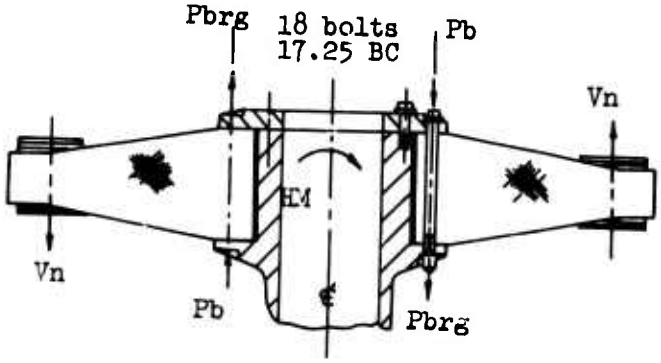

Figure 106. Head Moment Loads and Reactions.

HEAD MOMENT REACTION

P_B = Bolt load (tensile) lb, assuming no preload
P_{BRG} = Ring bearing load distribution, lb/in.
HM = Head moment, lb/in.
V_N = Thrust load, lb

Assume that the bolt load and ring bearing load are sinusoidally distributed.

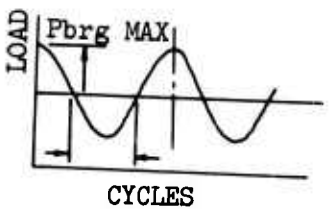

Figure 107. Assumed Bolt/Ring Load Distribution.

$$\frac{1}{2} HM = 2 \left[P_{\substack{BRG \\ MAX}} \quad R \int_0^{\pi} SIN\theta d\theta \quad x \; R \; SIN\theta \right]$$

$$\frac{1}{2} HM = 2 \left[P_{\substack{BRG \\ MAX}} \quad R^2 \int_0^{\pi} SIN^2\theta \; d\theta \right] = 2 P_{BRG} \; R^2 \left[\frac{\theta}{2} \quad \frac{SIN2\theta}{4} \right]_0^{\pi}$$

$$\frac{1}{2} HM = 2 \left[P_{\substack{BRG \\ MAX}} \; R^2 \left\{ \frac{\pi}{2} \quad \frac{SIN \; 2\pi}{4} \right\} \right] = 2 \left[P_{\substack{BRG \\ MAX}} \quad R^2 \quad \frac{\pi}{2} \right]$$

$$P_{\substack{BRG \\ MAX}} = \frac{1}{2} \left[\frac{HM}{\pi R^2} \right]$$

where $P_{\substack{BRG \\ MAX}}$ Reacts 1/2 HM

$$\tfrac{1}{2} HM = P_B \; R \; x \frac{\text{No. Bolts}}{2}$$

$$P_B = \frac{1}{2} \; \frac{HM}{R} \; x \; \frac{2}{\text{No. Bolts}}$$

where P_B Reacts 1/2 HM

THRUST REACTION

V_N is steady in all six arms of hub, so that thrust $_{TOTAL} = 6 \; V_N$.

$$P_{BRG} = \frac{1}{2} \left[\frac{6 \; V_N}{2\pi R} \right]$$

where P_{BRG} Reacts 1/2 V_N

$$P_B = \frac{1}{2} \left[\frac{6 \; V_N}{\text{No. Bolts}} \right]$$

where P_B Reacts 1/2 V_N

STATIC ULTIMATE CASE

$$HM = 2.25\ (10)^6$$

$$V_N = 31{,}250 \text{ lb}$$

$$P_{BRG} = \frac{1}{2}\left[\frac{6\ V_N}{2\pi R}\right] + \frac{1}{2}\left[\frac{HM}{\pi R^2}\right]$$

$$P_{BRG} = \frac{1}{2}\left[\frac{6x31250}{2\pi 8.625}\right] + \frac{1}{2}\left[\frac{2{,}250{,}000}{\pi x 8.625^2}\right]$$

$$P_{BRG} = \frac{1}{2}\left[\frac{187500}{54.192}\right] + \frac{1}{2}\left[\frac{2{,}250{,}000}{233.705}\right]$$

$$P_{BRG} = \frac{1}{2}\ 3460 + \frac{1}{2}\ \underline{9600}$$

$$P_{BRG} = 1730 + 4800 = 6580 \text{ lb/in.}$$

$$P_B = \frac{1}{2}\left[\frac{6\ V_N}{\text{No. Bolts}}\right] + \frac{1}{2}\left[\frac{HM/x2}{\text{R No. Bolts}}\right]$$

$$P_B = \frac{1}{2}\left[\frac{6x31250}{18}\right] + \frac{1}{2}\left[\frac{2{,}250{,}000}{8.625x18}\right]$$

$$P_B = \frac{1}{2}\left[\frac{187500}{18}\right] + \frac{1}{2}\left[\frac{4{,}500{,}000}{155.25}\right] = \underline{19700}\ \frac{\text{lb}}{\text{bolt}}$$

FATIGUE CASE

$$HM = \pm .8 \times 10^6 \text{ in.-lb}$$

$$V_N = 5790 \text{ lb}$$

$$P_{BRG} = \frac{1}{2}\left[\frac{6x5790}{2\pi 8.625} + \frac{+800{,}000}{\pi x 8.625^2}\right]$$

$$P_{BRG} = \frac{1}{2}\left[\frac{34740}{54.192}\right] + \frac{1}{2}\left[\frac{+800{,}000}{233.705}\right]$$

$$P_{BRG} = 321 \pm 1712\ \frac{\text{lb}}{\text{in.}}$$

CLAMP BOLT ANALYSIS (Reference Figure 65)

$$P_B = \frac{1}{2}\frac{6x5790}{18} + \frac{1}{2}\frac{+8000,000x2}{8.625x18}$$

$$P_B + \frac{1}{2}\frac{34740}{18} + \frac{1}{2}\frac{1,600,000}{155.25}$$

$$P_B = 965 \pm 5153 \text{ lb}$$

SPRING RATE OF BOLT

$$\frac{1}{K_B} = \frac{1}{E}\frac{.4d}{A_1} + \frac{L_1}{A_1} + \frac{L_2}{A_2} + \frac{L_3}{A_1} + \frac{L_4}{A_2} + \frac{L_5}{A_m} + \frac{.4d}{A_m}$$

where K_B = Spring Rate of Bolt lb/in.

d = Minor Thread Diameter = .5568 in.

$A_1 = .785 \times d^2 = .785x.6163^2 = .298$ sq in.

$A_2 = .785 \times d_2^2 = .785x500^2 = .196$ sq in.

A_m = Area of Minor Thread Diameter

$= .785 \times .5568^2 = .243$ sq in.

This formula considers the elastic deformation of the head and the engaged thread with a length of 0.4d. (0.4d = 0.4 x .5568 = .223 in.

$$\frac{1}{K_B} = \frac{1}{30x10^6}\frac{.223}{.298} + \frac{2.00}{.298} + \frac{2.750}{.196} + \frac{2.00}{.298} + \frac{2.750}{.196} + \frac{2.125}{.243} + \frac{.223}{.243}$$

$$\frac{1}{K_B} = \frac{1}{30x10^6} .748 + 6.711 + 14.031 + 6.711 + 14.031 + 8.745 + .918$$

$$\frac{1}{K_B} = \frac{1}{30x10^6} 51.895$$

$$K_B = 1.730x10^6 \text{ lb/in.}$$

Spring Rate of Ring

D_j = Effective Joint Dia. = 2.125

D_h = Hole Dia. = 1.125

L_j = Length of Joint = 1.250

TABLE 42. SPRING RATES

No	Component	E PSI	L in.	$A_{in.^2}$	x K_{10^6} lb/in.	
1	Bolt	30×10^6	.4d = .223	.298		
			l_1 = 2.000	.298		
			l_2 = 2.750	.196		
			l_3 = 2.000	.298		
			l_4 = 2.750	.196		
			l_5 = 2.125	.243		
			.4d = .223	.243		
	Bolt (total)	30×10^6			1.73	K_1
2	Ring	16×10^6	1.250	2.551	32.65	K_2
3	Top Cover	2.2×10^6	.25	2.551	22.45	K_3
4	(12) Laminates	10×10^6	3.00	2.551	8.50	K_4
5	(12) Spacers	2.1×10^6	6.00	2.551	.89	K_5
6	Bottom Cover	2.2×10^6	.25	2.551	22.45	K_6
7	Hub Lip	16×10^6	.875	2.551	46.65	K_7

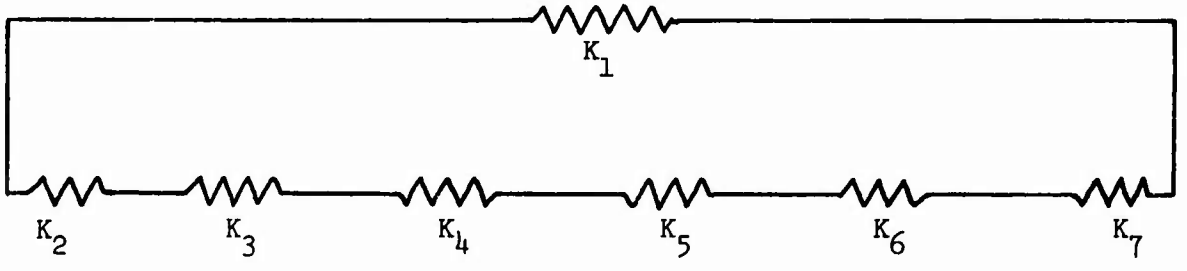

EQUIVALENT SPRING CIRCUIT

$$A = \frac{\pi}{4} (D_j^2 - D_n^2)$$

$$A = .785 (2.125^2 - 1.125^2) = .785 (4.516 - 1.266) = 2.551 \text{ sq in.}$$

$$K_j = \frac{EA}{L} = \frac{(16x10^6)(2.551)}{1.25} = 32.65x10^6 \text{ lb/in.}$$

Material Spring Rate

$$\frac{1}{K_m} = \frac{1}{K_2} + \frac{1}{K_3} + \frac{1}{K_4} + \frac{1}{K_5} + \frac{1}{K_6} + \frac{1}{K_7}$$

$$\frac{1}{K_m} = \frac{1}{32.65x10^6} + \frac{1}{22.45x10^6} + \frac{1}{8.50x10^6} + \frac{1}{22.45x10^6} + \frac{1}{46.65x10^6}$$

$$\frac{1}{K_m} = .031x10^{-6} + .045x10^{-6} + .118x10^{-6} + 1.124x10^{-6} + .045x10^{-6} + .021x10^{-6}$$

$$\frac{1}{K_m} = 1.384 \times 10^{-6}$$

$$K_m = .723 \times 10^6 \text{ lb/in.}$$

Preload on Bolt Due to Wrench Torque

$$P_p = \frac{T}{0.20d}$$

$$P_p = \frac{1940}{0.20x.5887}$$

$$P_p = 16,477 \text{ lb}$$

where T = Wrench Torque 5/18 -18 Bolt
= 1940 in.-lb
d = Pitch Dia. of Threads
= .5887 in.(Mean)
P_p= Preload, lb

or $P_p = \frac{P_p}{A_m}$

CLAMP TO HUB BOLT ANALYSIS (Reference Figure 67)

Head Moment Reaction

$$\Sigma M = M_B - M_{BRG} = 0$$

Since $\frac{1}{2}$ $HM = M_{BRG}$

$$M_B = \frac{1}{2} HM$$

or $\frac{1}{2} HM = M_B = P_B \frac{Rx\eta}{2}$

$$P_B = \frac{HM}{R\eta}$$

Thrust Reaction

$$P_B = \frac{1}{2} \frac{6 V_N}{n}$$

$$P_B = \frac{3 V_N}{n}$$

Static Ultimate Case

$HM = 1.5 \times 10^6$ in.- lb

$V_N = 31250$ lb

$$P_B = \frac{HM}{R\eta} + \frac{3 V_N}{\eta}$$

$$P_B = \frac{1.5 \times 10^6}{6.313 \times 24} + \frac{3 \times 31250}{24}$$

$$P_B = 9900 + 3906$$

$$\therefore P_B = \underline{\underline{13806}} \text{ lb}$$

Fatigue Case

$$HM = \pm .8 \times 10^6 \text{ in.-lb}$$

$$V_N = 5790 \text{ lb}$$

$$P_B = \frac{3 V_N}{n} + \frac{HM}{Rn}$$

$$P_B = \frac{3 \times 5790}{24} + \frac{.8 \times 10^6}{6.313 \times 24}$$

$$\therefore P_B = \underline{\underline{724 \pm 5280}} \text{ lb}$$

Spring Rate of Bolt

Where: $E = 30 \times 10^6$ psi

d = minor dia. = .4387

$A = .785 (.4387)^2 = .15107$

$L = 1.5$ in.

$$K_b = \frac{E A}{L}$$

$$K_b = \frac{(30 \times 10^6) .15107}{1.5}$$

$$K_b = \underline{\underline{3.021 \times 10^6}} \frac{\text{lb}}{\text{in.}}$$

Spring Rate of Ring

$E = 16 \times 10^6$

D_J = EFF. JOINT DIA. = 1.375

D_h = Hole Dia. = .875

$A = .785 (1.375^2 - .875^2)$

$A = .785 (1.890 - .765)$

$A = .283$

$L = 1.5$

$$K_m = \frac{(16 \times 10^6)\ .283}{1.5}$$

$$K_m = \frac{3.018 \times 10^6}{} \quad \frac{lb}{in.}$$

Preload on Bolt Due to Wrench Torque

where T = Wrench Torque for 1/2-20 bolt

= 960 in.-lb

d = Pitch Dia. of Thds

= .4643 in. (Min)

$$P_p = \frac{T}{0.20d}$$

$$P_p = \frac{960}{0.20 \times .4643}$$

$$P_p = \underline{10,338}\ lb$$

or

$$P_p = \frac{P_p}{A}$$

$$P_p = \frac{10338}{.15107} = \underline{68,433}\ psi$$

Load To Cause Separation of Materials

$$P_s = P_p \frac{K_b + K_m}{K_m}$$

$$P_s = 10338 \frac{3.021 \times 10^6 + 3.018 \times 10^6}{3.018 \times 10^6}$$

$$P_s = 10338 \frac{6.039 \times 10^6}{3.018 \times 10^6} = \underline{20,686}\ lb$$

or

$$P_s = \frac{P_p}{A}$$

$$P_s = \frac{20686}{.15107} = 136,932\ psi$$

LITERATURE CITED

1. ASTM, Special Technical Publications 497, COMPOSITE MATERIALS, TESTING AND DESIGN (Second Conference), Philadelphia, 1971.

2. Gessow & Myers, AERODYNAMICS OF THE HELICOPTER, New York, Frederick Ungar Publishing Co., 1967.

3. Faiz, L.,DESIGN ANALYSIS OF A MAIN ROTOR FABRICATED FROM COMPOSITE MATERIALS, Sikorsky Engineering Report 50784, October 1972.

4. Rimkunas, D.,STRUCTURAL ANALYSIS OF CH-53A MAIN ROTOR HEAD, Sikorsky Engineering Report 65303, December 1964.

5. LOADS FOR COMPOSITE MATERIAL HELICOPTER ROTOR HUB, Whittaker Report SDE-72-2, January 1972.

6. STRESS ANALYSIS - COMPOSITE MATERIAL HELICOPTER ROTOR HUB, Whittaker Report SDE-72-1, December 1971.

7. Sainsbury-Carter, B.J., ELASTIC ANALYSIS OF BONDED JOINTS AND REINFORCEMENTS, Sikorsky Engineering Report 50572, December, 1968.

8. Flonc, N., CHARACTERIZATION OF BORON, GRAPHITE AND GLASS FILAMENT/ORGANIC MATRIX COMPOSITE MATERIALS, Sikorsky Engineering Report 50644, January, 1970.

9. Levenetz, B., COMPOSITE MATERIAL ROTOR HUBS, Whittaker Corporation, USAAMRDL Technical Report 73-14, Eustis Directorate, U.S.Army Air Mobility Research and Development Laboratory, Fort Eustis, Virginia.

10. Cellotto, W., STRUCTURAL SUBSTANTIATION OF THE CH-54B MAIN ROTOR, Sikorsky Engineering Report 64515, June, 1969.

11. Clarke, A., STRUCTURAL SUBSTANTIATION OF THE CH-53A MAIN ROTOR, Sikorsky Engineering Report 65068, November 1965.

12. Cellotto, W., CH-54B MAIN ROTOR HEAD LOADS, Sikorsky Engineering Report 64514, November 1969.

13. METALLIC MATERIALS AND ELEMENTS FOR AEROSPACE VEHICLE STRUCTURES, Military Handbook 5A, Department of Defense, February 1966.

14. Degnan, W.G., FATIGUE PROPERTIES AND ANALYSIS, Sikorsky Engineering Report 50586, April, 1969.

15. Petersen, R.E., STRESS CONCENTRATION FACTORS, John Wiley and Sons, New York, 1953.

16. Lutz, W., BENDING AND TORSION OF THIN CIRCULATE RINGS OF CONSTANT CROSS SECTION, Sikorsky Engineering Report 50329, January 1963.

17. Roark, R.J., FORMULAS FOR STRESS AND STRAIN, McGraw-Hill Book Co. New York, 1954.

18. Conaway, J. H., THERMO-ELASTIC ANALYSIS OF LAMINATED SHELLS OF REVOLUTION, Sikorsky Engineering Report 50624, December 1969.